

2012

Fundamental Structure-Activity Relationships of TiO₂-Based Photocatalysts

Charles Alexander Roberts
Lehigh University

Follow this and additional works at: <http://preserve.lehigh.edu/etd>

Recommended Citation

Roberts, Charles Alexander, "Fundamental Structure-Activity Relationships of TiO₂-Based Photocatalysts" (2012). *Theses and Dissertations*. Paper 1205.

This Dissertation is brought to you for free and open access by Lehigh Preserve. It has been accepted for inclusion in Theses and Dissertations by an authorized administrator of Lehigh Preserve. For more information, please contact preserve@lehigh.edu.

Fundamental Structure-Activity Relationships of TiO₂-Based Photocatalysts

by

Charles A. Roberts

A Dissertation

Presented to the Graduate and Research Committee

of Lehigh University

in Candidacy for the Degree of

Doctor of Philosophy

in

Chemical Engineering

Lehigh University

January 2012

Copyright © 2012 by Charles A. Roberts

CERTIFICATE OF APPROVAL

Approved and recommended for acceptance as a dissertation in partial fulfillment of the requirements for the degree of Doctor of Philosophy.

Date

Dissertation Director:

Accepted Date

Dr. Israel E. Wachs, Ph.D.
Advisor and Committee Chairperson
G. Whitney Snyder Professor and
Professor of Chemical Engineering
Lehigh University

Date

Committee Members:

Dr. Hugo S. Caram, Ph.D.
Professor of Chemical Engineering
Lehigh University

Date

Dr. Mark A. Snyder, Ph.D.
P.C. Rossin Assistant Professor of
Chemical Engineering
Lehigh University

Date

Dr. Xingtao Gao, Ph.D.
Refining Catalyst R&D, GCC/CR
BASF Catalysts LLC

Date

ACKNOWLEDGEMENTS

This is a moment whose arrival I have been looking forward to for a long time. I think it is fair to say that those who have made it to this stage in the Ph.D. dissertation process would largely agree with the statement, “This would not have been possible without the help and support of faculty, colleagues, family and friends.” These next few pages will give me the opportunity to express my overwhelming gratitude to those people, and that is why I have been so eager to write these words. I, therefore, have every intention of getting the most out of this section of my dissertation. Whereas the main text of this work attempts to present the findings of my work over the last six and half years as precisely, concisely, and succinctly as possible; I intend to get my money’s worth with my acknowledgements. As anyone who has heard me tell a story, set up a joke, give a presentation (especially my Ph.D. oral defense), or had the pleasure of editing one of my manuscripts can tell you, I have never been one to spare words. I ask that the reader bear with me for the duration as all my powers of rhetoric will be on full display. It is my hope that those to whom I refer will read this and get the impression that I am saying, “Thank you,” in the way they would expect to hear it from me. If I accomplish this even in the least, then I will be delighted and I can simply ignore those who cringe at this sort of thing.

Israel E. Wachs has truly been the primary reason for my success as a graduate student. I have had many opportunities to speak with first-year graduate students and undergraduate students considering graduate education and the primary message I always try to convey to them is that the single most important decision they will make in graduate school is who they work for. I know that I made the right decision. I landed in Dr. Wachs’s research group simply because the stars and planets aligned at the right time. Lehigh University was the only graduate program that accepted me, I had no notion of what I wanted to study, and I took a class taught by Dr. Wachs as an elective in my first semester. The rest, as they say, is history. His advice, understanding, support, and encouragement all paid dividends over the years. His knowledge of the field is second to none and that quickly became apparent whenever I needed direction or suggestions in my research. I know no one that can pull journal references on catalysis from their memory like he does. He recognized the value of my work before I did, and his encouragement helped me push through the days when I would have preferred to wallow in my own

self doubt. Perhaps most of all, I thank him for his patience. “Chip, I think you like graduate school too much,” is a quote I will always remember. It was just the right thing to say. He allowed me to enjoy graduate school and all it had to offer in the way I wanted to, but always kept me moving in the right direction. I can think of no other person I would want in this role in my life. From the laboratory, to professional development and from world travel to my personal well-being; Dr. Wachs always had my best interest in mind. I am eternally grateful. (He will not get rid of me so easily though. We still have papers to publish!)

There are three important people that I must thank for doing so much more than just signing a piece of paper, and they are, of course, my Ph.D. committee members. Hugo Caram has been a constant joy to work and speak with over the years. I could always count on his support and encouragement. I do not know that I have ever met a person with such an uncanny ability to ask the right question to get to the heart of a problem in so many diverse topics. Mark Snyder is personally responsible for filling in the last piece of my Ph.D. puzzle. I should have asked him about making thin films of TiO_2 ages before I did. His insight into my work and his suggestions were always poignant and welcomed. I was truly honored that Xingtao Gao agreed to be on my committee. Not a week goes by in our laboratory that her name does not come up with regards to a paper she has written. If I or any group member needed to know about catalyst synthesis or UV-vis spectroscopy, chances are Xingtao wrote the paper that we consider gospel. She always made time to speak with me and often checked in on me unprompted. I also must thank Xingtao for her unsolicited help in my job search. Xingtao ignited my desire to always improve upon my work.

After six and half years in my research group, I have met and worked with many students, post-doctoral researchers, and scientists, many of whom I also have the privilege of counting as friends. I would love to say something about each and every one of them, but even I must place boundaries on my meandering. If any of them get the opportunity to read this, I want them to know that they hold a special place in my life. There are, however, some of these people that I must specifically mention.

Elizabeth Ross-Medgaarden set me on the path to catalysis. She was a person I could always look to for advice and instruction in my first two years at Lehigh. She encouraged me to explore the opportunities in Dr. Wachs's group and that alone deserves thanks. Peter Phivilay was my colleague in

photocatalysis research at Lehigh. I am insanely jealous of his multiple trips to Japan to study photocatalysis, but grateful that he went. Without the data he collected for me during those trips, this dissertation would have been impossible. I will jointly recognize Jih-Mirn Jehng and Edward Lee for teaching me the most about an aspect of graduate research that I did not realize required such a high level of proficiency; that being the role we play as technicians. I can now use Swagelok and replace thermocouples with the best of them. I will never undervalue that aspect of my experience. Sun-Jae Kim of Sejong University in Seoul, Korea came to our group with his titinate nanotubes and his humble, respectful demeanor. He left the group with my friendship and some really great Raman spectra of his samples. He was a pleasure to work with and the addition of our research to my dissertation truly enhanced the final product. I worked with Alexander Poretzky at Oak Ridge National Lab, and what we did there formed the basis for a large portion of my dissertation. Alex's expert advice was constantly needed and he never let me down. It was a pleasure to work with him at Oak Ridge because he always made sure we got everything done that we wanted to do.

I had the opportunity and pleasure of working for 5 months in Europe at universities in France and The Netherlands. Though a relatively short period of time in my entire graduate career, I managed not only to gain essential experience in my field of research, but also forge a basis for continued collaborations and meet and befriend some really amazing people.

In France I first studied at the Ecole Nationale Supérieure D'Ingenieurs de Caen in Caen. The laboratory there was where I first cut my teeth in infrared spectroscopy, but more significantly, it was where I had my first international experience. That experience could not have been more welcoming. Caen is a beautiful city and I worked with truly beautiful people. The laboratory was melting pot of students from France, Scotland, Poland, Portugal, and Romania. Spending time with them and learning that graduate students really are the same everywhere was invaluable to my development as a person. I then travelled to the École Nationale Supérieure de Chimie de Lille in Lille, France. There I worked with Elise Berrier who I will always count as a dear friend. Our work with Hervé Vezin made it into my dissertation, and served as one of the important starting points for the research that evolved into this final product. Elise, however, went so far above and beyond any of my expectations for the friends I made in Europe. My birthday is on January 5, and at that time I had already left Lille for Delft, The

Netherlands. I was in Delft for the holidays and it was my first time ever being away from family during that time of the year. I was still in touch with Elise and she offered to drive to Delft to visit me on my birthday. Her birthday is January 6, so we celebrated our birthdays together that day. This gesture was overwhelmingly kind. I have not the words to describe how appreciative I was. I will always have a place in my heart for Elise. *Merci beaucoup.*

Moving on to my time at the Technical University of Delft in Delft, The Netherlands, Guido Mul (now at the University of Twente in Enschede, The Netherlands) was my supervisor. He and his graduate students, Chieh-Chao Yang, Ana Rita Almeida, and Joana Carneiro, played an important role in my photocatalysis education. Our research group was working in the dark before the folks at TU Delft shined a light onto ATR infrared spectroscopy for us. I thank Guido for his patience and willingness to teach me despite our initial stumbles. Chieh-Chao (also now at Twente) and I continue to collaborate as I write these acknowledgements. His discussion is always challenging and thought provoking and his comments are always insightful. Rita is the main reason I know anything about ATR. She also made sure I had everything I needed when I came to Delft for the second time a little over one year later. Joana may not know it, but if it was not for her, I would have no chapter on cyclohexane photo-oxidation. I did the initial studies with her and it was not until 3 years later that we realized what we had with that data and pursued it further. Of these four people, only Guido is Dutch, but I think it is still appropriate to say *dank je wel* to all of them.

My friends are another large group of people who I would love to mention individually and wax poetic for pages on all of their fine points, but, alas, the bard doth not dare. I will say that in my opinion, my experiences with my friends were just as important a part of my graduate education as the academic aspects. Graduate school is an opportunity to spend time with a group of energetic, intelligent, and diverse individuals. It would be a shame to not take full advantage of the opportunity to learn about their culture, beliefs, or passions. I do, however, have to mention a few of my close personal friends, because they were the people that helped me deal with my life on a day to day basis, made me smile regularly, and were willing to put up with me.

I had two and half roommates over the years: Owen Finnegan, Chris Keturakis, and Patrick Robinson. Owen always had fresh baked brownies in the apartment and is just the sweetest four-year-

old stuck in a 6' 5" athletic frame that one could ever hope to befriend. I know he will be there whenever I need him, especially if I need a way to disappear on my future wedding day. And we started a fight club at Lehigh. Ooh-rah! Chris and I must have gravitated to each other. I reckon that we are the only two long-haired, heavy-metal-loving freaks on campus. Furthermore, we both work on catalysis in the same research group. Talk about a perfect match! We had a lot of great fun together going to concerts, discovering new bands, playing guitar, playing video games, lifting, the list goes on and on. Pat (the half roommate) kind of lived with Chris and me briefly, so thanks go to him for living on our couch that summer. There were some great times with Aqua Teens and Pucker on the rocks! Pat is a great friend who truly cares and showed me what it means to be passionate about one's research.

Jon Longley is counted among my best friends. When something happens in my life, good or bad, he is a person I want to share that experience with. I would be hard pressed to name a human being that I have met that is more charismatic than Jon. The number of conversations we have had on life, the universe, and everything is vastly numerous. We share a passion for good science, good friends, and good fun and anything we do together is likely to be good fun, at least in our opinion. Jon even brought out the adventurous side of me, and I am still trying to figure out how he convinced me to run a mile and a half up a mountain or to bike over twenty miles in a day when I had not biked that far cumulatively in my life! We have been through all the highs and lows of graduate student life together and I can foresee no point in my life when Jon is not my friend. We have a lot of mischief left to make and it will only build on our legend.

I would like to now to thank a few inanimate or abstract things that helped me get through graduate school. In no particular order: heavy metal, electric guitar, Guitar Hero, PS3, weightlifting, disc golf, racquetball, Harry Potter, The Lord of the Rings, H.P. Lovecraft, DVR, viral videos, Notre Dame Football, and party rocking. Thank you.

I have saved my most important words for last, and those are the words I wish to write to my family. I am truly blessed to have such a wonderful family and if there is truth to the idea of "nature vs. nurture," I would like to think I got the best of both worlds. I love each and every member of my family dearly and I thank them for supporting me at every turn.

My brother John has subjected himself to my shenanigans for his entire life, but I want him to know that in my old age I have truly come to appreciate how much I have enjoyed being his big brother. He provides a balance to my ridiculousness and I look forward to our conversations every time I get the chance to go home. I am so proud of all he has accomplished so far, even if he is a history major, and I say that with tongue firmly in cheek.

Lastly, I would like to address my parents, Charles and Diane Roberts, directly. Mom and Dad, thank you. It goes without saying that I could not be where I am today without you. There has never been a barrier I had to climb to pursue my dreams and you are responsible for that. I have been in school for a long time, and not once have I had to worry that I did not have your support. I consider myself so extremely lucky to have been raised by you. I do not know exactly what you did, but whatever it was, it worked. It would be easy to take for granted all the things you provided me with over the years and for me to become spoiled by your generosity, but I did not take that path and I am certain you are responsible for that. I do not voice my appreciation often, but I think that you know how I feel. Thank you for everything. No words or acts can repay you, but I know it is not necessary because everything you did for me was because you love me. I love you both so very much.

I think that covers everything. Graduate school was a defining experience in my life, and it allowed me to become a person that I am truly happy and proud to be. Now that it is over I will be moving into the real world (“Out of the frying pan and into the fire,” as Tolkien would say), but for now this dissertation is a celebration of some of the best times of my life. So even though my graduate student budget cannot afford many extravagances, I will still say, “Champagne, Champagne for everyone!”

TABLE OF CONTENTS

ACKNOWLEDGEMENTS	iv
TABLE OF CONTENTS	x
LIST OF TABLES	xv
LIST OF FIGURES	xvi
ABSTRACT	1
CHAPTER 1	4
Introduction	4
1. Background	5
1.1 Heterogeneous Photocatalysis	5
1.2 Mechanism of Photocatalytic Reactions	7
1.3 TiO ₂ Based Materials for Photocatalytic Reactions	9
1.3.1 Physical and Electronic Structure of TiO ₂ Supported on SiO ₂	12
1.3.2 Water Splitting Over TiO ₂	14
1.3.3 Cyclohexanone Photo-Oxidation Over TiO ₂	15
2. Techniques for Studying Photocatalytic Reaction and Photocatalyst Characterization	18
2.1 Batch Reactors for Product Detection	18
2.2 Characterization of Electronic Structure: UV-vis-NIR and Photoluminescence Spectroscopies	19
2.3 Vibrational Spectroscopy: ATR-FTIR and Raman	21
3. Approach and Outline	24
3.1 Approach	24
3.2 Outline	26
References	29
Tables	43
Figures	44
CHAPTER 2	49
Determination of a Structure-Photoactivity Relationship for Water Splitting on Well-Defined TiO_x Nanodomains	

Abstract	49
1. Introduction	50
2. Experimental	54
2.1 Catalyst Synthesis	54
2.2 Photoluminescence Spectroscopy	54
2.3 Photoluminescence Decay	55
2.4 Photocatalytic Water Splitting Activity	56
3. Results	56
3.1 Catalyst Structure: Physical and Electronic	56
3.2 Photoluminescence Properties: Peak Emission and Decay	57
3.3 Photocatalytic Splitting of Water to Produce H ₂	59
4. Discussion	60
4.1 Relationships between TiO ₂ nanodomain structure, photoluminescence decay, and UV-vis edge energy (E _g)	60
4.1.1 Effect of TiO ₂ nanodomain structure on photoluminescence lifetimes	60
4.1.2 Comparison of photoluminescence properties and UV- vis Edge Energy (E _g)	62
4.2 Effect of TiO ₂ Nanodomain on Photocatalytic Water Splitting Specific Activity	63
4.3 Effect of Photoluminescence Decay Components on Specific Activity	65
4.4 Surface and Bulk Considerations	70
5. Conclusions	73
Acknowledgments	74
References	75
Tables	81
Figures	83
Supporting Information	94
References	98
Tables	99
Figures	101
CHAPTER 3	102
Top Illumination Reactor and <i>In Situ</i> ATR-FTIR Investigation of Structure-Activity Relationships for Photo-Oxidation of Cyclohexane over Well-Defined TiO_x Nanodomains	

Abstract	102
1. Introduction	103
2. Experimental	107
2.1 Catalyst Synthesis	107
2.2 Cyclohexane Photo-Oxidation Reaction	108
2.3 Thin Film Preparation	109
2.4 <i>In Situ</i> ATR-FTIR During Photo-Oxidation of Cyclohexane	109
3. Results	110
3.1 Cyclohexanone Production and Activity: Top Illumination Reactor	110
3.2 <i>In Situ</i> ATR-FTIR of Supported TiO ₂ /SiO ₂ Catalysts during Photo-Oxidation of Cyclohexane.	113
4. Discussion	118
4.1 Cyclohexane Photo-Oxidation Structure-Activity Relationships as a Function of TiO _x Nanodomain Size	118
4.2 <i>In Situ</i> ATR-FTIR Evidence for the Dependence of Specific Activity on TiO _x Nanodomain Structure	122
4.3 Effect of TiO _x Nanodomain Size on Cyclohexane Photo-Oxidation Reaction Pathways	123
4.4 Relationships between Electronic Structure of TiO _x Nanodomains and Specific Photoactivity	125
4.5 Role of the SiO ₂ Support in Physical and Electronic Structure-Photoactivity Relationships	126
5. Conclusions	127
Acknowledgements	128
References	130
Tables	138
Figures	140
Supporting Information	151
Figures	153
CHAPTER 4	155
<i>In Situ</i> ATR-FTIR and Raman Spectroscopic Studies of Surface Reaction Intermediates during Photocatalytic Splitting of H₂O over TiO₂	
Abstract	155
1. Introduction	156

2. Experimental	160
2.1 Thin Film Preparation and SEM Imaging	160
2.2 ATR-FTIR Spectroscopy Theory, Calculations, and Determination of Thin Film Thickness	161
2.3 <i>In Situ</i> ATR-FTIR Spectroscopy	163
2.4 Raman Spectroscopy	165
2.5 <i>In Situ</i> Electron Paramagnetic Resonance Spectroscopy	166
3. Results	166
3.1 HOOH Adsorption and Intermediate Detection	166
3.2 <i>In Situ</i> ATR-FTIR and Raman Spectroscopy of Water Splitting on TiO ₂ Thin Films	168
3.2.1 ATR-FTIR Spectroscopy	168
3.2.2 Raman Spectroscopy	169
4. Discussion	170
4.1 Identification of Relevant Intermediates	171
4.2 Intermediates Detected During <i>In Situ</i> Spectroscopy of Water Splitting Over TiO ₂ Thin Films	172
4.3 ATR-FTIR in the Absence of H ₂ O	175
4.4 TiO ₂ Thin Film Thickness	176
5. Conclusions	178
Acknowledgements	179
References	180
Figures	185
 CHAPTER 5	 195
 Structure/Composition-Photoactivity Relationships for Titanate Nanotubes	
Abstract	195
1. Introduction	196
2. Experimental	199
2.1 Ti-NT Preparation and Imaging	199
2.2 Raman Spectroscopy	200
2.3 Photocatalytic Activity	201
3. Results	202
3.1 Raman Spectroscopy of As-Prepared and Dried Ti-NT	202
3.2 <i>In Situ</i> Raman Spectroscopy during Thermal Treatment of Ti- NT	203

3.3 Photocatalytic Activity of Ti-NT Samples	206
4. Discussion	207
4.1 Raman Spectroscopy of As-Prepared and Dried Ti-NT	207
4.2 Effect of Na Content on Raman Spectra of Ti-NT	209
4.3 Structure-Activity Relationships for Photocatalytic Reactions Over Ti-NT	210
5. Conclusion	213
Acknowledgements	214
References	215
Tables	225
Figures	226
Supporting Information	232
Figures	235
 CHAPTER 6	 240
 Conclusions and Future Outlook	
1. Conclusions	240
2. Future Outlook	245
References	250
Tables	252
Figures	253
 CURRICULUM VITAE	 254

LIST OF TABLES

CHAPTER 1

Table 1: Characteristic timescales of TiO ₂ photon activated states.	43
--	----

CHAPTER 2

Table 1: Nanodomain structure and size for TiO _x nanodomains in supported TiO ₂ /SiO ₂ catalysts as determined by Raman, XANES, and electron microscopy.	81
--	----

Table 2: Photoluminescence decay fit parameters from Eqn. 1 for supported TiO ₂ /SiO ₂ catalysts.	82
--	----

CHAPTER 2 SUPPORTING INFORMATION

Table S1: Dispersion and number of exposed sites for the supported TiO ₂ /SiO ₂ catalysts assuming a spherical domain shape for the 12 – 100% catalysts.	99
---	----

Table S2: Dispersion and number of exposed sites for the supported TiO ₂ /SiO ₂ catalysts accounting for the differing nanodomain shape.	100
---	-----

CHAPTER 3

Table 1: Summary of the structure and average size as determined by XANES and TEM, respectively, of the supported TiO ₂ nanodomains in the x% TiO ₂ /SiO ₂ catalysts and for pure TiO ₂ (anatase).	138
---	-----

Table 2: Dispersion and number of exposed sites for the supported TiO ₂ /SiO ₂ catalysts.	139
--	-----

CHAPTER 5

Table 1: H ₂ production over 5h during photocatalytic water splitting for Ti-NT catalysts with various pretreatment conditions. A TiO ₂ (P-25) catalyst is also shown for comparison.	225
--	-----

CHAPTER 6

Table 1: Activity for H ₂ production during photocatalytic water splitting over various novel metal oxides studied in the literature. The activity for TiO ₂ is shown for comparison.	252
--	-----

LIST OF FIGURES

CHAPTER 1

- Figure 1:** Number of publications regarding TiO₂ based photocatalysis, water splitting, and TiO₂ based water splitting in journals letters, reviews, books, and dissertations from 1980-2010. [Source: SciFinder Scholar (CAS) online search, September 21, 2011] 44
- Figure 2:** UV-vis E_g energies vs. x% TiO₂ loading on the SiO₂ support. Domain structure from Raman and XANES are indicated to emphasize electronic structure/structure correlation. 45
- Figure 3:** Schematic representation of the photocatalytic water splitting reaction on a semiconductor catalyst. 46
- Figure 4:** An internally illuminated batch reactor (a) for gaseous product detection during photocatalytic water splitting and a top illuminated reactor schematic (b) used for liquid sample withdrawal and product analysis during cyclohexane photo-oxidation. 47
- Figure 5:** Schematic of the IR beam path in typical ATR cell and IRE coated with a solid catalyst. The inset is a representation of the evanescent wave showing its penetration depth into the catalyst coating. 48

CHAPTER 2

- Figure 1:** UV-vis E_g energies vs. x% TiO₂ loading on the SiO₂ support. Domain structure from Raman and XANES are indicated to emphasize electronic structure/structure correlation. 83
- Figure 2:** PL spectroscopic wavelength maps for supported (a) 1, (b) 12, (c) 30 and (d) 60% TiO₂/SiO₂ catalysts. The red line towards the top of each figure represents the excitation wavelengths used to create the map and the emission intensity at each wavelength is given immediately below with color coding (red = very strong, yellow = strong, green = medium, light blue = weak and dark blue = very weak). For each map, the maximum intensity PL emission wavelength is labeled. 84
- Figure 3:** Photoluminescence decay data for a representative set of supported TiO₂/SiO₂ catalysts. 85

Figure 4: (a) “Fast”, t_1 , and “slow”, t_2 , decay times versus TiO_2 concentration of supported $\text{TiO}_2/\text{SiO}_2$ catalysts. (b) Relative amplitudes of the fast and slow PL decay components as a function of TiO_2 loading for supported $\text{TiO}_2/\text{SiO}_2$ catalysts. 86

Figure 5: Overall activity for H_2 production in $\mu\text{mol H}_2/\text{g cat/h}$ for water splitting as a function of TiO_2 loading for the supported $\text{TiO}_2/\text{SiO}_2$ photocatalysts. 87

Figure 6: Activity normalized by the (a) mass of Ti ($\mu\text{mol H}_2/\text{g Ti/hr}$) and (b) exposed Ti sites, defined as specific activity ($\mu\text{mol H}_2/\text{exposed Ti site/hr}$), as a function of TiO_2 loading. The domain structure is indicated for reference. 88

Figure 7: Specific activity ($\mu\text{mol H}_2/\text{exposed Ti site/hr}$) as a function of the average size of the TiO_2 nanodomains in the supported $\text{TiO}_2/\text{SiO}_2$ samples. The domain structure is indicated for reference. 89

Figure 8: Specific activity during H_2O splitting by supported $\text{TiO}_2/\text{SiO}_2$ catalysts and pure TiO_2 photocatalysts as a function of the decay time of PL emission (t_2). 90

Figure 9: Calculated number of sites exhibited fast recombination dynamics (black) and slow recombination dynamics (black) for the mass of supported $\text{TiO}_2/\text{SiO}_2$ catalyst used in the photo-reactor water splitting experiments. 91

Figure 10: Specific activity as a function of the (a) number of sites with slow decay dynamics and as a function of the (b) number of sites with fast decay dynamics. 92

Figure 11: Specific activity ($\mu\text{mol H}_2/\text{exposed Ti site/hr}$) as a function of edge energy values of the supported $\text{TiO}_2/\text{SiO}_2$ catalysts determined from UV-vis-NIR. The domain structure is indicated for reference. 93

CHAPTER 2 SUPPORTING INFORMATION

Figure S1: Specific activity adjusted to account for the 2D raft nanodomain shape as a function of average domain size in the supported $\text{TiO}_2/\text{SiO}_2$ catalysts. 101

CHAPTER 3

- Figure 1:** Production of cyclohexanone over 6h in the TIR for supported 1, 12, 30, and 60% TiO₂/SiO₂ catalysts. The supported 12 and 30% catalysts have had their production normalized to reflect the same mass of TiO₂ as the supported 60% TiO₂/SiO₂ catalyst. No detectable product formation was observed for the supported 1 and 5% catalysts. 140
- Figure 2:** Cyclohexanone production at 5h reaction time as a function of (a) wt.% loading of TiO₂ and (b) average domain size in the supported TiO₂/SiO₂ catalysts. Domain structure is indicated for reference. 141
- Figure 3:** Cyclohexane photo-oxidation activity (mmol cyclohexanone/g Ti/h) for cyclohexanone production on TiO₂ nanodomains as a function of the average domain size in the supported TiO₂/SiO₂ catalysts. The TiO₂ nanodomain structure is shown for reference. 142
- Figure 4:** Specific activity (mmol cyclohexanone/exposed Ti site/h) of TiO₂ nanodomains for cyclohexanone production during photo-oxidation of cyclohexane as function of average domain size. The TiO₂ nanodomain structure is shown for reference. 143
- Figure 5:** ATR-FTIR spectra of the supported TiO₂/SiO₂ catalysts after 100 minutes of illumination during photo-oxidation of cyclohexane. The spectrum for the pure SiO₂ support material is shown for reference. 144
- Figure 6:** ATR-FTIR spectra composing the time profile (0-100 mins of illumination) for photo-oxidation of cyclohexane over pure TiO₂ (anatase). Negative peaks are due to reactant consumption. Each spectrum represents a 10 min interval. 145
- Figure 7:** ATR-FTIR spectra composing the time profile (0-100 mins of illumination) for photo-oxidation of cyclohexane over the supported 60% TiO₂/SiO₂ catalyst containing ~11 nm spherical nanoparticles. Negative peaks are due to reactant consumption. Each spectrum represents a 10 min interval. 146
- Figure 8:** Comparison of the ATR-FTIR spectra composing the time profile (0-100 mins of illumination) for photo-oxidation of cyclohexane over pure TiO₂ (anatase) and a physical mixture of 60% TiO₂ (anatase) and 40% SiO₂ support by weight. The peaks highlighted in red correspond to cyclohexanone vibrations and the peaks highlighted in blue correspond to carbonate/carboxylate vibrations. 147

Figure 9: Specific activity (mmol cyclohexanone/exposed Ti site/h) of TiO₂ nanodomains for cyclohexanone production during photo-oxidation of cyclohexane as function of the relative contribution of the number of Ti sites producing electrons with (a) fast and (b) slow recombination dynamics. 148

Figure 10: Evolution of the peak intensity for desorbed cyclohexanone (1710 cm⁻¹), adsorbed cyclohexanone (1680 cm⁻¹), carboxylates (1580 cm⁻¹), and carbonates (1414 cm⁻¹) over 100 mins of illumination time for pure (a) TiO₂ (anatase) and (b) 60% TiO₂/SiO₂. 149

Figure 11: Specific activity (mmol cyclohexanone/exposed Ti site/h) of TiO₂ nanodomains for cyclohexanone production during photo-oxidation of cyclohexane as function of edge energy, Eg. The TiO₂ nanodomain structure and the exact Eg value are shown for reference. 150

CHAPTER 3 SUPPORTING INFORMATION

Figure S1: Dispersion (black) and the number of exposed Ti sites (blue) as a function of the average domain size in the supported TiO₂/SiO₂ catalysts. TiO₂ domain structure is indicated for reference. 153

Figure S2: Specific activity (mmol/exposed Ti site/h) of TiO₂ nanodomains for cyclohexanone production during photo-oxidation of cyclohexane as function of the slow decay time, t₂, as determined the exponential decay of photoluminescence of the supported TiO₂/SiO₂ catalysts. 154

CHAPTER 4

Figure 1: Theoretical estimation of the penetration depth of the evanescent wave as a function of the wavelength (expressed in wavenumbers) of IR light for a TiO₂ thin film with various porosities on a ZnSe IRE. The pores are assumed to be filled with water. 185

Figure 2: SEM image of the TiO₂ thin film thickness as prepared on a glass slide. 186

Figure 3: (a) Top view of the top plate of the ATR flow through cell. (b) *In situ* ATR experimental setup for illumination during photocatalytic water splitting. 187

Figure 4: Time profile of ATR-FTIR spectra centered around the peroxide spectral region during HOOH adsorption on a TiO₂ thin film under ambient conditions using a 30% HOOH/H₂O solution. The background used was TiO₂ in H₂O. 188

Figure 5: Time profile of ATR-FTIR spectra centered around the superoxide spectral region during HOOH adsorption on a TiO₂ thin film under ambient conditions using a 30% HOOH/H₂O solution. The background used was TiO₂ in H₂O. 189

Figure 6: Visible (532 nm) Raman spectra during HOOH adsorption on a TiO₂ thin film under ambient conditions using (a) 1.0% and (b) 0.1% HOOH/H₂O solution. Note that the convention of plotting as function of decreasing wavenumber is adopted for ease of comparison to the ATR-FTIR spectra. 190

Figure 7: (a) Time profile 2D contour map of *in situ* ATR-FTIR spectra during photocatalytic water splitting on a TiO₂ thin film and under dark and illuminated conditions. (b) Peak area (1000-1200 cm⁻¹) as a function of time for the same experiment. The background used was TiO₂ in H₂O under dark conditions. 191

Figure 8: Peak area (1000-1200 cm⁻¹) as a function of time for *in situ* ATR-FTIR during photocatalytic water splitting on a TiO₂ thin film and under dark and illuminated conditions (Red). The black curve is the same experiment in the absence of H₂O reactant. 192

Figure 9: UV Raman spectra after 10 min of excitation using the UV laser line (325 nm) in absence of H₂O and in the presence of various reactants (H₂O, 10 mM Fe³⁺/H₂O, and D₂O) 193

Figure 10: *In situ* EPR spectra of TiO₂ under reducing conditions (red) followed by the introduction of 10% O₂/He flow (black) at elevated temperature. 194

CHAPTER 5

Figure 1: Raman spectra of the as-prepared titanate powders with negligible Na content (H-Ti-NT) and with 7.02 at% Na content (Na/H-Ti-NT) under ambient conditions. 226

Figure 2: Raman spectra of the titanate powders with negligible Na content (H-Ti-NT) freeze-dried multiple times (a) and of the powders with various drying methods (b) under ambient conditions. 227

Figure 3: *In situ* Raman spectra of the titanate powders (a) with negligible Na content (H-Ti-NT) and (b) with 7.02 atom % Na content (Na/H-Ti-NT) taken at temperatures of 100 °C to 550 °C with a flowing 10% O₂/Ar (30 sccm). 228

Figure 4: TEM image for the H-Ti-NT powder after heat treatment at 400 °C for 30 minutes in air. 229

Figure 5: Raman spectra of the titanate powders with negligible Na content (H-Ti-NT) and with 7.02 at% Na content (Na/H-Ti-NT) under ambient conditions after calcining at 700 °C for 3 hrs in air. (A: anatase phase, R: rutile phase) 230

Figure 6: Photocatalytic decomposition of 4-chlorophenol over Ti-NT catalysts after various pretreatment procedures. A pure TiO₂ (P-25) sample was also run for comparison. 231

CHAPTER 5 SUPPORTING INFORMATION

Figure S1: Reference Raman spectra for different TiO₂ phases compared to the Raman Spectrum of as-prepared H-Ti-NT powder. Dashed lines indicate major Raman bands present for the H-Ti-NT spectrum. 235

Figure S2: Ambient Raman spectra of physically mixed H-Ti-NT powders and TiO₂ powders as a function of different weight ratios. 236

Figure S3: Phase intensities (%) of anatase TiO₂ phase at 138 cm⁻¹ and H-Ti-NT phase at 288 cm⁻¹ estimated from the ambient Raman spectra presented in Figure S1. 237

Figure S4: In-situ Raman spectra for ammonium metatungstate supported on Na/H-Ti-NT and H-Ti-NT powders obtained during calcination at 700 °C in presence of 10% O₂/Ar. 238

Figure S5: STEM-HAADF images of 11.2% WO_x impregnated on H-Ti-NT (0.12% Na) and calcined at 550 °C showing both nanotube structure (a) and nanowire structures (b). For the nanotube structure in (a) the yellow lines indicate the outer wall and the red lines indicate the inner wall. 239

CHAPTER 6

Figure 1: Typical ATR-FTIR spectrum for H₂O on a ZnSe IRE. 253

ABSTRACT

Heterogeneous photocatalysis has been identified as a means of using renewable solar energy to produce the sustainable, non-carbon fuel H_2 and a variety of useful chemical intermediates. Currently, however, heterogeneous photocatalytic reactions are too inefficient to be industrially relevant and a deeper understanding of the effect of fundamental photocatalytic material properties on photoactivity is needed to further enhance the yields of desired products. In the general field of heterogeneous catalysis, structure-activity relationships aid in the rational design of improved catalysts and this ideology was applied to photocatalytic reactions over TiO_2 based photocatalysts and model supported TiO_2/SiO_2 catalysts in this study. The model supported TiO_2/SiO_2 catalysts contain well-defined TiO_x nanodomain structures that vary in domain size and electronic structure and greatly facilitate the determination of structure-photoactivity relationships. These catalysts were used in reactor studies during photocatalytic water splitting and cyclohexane photo-oxidation, and were monitored for production of H_2 and cyclohexanone, respectively. It was found that for both reactions the trend in photoactivity for the TiO_x nanodomains proceeded as: pure TiO_2 (anatase) (24 nm) > TiO_2 (anatase) nanoparticles (4-11 nm) > polymeric surface TiO_5 (~1 nm) > surface isolated TiO_4 (~0.4 nm).

Photoluminescence (PL) spectroscopy was employed to yield insight into how exciton generation and recombination are related to TiO_x domain size and, thus, to the photoactivity of the examined reactions. Transient PL decay studies determined that the larger bulk structure found in TiO_2 (anatase) nanoparticles (NPs) acts as a reservoir

for excitons exhibiting slow recombination kinetics, which have an increased opportunity to participate in photochemistry at the surface active sites. The reactions were also studied using *in situ* attenuated total reflectance (ATR) Fourier transform infrared spectroscopy (FTIR) to observe the formation of adsorbed intermediates and products. For cyclohexane photo-oxidation, cyclohexanone intermediates and products were identified and the high photoactivity of the unsupported TiO₂ (anatase) NPs was attributed to improved product desorption characteristics. The identification of intermediates during water splitting is made difficult by the extremely high absorption of infrared wavelengths by H₂O. ATR-FTIR and Raman spectroscopy measurements were performed during photocatalytic splitting of water in an attempt to confirm the surface reaction intermediates currently identified in the literature and evidence for both superoxide (O₂^{·-}) and peroxide (O₂²⁻) adsorbed species were found by ATR-FTIR, but no surface Ti-OOH was detected by Raman. Finally, alternate Ti-containing structures, titanate and TiO₂ (anatase) nanotubes, were characterized with Raman spectroscopy and screened for their photocatalytic activity. Depending on the photo-reaction (4-chlorophenol decomposition or water splitting), thermal treatment to form the anatase phase in the nanotubular structure is a benefit to photoactivity due to the increased crystallinity. For water splitting, however, the structure-activity relationship found for supported TiO₂/SiO₂ holds, and the presence of a larger bulk structure yields the best H₂ production photoactivity.

The *structure-photoactivity relationship* in this dissertation exists for two different photo-reactions and is expected to be a beneficial aid to future studies on the rational design of new and novel photocatalysts.

CHAPTER 1

Introduction

One of the challenges faced by scientists and engineers in the 21st century is to learn how to efficiently convert naturally abundant, inexpensive, renewable resources into a variety of useful chemical intermediates and sustainable fuels sources, such as non-carbon based H₂ fuel. To this end, heterogeneous photocatalysis has been the topic generating interest because of its ability to use renewable solar energy in catalytic processes rather than the elevated temperatures of conventional heterogeneous catalysis. At the laboratory scale, heterogeneous photocatalysis has shown promise for the production of commercially important intermediates like cyclohexanone and the conversion of water into non-carbon H₂ fuel. Currently these processes are largely too inefficient to be applied at the industrial level and much research is still required to develop new photocatalytically active materials and to understand the fundamental processes that occur during photocatalytic reactions. The work presented in this dissertation focuses on photocatalytic reaction over TiO₂ based catalysts and attempts to increase the fundamental understanding of how TiO₂ structure relates to photoactivity. Reactor and spectroscopic studies are combined to yield insight into how overall photocatalytic activity is affected by physical/electronic structure of TiO₂ domains and the formation of reactive intermediates at surface active sites. The

studies herein attempt to provide the necessary information to form fundamental structure-activity relationships for TiO₂ catalysts across multiple photocatalytic reactions and will lead to future rational design of advanced TiO₂ photocatalysts.

This opening chapter presents a theoretical basis for understanding the topics in subsequent chapters regarding heterogeneous photocatalysis reaction mechanism, important physical/electronic properties of TiO₂ photocatalysts, and the applied reactor and spectroscopic techniques. The chosen approach and an outline of the structure of this research is also presented.

It has been noted by chemist Daniel G. Nocera in a 2007 article on production of H₂ with solar energy that, “A failing of energy R&D for the last 30 years in the United States has been that it has been treated as an engineering problem, with a little ‘r’ component and a big ‘D.’ There needs to be an ‘R’ bigger than the ‘D.’”¹ This quote has been a source of personal motivation and it is intended by the author that this research be a step towards remedying the problem identified by Nocera.

1. Background

1.1 Heterogeneous Photocatalysis

A conventional heterogeneous catalytic reaction is thermally activated, and though the reaction’s thermal efficiency and selectivity are greatly improved; the process still generally requires a significant energy input. In heterogeneous photocatalysis, activation of the catalyst occurs by the absorption of photons of light, a readily abundant resource provided by our planet’s sun. Photocatalytically active materials

are typical semiconductors and most commonly are metal oxides or sulfides such as TiO₂, ZnO, ZrO₂, CeO₂, SnO₂, CdS, ZnS, etc.²

By far the most used and studied photocatalyst is TiO₂. The pioneering discovery of the photoelectric effect of TiO₂ electrodes for the electrolysis of H₂O into H₂ and O₂ by Fujishima and Honda in 1972 can be credited for generating the large interest that followed.³ Titania-based photocatalysis is a rapidly growing field with the number of publications over the last 30 years experiencing a dramatic increase (Figure 1). The majority of the studies focus on the applications that have become commercially viable and environmentally important. Such applications include the purification of water by the degradation of organic compounds,⁴⁻⁸ purification of air,^{2,9-11} and the oxidation of toxic chlorinated industrial solvents such as trichloroethane.¹⁰ Titania is already being applied in a variety of applications as a self-cleaning or self-sterilizing surface.¹² Furthermore, TiO₂ has a broad range of photo-related applications as a white-paint pigment, cosmetic, and sun-blocking material (where it functions to absorb harmful UV radiation).¹³

At the academic and laboratory level, many other reactions are being studied. It is quite possible, though often with low efficiency, to perform a variety of photo-oxidations, -reductions, -substitutions, and polymerizations over TiO₂ catalysts.¹⁴ The prospect of improving the efficiency of these reactions to compete with commercially viable thermal processes has attracted many researchers to closely examine these reactions and a number of excellent reviews on the subject have been published.^{2,4,7,10,14,15} Of particular interest is the photocatalytic splitting of H₂O to H₂

and O₂. The push to convert naturally abundant H₂O to clean H₂ as alternative, sustainable non-carbon fuel has been the motivation for these studies.¹ The publications on TiO₂ for this reaction are beginning to have a larger contribution to the overall TiO₂ based photocatalysis field and a consistent contribution to the overall water splitting field as indicated in Figure 1 indicate. Water splitting, however, has been recently dominated by alternative, novel metal oxides and materials.¹⁶⁻²² These materials, however, are still not commercially viable as their quantum efficiency (percentage of photons exciting a photocatalyst that actually contribute to the photo-reaction) is still below the desired mark for conversion of the overall solar energy spectrum.²³ Fortunately the study of TiO₂ based catalysts for water splitting and other reactions where it exhibits low efficiency remains a viable way to achieve fundamental understanding of the photocatalytic process and can yield valuable information for the design of improved photocatalysts.

1.2 Mechanism of Photocatalytic Reactions

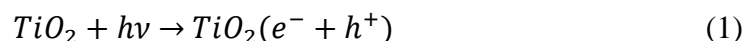
Regardless of the phase of the application, photocatalytic reactions proceed via several fundamental steps:²

- 1) Transfer of the reactants to the catalyst surface
- 2) Adsorption of the reactants
- 3) Absorption of light photons by the catalyst
- 4) Formation of excitons in the form of electron (e⁻)-hole (h⁺) pairs
- 5) Migration of e⁻ and h⁺ to surface catalytic active sites
- 6) Reaction of the adsorbed reactant species to an adsorbed reaction product(s)

- 7) Desorption of product(s)
- 8) Removal of product(s) from the catalyst surface region

It is important to note that these eight steps can be viewed as three distinct areas: surface chemical reactions, electronic reactions, and mass transfer steps (Steps 1 and 8). Although the mass transfer of molecules at interfaces is well known, having to consider both surface chemical reactions and electronic reactions when studying photocatalytic reaction and often makes the task quite challenging.

The ability of a semiconductor like TiO_2 to generate e^- and h^+ during photocatalytic reactions is largely dependent on the material's bandgap. When a photo-active material is illuminated by photons with energy exceeding the bandgap energy of the material, an electron is excited from the valence band to the conduction band, simultaneously forming a hole in the valence band. The formation of these excitons is represented by:



The electrons and holes can then undergo a variety of processes. Immediate recombination of e^-/h^+ pairs occurs readily and is one of the biggest detriments to catalytic efficiency as it has been found by high temporal resolution transient photoluminescence spectroscopy that at least 90% of the e^-/h^+ pairs recombine within 10 ns, negating their ability to perform useful chemistry.²⁴ In this case, the energy input from the illumination photons is lost as heat. If recombination of e^-/h^+ pairs does not immediately take place then it is possible for the e^- and h^+ to migrate to surface catalytic active sites (Step 5 above) and take part in surface reactions. To initiate such

reactions, it is believed that active form of oxygen such as superoxide radicals (O_2^-) must be formed through reduction by e^- and that the oxidizing h^+ excitons can generate surface hydroxyl radicals ($\bullet OH$).^{5,14} The formation of such strongly oxidizing radicals is believed to be the main driving force behind photocatalytic reactions on TiO_2 surfaces¹⁴ and is in agreement with recent density functional theory (DFT) studies.²⁵

Another important reaction is the trapping of electrons at Ti^{4+} sites:



Depending if these trap states are at surface sites or within the bulk a material, they can be beneficial or a deterrent to the photocatalytic process.

The electronic reactions discussed above each have characteristic time scales which have been determined in the literature and are summarized for TiO_2 photon activated states in Table 1.^{5,26} It can be seen that the reactions at the surface in typical photocatalytic process occur with a much slower characteristic time (100 ns - ns) as opposed to recombination and trapping (100 ps – 100 ns). This simple comparison makes it obvious why photocatalytic reactions typically have such low quantum efficiencies.

1.3 TiO_2 Based Materials for Photocatalytic Reactions

TiO_2 based photocatalysts have already been shown to be active for a large and diverse set of photo-reactions. There are several intrinsic properties that make it the oxide semiconductor of choice in photocatalytic applications. The TiO_2 is found to naturally exist in three primary crystal phase: anatase, rutile, and brookite.^{27,28} Rutile is the more thermodynamically stable phase over a large range of temperatures and

pressures; however, under normal condition and those applicable to photo-reactions, anatase is also very stable and does not transition to rutile with any detectable rate until it reaches temperatures $> 600\text{ }^{\circ}\text{C}$.^{29,30} In the case of photoelectrochemistry, only anatase and rutile have bandgaps (3.2 and 3.0 eV, respectively) with a conduction band positioned such that the reduction of H^+ to H_2 is possible.⁵ Brookite is not thermodynamically stable, readily transitioning to rutile, and has been shown to be an indirect bandgap semiconductor and, therefore, an inefficient absorbing material.³¹

The photo-activity of TiO_2 is dependent on the interplay of several factors relating to the structure of the catalyst. The intrinsic properties of TiO_2 include the crystal phase (anatase or rutile), quality of the crystal structure (number of defects), catalyst surface area, and the density of surface hydroxyl groups which play a role in the possible formation of hydroxyl radicals and participate as catalytic active sites. Researchers have recognized these factors and work has already been done in an attempt to understand their role in photocatalytic activity.^{2,32-37} Factors that are extrinsic to the catalyst structure are have also garnered attention in studies on reactor design,^{33,38-40} light intensity and wavelength,^{33,41} and temperature.⁴²

The largest contributor to the low quantum efficiency of TiO_2 photocatalysts is its wide band gap (3.0 – 3.2 eV for rutile and anatase, respectively). Though titania absorbs light into the visible spectrum, generally wavelengths of light less than 400 nm are required to activate the catalyst.³⁰ It is known that the properties of TiO_2 can be modified by such methods as doping of transition and/or noble metals, synthesis of nanostructures (nanotubes, -wires, -rods), and by supporting TiO_2 nanoparticles on an

inert metal oxide support. These modifications of TiO₂ typically attempt to improve photocatalytic activity by:

- 1) Broadening light absorption into the visible range of the spectrum
- 2) Prevent recombination of e⁻/h⁺ pairs by accumulating electrons and holes in two different semiconductor layers
- 3) Increase the intrinsic surface properties of TiO₂, i.e. increased surface area or hydroxyl concentration

A multitude of studies using these modification techniques can be found throughout the literature.^{21,43-46} An excellent review of transition metal ion doping in heterogeneous photocatalysis was made by Litter.⁴⁷ The drive to use sunlight as a clean, renewable energy source has led to large subset of these publications focusing on doping and/or compositing processes which broaden light absorption into the visible spectrum, thereby making more efficient use of the sun's energy.^{8,15,21,48-50}

Regarding the surface area of TiO₂ based photocatalysts; it is possible to create nanotube structures with an outer diameter of ~1 nm and an internal diameter of ~0.6-0.8 nm which yield increased surface areas over particulate structures. Titanate nanotube structures are typically synthesized using a hydrothermal preparation method⁵¹ and have a high potential as heterogeneous catalysts,⁵²⁻⁵⁵ hydrogen storage materials,^{56,57} and secondary batteries.⁵⁸⁻⁶⁰ The hydrothermal preparation method, however, forms titanate structures which lack the benefits of crystalline TiO₂ structures and often residual Na impurities are found which act as a poison to photo-reactions.^{36,61} Thus, in addition to the modification by doping, titanate nanotubes are

often subjected to thermal treatments to create stable crystalline TiO₂ (anatase) nanotubes.^{36,62-69} The thermal treatment and Na impurity removal of titanate nanotubes for improved photocatalytic performance will be the subject of a later chapter.

1.3.1 Physical and Electronic Structure of TiO₂ Supported on SiO₂

Supporting TiO₂ with various weight percent loadings on SiO₂ is another way to alter the structure of the TiO₂ photo-catalyst and is a catalyst preparation technique of particular interest to the studies in subsequent chapters of this dissertation. As a metal oxide, both the TiO₂ structure and catalytic activity can be affected by supporting titania material on an inert, high surface area metal oxide.⁷⁰⁻⁷² In particular, it has been shown that the structure of TiO_x supported on SiO₂ varies with the weight percent loading of titania and these structures can be controlled during catalyst synthesis.^{71,72} Furthermore, the electronic properties of metal oxides (band gap or edge energy) can be controlled by changing the nanodomain structure because the local electron density is affected by the metal oxide domain size; the local electron density increases for smaller dimensions and the electrons become more delocalized for larger dimensions.⁷³ The support effect on the edge energy E_g, as determined by UV-vis-NIR spectroscopy, and its relationship to physical structure has been demonstrated for supported VO_x,⁷⁴ WO_x,⁷⁵ and MoO_x.⁷⁶

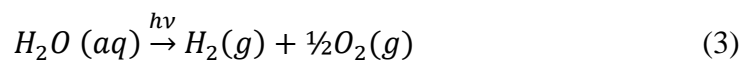
The electronic structure of well-defined TiO_x domains present in supported TiO₂/SiO₂ materials has similarly been probed with *in situ* UV-vis-NIR diffuse reflectance spectroscopy (DRS). First the physical structure of the TiO₂/SiO₂ catalysts

was determined by using a variety of characterization techniques including Raman spectroscopy, x-ray absorption near edge structure (XANES), and transmission electron microscopy. The nature of the supported TiO₂ nanodomain varied in the following manner as a function of the titania loading: isolated surface site (1% TiO₂/SiO₂), polymeric surface chain (12% TiO₂/SiO₂), TiO₂ (anatase) 2D rafts (20-40% TiO₂/SiO₂) and TiO₂ (anatase) 3D nanoclusters (60% TiO₂/SiO₂). The electron density of these structures is reflected in the optical band gap or E_g value yielded from the UV-vis-NIR DRS data. For supported TiO₂/SiO₂, the E_g value for the TiO_x domain increases as domain size decreases as shown in Figure 2. The nanoparticles present at ~40 weight percent loading and higher exhibit E_g values that are the same as pure TiO₂ (anatase), E_g = 3.2 eV indicating that the photoelectric effect is initiated with the same minimum wavelength of light for those nanodomains.^{71,77}

Because the bandgap plays a critical role in the photocatalysts ability to generate electrons and holes under illumination, the discovery of the relationship between physical nanodomain structure and electronic structure makes the study of supported TiO_x nanodomain size/structure on photocatalytic activity an interesting topic. It has been proposed by Anpo *et al.* that a single site tetrahedral TiO₄ titanium oxide species incorporated in a zeolite framework has a relatively high activity in the reduction of CO₂ with H₂O and the decomposition of NO into N₂ and O₂.¹⁵ However, it is yet to be seen if this is a structure that is generally preferred for a larger range of photo-reaction, and studies of TiO_x nanodomain photo-activity on two separate photo-reactions will be the topic of two subsequent chapters.

1.3.2 Water Splitting Over TiO₂

Photocatalytic decomposition of H₂O to H₂ and O₂, the so-called water splitting reaction, occurs via the half reaction:



The mechanism of water splitting proceeds in three main steps, qualitatively described as: 1) absorption of photons to form electron and hole pairs, 2) electron and hole separation and migration to surface catalytic active sites, and 3) the overall surface chemical reactions described by Equation 3.⁷⁸ (Note that these steps are a condensed version of the 8-steps outlined for all photocatalytic reactions, not an exclusion of the other processes that must occur.) The reaction steps of water splitting are schematically shown in Figure 3. It is proposed that water is oxidized to form O₂ at surface catalytic active sites associated with positively charge holes and that H⁺ is reduced to H₂ at surface catalytic active sites associated with electrons. The schematic in Figure 3 is also a useful visually aid for understanding the electronic steps of photocatalytic reaction (i.e. the excitation of an electron to the conduction band, the formation of a hole in the valence band, and the migration of those excitons to surface active sites).

Although TiO₂ is the most studied semiconductor photocatalyst, researchers have found that for water splitting there are also other inorganic semiconductor oxide materials that exhibit markedly higher water splitting activity. There have been many applied studies that have generated new, novel photocatalysts for water splitting.^{16-21,78} The search for improved water splitting catalysts largely focuses on tailoring the

bandgap of the material around the standard redox potential of water (1.23 V),²⁰ but more must be done to understand the fundamental physical/electronic structure-activity relationships inherent to the water splitting reaction given that TiO₂ fits this description and still does not provide adequate quantum efficiency. Furthermore, fundamental surface characterization studies on the novel water splitting catalysts still have not been reported. Therefore, despite the relatively low efficiency and activity of the reaction on TiO₂, investigation of fully characterized, well-defined TiO_x nanodomains will greatly add to the fundamental understanding of the photocatalytic water splitting reaction.

1.3.3 Cyclohexanone Photo-Oxidation Over TiO₂

Cyclohexane oxidation is a commercially important reaction for the production of cyclohexanone and cyclohexanol over a homogeneous catalyst with a selectivity of 70-80%. The reaction products are used to as chemical intermediates in the production of nylon-6 and nylon-6,6.²⁶ Because of the high pressure in the homogeneous catalytic reaction (8-12 bar), it is desirable to find an alternative process that is not only more selective but also safer. Photo-oxidation is a potential route to meet both requirements as it is performed under ambient conditions and the initial report of the photo-reaction indicated high selectivity to the ketone product of cyclohexanone over TiO₂ anatase (100% cyclohexanone) and TiO₂ rutile (90% cyclohexanone, 10% CO₂).⁷⁹

The cyclohexane photo-oxidation reaction can be understood to undergo the same basic 8-step process of all photocatalytic reactions. Over a TiO₂ catalyst the electronic

reactions will generally be the same with regards to formation of electrons and holes, e^-/h^+ pair recombination, and migration of charged species to the surface catalytic active sites. The surface reaction mechanism, however, will differ when compared to water splitting because the reactants are cyclohexane and O_2 . This difference will have a profound effect on the mechanism and how surface hydroxyls play a role in the photo-chemistry.

The proposed mechanism of cyclohexane photo-oxidation over TiO_2 has been studied and published by several researchers,^{33,80-82} however, spectroscopic evidence for the mechanism during photocatalysis is scarce. Recently, with aid of the attenuated total reflectance infrared spectroscopy (ATR-IR) technique, Almeida *et al.* have identified key adsorbed intermediates, tracked product desorption, and proposed a possible reasonable mechanism.^{42,83-85} The initial activation of the TiO_2 catalyst occurs when photo-generated holes interact surface OH groups to form surface hydroxyl radicals $\bullet OH$. Photo-generated holes are predicted to interact with adsorbed O_2 to form superoxides (O_2^-). The ATR-IR results do not give spectroscopic evidence for this but it is in agreement with the predicted activation of photocatalytic surfaces discussed above. The cyclohexane photo-oxidation then proceeds via the following steps:⁸³

- 1) A surface hydroxyl radical reacts with adsorbed cyclohexane to form a surface adsorbed cyclohexyl radical and water.
- 2) The cyclohexyl radical reacts with the O_2^- ion to yield an adsorbed cyclohexyl peroxide intermediate.

- 3) Adsorbed cyclohexanone formation occurs by decomposition of the peroxide intermediate upon reaction at the Ti sites with OH vacancies formed during initiation.
- 4) Cyclohexanone desorption occurs to form products or are further oxidized to form carboxylates, which can be subsequently oxidized to form carbonates and, finally, CO₂ and H₂O.

It is predicted that accumulation of unwanted, non-selective carbonates and carboxylates species contribute to the deactivation of the TiO₂ surface with reaction time.^{40,83} Strong spectroscopic evidence is given for Steps 2-4 of the proposed mechanism, while Step 2 is indirectly observed by the formation of H₂O. The formation of radicals during initiation and Step 1, however, lacks spectroscopic proof.

The extrinsic properties of the photo-oxidation of cyclohexanone over TiO₂ have been studied as well and include reactor design,^{33,38-40} intensity and wavelength of illumination,^{33,41} solvent,⁸⁰ and oxidizing reactants (O₂, H₂O).^{80,86} The TiO₂ catalyst structure has also been subjected to studies of the effect of surface area,³³ pretreatment conditions (calcinations temperature and environment),³³ particle size and crystallinity,³⁴ crystal phase,³⁷ and dopants (Ag and Au).⁴³⁻⁴⁶ The influence of these intrinsic TiO₂ properties relates to the determination of structure-activity relationships. Carneiro *et al.* have studied the effect of TiO₂ (anatase) hydroxyl concentration and particle size for cyclohexane photo-oxidation and found that a high concentration of surface hydroxyls on small particle sizes TiO₂ (anatase) was beneficial to cyclohexanone activity, but large particles were more efficient at desorbing

cyclohexanone.³⁴ Because this study was done over pure TiO₂ (anatase) crystal particles, performing similar experiments coupled with several spectroscopic techniques using well-defined TiO_x nanodomains, will add to a deeper understanding of the structure-activity relationships.

2. Techniques for Studying Photocatalytic Reactions and Photocatalyst Characterization

2.1 Batch Reactors for Product Detection

The most common technique for analyzing the activity of a TiO₂ photocatalytic reaction, including water splitting and cyclohexanone photo-oxidation, is the detection of product formation in a batch reactor. Typically a slurry is created where the catalyst material is suspended in the reactant liquid (with gaseous reactant bubbled into the reactor). The slurry is illuminated using a UV lamp (usually Hg or Xe arc lamps with strong radiation intensities below ~400nm). The slurry concentration becomes very important when considering that the efficiency of absorption of light can decrease in slurries that have too high a concentration.³³ The illumination can occur from the top of the reactor (top illumination reactor, TIR) or internally in the so-called monolith reactor with internal illumination. Product detection is accomplished by sample withdrawal and analysis by gas chromatography. If low yields of a gaseous product are expected, as is the case with H₂ production during water splitting, the empty volume of the reactor can be evacuated prior to the reaction. Figure 4a shows a picture of the internally illuminated reactor for gaseous product analysis used in the

water splitting studies of Chapter 2. Figure 4b shows a schematic of the TIR used for cyclohexanone product detection in Chapter 3. Complete experimental details for these reactors can be found in the respective chapters. The reader is referred to Maeda *et al.* for a water splitting study using the internally illuminated reactor¹⁹ and to the references of Du and Carneiro for examples of studies performed in a TIR reactor.^{30,33-}

35,37-40,44-46,86

2.2 Characterization of Electronic Structure: UV-vis-NIR and Photoluminescence Spectroscopy

Ultraviolet-visible-near infrared (UV-vis-NIR) diffuse reflectance spectroscopy (DRS) is a powerful tool for studying most photocatalytic materials. As indicated above, UV-vis-NIR can yield information on the edge energy E_g of a material which is related to the bandgap. The bandgap has a direct influence on the ability of a photocatalyst to generate electrons and holes upon illumination with a given energy of light. The energy of the photons absorbed by the material must exceed the bandgap for any generation of excitons to occur and without this initiation, photocatalysis cannot occur. Another benefit of UV-vis-NIR DRS is the ability to perform experiments *in situ* allowing for various pretreatment conditions, both thermal and atmospheric, and the monitoring of electronic states under reaction conditions.⁸⁷ This is of the utmost importance for supported metal oxide catalysts since moisture has been shown to affect the physical structure of supported oxide, in turn affecting the E_g .^{71,72} The effect of supported TiO_x domain structure on electron localization and E_g has already been discussed above and the reader is directed to the appropriate

references.^{71,73-77} A drawback of the E_g energy as determined by UV-vis-NIR spectroscopy is that it is a bulk property, that is it reflects the electronic structure of the material as a whole and is not specific to the surface where photo-reactions take place.

Photoluminescence (PL) spectroscopy is complementary to UV-vis-NIR DRS in its ability to yield electronic structural information for TiO_2 .⁴⁹ Because the entirety of the sample is excited during the collection of PL emission intensity, it too can be considered a bulk technique and information on surface electronic structure is limited to analysis of a surface species indirect effect on the PL emission spectrum. Photoluminescence occurs when excitons undergo energy loss in the form of photons of light. This process can occur in several ways, most importantly by the relaxation of electrons in the conduction band back to their ground state in the valence band or by the annihilation of e^-/h^+ pairs through recombination. Thus, PL spectroscopy can yield direct information on the fundamental electronic processes that influence the photoactivity of TiO_2 catalysts. The recombination of e^-/h^+ pairs can be probed directly using ultra-high temporal resolution, transient PL spectroscopy experiments and by fitting to the decay of the emission.

It was shown by Tang *et al.* that the lifetime of photo-generated holes in TiO_2 is a strong determinant of the ability of TiO_2 to split water.⁸⁸ Furthermore, PL spectroscopy, though a bulk technique, can indirectly yield information about the surface since electrons can migrate and interact with adsorbed species or emit PL from surface sites.^{15,49,89} Combining the two above findings, it can be inferred that electrons

and holes that result in long PL lifetimes will be more likely to participate in surface reactions which is in agreement with the characteristic times of photon process found in Table 1. PL spectroscopy and the high temporal resolution, transient PL decay techniques, including experimental details, spectral analysis, and decay profile analysis, are discussed in detail in Chapters 2 and 3.

2.3 Vibrational Spectroscopy: ATR-FTIR and Raman

Direct molecular information about surface adsorbed reaction intermediates and active site structure can be obtained through vibrational spectroscopy, i.e. infrared (IR) and Raman spectroscopy. The two techniques have been found to be complementary to one another. Whereas IR spectroscopy detects vibrations involving a change in dipole moment, Raman spectroscopy detects vibrations involving a change in polarizability. These complementary selection rules result in Raman spectroscopy generally being more sensitive to symmetric modes and IR spectroscopy typically being more sensitive to asymmetric modes.⁹⁰ Another important difference is the ability of Raman spectroscopy to readily collect spectra in an aqueous phase.^{76,90,91} Conversely, water largely absorbs IR energy and produces significant, broad vibrations in regions relevant to adsorbed oxygen and hydroxyl species that participate in the photocatalytic process.^{92,93} It is therefore possible that Raman spectroscopy could be useful in detection of such elusive intermediates in the aqueous phase. It is also proposed that by using a laser with a UV wavelength, it would be possible to simultaneously initiate photo-reactions and obtain spectra of the working catalyst.

The possibility of using Raman spectroscopy under photocatalytic conditions will be considered in Chapter 4.

It has been found that the difficulties of collecting IR spectra in the liquid phase can largely be overcome by the use of attenuated total reflectance (ATR) Fourier transform infrared (FTIR) spectroscopy. ATR-FTIR has been shown to be a technique that can successfully probe the solid-liquid interface that exists in many photocatalytic reaction systems.⁹⁴⁻⁹⁸ The ATR technique is an internal reflection spectroscopy that requires the sample to be in direct contact with an internal reflection element (IRE) with a high refractive index. Typically a thin film of a catalyst sample is coated onto the IRE. Incident IR light travels through the IRE and bounces on the interfaces between the sample and IRE. The angle of the incident light is adjusted to the critical angle of the IRE so that total internal reflection is achieved. Despite the total internal reflection, the electromagnetic field of the light extends beyond the interface into the sample, and this phenomenon is known as an evanescent wave.⁹⁴ The evanescent wave can be absorbed by the sample and the absorption causes the initial IR beam to be attenuated and the resultant spectrum can be obtained. A schematic of a typical ATR cell, sample thin film, and the resulting IR beam and evanescent wave is shown in Figure 5.

The evanescent wave is a standing wave and forms perpendicular to the IRE surface with a penetration depth d_p into the sample that is dependent on the wavelength of light λ , the angle of incidence θ , and the refractive indices of the IRE and the sample:

$$d_p = \frac{\lambda}{2\pi \sqrt{(n_1^2 \sin^2 \theta - n_2^2)}} \quad (4)$$

where n_1 is the refractive index of the IRE and n_2 is the refractive index of the sample.⁹⁸ The calculation of penetration depth is complicated by the fact that the index of refractive of the sample is affected by the relative porosity of the material and by the material filling the pores. Mojet *et al.* calculated that the penetration depth for a sample with pores filled with water increased 1.3 times over a one with pores filled with air.⁹⁴ The effect of the porosity and material filling the pore space can be reflected in a calculation of the effective refractive index n_{eff} of the sample:

$$n_{eff} = \sqrt{(1 - \phi)n_c^2 + \phi n_p^2} \quad (5)$$

where ϕ is the relative porosity and n_c and n_p are the refractive indices of the catalyst and the material filling the pores, respectively.

The goal of the above theoretical look at ATR-IR is to understand that the evanescent wave will only be attenuated by the sample and reactants that are within the penetration depth. Therefore, it is possible to minimize the contribution of the liquid phase on the resulting spectrum. Ideally the solid/liquid interface should be at the penetration depth of the evanescent wave. In practice, the theoretical model does not give the best results under the real reaction conditions due to the difficulties involved in creating an ideal sample thin film. Ortiz-Hernandez *et al.* studied the effect of film thickness on the contribution of the liquid to the ATR-IR spectrum. They found that a film of thickness $5d_p$ was required to avoid sampling liquid that is outside of the film, which corresponded to a film thickness of around 9-10 μm . It

must be stressed that their findings are specific to the catalyst and reaction system, and IRE used in the study. Possible IRE materials include a long list of high refractive index crystal, but the most common are ZnSe, diamond, and germanium. The choice of IRE is dependent several factors, including the spectral range of interest, sample material, solvent, pH, and cost. ZnSe was used throughout this research because of its wide spectral (20,000 – 700 cm^{-1}).⁹⁵

The ATR-FTIR technique has already been shown to be useful in for probing the TiO_2 -cyclohexane, solid-liquid interface for photo-oxidation of cyclohexane by Almeida *et al.* and led to the identification of key adsorbed intermediates and the determination of a possible reaction mechanism.^{42,83-85} The probing of the catalyst-water interface is more challenging but has been shown to be possible,⁹⁹ especially in the case when the characteristic peaks of the adsorbed species, such as CO, do not overlap with the IR bands of H_2O .⁹⁴ ATR-FTIR has been used specifically for the photo-oxidation of water, however Fe^{3+} ions were added using FeCl_3 to act as electron scavengers.^{92,93} This Fe^{3+} aqueous solution does not reflect from the real conditions that one would hope to use for this reaction since the use of FeCl_3 renders the solution quite toxic. Chapter 4 deals with identification of the intermediates of water splitting using ATR-FTIR using pure H_2O as the reactant liquid.

3. Approach and Outline

3.1 Approach

Heterogeneous photocatalysis has been identified as a potential alternative to conventional thermally activated catalytic process for the sustainable production of industrially important chemical intermediates and non-carbon H₂ fuel. Currently the materials used as photocatalysts do not use light or solar energy with a high enough efficiency to become commercially viable. This introductory chapter has shown that TiO₂ based photocatalysts provide an excellent basis for studying the fundamental physical/electronic structures that yield higher photocatalytic activity. Furthermore, the development of new techniques that can probe the surface intermediates involved in the photocatalytic mechanism is providing unprecedented access to information affecting structure-activity relationships in photo-reactions. Researchers have recognized the importance of determining structure-activity relationships in photocatalysis for the future rational design and discovery of improved photocatalyst materials

The research described in this dissertation will focus on the development of fundamental structure-activity relationships for photocatalytic reactions. The use of well-defined supported TiO₂/SiO₂ catalysts will facilitate the development of those relationships as well as introduce nanodomain structures that have not previously been considered. The use of a complete series of well-defined TiO₂ nanodomains makes this work internally consistent and will add new insight to the interpretation of data collected by the typical experimental techniques employed by photocatalysis researchers, such as UV-vis-NIR, PL spectroscopy, and batch reactor product detection.

The structure-activity relationships found will be tested for two different reactions and then an improvement on photo-activity will be attempted through the use of a different TiO₂ structure that reflects the beneficial properties of the structure-activity relationship. The use of ATR-FTIR will supplement the research by yielding information about the relationship between adsorbed intermediates under photo-reaction conditions and photocatalyst structure-activity relationships. ATR-FTIR and Raman spectroscopies also provide a basis for determining the relevant intermediates in the water splitting reaction, the identification of which has been largely speculative or done under conditions that are not applicable to the relevant photo-reaction conditions.

3.2 Outline

Chapter 2

The supported TiO₂/SiO₂ catalysts will be characterized for the effect of the various TiO₂ (anatase) nanodomain structures on their PL emission spectrum and the decay of PL will be related to the recombination dynamics of e⁻/h⁺ pairs. The electronic properties determined by PL spectroscopy will be shown to relate to the physical structure of the TiO₂ nanodomains. Combining the physical/electronic structural information with reactor data for the production of H₂ during the water splitting reaction will provide a basis for determining photo-reaction structure-activity relationships.

Chapter 3

This research is analogous to that of Chapter 2 in its use of the well defined TiO₂ (anatase) nanodomains of the supported TiO₂/SiO₂ catalysts, however, the reaction studied is quite different. The production of cyclohexanone by photo-oxidation of cyclohexane will be the photo-reaction and a structure-activity relationship will be developed using the same characterization techniques. In addition, *in situ* ATR-FTIR will be employed to relate the effect of structure on the adsorbed intermediates and product desorption during cyclohexane photo-oxidation

Chapter 4

Identification of the intermediates present during the photocatalytic splitting of H₂O on TiO₂ will be attempted using ATR-FTIR and Raman spectroscopy. The difficulties of this endeavor will be highlighted and several discrepancies in the literature will be discussed and investigated. The experimental focus of the spectroscopic studies will be to identify intermediates under the relevant photo-reaction conditions necessary for the splitting of water to H₂ and O₂.

Chapter 5

Titanate nanotubes have been identified as a promising material for a variety of reactions and the thermal transformation of this material into the photocatalytically more active anatase phase will be characterized. The removal of Na impurities that are residuals of the synthesis procedure will be shown to be possible with a washing procedure and the positive effect of removing this photocatalytic activity poison are demonstrated for the water splitting reaction. High surface area and crystallinity have

been shown to be important factors in increasing photo-activity and will be considered for the water splitting reaction and for the decomposition of 4-chlorophenol.

Chapter 6

A summary of the most important conclusions of the research in this dissertation will be presented. The future outlook for research continuing in the vein of this dissertation will be discussed, especially regarding the development of photocatalytic structure-activity relationships and the work necessary to improve the identification of water splitting reaction intermediates.

References

- (1) Service, R.F. "Hydrogen Economy? Let Sunlight Do the Work," *Science*, **2007**, 315, 789.
- (2) Herrmann, J. –M. "Heterogeneous photocatalysis: state of the art and present applications," *Top. Catal.* **2005**, 34, 49-65.
- (3) Fujishima, A.; Honda, K. "Electrochemical photolysis of water at a semiconductor electrode," *Nature* **1972**, 238, 37-38.
- (4) Mills, A.; Davies, R. H.; Worsley, D. "Water purification by semiconductor photocatalysis," *Chem. Soc. Rev.* **1993**, 22, 417-425.
- (5) Mills, A.; Le Hunte, S. "An overview of semiconductor photocatalysis," *J. Photochem. Photobiol, A* **1997**, 108, 1-35.
- (6) Herrmann, J. M. "Heterogeneous photocatalysis: fundamentals and applications to the removal of various types of aqueous pollutants," *Catal. Today* **1999**, 53, 115-129.
- (7) Alfano, O. M.; Bahnemann, D.; Cassano, A. E.; Dillert, R.; Goslich, R. "Photocatalysis in water environments using artificial and solar light," *Catal. Today* **2000**, 58, 199-230.
- (8) Nishijima, K.; Ohtani, B.; Yan, X.; Kamai, T.; Chiyoya, T.; Tsubota, T.; Murakami, N.; Ohno, T. "Incident light dependence for photocatalytic degradation of acetaldehyde and acetic acid on S-doped and N-doped TiO₂ photocatalysts," *Chem. Phys.* **2007**, 339, 64-72.

- (9) Pearl, J.; Ollis, D. F. "Heterogeneous photocatalytic oxidation of gas-phase organics for air purification: acetone, 1-butanol, butyraldehyde, formaldehyde, and m-xylene oxidation," *J. Catal.* **1992**, 136, 554-565.
- (10) Linsebigler, A. L.; Lu, G.; Yates, J. T. Jr., "Photocatalysis on TiO₂ Surfaces: Principles, Mechanism, and Selected Results," *Chem. Rev.* **1995**, 95, 735-758.
- (11) Paz, Y. "Application of TiO₂ photocatalysis for air treatment: Patents' overview," *Appl. Catal.* **2010**, 99, 448-460.
- (12) Fujishima, A.; Zhang, X. "Titanium dioxide photocatalysis: present situation and future approaches," *C. R. Chim.* **2006**, 9, 750-760.
- (13) Salem, I. "Recent studies on the catalytic activity of titanium, zirconium, and hafnium oxides," *Catal. Rev.* **2003**, 45, 205-296.
- (14) Fox, M. A.; Dulay, M. T. "Heterogeneous Photocatalysis," *Chem. Rev.* **1993**, 93, 341-357.
- (15) Anpo, M.; Takeuchi, M. "The design and development of highly reactive titanium oxide photocatalysts operating under visible light irradiation," *J. Catal.* **2003**, 216, 505-516.
- (16) Domen, K.; Naito, S.; Onishi, T.; Tamaru, K. "Photocatalytic decomposition of liquid water on a nickel(II) oxide-strontium titanate (SrTiO₃) catalyst," *Chem. Phys. Lett.* **1982**, 92, 433-434.
- (17) Kato, H.; Kudo, A. "New tantalate photocatalysts for water decomposition into H₂ and O₂," *Chem. Phys. Lett.* **1998**, 295, 487-492.

- (18) Maeda, K.; Takate, T.; Hara, M.; Saito, N.; Inoue, Y.; Kobayashi, H.; Domen, K. "GaN:ZnO Solid Solution as a Photocatalyst for Visible-Light-Driven Overall Water Splitting," *J. Am. Chem. Soc.* **2005**, 127, 8286-8287.
- (19) Maeda, K.; Teramura, K.; Saito, N.; Inoue, Y.; Domen, K. "Improvement of photocatalytic activity of $(\text{Ga}_{1-x}\text{Zn}_x)(\text{N}_{1-x}\text{O}_x)$ solid solution for overall water splitting by co-loading Cr and another transition metal," *J. Catal.* **2006**, 243, 303-308.
- (20) Maeda, K.; Domen, K. "New Non-Oxide Photocatalysts Designed for Overall Water Splitting under Visible Light," *J. Phys. Chem. C* **2007**, 111, 7851-7861.
- (21) Osterloh, F. E.; "Inorganic Materials as Catalysts for Photochemical Splitting of Water," *Chem. Mater.* **2008**, 20, 35-54.
- (22) Kudo, A.; Miseki, Y.; "Heterogeneous Materials for Water Splitting," *Chem. Soc. Rev.* **2009**, 38, 253-278.
- (23) Miller, E. L.; Marsen, B.; Paluselli, D. Rocheleau, R. "Optimization of Hybrid Photoelectrodes for Solar Water-Splitting," *Electrochem. Solid State Lett.* **2005**, 8, A247-A249.
- (24) Serpone, N.; Lawless, D.; Khairutdinov, R.; Pelizzetti, E. "Subnanosecond Relaxation Dynamics in TiO_2 Colloidal Sols (Particle Sizes $R_p = 1.0\text{-}13.4$ nm). Relevance to Heterogeneous Catalysis," *J. Phys. Chem.* **1995**, 99, 16655-16661.
- (25) Valdés, A.; Qu, Z.-W.; Kroes, G.-J.; Rossmeisl, J.; Nørskov, J. K. "Oxidation and Photo-Oxidation of Water on TiO_2 Surface," *J. Phys. Chem. C* **2008**, 112, 9872-9879.

- (26) Almeida, A. R. *Cyclohexane photo-catalytic oxidation on TiO₂, an in situ ATR-FTIR mechanistic and kinetic study*. Ph.D. dissertation, Technical University of Delft, **2010**.
- (27) Wells, A. F. *Structural Inorganic Chemistry*. 5 Ed. Oxford University Press, USA, **1984**.
- (28) Mo, S. -D.; Ching, W. Y. "Electronic and optical properties of three phases of titanium dioxide: Rutile, anatase, and brookite," *Phys. Rev. B* **1995**, 51, 13023-13032.
- (29) Kumar, K. -N. P.; Keizer, K.; Burggraaf, A. J.; Okubo, T.; Nagamoto, H.; Morooka, S. "Densification of nanostructured titania assisted by a phase transformation," *Nature* **1992**, 358, 48-51.
- (30) Du, P. *Catalysis Engineering of Light Induced Dye Degradation and Cyclohexane Photo-Oxidation*. Ph.D. Dissertation, Technical University of Delft, **2008**.
- (31) Zallen, R.; Moret, M. P. "The optical absorption edge of brookite TiO₂," *Solid State Commun.* **2006**, 137, 154-157.
- (32) Abe, R.; Kazuhiro, S.; Domen, K.; Arakawa, H. "A new type of water splitting system composed of two different TiO₂ photocatalysts (anatase, rutile) and a IO₃⁻/I⁻ shuttle redox mediator," *Chem. Phys. Lett.* **2001**, 344, 339-344.
- (33) Du, P.; Moulijn, J. A.; Mul, G. "Selective photo(catalytic)-oxidation of cyclohexane: Effect of wavelength and TiO₂ structure on product yields," *J. Catal.* **2006**, 238, 342-352.

- (34) Carneiro, J. T.; Almeida, A. R.; Moulijn, J. A.; Mul, G. "Cyclohexane selective photocatalytic oxidation by anatase TiO₂: influence of particle size and crystallinity," *Phys. Chem. Chem. Phys.* **2010**, 12, 2744-2750.
- (35) Carneiro, J. T.; Savenije, T. J.; Moulijn, J. A.; Mul, G. "Toward a Physically Sound Structure-Activity Relationship of TiO₂-Based Photocatalysts," *J. Phys. Chem. C* **2010**, 114, 327.
- (36) Bavykin, D. V.; Walsh, F. C. *Titanate and Titania Nanotubes: Synthesis, Properties and Applications*, RSC Publishing, Cambridge, UK, **2010**.
- (37) Carneiro, J. T.; Savenije, T. J.; Moulijn, J. A.; Mul, G. "How Phase Composition Influences Optoelectronic and Photocatalytic Properties of TiO₂," *J. Phys. Chem. C* **2011**, 115, 2211-2217.
- (38) Du, Peng; Carneiro, J. T.; Moulijn, J. A.; Mul, G. "A novel photocatalytic monolith reactor for multiphase heterogeneous photocatalysis," *Appl. Catal.* **2008**, 334, 119-128.
- (39) Carneiro, J. T.; Berger, R.; Moulijn, J. A.; Mul, G. "An internally illuminated monolith reactor: Pros and cons relative to a slurry reactor," *Catal. Today* **2009**, 147S, S324-S329.
- (40) Carneiro, J. T.; Moulijn, J. A.; Mul, G. "Photocatalytic oxidation of cyclohexane by titanium dioxide: Catalyst deactivation and regeneration," *J. Catal.* **2010**, 273, 199-210.

- (41) Brusa, M. A.; Grela, M. A. "Photon Flux and Wavelength Effects on the Selectivity and Product Yields of the Photocatalytic Air Oxidation of Neat Cyclohexane on TiO₂ Particles," *J. Phys. Chem. B* **2005**, 109, 1914-1918.
- (42) Almeida, A. R.; Berger, R.; Moulijn, J. A.; Mul, G. "Photo-catalytic oxidation of cyclohexane over TiO₂: A novel interpretation of temperature dependent performance," *Phys. Chem. Chem. Phys.* **2011**, 13, 1345-1355.
- (43) Vinu, R.; Madras, G. "Photocatalytic activity of Ag-substituted and impregnated nano-TiO₂," *Appl. Catal. A*, **2009**, 366, 130-140.
- (44) Carneiro, J. T.; Savenije, T. J.; Mul, G. "Experimental evidence for electron localization on Au upon photo-activation of Au/anatase catalysts," *Phys. Chem. Chem. Phys.* **2009**, 11, 2708-2714.
- (45) Carneiro, J. T.; Yang, C. -C.; Moma, J. A.; Moulijn, J. A.; Mul, G. "How Gold Deposition Affects Anatase Performance in the Photocatalytic Oxidation of Cyclohexane," *Catal. Lett.* **2009**, 129, 12-19.
- (46) Carneiro, J. T.; Savenije, T. J.; Moulijn, J. A.; Mul, G. "The effect of Au on TiO₂ catalyzed selective photocatalytic oxidation of cyclohexane," *J. Photochem. Photobiol. A* **2011**, 217, 326-332.
- (47) Litter, M. I. "Heterogeneous photocatalysis, Transition metal ions in photocatalytic systems," *Appl. Catal. B* **1999**, 23, 89-114.
- (48) Usseglio, S.; Damin, A.; Scarano, D.; Bordiga, S.; Zecchina, A.; Lamberti, C. "(I₂)_n Encapsulation inside TiO₂: A Way to Tune Photoactivity in the Visible Region," *J. Am. Chem. Soc.* **2007**, 129, 2822-2828.

(49) Shi, J.; Chen, J.; Feng, Z.; Chen, T.; Lian, Y.; Wang, X.; Li, C. "Photoluminescence Characteristics of TiO₂ and Their Relationship to the Photoassisted Reaction of Water/Methanol Mixture," *J. Phys. Chem. C* **2007**, 111, 693-699.

(50) Ingram, D. B.; Linic, S. "Water Splitting on Composite Plasmonic-Metal/Semiconductor Photoelectrodes: Evidence for the Selective Plasmon-Induced Formation of Charge Carriers near the Semiconductor Surface," *J. Am. Chem. Soc.* **2011**, 133, 5202-5205.

(51) Qamar, M.; Yoon, C. R.; Oh, H. J.; Lee, N. H.; Park, K.; Kim, D. H.; Lee, K. S.; Lee, W. J.; Kim, S. J., Preparation and photocatalytic activity of nanotubes obtained from titanium dioxide," *Catal. Today* **2008**, 131, 3-14.

(52) Kasuga, T. "Formation of titanium oxide nanotubes using chemical treatments and their characteristic properties," *Thin Solid Films* **2005**, 496, 141-145.

(53) Cortes-Jacome, M. A.; Angeles-Chaves, C.; Morales, M.; Lopez-Salinas, E.; Toledo-Antonio, J. A. "Evolution of titania nanotubes-supported WO_x species by in situ thermo-Raman spectroscopy, X-ray diffraction and high resolution transmission electron microscopy," *J. Solid State Chem.* **2007**, 180, 2682-2689.

(54) Cortes-Jacome, M. A.; Ferrat-Torres, G.; Ortiz, L. F. F.; Angeles-Chavez, C.; Lopez-Salinas, E.; Escobar, J.; Mosqueira, M. L.; Toledo-Antonio, J. A. "In situ thermo-Raman study of titanium oxide nanotubes," *Catal. Today* **2007**, 126, 248-255.

- (55) Yu, K.-P.; Yu, W.-Y.; Kuo, M.-C.; Liou, Y.-C.; Chien, S.-H. "Pt/titania-nanotube: A potential catalyst for CO₂ adsorption and hydrogenation." *Appl. Catal. B* **2008**, 84, 112-118.
- (56) Lim, S. H.; Luo, J.; Zhong, Z.; Ji, W.; Lin, J. "Room-Temperature Hydrogen Uptake by TiO₂ Nanotubes," *Inorg. Chem.* **2005**, 44, 4124-4126.
- (57) Jung, Y. H.; Kim, D. H.; Kim, S. J.; Lee, K. S. "Synthesis and Characterization of Titanate Nanotube for Hydrogen Storage Using Hydrothermal Method with Various Alkaline Treatment," *J. Nanosci. Nanotechnol.* **2008**, 8, 5094-5097.
- (58) Zhang, H.; Gao, X. P.; Li, G. R.; Yan, T. Y.; Zhu, H. Y. "Electrochemical lithium storage of sodium titanate nanotubes and nanorods," *Electrochim. Acta* **2008**, 53, 7061-7068.
- (59) Kim, D. H.; Lee, K. S.; Yoon, J. H.; Jang, J. S.; Choi, D.-K.; Sun, Y.-K.; Kim, S.-J.; Lee, K. S. "Synthesis and electrochemical properties of Ni doped titanate nanotubes for lithium ion storage," *Applied Surface Science* **2008**, 254, 7718-7722.
- (60) Zhao, Z. W.; Guo, Z. P.; Wexler, D.; Ma, Z. F.; Liu, H. K. "Titania nanotube supported tin anodes for lithium intercalation," *Electrochem. Commun.* **2007**, 9, 697-702.
- (61) Suetake, J.; Nosaka, A. Y.; Hodouchi, K.; Matsubara, H.; Nosaka, Y. "Characteristics of Titanate Nanotube and the States of the Confined Sodium Ions," *J. Phys. Chem. C* **2008**, 112, 18474-18482.

- (62) Lin, C. -H.; Lee, C. -H.; Chao, J. -H.; Kuo, C. -Y.; Cheng, Y. -C.; Huang, W. -N.; Chang, H. -W.; Huang, Y. -M.; Shih, M. -K. "Photocatalytic Generation of H₂ Gas from Neat Ethanol over Pt/TiO₂ Nanotube Catalysts," *Catal. Lett.* **2004**, 98, 61-66.
- (63) Hodos, M.; Horvath, E.; Haspel, H.; Kukovecz, A.; Konya, Z.; Kiricsi, I. "Photosensitization of ion-exchangeable titanate nanotubes by CdS nanoparticles," *Chem. Phys. Lett.* **2004**, 399, 512-515.
- (64) Yu, J.; Yu, H.; Cheng, B.; Trapalis, C. "Effects of calcination temperature on the microstructures and photocatalytic activity of titanate nanotubes," *J. Molec. Catal. A* **2006**, 249, 135-142.
- (65) Yu, H.; Yu, J.; Cheng, B. "Preparation, characterization and photocatalytic activity of novel TiO₂ nanoparticle-coated titanate nanorods," *J. Molec. Catal. A* **2006**, 253, 99-106.
- (66) Zhou, H.; Park, T. -J.; Wong, S. S. "Synthesis, characterization, and photocatalytic properties of pyrochlore Bi₂Ti₂O₇ nanotubes," *J. Mater. Res.* **2006**, 21, 2941-2947.
- (67) Song, H.; Jiang, H.; Liu, T.; Liu, X.; Meng, G. "Preparation and photocatalytic activity of alkali titanate nano materials A₂Ti_nO_{2n+1} (A = Li, Na and K)," *Mater. Res. Bull.* **2007**, 42, 334-344.
- (68) Yu, Y.; Xu, D. "Single-crystalline TiO₂ nanorods: Highly active and easily recycled photocatalysts," *Appl. Catal. B* **2007**, 73, 166-171.

- (69) Xiao, M.-W.; Wang, L. -S.; Wu, Y.-Dan; Huang, X. -J.; Dang, Z. "Preparation and characterization of CdS nanoparticles decorated into titanate nanotubes and their photocatalytic properties," *Nanotechnology* **2008**, 015706/1-015706/7.
- (70) Deo, G; Andrzej, M.; Wachs, I. E.; Huybrechts, D. R. C.; Jacobs, P. A. "Characterization of titania silicalites," *Zeolites*, **1993**, 13, 365-373.
- (71) Gao, X.; Bare, S.R.; Fierro, J. L. G.; Banares, M. A.; and Wachs, I. E. "Preparation and in-Situ Spectroscopic Characterization of Molecularly Dispersed Titanium Oxide on Silica," *J. Phys. Chem. B* **1998**, 102, 5653-5666.
- (72) Lee, E. L.; Wachs, I. E. "Molecular Design and In Situ Spectroscopic Investigation of Multilayered Supported M1Ox/M2Ox/SiO2 Catalysts," *J. Phys. Chem. C*, **2008**, 112, 20418-20428.
- (73) Weber, R. S. "Effect of Local Structure on the UV-Visible Absorption Edges of Molybdenum Oxide Clusters and Supported Molybdenum Oxides," *J. Catal.* **1995**, 151, 470-474.
- (74) Gao, X.; Wachs, I. E. "Investigation of Surface Structures of Supported Vanadium Oxide Catalysts by UV-vis-NIR Diffuse Reflectance Spectroscopy," *J. Phys. Chem. B* **2000**, 104, 1261-1268.
- (75) Ross-Medgaarden, E. I.; Wachs, I. E. "Structural Determination of Bulk and Surface Tungsten Oxides with UV-vis Diffuse Reflectance Spectroscopy," *J. Phys. Chem. C* **2007**, 111, 15089-15099.

- (76) Tian, H.; Roberts, C. A.; Wachs, I. E. "Molecular Structural Determination of Molybdena in Different Environments: Aqueous Solutions, Bulk Mixed Oxides, and Supported MoO₃ Catalysts," *J. Phys. Chem. C* **2010**, 114, 14110-14120.
- (77) Ross-Medgaarden, E. I.; Wachs, I. E.; Knowles, W. V.; Burrows, A.; Kiely, C. J.; Wong, M. S. "Tuning the Electronic and Molecular Structures of Catalytic Active Sites with Titania Nanoligands," *J. Am. Chem. Soc.* **2009**, 131, 680-687.
- (78) Kudo, A.; Kato, H.; Tsuji, I. "Strategies for the Development of Visible-light-driven Photocatalysts for Water Splitting," *Chem. Lett.* **2004**, 33, 1534-1539.
- (79) Giannotti, C.; Le Greneur, S.; Watts, O. "Photooxidation of alkanes by metal oxide semiconductors," *Tetrahedron Lett.* **1983**, 24, 5071-5072.
- (80) Boarini, P.; Carassiti, V.; Maldotti, A.; Amadelli, R. "Photocatalytic Oxygenation of Cyclohexane on Titanium Dioxide Suspensions: Effect of the Solvent and of Oxygen," *Langmuir* **1998**, 14, 2080-2085.
- (81) Almquist, C. B.; Biswas, P. "The photo-oxidation of cyclohexane on titanium dioxide: an investigation of competitive adsorption and its effects on product formation and selectivity," *Appl. Catal., A* **2001**, 214, 259-271.
- (82) Brusa, M. A.; Grela, M. A. "Photon Flux and Wavelength Effects on the Selectivity and Product Yields of the Photocatalytic Air Oxidation of Neat Cyclohexane on TiO₂ Particles," *J. Phys. Chem. B* **2005**, 109, 1914-1918.
- (83) Almeida, A. R.; Moulijn, J. A.; Mul, G. "In Situ ATR-FTIR Study on the Selective Photo-oxidation of Cyclohexane over Anatase TiO₂," *J. Phys. Chem. C* **2008**, 112, 1552-1561.

(84) Almeida, A. R.; Carneiro, J. T.; Moulijn, J. A.; Mul, G. "Improved performance of TiO₂ in the selective photocatalytic oxidation of cyclohexane by increasing the rate of desorption through surface silylation," *J. Catal.* **2010**, 273, 116-124.

(85) Almeida, A. R.; Moulijn, J. A.; Mul, G. "Photocatalytic oxidation of cyclohexane over TiO₂: evidence for a Mars-van Krevelen mechanism," *J. Phys. Chem. C* **2011**, 115, 1330-1338.

(86) Carneiro, J. T.; Yang, C. -C.; Moulijn, J. A.; Mul, G. "The effect of water on the performance of TiO₂ in photocatalytic selective alkane oxidation," *J. Catal.* **2011**, 277, 129-133.

(87) Ross-Medgaarden, E. I.; Knowles, W. V.; Kim, T.; Wong, M. S.; Zhou, W.; Kiely, C. J.; Wachs, I. E. "New insights into the nature of the acidic catalytic sites present in ZrO₂-supported tungsten oxide catalysts," *J. Catal.* **2008**, 256, 108-125.

(88) Tang, J.; Durrant, J. R.; Klug, D. R. "Mechanism of Photocatalytic Water Splitting in TiO₂. Reaction of Water with Photoholes, Importance of Charge Carrier Dynamics, and Evidence for Four-Hole Chemistry," *J. Am. Chem. Soc.* **2008**, 130, 13885-13891.

(89) Anpo, M.; Higashimoto, S.; Matsuoka, M.; Zhanpeisov, N.; Shioya, Y.; Stanislaw, D.; Che, M. "The effect of the framework structure on the chemical properties of the vanadium oxide species incorporated within zeolites," *Catal. Today* **2003**, 78, 211-217.

- (90) Wachs, I. E.; Roberts, C. A. "Monitoring surface metal oxide catalytic active sites with Raman spectroscopy," *Chem. Soc. Rev.* **2010**, 39, 5002-5017.
- (91) Molinari, J. E.; Wachs, I. E. "Presence of Surface Vanadium Peroxo-oxo Umbrella Structures in Supported Vanadium Oxide Catalysts: Fact or Fiction?" *J. Am. Chem. Soc.* **2010**, 132, 12559-12561.
- (92) Nakamura, R.; Imanishi, A.; Murakoshi, K.; Nakaoto, Y. "In Situ FTIR Studies of Primary Intermediates of Photocatalytic Reactions on Nanocrystalline TiO₂ Films in Contact with Aqueous Solutions," *J. Am. Chem. Soc.* **2003**, 125, 7443-7450.
- (93) Nakamura, R.; Nakato, Y. "Primary Intermediates of Oxygen Photoevolution Reaction on TiO₂ (Rutile) Particles, Revealed by in Situ FTIR Absorption and Photoluminescence Measurements," *J. Am. Chem. Soc.* **2004**, 126, 1290-1298.
- (94) Mojet, B. L.; Ebbeson, S. D.; Lefferts, L. "Light at the interface: the potential of attenuated total reflection infrared spectroscopy for understanding heterogeneous catalysis in water." *Chem. Soc. Rev.* **2010**, 39, 3643-4655.
- (95) Hind, A. R.; Bhargava, S. K.; McKinnon, A. "At the solid/liquid interface: FTIR/ATR – the tool of choice," *Adv. Coll. Int. Sci.* **2001**, 93, 91-114.
- (96) Bürgi, T.; Baiker, A. "In Situ Infrared Spectroscopy of Catalytic Solid-Liquid Interfaces Using Phase-Sensitive Detection: Enantioselective Hydrogenation of a Pyrone over Pd/TiO₂," *J. Phys. Chem. B* **2002**, 106, 10649-10658.
- (97) Ortiz-Hernandez, I.; Williams, C. T. "In Situ Investigation of Solid-Liquid Interfaces by Attenuated Total Reflection Infrared Spectroscopy," *Langmuir* **2003**, 19, 2956-2962.

(98) Andanson, J. -M.; Baiker, A. "Exploring catalytic solid/liquid interfaces by *in situ* attenuated total reflection infrared spectroscopy." *Chem. Soc. Rev.* **2010**, 39, 4571-4584.

(99) Warren, D. S.; McQuillan, A. J. "Influence of Adsorbed Water on Phonon and UV-Induced IR Absorptions of TiO₂ Photocatalytic Particle Films," *J. Phys. Chem. B* **2004**, 108, 19373-19379.

Table 1: Characteristic timescales of TiO₂ photon activated states.⁵

Primary Process	Characteristic Time
Generation of electron/hole pair:	
$TiO_2 + h\nu \rightarrow TiO_2(e^- + h^+)$	fs (very fast)
Trapping of electron/hole pairs:	
$h^+ + Ti^{IV}OH \rightarrow \{Ti^{IV}OH^+\}$	10 ns (fast)
$e^- + Ti^{IV}OH \rightarrow \{Ti^{III}OH\}$	100 ps (shallow trap)
$e^- + Ti^{IV} \rightarrow Ti^{III}$	10 ns (deep trap)
Electron/hole recombination:	
$e^- + \{Ti^{IV}OH^+\} \rightarrow Ti^{IV}OH$	100 ns (slow)
$h^+ + \{Ti^{III}OH\} \rightarrow Ti^{IV}OH$	10 ns (fast)
Reaction at the surface:	
$\{Ti^{IV}OH^+\} + organic \rightarrow Ti^{IV}OH + oxidized\ organic$	100 ns (slow)
$\{Ti^{III}OH\} + O_2 \rightarrow Ti^{IV}OH + O_2^-$	ms (very slow)

Figure 1: Number of publications regarding TiO₂ based photocatalysis, water splitting, and TiO₂ based water splitting in journals letters, reviews, books, and dissertations from 1980-2010. [Source: SciFinder Scholar (CAS) online search, September 21, 2011]

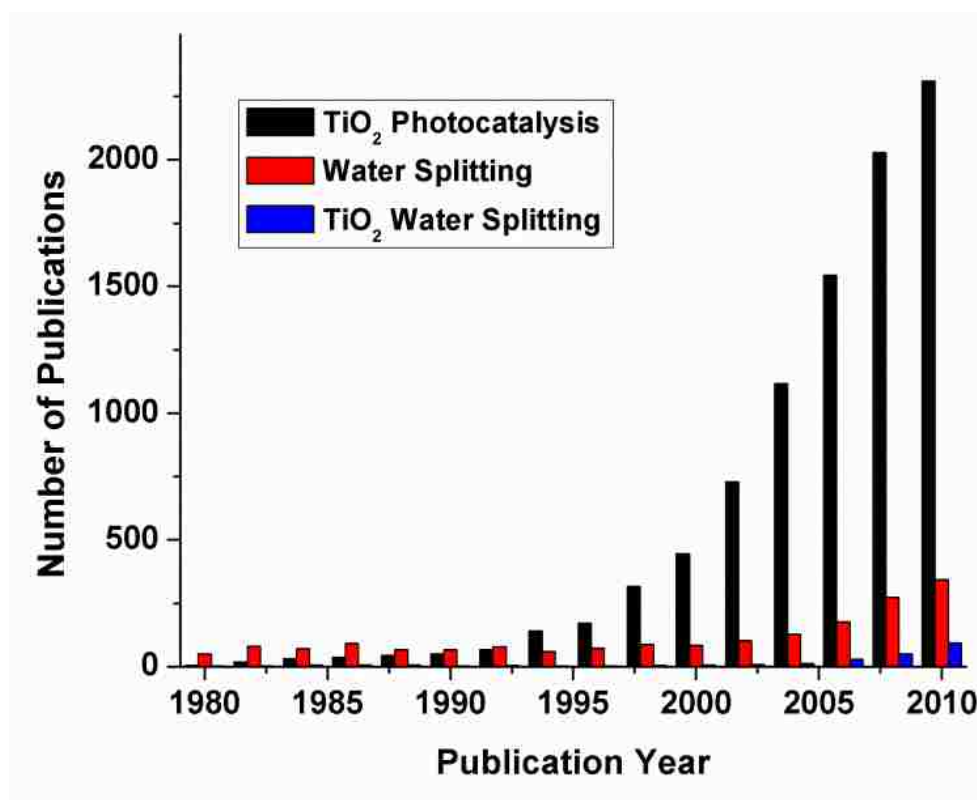


Figure 2: UV-vis E_g energies vs. x% TiO_2 loading on the SiO_2 support. Domain structure from Raman and XANES are indicated to emphasize electronic structure/structure correlation. Reproduced from reference 77.

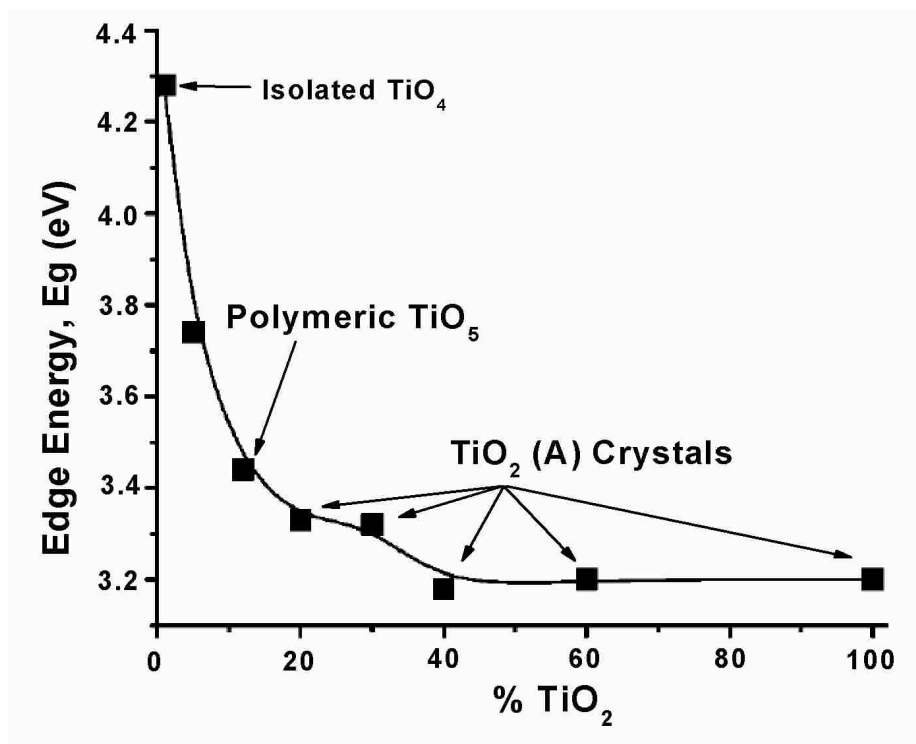


Figure 3: Schematic representation of the photocatalytic water splitting reaction on a semiconductor catalyst.

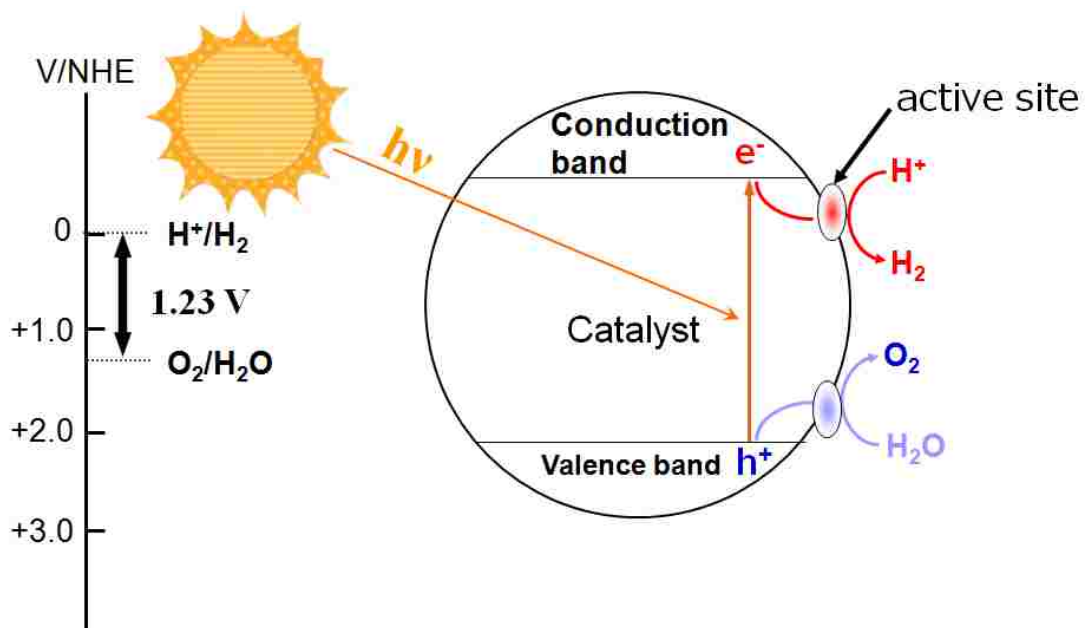


Figure 4: An internally illuminated batch reactor (a) for gaseous product detection during photocatalytic water splitting and a top illuminated reactor schematic (b) used for liquid sample withdrawal and product analysis during cyclohexane photo-oxidation. The schematic in (b) is reproduced from Carneiro *et al.*³⁹

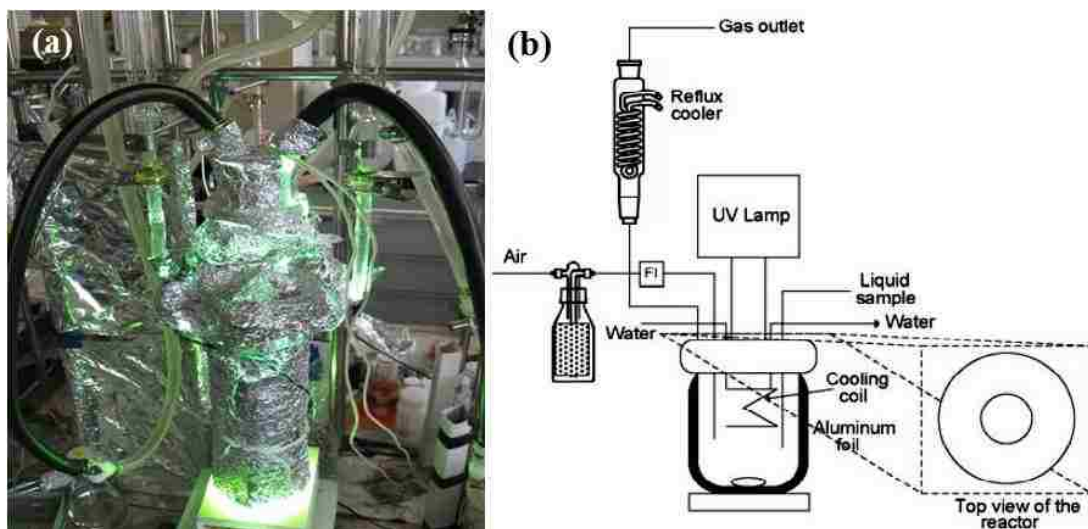
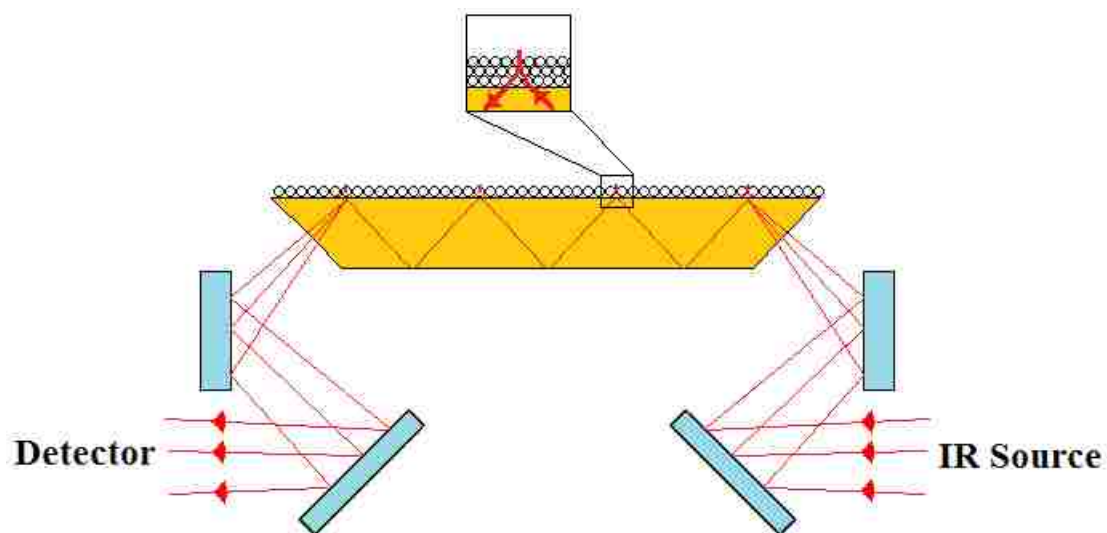


Figure 5: Schematic of the IR beam path in typical ATR cell and IRE coated with a solid catalyst. The inset is a representation of the evanescent wave showing its penetration depth into the catalyst coating.



CHAPTER 2

Determination of a Structure-Photoactivity Relationship for Water Splitting on Well-Defined TiO_x Nanodomains

Abstract

Photocatalytic H₂O splitting to H₂ and O₂ on well-defined TiO₂ nanodomains supported on SiO₂ was investigated to explore the existence of a structure-photocatalytic relationship. The model supported 1-60% TiO₂/SiO₂ photocatalysts were synthesized by incipient wetness impregnation of Ti-isopropoxide/isopropanol solutions into a SiO₂ support in a N₂ environment. Earlier studies reported that the nature of the supported TiO₂ nanodomain varied in the following manner as a function of the titania loading: isolated site (1% TiO₂/SiO₂), polymeric chain (12% TiO₂/SiO₂), 2D rafts (20-40% TiO₂/SiO₂) and 3D nanoclusters (60% TiO₂/SiO₂). *In situ* photoluminescence (PL) spectroscopic measurements showed the PL emission peak shifts to higher excitation wavelength with increasing titania domain size indicating a fundamental difference in electronic structure of the various TiO₂ domains present. *In situ* photo-excitation emission decay studies, with a pulsed tunable laser and a gated detector with a gate width of ~ 300 picoseconds, revealed that the decay time monotonically decreases with increasing TiO₂ nanodomain size. Photocatalytic

splitting of H₂O, in a UV irradiated batch reactor, exhibited enhanced H₂ production with increasing titania domain size. Normalization of the H₂ production by exposed Ti site to yield a specific activity confirmed that isolated TiO₄ sites were the least active for water splitting despite their slow decay rate. However a direct relationship between the number of Ti sites producing electrons with a high contribution of the slow component of decay and high photocatalytic activity was found, thus, providing an explanation for the effect of titania domain size on photocatalysis production. These photocatalytic structure-activity relationships with model supported titania domains should be beneficial for future studies of the rational design of novel photocatalysts for H₂O splitting.

1. Introduction

Photocatalysis by TiO₂ semiconductors has received much attention since the pioneering discovery of the effect of photosensitization of TiO₂ electrodes on the electrolysis of H₂O into H₂ and O₂ by Fujishima and Honda in 1972.¹ These studies have been motivated by the push to convert naturally abundant H₂O to clean H₂ as an alternative, sustainable non-carbon fuel.² The photocatalytic efficiency of TiO₂ has been improved over the years by the addition of various metals or metal oxides.³ The functions of these dopants generally fall into two categories: (1) to broaden light absorption into the visible range or (2) to prevent the recombination of electron/hole pairs by accumulating electrons and holes in two different semiconductor layers. The second category is of particular interest to understanding the mechanism of

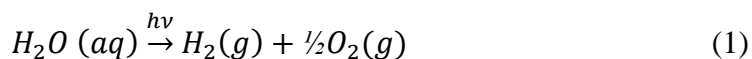
photocatalytic reactions as Serpone *et al.* found that at least 90% of the photo-generated electron/hole pairs recombined within 10 ns, negating their ability to perform useful chemistry.⁴

The majority of photocatalytic reactions utilizing TiO₂ are processes that degrade organic compounds in air or water.⁵⁻⁹ An application such as photo-oxidation of industrial solvents such as trichloroethane and other toxic chlorinated materials have obvious environmental benefits.⁶ TiO₂ based catalysts have also been modified or tailored to increase photo-activity, trap photo-generated holes, or shift the activity to the visible region of the spectrum.^{3,9-13}

The structure and catalytic activity of TiO₂ can be significantly affected by supporting titania on inert, high surface area oxides.¹⁴⁻¹⁶ In particular, it has been shown that the structure of TiO_x supported on SiO₂ varies with the weight percent loading of titania and these structures can be controlled during catalyst synthesis.^{16,17} The electron density of nanostructured metal oxide clusters is known to be dependent on the metal oxide domain size, with the local electron density increasing for smaller dimensions and the electrons becoming more delocalized for larger dimensions.¹⁸ The electronic structure of well-defined TiO_x domains present in supported TiO₂/SiO₂ materials has been probed with *in situ* UV-vis-NIR diffuse reflectance spectroscopy (DRS), which contains the optical bandgap or edge energy. For supported TiO₂/SiO₂, the E_g value for the TiO_x domain has been found to increase as domain size decreases and nanoparticles (NPs) of 5-9 and higher exhibit E_g values that are the same as pure TiO₂ (anatase), E_g = 3.2 eV (Figure 1).^{15,19}

Although TiO₂ is the most studied semiconductor photocatalyst, researchers have found that there are other inorganic semiconductor oxide materials that exhibit improved water splitting properties. There have been many applied studies that have generated new, novel photocatalysts for water splitting,²⁰⁻²² but their efficiency is still below the desired target of 10% conversion of the overall solar energy spectrum.²³

Photocatalytic degradation of H₂O to H₂ and O₂, the so-called water splitting reaction, occurs via the half reaction:



The mechanism of water splitting proceeds in three steps, qualitatively described as: 1) absorption of photons to form electron and hole pairs, 2) electron and hole separation and migration to surface reaction sites, and 3) the surface chemical reactions described by the water splitting reaction above.²² All photocatalytic reactions proceed through the initial photon absorption step that generates electron (e⁻) and hole (h⁺) pairs.^{7,22} It is, therefore, likely that the semiconductor electronic structure will have an effect on this step of the water splitting reaction. The generation of e⁻/h⁺ pairs takes place extremely fast on the femtosecond scale. The recombination of the e⁻/h⁺ pairs, however, occurs faster (10-100 ns) on average than the reaction at the catalyst surface (> 100 ns).²⁴ Therefore, it is of interest to characterize the recombination of e⁻/h⁺ pairs with ultra-high temporal resolution in order to determine if the photocatalytic phenomenon is affected by the electronic and molecular structure of the TiO_x domain.

Photoluminescence (PL) spectroscopy is complementary to UV-vis-NIR DRS in its ability to yield electronic structural information for TiO₂ and both techniques yield

information related to the bandgap or edge energy of a semiconductor oxide material.^{25,26} The recombination of e^-/h^+ pairs can be probed directly using ultra-high temporal resolution, transient PL spectroscopy experiments and by the decay of the emission. It was shown by Tang *et al.* that the lifetime of photo-generated holes in TiO_2 is a strong determinant of the ability of TiO_2 to split water.²⁷ The PL emission decay is related to the lifetime of photo-generated holes (i.e. the slower the decay, the longer the lifetime) since PL emission is indicative of recombination of e^-/h^+ pairs. The quenching of the PL emission and decrease of the PL lifetime and intensity also reflects the trapping efficiency of the electrons and holes at various sites such as surface states and the bulk defect sites of the catalyst. The following work will build on the groundbreaking work by Tang *e. al.* by further analyzing the relationship between photoactivity of H_2O splitting and the lifetime of photo-generated e^-/h^+ pairs with higher temporal resolution in order to examine how nanodomain structure affects the lifetime of photo-generated e^-/h^+ pairs.

It is hypothesized that emission decay from the recombination of e^-/h^+ pairs, a phenomenon that is readily characterized with transient PL spectroscopy, may be correlated with the known nanodomain structures of the well-defined TiO_2/SiO_2 model catalysts to establish structure-photoactivity relationships for TiO_x nanodomains. It is also known that PL spectroscopy is a technique that is not surface sensitive and simultaneously probes the bulk and surfaces semiconductor oxides. PL spectroscopy will not differentiate between e^-/h^+ pairs that recombine in the bulk or at the surface. The migration of e^-/h^+ pairs to surface reaction sites in step 2 of the photocatalytic

process, while related to the surface, can be hindered by bulk recombination of e^-/h^+ pairs, therefore PL spectroscopy may indirectly be related to the surface steps of photocatalysis. This study will also explore the relative usefulness of using a bulk property to determine a structure-photoactivity relationship.

2. Experimental

2.1 Catalyst Synthesis

Model supported TiO_2/SiO_2 catalysts were synthesized from Ti-isopropoxide/isopropanol precursor solutions and a SiO_2 support by incipient-wetness impregnation of varying amounts of Ti precursor, followed by drying and calcination in air (a more complete description for obtaining various Ti loadings can be found in reference 15). The silica support for this study was Cab-O-Sil (Cabot, EH-5) and this material was treated with water in order to condense its volume for easier handling. The wet SiO_2 was dried at 120 °C and subsequently calcined at 500 °C overnight. The resulting BET surface area was 332 m^2/g . Titanium isopropoxide was obtained from Alfa Aesar (99.999% purity) and preparation was performed inside a glove-box with continuous flowing N_2 . The samples were subsequently dried at 120 °C in flowing N_2 for 1 h and calcined at 500 °C in flowing air for 4 h.

2.2 Photoluminescence Spectroscopy

In situ PL-spectroscopy was done using a Jobin-Yvon Fluorolog system modified to use a quartz u-tube cell. The supported TiO_2/SiO_2 samples were heated at 10 °C/min to 400 °C in flowing 10% O_2/N_2 (30 sccm) to remove adsorbed water, since moisture

causes quenching of the PL signal,²⁸ and fully oxidize the model catalysts. Upon cooling to room temperature in flowing inert gas (N₂, 30 sccm), the PL spectra were taken in the flowing inert gas. The PL spectra were taken at incremental light excitation wavelengths from 300 to 500 nm and the emission was measured from 300 to 600 nm. This allowed for multiple spectra to be combined in creating emission maps for each sample. The maps were used to determine the optimum excitation wavelength of light to use for the excitation lifetime measurements.

2.3 Photoluminescence Decay

Spectrally resolved PL lifetime measurements were conducted using a Ti:sapphire laser (Coherent Mira 900), tunable in the 685-1000 nm spectra range, generating 5 ps pulses with a 76 MHz repetition rate, pumped with a frequency-doubled Nd:YVO₄ laser (Coherent Verdi V-18). The output of the laser was frequency doubled using an ultrafast harmonic generator (Coherent 5-050). To perform the luminescence measurements, the excitation light at 400 nm was directed toward a microscope of a tunable micro-, macro-Raman/photoluminescence system (Jobin Yvon Horiba, T6400) and was focused using a long distance objective (50x, N/A=0.5) onto a sample to a spot size of ~ 2 μm. The photocatalyst sample was placed into a high temperature *in situ* microscopy stage (Linkam, TS-1500) and pretreated according to the procedure described above. The luminescence light was collected through the same objective in backscattering geometry and focused onto a slit of the triple-monochromator equipped with a fast gated intensified charge coupled device (ICCD) camera collecting in the 350-900 nm range (LaVision, Picostar HR12). The ICCD camera was gated using a

sequence of 76 MHz pulses propagating with a variable delay relative to the original train of trigger pulses (76 MHz) from a photodiode in a Ti:sapphire laser. The minimum gate width was 300 ps and the maximum delay was defined by the laser repetition rate (~13.2 ns). The laser energy at the sample was maintained at approximately 1.6 mW to prevent photo-degradation of the photocatalyst sample. The experimental decay curves were then fit to a double first-order exponential decay model to account for an observed “fast” (t_1) and “slow” (t_2) components:²⁹

$$y = A1 \cdot \exp\left(\frac{-t}{t_1}\right) + A2 \cdot \exp\left(\frac{-t}{t_2}\right) + y_0 \quad (2)$$

2.4 Photocatalytic Water Splitting Activity

The H₂O splitting photocatalytic activity of the model supported TiO₂/SiO₂ catalysts was determined with UV (wavelengths > 290 nm) irradiation using a 450 W Hg lamp. A reaction cell made of Pyrex was employed and filled with 250 mL condensed liquid-phase water. The reactor was connected to a glass, closed-gas circulation system. About 200 mg of the photocatalyst was suspended in the reaction cell and stirred with a magnetic stir bar. The air in the remaining volume of the reactor was evacuated to facilitate product detection. The reactor was maintained at room temperature and gas chromatography was used to analyze H₂ production for 5 hours.

3. Results

3.1 Catalyst Structure: Physical and Electronic

The silica-supported titania phases were extensively characterized during previous work from our group with atomic absorption, *in situ* (dehydrated) Raman, IR, UV-vis,

XANES and electron microscopy (aberration corrected HR-TEM) to determine their molecular and electronic structures as well as domain size.^{15,17,19} The resulting model supported catalysts (denoted x% TiO₂/SiO₂) were found to consist of monotonically increasing titania nanodomains on the SiO₂ substrate with increasing TiO₂ loading. The supported 1% TiO₂/SiO₂ catalyst possesses isolated surface TiO₄ sites (~0.4 nm) and the supported 12% TiO₂/SiO₂ catalyst is populated by polymeric surface TiO₅ chains (~1 nm). For the supported 20-30% TiO₂/SiO₂ catalyst, the dominant titania phase is present as thin, two-dimensional TiO₂ (anatase) rafts (~2-5 nm) that become three-dimensional TiO₂ (anatase) NPs (~5-11 nm) at 40-60% loadings. The structures of each of the individual catalysts are summarized in Table 1. The electronic structure as determined from the E_g values of the *in situ* UV-vis-NIR DRS measurements has already been discussed in the introduction of this chapter and the results are reproduced for the samples used in the current study in Figure 1 as a function of TiO₂ loading.

3.2 Photoluminescence Properties: Peak Emission and Decay

The photoluminescence maps in Figure 2 display the emission data for a representative set of supported TiO₂/SiO₂ catalysts. The red line through the top portion of the map is due to the elastically scattered excitation light (Rayleigh scattering). For each of the maps the peak emission wavelength was determined and found to blue shift, higher energy corresponding to lower nm values, with decreasing TiO₂ loading. This trend is true regardless of the excitation wavelength used to generate the PL emission. The broad shape of the emission over all excitations

wavelengths is attributed to the heterogeneity of the TiO_x nanodomains on the silica support within each photocatalyst.

The decay curves for a representative group of supported $\text{TiO}_2/\text{SiO}_2$ catalysts are presented in Figure 3. The decay curves were measured by acquiring the emission spectra in a relatively narrow spectral range, 514 to 526 nm, followed by integration over this spectral region for every delay time. By closely examining the appearance of the curves, the existence of both “fast” and “slow” components of the decay can qualitatively be observed. The samples with lower TiO_2 loading correspond to samples that have domains containing isolated surface sites or polymeric surface structures and have a steeper or faster initial component of the decay. The decay fit parameters for each of the photocatalysts are given in Table 2. The parameters denoted t_1 and t_2 refer to the decay constants for the “fast” and “slow” decay components, respectively, with A_1 and A_2 referring to the amplitudes of the “fast” and “slow” components, respectively, and the relative amplitudes for each photocatalyst are also reported in Table 2.

The dependence of the decay rate parameters t_1 and t_2 on TiO_2 loading is plotted in Figure 4a. The decay constant of the fast component (t_1) does not change significantly and remains almost constant over the whole concentration range. The slow decay time (t_2) decreases with increasing TiO_2 loading and is longest for the lowest titania loading (1% $\text{TiO}_2/\text{SiO}_2$). The relative amplitudes of these two components depend on the TiO_2 loading of the supported $\text{TiO}_2/\text{SiO}_2$ catalysts as shown in Figure 4b. The relative amplitude of the fast component decreases

monotonically as the TiO₂ loading increases. The opposite trend is observed for the slow component and the pure TiO₂ sample displays the largest contribution from the slow component of the decay. At low concentrations of TiO₂/SiO₂ (1-12% TiO₂), the PL decay can be characterized by two components with approximately equal amplitudes and significantly different lifetimes (Fig 4a and 4b).

It is important to note that the PL decay measurements were obtained in the diffuse-reflectance mode for powder samples. Slight differences in the objective height and sample surface can lead to changes in the intensity of PL detected during the experiment. It is, therefore, not possible to quantify these data so that the difference in total excited electrons for the various supported TiO₂/SiO₂ samples can be precisely determined. However, the relative amplitudes of the fast and slow components are quantities that can be applied to other systems with a known number of excitons.

3.3 Photocatalytic Splitting of Water to Produce H₂

The overall activity for H₂ production during photocatalytic splitting of H₂O over 5h (units of μmol H₂/g catalyst/h) for the supported TiO₂/SiO₂ catalysts as a function of TiO₂ loading is presented in Figure 5. The production of H₂ increases monotonically from 1% to 60% TiO₂/SiO₂ by factor of nearly 10 and further increases by another factor of ~7 from 60% TiO₂/SiO₂ to pure TiO₂. Normalized activity of the H₂ production rate for each catalyst was determined by normalizing the rate both by the total mass of Ti and by the number of exposed Ti sites and are presented in Figure 6.

The number of exposed Ti sites was calculated by first estimating the dispersion from the known average domain size (Table 1) and by assuming a spherical domain

shape.³⁰ The calculation of exposed sites is detailed in the supporting information of this chapter and the number of exposed Ti sites for each TiO₂ nanodomain-containing sample is summarized in Table S1. A discussion of the assumption that the nanodomains all have spherical particle shape can also be found in the supporting information. The activity normalized by exposed Ti sites (Figure 6b) will be referred to as the specific activity and more closely mirrors that of the overall activity for H₂ production per mass of catalyst (Figure 5).

4. Discussion

4.1 Relationships between TiO₂ nanodomain structure, photoluminescence decay, and UV-vis edge energy (E_g).

As already indicated (see Table 1), the TiO₂ nanodomain structure is dependent on titania loading on SiO₂ and varies from isolated polymeric surface species (~0.4 – 1 nm), TiO₂ (anatase) rafts (2 – 5 nm) and 3D TiO₂ (anatase) NPs (~5 – 11 nm), while unsupported TiO₂ (anatase) employed in this study has a domain size of ~25 nm. The UV-vis bandgap or edge energy of a semiconductor material is dependent on the domain size^{15,19} and the photoluminescence is related to the band gap of a semiconductor oxide material.²⁶ Consequently, the photoluminescence characteristics of TiO₂ domains are also hypothesized to be related to the titania domain size.

4.1.1 Effect of TiO₂ nanodomain structure on photoluminescence lifetimes.

The qualitative observation of “fast” and “slow” PL decay components in photoluminescence response curves in Figure 3 led to the use of a double first-order

(biexponential) model to fit the response curves. Quickenden *et al.* have suggested that the simplest phenomenological explanation for bimolecular modeling of the decay of luminescence is that two excited species are decaying back to their ground states independently of one another.³¹ This scenario is applicable to the supported TiO₂/SiO₂ photocatalysts since in some cases more than one type of TiO₂ nanodomain can be found on the SiO₂ support for the same sample. Furthermore, the support itself could also be part of an excited species undergoing decay and this possibility will subsequently be addressed below.

The excitons, i.e. electrons and holes (e⁻ and h⁺, respectively), may also decay with different kinetics. Another benefit of the biexponential model is that further analysis of the two components can yield insight into the recombination dynamics of e⁻/h⁺ pairs that are dominant in a particular domain size.³¹⁻³⁵ The fast component of decay is attributable to recombination by multiexcitons. Multiexciton recombination kinetics are relatively fast (10-100 ps) and are characterized by e⁻/h⁺ annihilation caused by Coulomb interaction (Auger-like effect). The slow component of decay is attributable to single exciton recombination kinetics. Single exciton recombination occurs relatively slowly (10-100 ns) and is characterized by simple relaxation of a photo-excited electron to its ground state. It is believed that the multiexciton kinetics readily occur in materials exhibiting charge multiplication that occurs when more than one electron and hole are generated after absorption of a single photon.³⁵ The current data does not allow confirmation of whether the charge multiplication phenomenon is responsible for the fast component found for the TiO₂/SiO₂ catalysts. The time scale of

the fast component, however, is indicative of e^-/h^+ annihilation rather than relaxation to the ground state.

The fast and slow components of PL decay for the titania nanodomains, tabulated in Table 2, have t_1 and t_2 parameters on the time scale of single exciton and multiexciton recombination kinetics, respectively. Furthermore, the relative contribution of the fast and slow components indicate that the slow component becomes more prevalent with increasing titania domain size on the silica support and is most significant in the pure TiO_2 sample (Figure 4b).

4.1.2 Comparison of photoluminescence properties and UV-vis Edge Energy (E_g)

The photoluminescence maps in Figure 2 agree with the previous UV-vis-NIR data showing that the optical edge energy values of the TiO_2 domains increase as the domain size decreases (Figure 1), thus, illustrating the complementary nature of the two optical spectroscopic techniques. For example, the largest E_g value found from the UV-vis-NIR data corresponds to the supported 1% $\text{TiO}_2/\text{SiO}_2$ photocatalyst sample, which consists of isolated surface TiO_4 domains. This high E_g value is manifested in the corresponding blue-shifted PL emission spectrum map of the same catalyst. A higher E_g value requires that the excitation photon is of a higher energy to be able to excite the electrons in the material from the valence band to the conduction band. Subsequently, the observed emission is also of a higher energy when the electrons relax to their ground state in higher E_g materials. This result is not

unexpected given that both techniques are intimately connected to the E_g of a semiconductor oxide material.²⁶

It should also be noted that the maps were obtained *in situ* after dehydration at 400 °C. This is important as it has been shown that reactant molecules will induce quenching of the PL signal.²⁸ The ability to perform these experiments *in situ* allows the researcher control over the state of the surface of the catalyst and, in this case, to specifically focus on the initial formation of e^-/h^+ pairs. The PL maps of the photocatalysts also served as a guide for choosing an excitation wavelength for emission decay experiments. Though not the optimal excitation wavelength for all the samples, 400 nm light was chosen during the excitation lifetime measurements as it would provide sufficient energy for excitation of all the titania domains. The dependence of excitation wavelength on activity, though important, is outside of the scope of the current study.

4.2 Effect of TiO₂ Nanodomain Structure on Photocatalytic Water Splitting Specific Activity.

It is desirable to couple the quantitative structural properties with photocatalytic activity rate data to form structure-activity relationships. This kind of relationship is important as it allows one to make critical decisions when designing a photocatalyst to maximize water splitting activity.³⁶ The plot of specific photocatalytic activity as a function of TiO₂ loading in Figure 6b establishes a *structure-activity relationship* for photocatalytic H₂O splitting on supported TiO_x nanodomains with increasing nanodomain size responsible for higher photocatalytic water splitting specific activity.

Since the loading of titania on the silica support is directly related to the nanodomain size, the structure-activity relationship can be made clearer by plotting specific activity as a function of average domain size (Figure 7). The trend in Figure 8 mirrors that of Figure 6b because the weight percent loading directly affects the size of the nanodomains in the SiO₂ support.

The high activity of pure TiO₂ with a particle size of ~24 nm is a finding of interest because it is largely believed that larger crystalline structures likely contain a greater number of defects that act as recombination centers which are detrimental to photocatalytic activity.²² If, however, the crystal is of high quality, i.e. containing a low number of defects, the increased crystallinity of the higher loading samples would be beneficial. The effect of particle size can be explained by examining the second step of the water splitting reaction (separation of photo-generated e⁻/h⁺ pairs and their migration to the surface catalytic sites). The benefit of a smaller particle size is that it yields a shorter distance for holes and electrons to migrate to surface active sites decreasing the probability of recombination.²² In the case of water splitting on TiO₂ nanodomains, the size effect on recombination of e⁻/h⁺ pairs is negligible in determining the overall best catalyst as pure TiO₂, rather it is the increasing amount of bulk, high crystallinity TiO₂ that is the better indicator of high specific activity.

Theory can give further insight as to why the bulk TiO₂ catalyst is preferred to the supported TiO₂ domains. In a density functional theory (DFT) study of the photo-oxidation of water on TiO₂ surfaces by Valdés *et al.* it was found that a TiO₂ surface containing oxygen in coordinatively unsaturated sites is the most stable.³⁷ This

surface yielded the lowest energetics for the water oxidation reaction. Furthermore, it found that while a pathway for water oxidation via breaking of a Ti-O-Ti bond was possible, the barrier was much too high for it to be favored. In the current study the catalysts containing 3D TiO₂ (anatase) NPs will have surfaces with the highest concentration of coordinatively unsaturated sites relative to Ti-O-Ti sites. As the loading is decreased, and especially in the case of polymeric domains, the relative amount of inactive Ti-O-Ti sites increases. This is an indication that despite the importance of the generating electrons and holes, the surface reaction is rate-determining for water splitting on TiO₂ nanodomains. Indeed, Valdés *et al.* find that the formation of hydroxyl groups at the coordinatively unsaturated TiO₂ sites is the rate-determining-step. This does not the ~7 times greater activity of the pure TiO₂ (anatase) NPs (24 nm) over the supported 60% TiO₂/SiO₂ catalyst containing 11 nm TiO₂ (anatase) NPs. This difference suggests that the support could lead to the inactivity of trapped electrons and holes associated with the SiO₂ support and analysis of PL decay will help to determine if this is indeed the case.

4.3 Effect of Photoluminescence Decay Components on Specific Activity

Recalling that the PL lifetime of the photocatalyst sample is directly related to the nanodomain structure (Figure 4a), it is logical to examine the specific photocatalytic activity as a function of PL lifetime. Using the slow decay time t_2 as an indicator of overall PL lifetime, this plot can be seen in Figure 8. Despite having the highest value of t_2 , the supported 1% TiO₂/SiO₂ catalyst has a specific activity lower than those samples containing TiO₂ (anatase) nanoparticles and pure TiO₂ is 10 times more

active. Thus, the plot of specific activity as a function of PL lifetime in Figure 8 fails to establish an electronic structure-activity relationship because the slow component decay rate is less significant as loading decreases (see Figure 4b). Though t_2 can be considered an indication of the overall lifetime of excited e^-/h^+ ,²⁷ it is not always significant for a particular catalyst. This is especially true given that the multiexciton recombination kinetics occur on a timescale several orders of magnitude less than the timescale of the surface reaction (100 ps compared to >100 ns).²⁴ Therefore, the relative contribution of the slow component is predicted to be a better indication of photocatalytic activity.

The apparent contradiction in Figure 8 is rectified by considering the origin and the relative contribution of the fast and the slow components of decay. As stated earlier, the origin of the two components of decay is believed to be from multiexciton and single exciton recombination kinetics, respectively.³²⁻³⁵ Figure 4b shows that the relative contribution of the fast component is highest for the supported 1% TiO₂/SiO₂ photocatalyst and that the relative contribution of the slow component is highest for pure TiO₂. This means that the majority of recombinations are occurring with relatively fast kinetics for the isolated TiO₄ domains. Conversely, the majority of recombinations in the pure TiO₂ occur with relatively slow kinetics. The exact total number of excited electrons in each supported TiO₂/SiO₂ sample is unknown, but it can be assumed that a greater quantity of electrons will be excited for catalysts with a greater quantity of Ti sites. The generation of electrons is related to the first step of the photocatalytic process:



Therefore, if a greater percentage of the total Ti sites produce electrons that decay with slow kinetics it is a benefit for photocatalytic activity as a greater number of e^-/h^+ pairs have the opportunity to migrate to surface sites to split water.

The relative contribution of the components of decay allows for the semi-quantitative determination of the number of Ti sites that, upon absorption of a photon, generate excitons that decay with fast or slow kinetics. Though it not likely that each individual Ti site in a given supported TiO_2/SiO_2 catalyst produces excitons under reactions conditions, it can be assumed that those that do produce excitons will exhibit recombination kinetics related to the contribution of the fast and slow components of decay. Therefore, multiplying the total number of Ti sites by the relative contribution of the fast and slow component will yield the number of Ti sites that generate excitons that decay with fast and slow kinetics, respectively. The basis for invoking this relationship is that photons with UV wavelengths will be absorbed throughout the entirety of the TiO_x nanodomain sizes found in this study because it has been shown that the absorption coefficient for TiO_2 coatings up to 2 μm thick is still significant at wavelengths $< \sim 410$ nm.³⁸ The cumulative absorbed photon flux, however, is directly related to the depth and cross sectional area of the particle.³⁸ It follows that larger TiO_2 (anatase) NPs, with their higher average size and larger cross sectional area, will cumulatively absorb more photons at Ti sites in at the surface *and* bulk of the catalysts particle. Thus, the larger bulk of the TiO_2 NPs (> 11 nm) can be viewed as a reservoir of photon-absorbing Ti sites that generate excitons.

The number of Ti sites, N_s , is calculated from the mass of the supported $\text{TiO}_2/\text{SiO}_2$ catalyst used in the batch photo-reactor experiments. The results of this calculation are summarized in Figure 9. The number of Ti sites that produce electrons with slow recombination kinetics increases monotonically with wt% loading of TiO_2 , whereas the number of Ti sites that produce electrons with fast kinetics increases until TiO_2 (anatase) NPs are formed and then becomes independent of particle size. The high number of slow recombinations is likely related to the existence of a more significant bulk structure as particle size increases.

The effect of having a large number of Ti sites having slow recombination kinetics can be seen in Figure 10a, which exhibits a strong correlation between this property and the specific activity. The slow decay of excited electrons yields a greater opportunity to do photocatalytic water splitting at the surface active sites. This conclusion is supported by Figure 10b, which shows that there is no correlation between specific activity and the number of Ti sites producing electrons with fast recombination kinetics. Given the fast recombination occur on the time scale of 0-100 ps, this lack of correlation is to be expected, since the surface reaction occurs on a time scale several orders of magnitude slower. Electrons and holes that decay with fast kinetics are very unlikely to participate in surface photocatalytic reactions.

Another reason that the isolated TiO_4 sites in the supported 1% $\text{TiO}_2/\text{SiO}_2$ catalyst show low activity despite having a slower rate of decay may have to do with the SiO_2 support. Table 2 shows the decay component analysis for the pure SiO_2 support. The SiO_2 actually has the slowest decay rate and a strong contribution from the slow

component of decay. The pure SiO₂ support, however, shows negligible production of H₂ (~1 μmol of H₂ over 5h) under the same reaction conditions used to test the TiO₂ nanodomains. It is believed that the SiO₂ is contributing this slow decay rate to the smaller TiO₂ domains, however, the trap states are inactive for water splitting, indicating the electrons and holes are unavailable to perform the surface reactions. The low loading samples, especially 1 and 12% with isolated and polymeric domains, respectively, contain a larger percentage of exposed metal-support Ti-O-Si bonds. Trapping charges at the silica hydroxyls at Ti-O-Si interfacial sites could result in increase of the separation distance between electrons and holes that in turn slows down their recombination, but this does not necessitate that these electrons and holes are active as they may not be found at active surface sites.

The structure-activity relationship, when combined with the relationship between specific activity and contribution of slow decay has determined that the reason for high activity on large TiO₂ (anatase) nanoparticles is three-fold. First, the increased crystallinity of large NPs deters rapid recombination of electrons and is manifested in the large contribution of slow decaying excitons in the largest NPs found on pure TiO₂. The bulk large bulk structural contribution acts as a reservoir for these excitons. Second, the catalysts containing 3D NP domain structures have relatively fewer Ti-O-Ti sites that are inactive according to DFT calculations. Finally, the effect of trap states on the SiO₂ support further explains the low activity of the isolated TiO₄ and polymeric TiO₅ and gives a possible reason for the lower activity of 11 nm TiO₂ (anatase) NPs compared to 24 nm TiO₂ (anatase) NPs.

4.4 Surface and Bulk Considerations

Although electrons and holes can be generated throughout the bulk of a semiconductor photocatalyst, the water splitting reaction can only occur at surface active sites. For example, comparing the activity normalized by the mass of Ti ($\mu\text{mol H}_2/\text{g Ti/hr}$) in Figure 6a to the specific activity ($\mu\text{mol H}_2/\text{exposed Ti site/hr}$) in Figure 7 illustrates one of the most basic principles of catalysis science: barring any surface reconstruction, metal atoms that are not on the surface cannot active as active sites for adsorption. The high activity of the isolated TiO_4 site in the activity plot of Figure 5 gives evidence that the surface reaction does not involve the bulk and that specific activity is a more accurate representation of the structure-activity relationship that exists for water splitting over TiO_2 nanodomains. Therefore it is reasonable to question the usefulness of employing bulk techniques such as PL spectroscopy or UV-vis-NIR spectroscopy to find structure activity relationships.

If specific activity for H_2 production during water splitting for the supported $\text{TiO}_2/\text{SiO}_2$ samples is plotted as a function of their corresponding E_g values from UV-vis DRS measurements, a clear correlation does not result as shown in Figure 11. The lack of any relationship is because catalysts with as little as 40% loading of TiO_2 already contain nanocrystals that exhibit the same E_g value as bulk TiO_2 . Although UV-vis DRS is useful in determining if a material has a bandgap sufficient to perform photocatalysis under certain wavelengths of light, the bulk E_g value is not an indication of the specific photoactivity of a semiconductor oxide material.

It was already shown that the relationship between specific activity and decay rate in Figure 8 does not hold for the hypothesis that a slow decay rate will yield a longer lifetime. Once again, PL spectroscopy is a bulk technique, so it is tempting to argue that based on the lack correlation that PL spectroscopy does not offer useful insight into photocatalytic water splitting. However, unlike the E_g values of UV-vis DRS, PL spectra yield information on the kinetics of electron and hole formation. The importance of having a bulk structure in the generation of a large number of electrons and holes is reflected in Figure 9 illustrating the strong relationship between slow PL decay and large titania domain size. More specifically, a good photocatalyst must generate a large number of electrons and holes that recombine with slow kinetics. Figure 10 shows that for photocatalytic water splitting on TiO_2 nanodomains, there is a strong relationship between specific activity and the number of Ti sites generating electrons with slow recombination kinetics. The slow recombinations are on a time scale that indicates that the kinetics are characterized by single exciton relaxation (10-100 ns). While PL spectroscopy cannot discriminate between e^-/h^+ pairs that recombine in the bulk and e^-/h^+ pairs that migrate to the surface and become available to do surface chemistry, it can give an indication that certain domains promote a greater opportunity for this to occur via slower recombination kinetics. The correlation in Figure 10 supports this electronic structure-activity relationship.

The affect of TiO_x structure on other photocatalytic reactions has also been studied in the literature and it is useful to compare the structure-photoactivity relationships. It has been proposed by that a single site tetrahedral TiO_4 titanium oxide species

incorporated in a zeolite framework has a relatively high activity in the reduction of CO₂ with H₂O and the decomposition of NO into N₂ and O₂.^{11,39} It has been shown by Yang *et al.* that carbon residue in the reactor during CO₂ photo-reduction with H₂O can lead to false positive results for the activity of this reaction.⁴⁰ Therefore, it is unclear whether the TiO₄ site is truly active and the current work finds the opposite to be true for water splitting. Also, Carneiro *et al.* have studied the effect of TiO₂ (anatase) hydroxyl concentration and particle size for cyclohexane photo-oxidation and found that a high concentration of surface hydroxyls on small particle sizes TiO₂ (anatase) due to their higher surface area was beneficial to cyclohexanone activity, but large particles were more efficient at desorbing cyclohexanone.⁴¹ Because the activity of photocatalytic reactions depends on an interplay of many factors, i.e. crystal phase (anatase or rutile), quality of the crystal structure (number of defects), catalyst surface area, and the density of surface hydroxyl groups, and the importance of these factors likely varies among different photocatalytic reactions, it is difficult to determine exactly why water splitting activity favors the large bulk structure of supported TiO₂ nanodomains. If the support indeed plays a role trapping electrons at inactive Si-OH as indicated above, then it could be that the larger domains have a high active surface hydroxyl concentration. However, if the water splitting is severely desorption limited, similar to cyclohexanone photo-oxidation, the large particles and the reservoir of long lived excitons in the bulk structure would be a significant contributor to the higher activity.

5. Conclusions

An investigation into the existence of a structure-photoactivity relationship for photocatalytic water splitting on well-defined TiO₂ nanodomains was performed. The trend in H₂ production for the nanodomains proceeded as: pure TiO₂ (anatase) (24 nm) > TiO₂ nanoparticles (4-11 nm) > polymeric TiO₅ (~1 nm) > isolated TiO₄ (~0.4 nm). Photoluminescence spectroscopy showed that, like UV-vis-NIR E_g values, there is a distinct difference in electronic structure between the nanodomains that is manifested in the degree to which electrons and holes recombine with slow kinetics. The high activity of the pure TiO₂ is attributed its significant bulk structure which acts as a reservoir for the generation of a greater number of electrons with slow recombination kinetics as well as its larger concentration of active exposed Ti sites. Bulk techniques such as UV-vis DRS and PL spectroscopy are useful in obtaining information about electronic structure, UV-vis DRS edge energy, however is not related to specific photoactivity. PL spectroscopy can yield useful surface information because a slow rate of recombination allows a greater opportunity for excitons to migrate to surface active sites.

While the current study did not yield a new superior water splitting material, the benefits of such a fundamental study should not be ignored. In attempting to determine a structure-activity relationship for photocatalytic H₂O splitting over various TiO_x nanodomains, the study was successful. Of course, it is quite obvious from the literature that TiO₂-based materials are not the best for water-splitting, but the current well-defined model photocatalysts were employed to provide insight into

the fundamental structure effects on photocatalytic activity. If the relationship found here holds true for doped TiO₂ based catalysts or other novel metal oxide catalysts, rational design of improved photocatalysts can be achieved.

Acknowledgements:

This research was financially supported by Department of Energy-Basic Energy Sciences grant DE-FG02-93ER14350. Research was conducted at the Center for Nanophase Materials Sciences, which is sponsored at Oak Ridge National Laboratory by the Division of Scientific User Facilities, U.S. Department of Energy and in conjunction with User Project CNMS2008-075. Somphonh P. Phivilay of Lehigh University and Naoyuki Sakamoto, Dr. Kazuhiko Maeda, and Dr. Kazunari Domen at the University of Tokyo are thanked for assistance in obtaining the water splitting photoactivity data.

References

- (1) Fujishima, A.; Honda, K. "Electrochemical photolysis of water at a semiconductor electrode," *Nature* **1972**, 238, 37-38.
- (2) Service, R.F. "Hydrogen Economy? Let Sunlight Do the Work," *Science*, **2007**, 315, 789.
- (3) Irie, H.; Miura, S.; Kamiya, K.; Hashimoto, K. "Efficient visible light-sensitive photocatalysts: Grafting Cu(II) ions onto TiO₂ and WO₃ photocatalysts," *Chem. Phys. Lett.* **2008**, 457, 202-205.
- (4) Serpone, N.; Lawless, D.; Khairutdinov, R.; Pelizzetti, E. "Subnanosecond Relaxation Dynamics in TiO₂ Colloidal Sols (Particle Sizes R_p = 1.0-13.4 nm). Relevance to Heterogeneous Catalysis," *J. Phys. Chem.* **1995**, 99, 16655-16661.
- (5) Mills, A.; Davies, R. H.; Worsley, D. "Water purification by semiconductor photocatalysis," *Chem. Soc. Rev.* **1993**, 22, 417-425.
- (6) Linsebigler, A. L.; Lu, G.; Yates, J. T. Jr., "Photocatalysis on TiO₂ Surfaces: Principles, Mechanism, and Selected Results," *Chem. Rev.* **1995**, 95, 735-758.
- (7) Herrmann, J. M. "Heterogeneous photocatalysis: fundamentals and applications to the removal of various types of aqueous pollutants," *Catal. Today* **1999**, 53, 115-129.
- (8) Alfano, O. M.; Bahnemann, D.; Cassano, A. E.; Dillert, R.; Goslich, R. "Photocatalysis in water environments using artificial and solar light," *Catal. Today* **2000**, 58, 199-230.

- (9) Nishijima, K.; Ohtani, B.; Yan, X.; Kamai, T.; Chiyoya, T.; Tsubota, T.; Murakami, N.; Ohno, T. "Incident light dependence for photocatalytic degradation of acetaldehyde and acetic acid on S-doped and N-doped TiO₂ photocatalysts," *Chem. Phys.* **2007**, 339, 64-72.
- (10) Abe, R.; Kazuhiro, S.; Domen, K.; Arakawa, H. "A new type of water splitting system composed of two different TiO₂ photocatalysts (anatase, rutile) and a IO₃⁻/I⁻ shuttle redox mediator," *Chem. Phys. Lett.* **2001**, 344, 339-344.
- (11) Anpo, M.; Takeuchi, M. "The design and development of highly reactive titanium oxide photocatalysts operating under visible light irradiation," *J. Catal.* **2003**, 216, 505-516.
- (12) Kudo, A.; Kato, H.; Tsuji, I. "Strategies for the Development of Visible-light-driven Photocatalysts for Water Splitting," *Chem. Lett.* **2004**, 33, 1534-1539.
- (13) Usseglio, S.; Damin, A.; Scarano, D.; Bordiga, S.; Zecchina, A.; Lamberti, C. "(I₂)_n Encapsulation inside TiO₂: A Way to Tune Photoactivity in the Visible Region," *J. Am. Chem. Soc.* **2007**, 129, 2822-2828.
- (14) Deo, G.; Andrzej, M.; Wachs, I. E.; Huybrechts, D. R. C.; Jacobs, P. A. "Characterization of titania silicalites," *Zeolites*, **1993**, 13, 365-373.
- (15) Gao, X.; Bare, S.R.; Fierro, J. L. G.; Banares, M. A.; and Wachs, I. E. "Preparation and in-Situ Spectroscopic Characterization of Molecularly Dispersed Titanium Oxide on Silica," *J. Phys. Chem. B* **1998**, 102, 5653-5666.

- (16) Lee, E. L.; Wachs, I. E. "Molecular Design and In Situ Spectroscopic Investigation of Multilayered Supported M1Ox/M2Ox/SiO2 Catalysts," *J. Phys. Chem. C*, **2008**, 112, 20418-20428.
- (17) Gao, X.; Wachs, I. E. "Titania-silica as catalysts: molecular structural characteristics and physico-chemical properties," *Catal. Today* **1999**, 51, 233-254.
- (18) Weber, R. S. "Effect of Local Structure on the UV-Visible Absorption Edges of Molybdenum Oxide Clusters and Supported Molybdenum Oxides," *J. Catal.* **1995**, 151, 470-474.
- (19) Ross-Medgaarden, E. I.; Wachs, I. E.; Knowles, W. V.; Burrows, A.; Kiely, C. J.; Wong, M. S. "Tuning the Electronic and Molecular Structures of Catalytic Active Sites with Titania Nanoligands," *J. Am. Chem. Soc.* **2009**, 131, 680-687.
- (20) Maeda, K.; Domen, K. "New Non-Oxide Photocatalysts Designed for Overall Water Splitting under Visible Light," *J. Phys. Chem. C* **2007**, 111, 7851-7861.
- (21) Osterloh, F. E.; "Inorganic Materials as Catalysts for Photochemical Splitting of Water," *Chem. Mater.* **2008**, 20, 35-54.
- (22) Kudo, A.; Miseki, Y.; "Heterogeneous Materials for Water Splitting," *Chem. Soc. Rev.* **2009**, 38, 253-278.
- (23) Miller, E. L.; Marsen, B.; Paluselli, D. Rocheleau, R. "Optimization of Hybrid Photoelectrodes for Solar Water-Splitting," *Electrochem. Solid State Lett.* **2005**, 8, A247-A249.
- (24) Mills, A.; Le Hunte, S. "An overview of semiconductor photocatalysis," *J. Photochem. Photobiol. A* **1997**, 108, 1-35.

- (25) Shi, J.; Chen, J.; Feng, Z.; Chen, T.; Lian, Y.; Wang, X.; Li, C. "Photoluminescence Characteristics of TiO₂ and Their Relationship to the Photoassisted Reaction of Water/Methanol Mixture," *J. Phys. Chem. C* **2007**, 111, 693-699.
- (26) Singha, A.; Dhar, P.; Roy, A. "A nondestructive tool for nanomaterials: Raman and photoluminescence spectroscopy," *Am. J. Phys.* **2005**, 73, 224-233.
- (27) Tang, J.; Durrant, J. R.; Klug, D. R. "Mechanism of Photocatalytic Water Splitting in TiO₂. Reaction of Water with Photoholes, Importance of Charge Carrier Dynamics, and Evidence for Four-Hole Chemistry," *J. Am. Chem. Soc.* **2008**, 130, 13885-13891.
- (28) Anpo, M.; Higashimoto, S.; Matsuoka, M.; Zhanpeisov, N.; Shioya, Y.; Stanislaw, D.; Che, M. "The effect of the framework structure on the chemical properties of the vanadium oxide species incorporated within zeolites," *Catal. Today* **2003**, 78, 211-217.
- (29) Selby, B. J.; Quickenden, T. I.; Freeman, C. G. "The Fitting of Luminescence Rises and Decays," *Kinetics and Catalysis* **2003**, 44, 5-15.
- (30) Boudart, M.; Djéga-Mariadassou, G. *Kinetics of Heterogenous Catalytic Reactions*, Princeton University Press, Princeton, NJ, **1984**.
- (31) Quickenden, T. I.; Green, T. A.; Lennon, D. "Luminescence from UV-Irradiated Amorphous H₂O Ice," *J. Phys. Chem.* **1996**, 100, 16801-16807.

(32) McGuire, J. A.; Joo, J.; Pietryga, J. M.; Schaller, R. D.; Klimov, V. I. "New Aspects of Carrier Multiplication in Semiconductor Nanocrystals," *Acc. Chem. Res.* **2008**, 41, 1810-1819.

(33) Shen, Q.; Katayama, K.; Sawada, T.; Toyoda, T. "Characterization of the electron transfer from CdSe quantum dots to nanostructured TiO₂ electrode using a near-field heterodyne transient grating technique," *Thin Solid Films*, **2008**, 516, 5927-5930.

(34) Trinh, M. T.; Houtepen, A. J.; Schins, J. M.; Hanrath, T.; Piris, J.; Knulst, W.; Goossens, A. P. L. M.; Siebbeles, L. D. A. "In Spite of Recent Doubts Carrier Multiplication Does Occur in PbSe Nanocrystals," *Nano Lett.*, **2008**, 8, 1713.

(35) Nair, G.; Chang, L.-Y.; Geyer, S. M.; Bawendi, M. G. "Perspective on the Prospects of a Carrier Multiplication Nanocrystal Solar Cell," *Nano Lett.*, **2011**, 11, 2145-2151.

(36) Wachs, I. E.; Roberts, C. A. "Monitoring surface metal oxide catalytic active sites with Raman spectroscopy," *Chem. Soc. Rev.* **2010**, 39, 5002-5017.

(37) Valdés, A.; Qu, Z.-W.; Kroes, G.-J.; Rossmeisl, J.; Nørskov, J. K. "Oxidation and Photo-Oxidation of Water on TiO₂ Surface," *J. Phys. Chem. C* **2008**, 112, 9872-9879.

(38) Murphy, A. B. "Band-gap determination from diffuse reflectance measurements of semiconductor films, and application to photoelectrochemical water-splitting," *Sol. Energy Mater. Sol. Cells* **2007**, 91, 1326-1337.

(39) Takeuchi, M.; Sakai, S.; Ebrahimi, A.; Matsuoka, M.; Anpo, M. "Application of Highly Functional Ti-Oxide-Based Photocatalysts in Clean Technologies," *Top. Catal.* **2009**, 52, 1651-1659.

(40) Yang, C. -C.; Yu, Y. -H.; van der Linden, B.; Wu, J. C. S.; Mul, G. "Artificial Photosynthesis over Crystalline TiO₂-Based Catalysts: Fact of Fiction?" *J. Am. Chem. Soc.* **2010**, 132, 8396-8406.

(41) Carneiro, J. T.; Almeida, A. R.; Moulijn, J. A.; Mul, G. "Cyclohexane selective photocatalytic oxidation by anatase TiO₂: influence of particle size and crystallinity," *Phys. Chem. Chem. Phys.* **2010**, 12, 2744-2750.

Table 1: Nanodomain structure of TiO_x nanodomains in supported $\text{TiO}_2/\text{SiO}_2$ catalysts as determined by Raman, XANES, and electron microscopy. Generated from data in references 15 and 19.

Catalyst	Structure	Domain Size (nm)
1% $\text{TiO}_2/\text{SiO}_2$	Isolated surface TiO_4 species	~0.4
12% $\text{TiO}_2/\text{SiO}_2$	Polymeric surface TiO_5 species	~1
30% $\text{TiO}_2/\text{SiO}_2$	TiO_2 (anatase) – 2D Rafts	4.0
40% $\text{TiO}_2/\text{SiO}_2$	TiO_2 (anatase) – 2D Rafts	7.0
50% $\text{TiO}_2/\text{SiO}_2$	TiO_2 (anatase) – NPs	9.0
60 $\text{TiO}_2/\text{SiO}_2$	TiO_2 (anatase) – NPs	11
Pure TiO_2	TiO_2 (anatase) – NPs	24

Table 2: Photoluminescence decay fit parameters from Eqn. 1 for supported TiO₂/SiO₂ catalysts.

% TiO₂ Loading	t1 (ps)	t2 (ps)	A1	A2	A1/(A1+A2)	A2/(A1+A2)
	fast	slow	fast	slow	fast	Slow
0	1271	4044	2028	3069	0.40	0.60
1	507	3712	1834	1491	0.55	0.45
8	470	3120	31779	31858	0.50	0.50
12	484	3178	9940	9752	0.50	0.50
15	474	2600	6722	7385	0.48	0.52
30	378	1245	728	1143	0.39	0.61
40	510	2748	554	1733	0.24	0.76
60	180	2802	283	1117	0.20	0.80
100	290	1320	125	1137	0.10	0.90

Figure 1: UV-vis E_g energies vs. x% TiO_2 loading on the SiO_2 support. Domain structure from Raman and XANES are indicated to emphasize electronic structure/structure correlation. Data reproduced for catalysts used in the current study from reference 19.

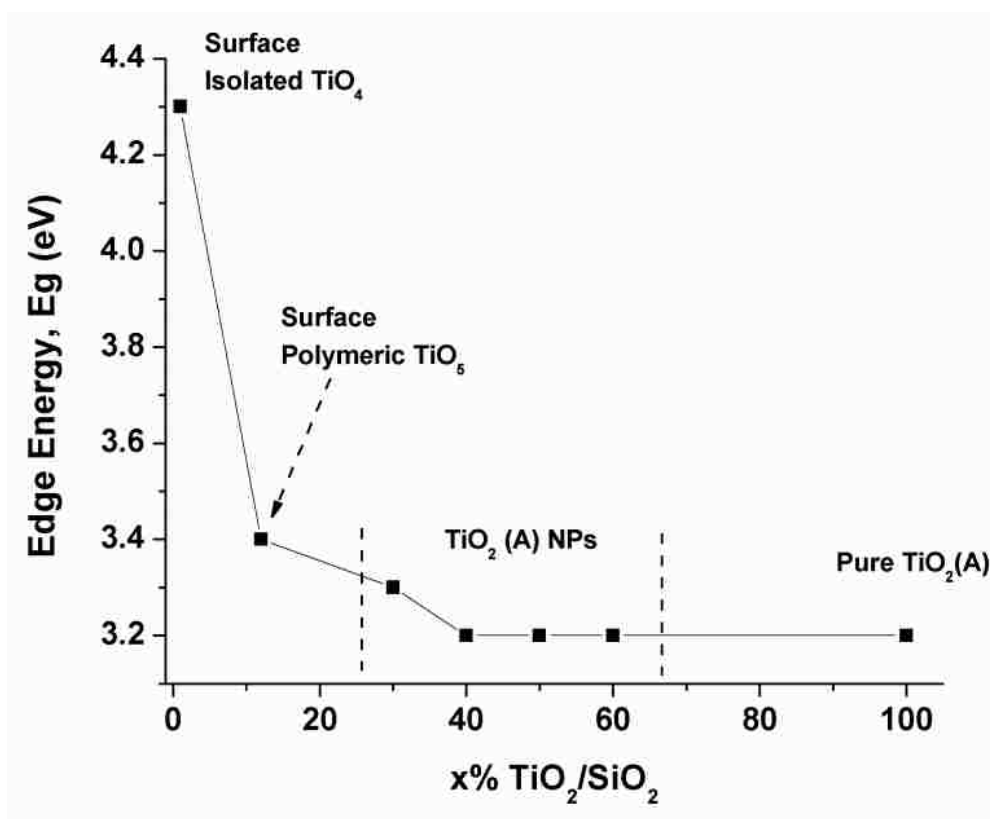


Figure 2: PL spectroscopic wavelength maps for supported (a) 1, (b) 12, (c) 30 and (d) 60% TiO₂/SiO₂ catalysts. The red line towards the top of each figure represents the excitation wavelengths used to create the map and the emission intensity at each wavelength is given immediately below with color coding (red = very strong, yellow = strong, green = medium, light blue = weak and dark blue = very weak). For each map, the maximum intensity PL emission wavelength is labeled.

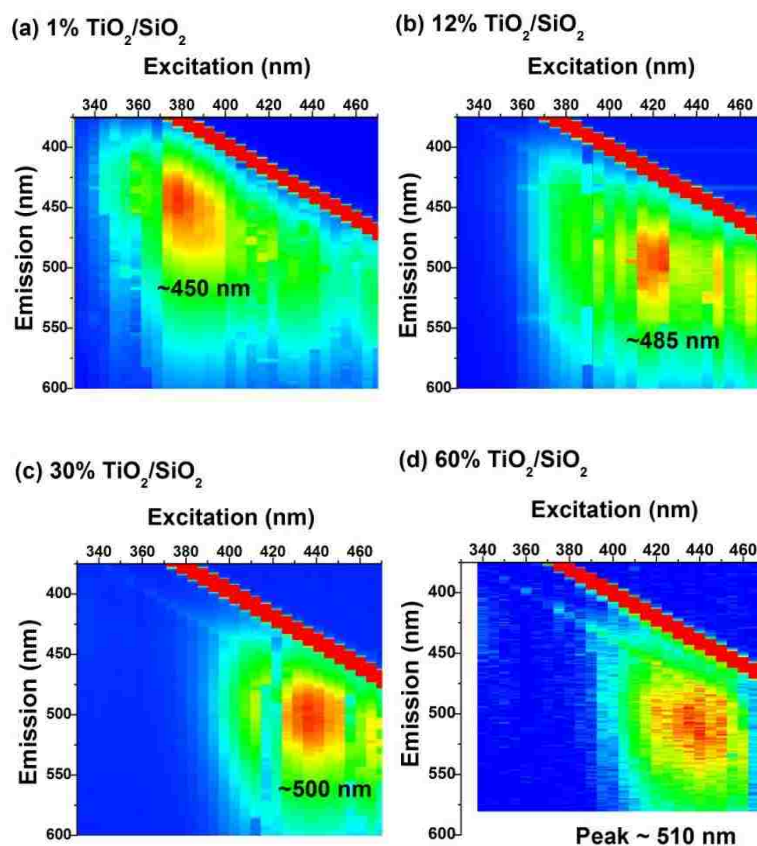


Figure 3: Photoluminescence decay data for a representative set of supported $\text{TiO}_2/\text{SiO}_2$ catalysts.

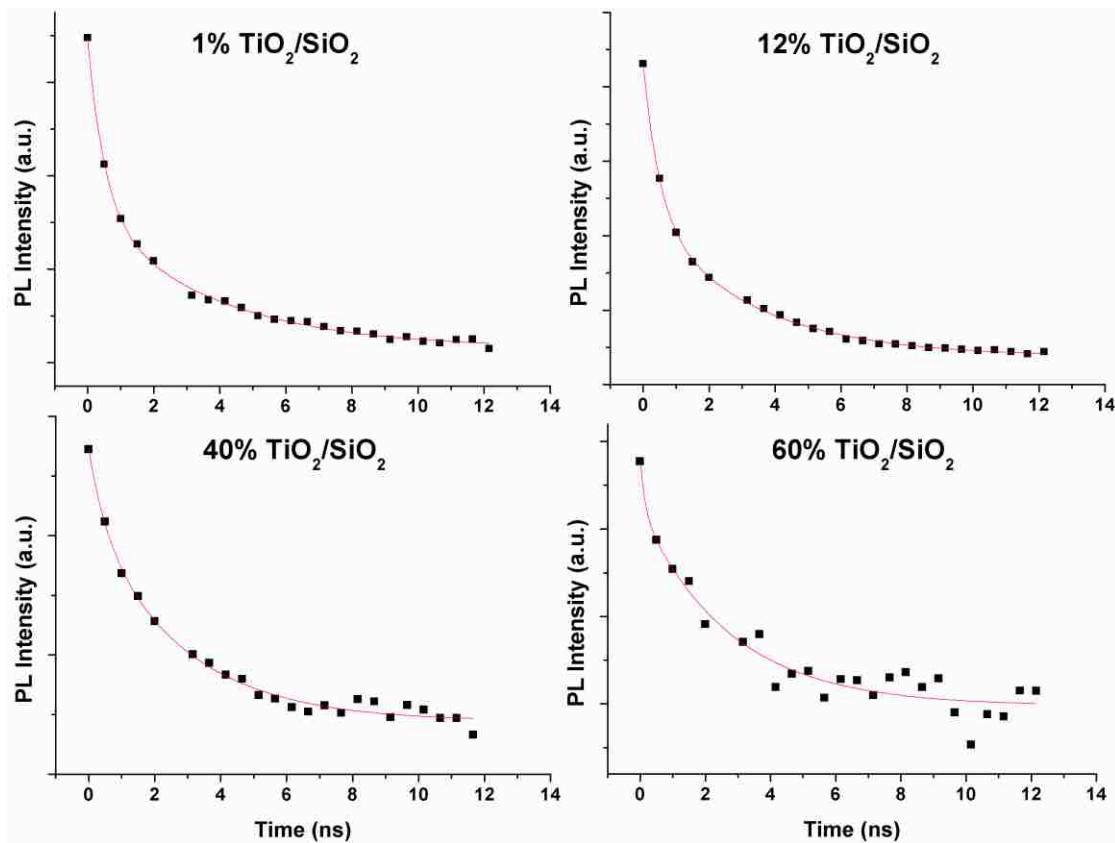


Figure 4: (a) “Fast”, t_1 , and “slow”, t_2 , decay times versus TiO_2 concentration of supported $\text{TiO}_2/\text{SiO}_2$ catalysts. (b) Relative amplitudes of the fast and slow PL decay components as a function of TiO_2 loading for supported $\text{TiO}_2/\text{SiO}_2$ catalysts.

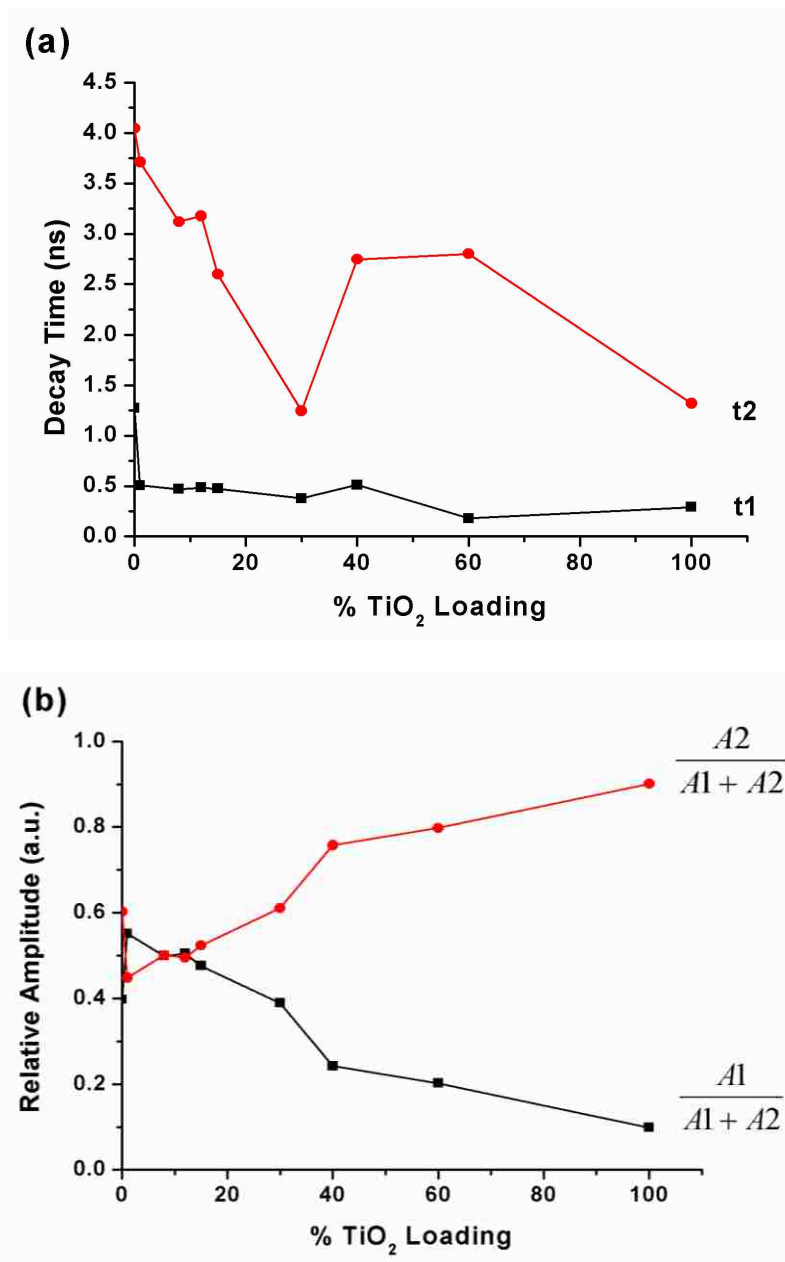


Figure 5: Overall activity for H₂ production in $\mu\text{mol H}_2/\text{g cat/h}$ for water splitting as a function of TiO₂ loading for the supported TiO₂/SiO₂ photocatalysts.

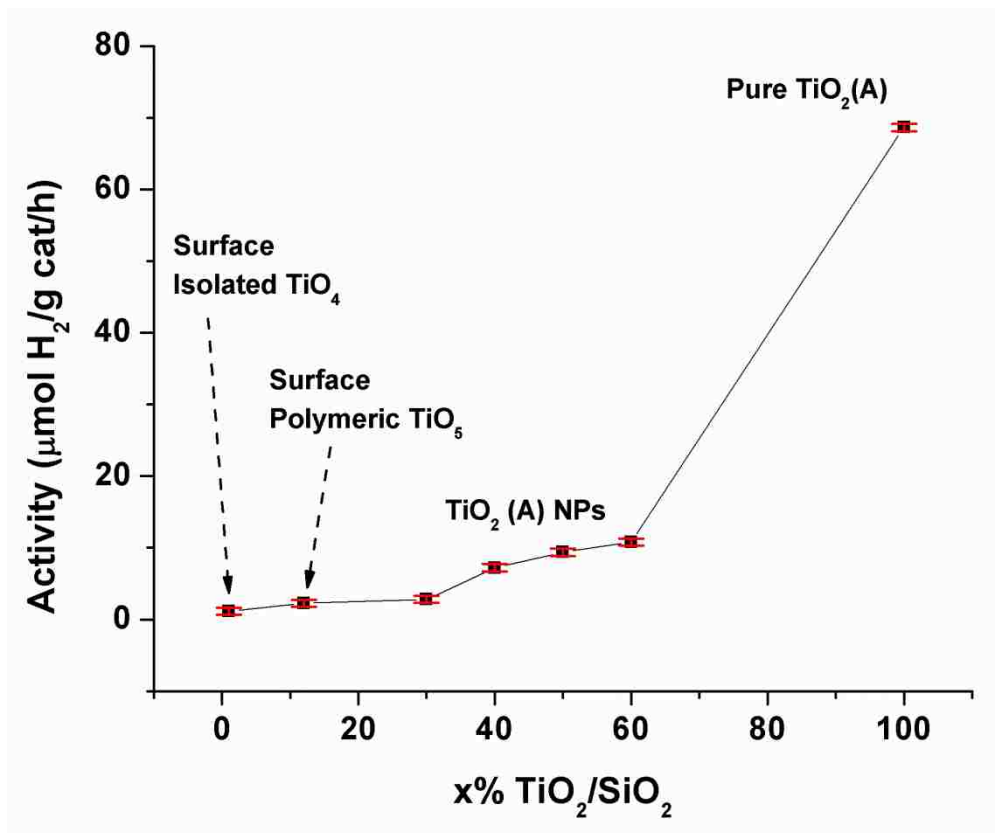


Figure 6: Activity normalized by the (a) mass of Ti ($\mu\text{mol H}_2/\text{g Ti/hr}$) and (b) exposed Ti sites, defined as specific activity ($\mu\text{mol H}_2/\text{exposed Ti site/hr}$), as a function of TiO_2 loading. The domain structure is indicated for reference.

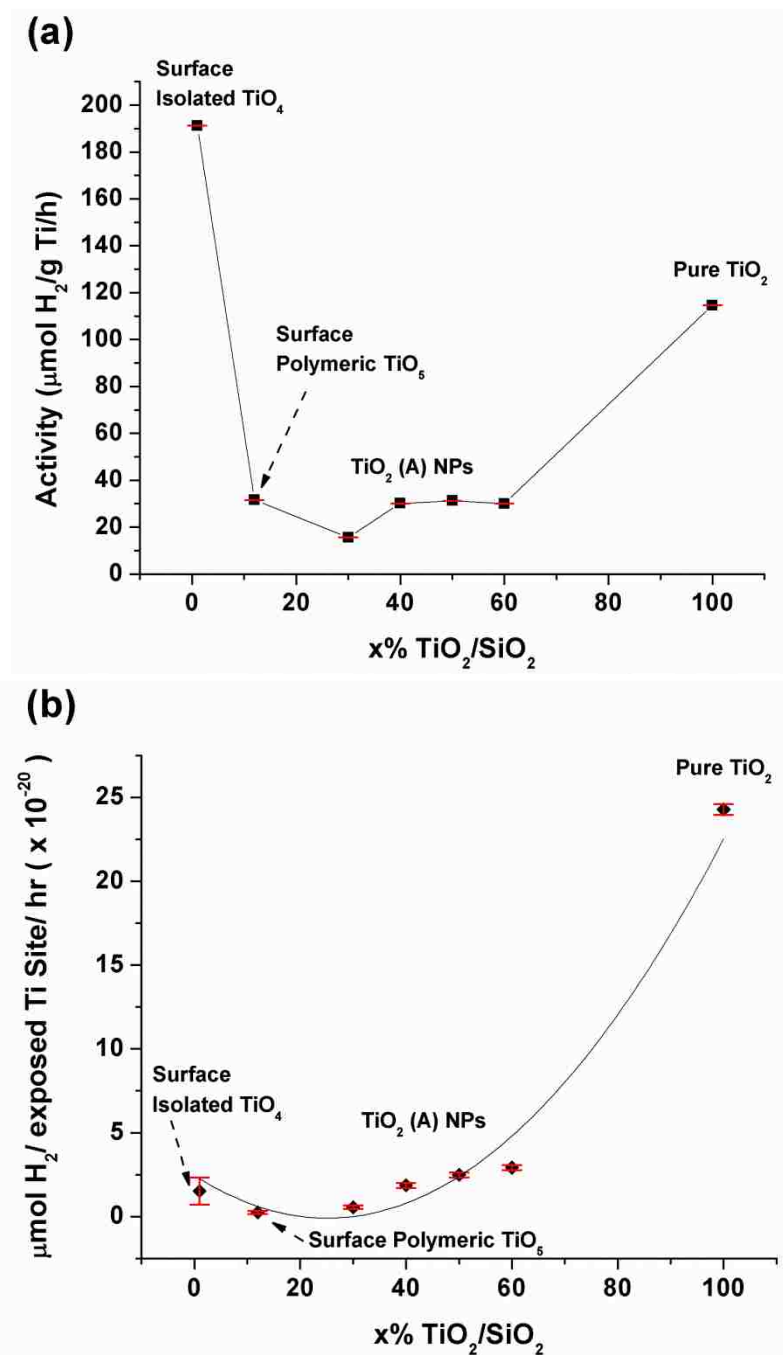


Figure 7: Specific activity ($\mu\text{mol H}_2/\text{exposed Ti site/hr}$) as a function of the average size of the TiO_2 nanodomains in the supported $\text{TiO}_2/\text{SiO}_2$ samples. The domain structure is indicated for reference.

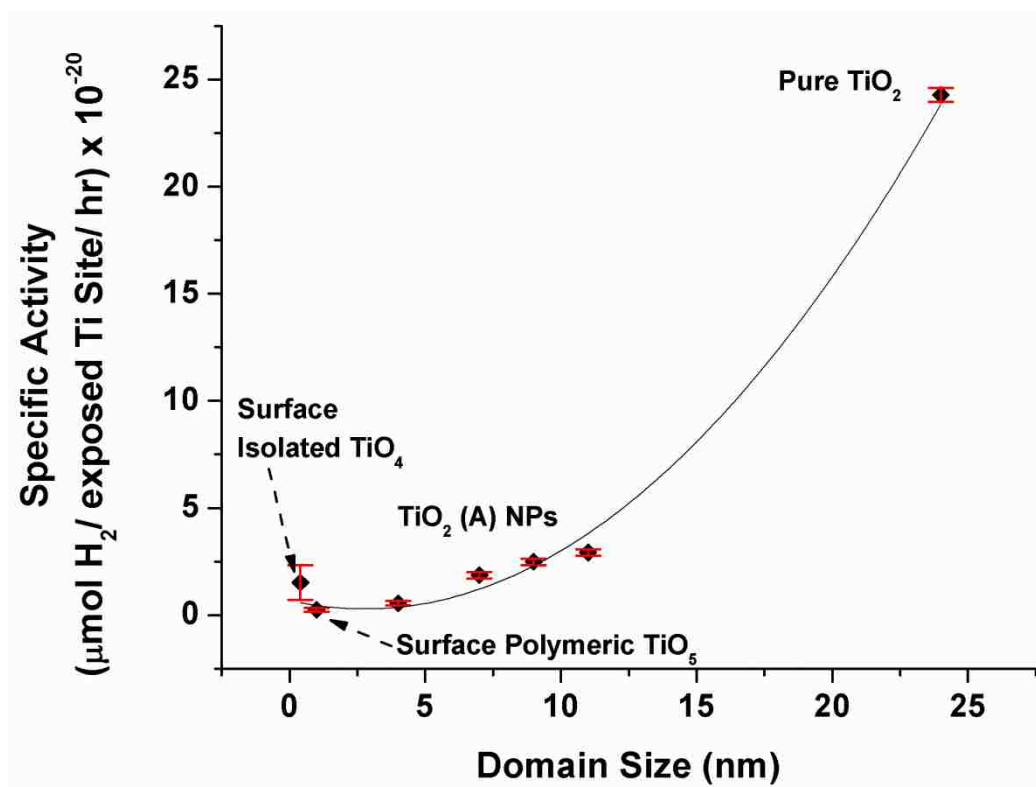


Figure 8: Specific activity during H₂O splitting by supported TiO₂/SiO₂ and pure TiO₂ photocatalysts as a function of the decay time of PL emission (t₂).

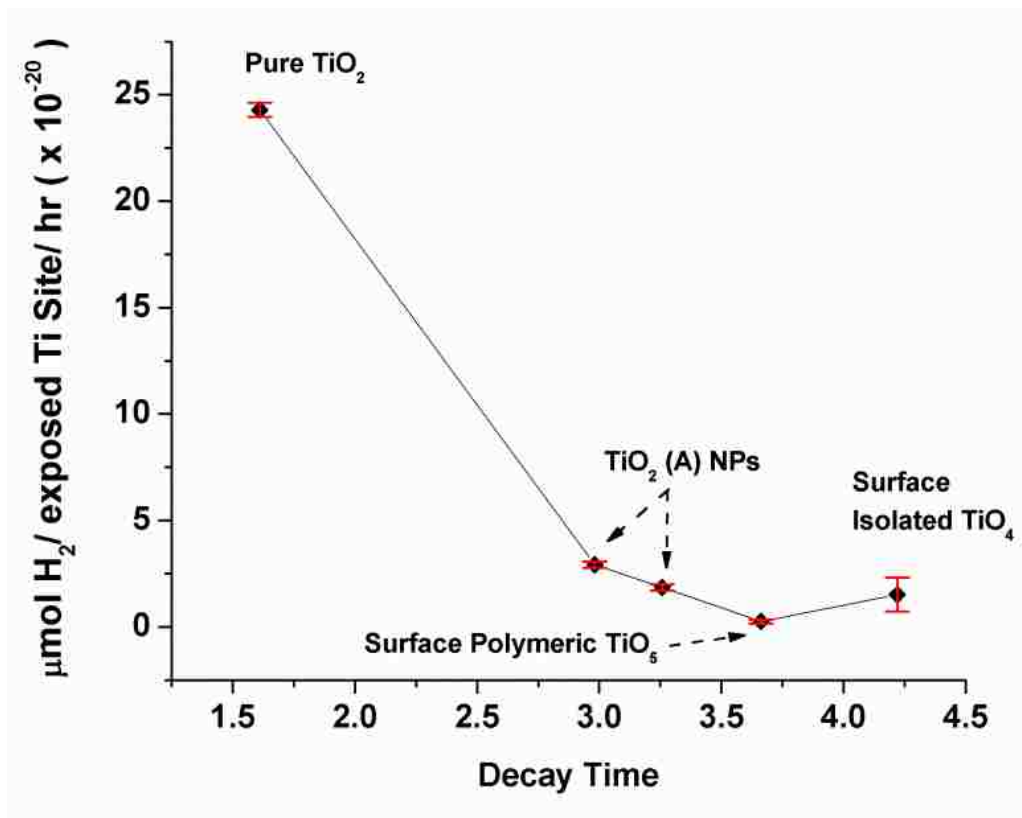


Figure 9: Calculated number of sites exhibited fast recombination dynamics (black) and slow recombination dynamics (black) for the mass of supported $\text{TiO}_2/\text{SiO}_2$ catalyst used in the photo-reactor water splitting experiments.

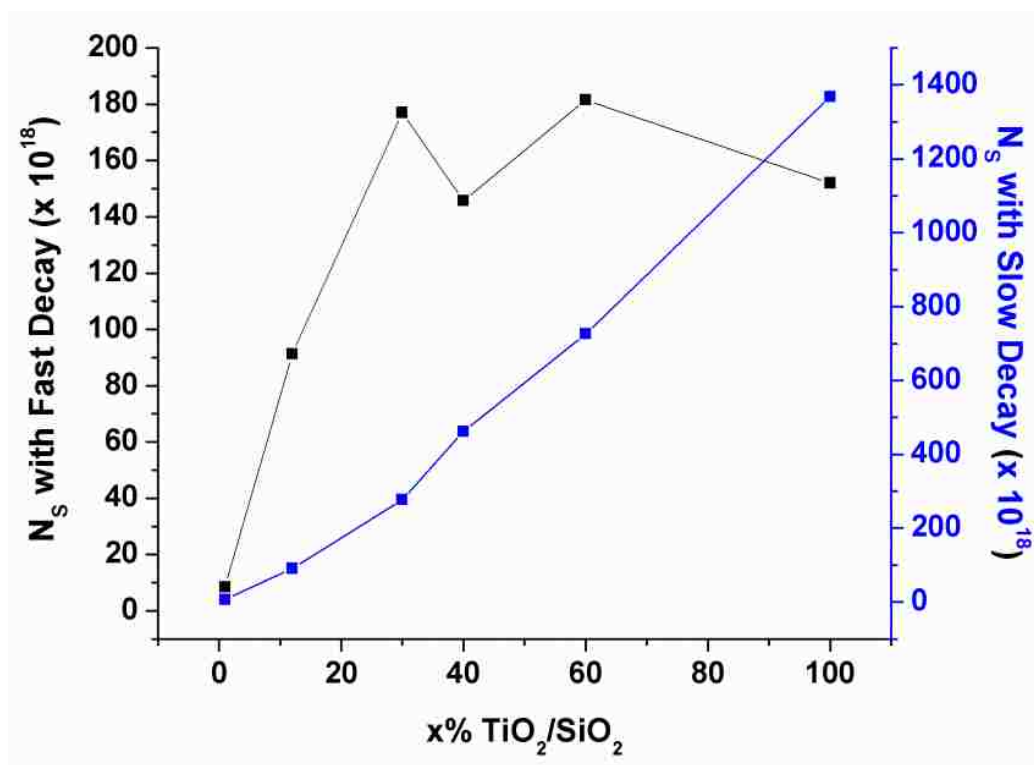


Figure 10: Specific activity as a function of the (a) number of sites with slow decay dynamics and as a function of the (b) number of sites with fast decay dynamics.

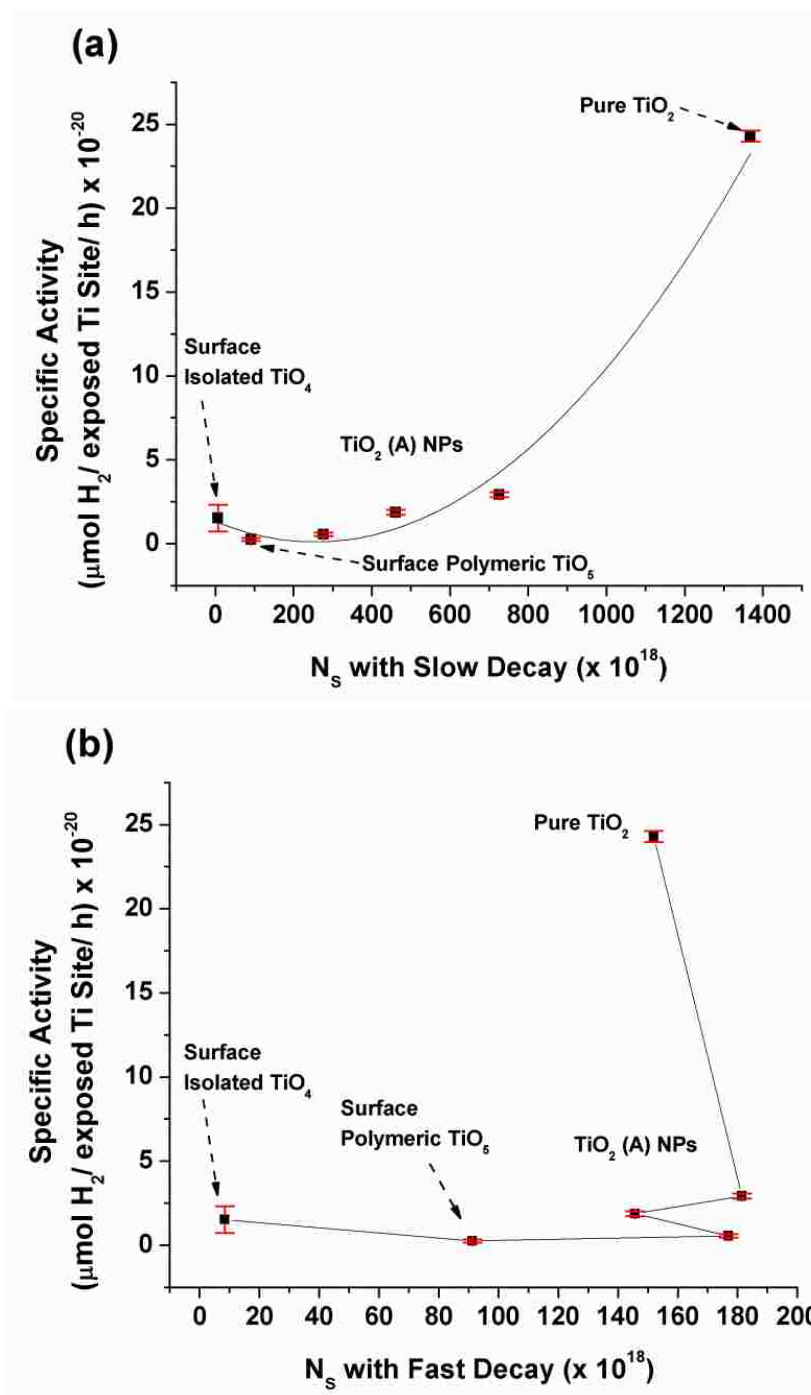
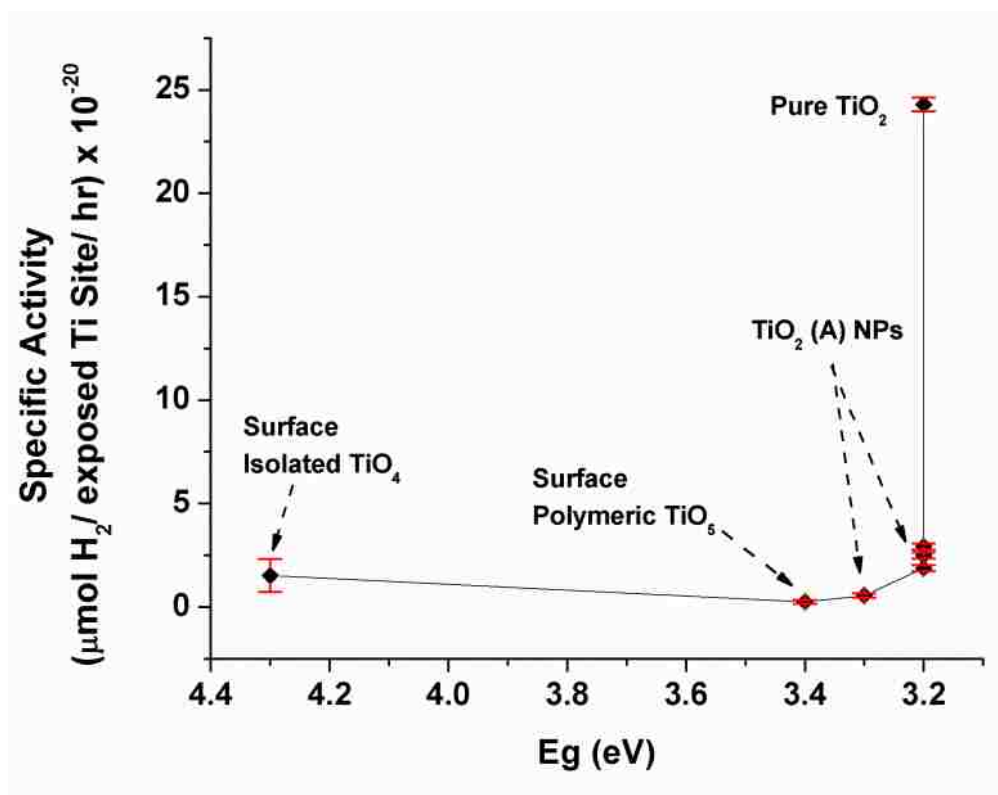


Figure 11: Specific activity ($\mu\text{mol}/\text{exposed Ti site}/\text{hr}$) as a function of edge energy values of the supported $\text{TiO}_2/\text{SiO}_2$ catalysts determined from UV-vis-NIR. The domain structure is indicated for reference.



Chapter 2

Supporting Information

The calculation of the exposed Ti sites in the supported TiO₂/SiO₂ samples was made using the known mass of catalyst used for each experiment. From that mass, the number of exposed sites can be estimated using the weight percent loading of TiO₂ for each sample and by estimating the dispersion (D) from the average domain size (d) for each catalyst. The average domain size was taken from Ross *et al.* and was determined by high resolution transmission electron microscopy for the samples containing TiO₂ (anatase) nanoparticles and for the pure TiO₂ (anatase) powder.¹ The supported 1% and 12% TiO₂/SiO₂ catalyst domain sizes were estimated for an isolated TiO₄ unit and a chain of three surface TiO₅ units, respectively. The domain sizes are summarized in Table 1 in Chapter 2.

The dispersion is defined as the ratio of exposed metal atoms to the total metal atoms in the catalyst. It was determined by Boudart that for a spherical metal particle that the dispersion can be estimated by:

$$D = \frac{0.9}{d} \quad (1)$$

where d is defined in nanometers.² Using this equation the total exposed Ti sites for each supported TiO₂/SiO₂ catalyst can be calculated in the following manner:

$$\text{Exposed Ti Sites} = \text{Mass of Catalyst} \times \frac{x}{100} \times \frac{1}{MW \text{ TiO}_2} \times 6.02 \times 10^{23} \times D \quad (2)$$

where x is the weight percent loading of TiO_2 in each sample. The dispersion and number of exposed sites is summarized in Table S1. The dispersion for the supported 1% $\text{TiO}_2/\text{SiO}_2$ catalyst is assumed to be 100% ($D = 1$) since it contains only surface isolated TiO_4 sites (0.4 nm). Also, particles sizes less than 0.9 nm are not valid for equation 1. Because the supported 12% $\text{TiO}_2/\text{SiO}_2$ catalyst was estimated to have a particle size of ~ 1 nm, the resulting dispersion for this nanodomain was calculated to be $D = 0.9$, which is believed to be a reasonable number for surface polymeric TiO_5 .

There is an associated error with this calculation due to error in the measurement of the mass of catalyst used and the estimation of the domain size. The error in mass was estimated to be ± 0.5 mg and the error in particle size was ± 0.3 nm. The error in dispersion was first calculated to simplify the error propagation analysis and was found using the following equation:

$$\delta D = \sqrt{\left(-0.9 \times \frac{\delta d}{d} \times D\right)^2} \quad (3)$$

Once the error in dispersion was determined for each catalyst the calculation of error for the number of exposed Ti sites and for the specific activity was easily made using standard propagation of error calculations for multiplication.

The validity of the assumption that the supported 1-60% $\text{TiO}_2/\text{SiO}_2$ catalysts contain only spherical particles is called into question by the observation in the TEM of the existence of “2D raft” structures. If the structures were truly 2-dimensional then they would also show 100% dispersion. The labeling of the structures as 2D, while convenient, is in reality a misnomer because they have a clear crystal structure so they must contain multiple layers. Therefore, according to Boudart, the shape of the

particles is actually plates which have a different shape factor f , than spherical particles.² The shape factor is used to calculate the particle size by the equation:

$$d = f \frac{V_{sp}}{S_M} \quad (4)$$

where V_{sp} is the specific volume of the metal and S_M is the specific surface area of the metal. The values of V_{sp} and S_M are unknown for the nanodomains in the supported $\text{TiO}_2/\text{SiO}_2$ catalysts, but estimation of the increase in dispersion due to the lower shaper factor for plate particles can be made. The shape factor for a spherical particle and a plate particle is $f = 6$ and $f = 2$, respectively. This difference of a factor of 3 can be carried through to the calculation of dispersion and then further to the calculation of number of exposed Ti sites. The calculation was then done for the samples found to contain 2D rafts, i.e. the supported 30 and 40% $\text{TiO}_2/\text{SiO}_2$ catalysts, and the results summarized in Table S2.

Furthermore, the specific activity was calculated with the adjusted number of exposed sites and is plotted as a function of average domain size in Figure S1. Figure S1 corresponds to Figure 9 of Chapter 2. A qualitative comparison of the two figures shows that the adjusted specific activity for the supported 30 and 40% $\text{TiO}_2/\text{SiO}_2$ 2D raft nanodomains has slightly decreased and yields a slightly better fit as function of average domain size. Overall, the trend that specific activity increases with average domain size still holds and is only affected minimally. On this basis alone, it would appear logical to use the adjusted specific activity throughout Chapter 2, however there are several reasons to avoid the additional assumption required to calculate the adjusted specific activity. It is known from the UV-vis-NIR data that the supported

40% TiO₂/SiO₂ catalyst has an edge energy of $E_g = 3.2$ eV. This value is identical to that of supported 50 and 60% TiO₂/SiO₂ catalysts and pure TiO₂ (anatase). This is a clear indication that despite the presence of 2D rafts, the supported 40% TiO₂/SiO₂ catalyst is far from containing purely that structure. The same is then true of the supported 30% TiO₂/SiO₂ catalyst given its E_g value of 3.3 eV. It is more likely that there is a distribution of nanodomain shapes in the samples containing TiO₂ (anatase) nanoparticles. Therefore, without any knowledge of this distribution, it would simply be guessing to try to assign the correct shape or some weighted average of shapes to calculate a more accurate dispersion. The most accurate determination of dispersion is by performing a chemisorption experiment.² However in the absence of any knowledge of the active site or the relevant adsorbed species/intermediate, this data is not available. Therefore, for the purposes of the study in Chapter 2, the simplest solution was to use the single assumption that all TiO₂ (anatase) nanodomains are particles with a spherical shape. Comparing Figures 9 and S2, it can be seen that the overall trend of increasing specific activity with average domain size is minimally affected by the exact dispersion as determined by the shape and size of the domains in the supported TiO₂/SiO₂ catalysts.

References

- (1) Ross-Medgaarden, E. I.; Wachs, I. E.; Knowles, W. V.; Burrows, A.; Kiely, C. J.; Wong, M. S. "Tuning the Electronic and Molecular Structures of Catalytic Active Sites with Titania Nanoligands," *J. Am. Chem. Soc.* **2009**, 131, 680-687.
- (2) Boudart, M.; Djéga-Mariadassou, G. *Kinetics of Heterogeneous Catalytic Reactions*, Princeton University Press, Princeton, NJ, **1984**.

Table S1: Dispersion and number of exposed sites for the supported TiO₂/SiO₂ catalysts assuming a spherical domain shape for the 12 – 100% catalysts.

x% TiO₂/SiO₂	Dispersion	Exposed Sites (x 10¹⁹)
1	1.00*	1.52
12	0.90	16.4
30	0.23	10.2
40	0.13	7.81
50	0.10	7.56
60	0.08	7.43
100	0.04	5.70

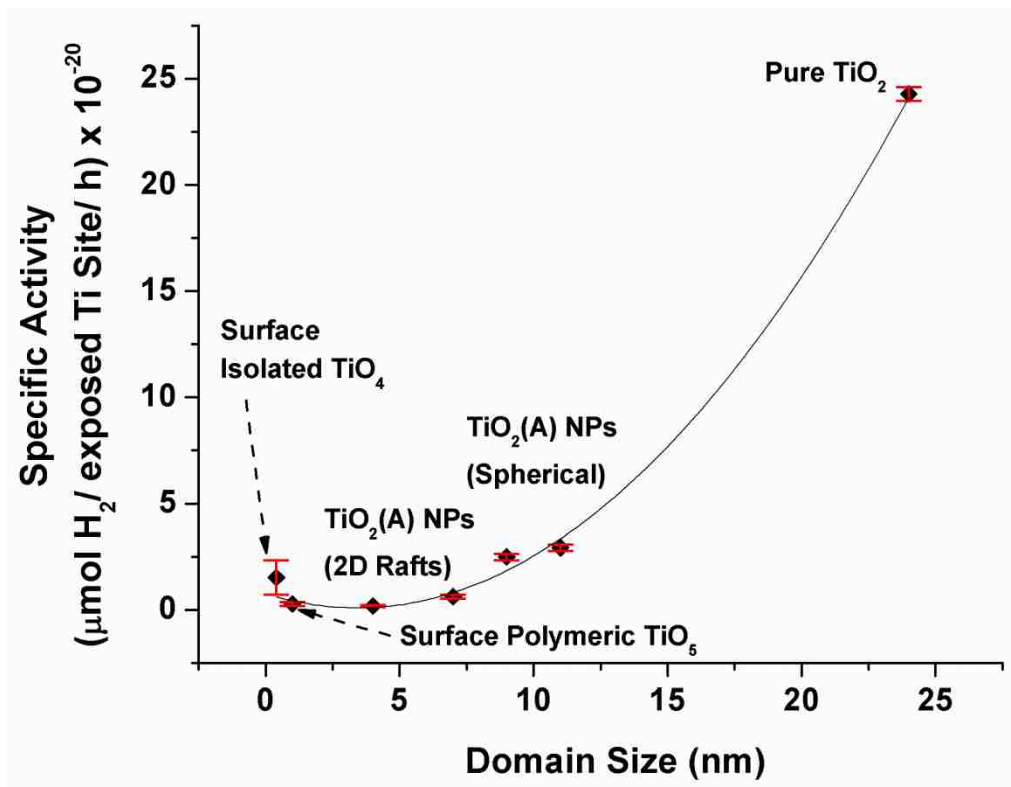
*Assumed to be fully dispersed since the sample contains only surface isolated TiO₄ sites.

Table S2: Dispersion and number of exposed sites for the supported TiO₂/SiO₂ catalysts accounting for the differing nanodomain shape.

x% TiO₂/SiO₂	Shape	Dispersion	Exposed Sites (x 10¹⁹)
1	N.A.	1.00*	1.52
12	N.A.	0.90	16.4
30	Plate	0.68	30.1
40	Plate	0.39	23.4
50	Sphere	0.10	7.56
60	Sphere	0.08	7.43
100	Sphere	0.04	5.70

*Assumed to be fully dispersed since the sample contains only surface isolated TiO₄ sites.

Figure S1: Specific activity adjusted to account for the 2D raft nanodomain shape as a function of the size of the nanodomain in the supported $\text{TiO}_2/\text{SiO}_2$ catalysts.



CHAPTER 3

Top Illumination Reactor and *In Situ* ATR-FTIR Investigation of Structure-Activity Relationships for Photo-Oxidation of Cyclohexane over Well-Defined TiO_x Nanodomains

Abstract

Photo-oxidation of cyclohexane on well-defined TiO_x nanodomains was investigated to determine the existence of a structure-activity relationship. The model supported 1-60% TiO₂/SiO₂ photocatalysts were synthesized by incipient wetness impregnation of Ti-isopropoxide/isopropanol solutions into a SiO₂ support in a N₂ environment. Earlier studies reported that the nature of the supported TiO₂ nanodomain varied in the following manner as a function of the titania loading: isolated site (1% TiO₂/SiO₂), polymeric chain (12% TiO₂/SiO₂), 2D rafts (20-40% TiO₂/SiO₂) and 3D nanoclusters (60% TiO₂/SiO₂). A top illumination reactor equipped with a 50 W Hg lamp was used to initiate photo-oxidation in a slurry of catalyst in cyclohexane (~1.0 g/L) with simultaneous product sampling over 6h followed by GC analysis. The production of cyclohexanone was used to calculate the specific activity (mmol cyclohexanone/exposed Ti site/h) and was shown to produce a structure-photoactivity relationship that revealed that a large contribution of a bulk structure in TiO_x nanodomains yields higher specific activity. The contribution of the bulk structure to

high specific photoactivity was analyzed by means of photoluminescence decay spectroscopy for the TiO_x nanodomains and shown to be related to the ability of the bulk to act as reservoir for excitons able to participate in the surface photo-oxidation reaction. *In situ* ATR-FTIR experiments were performed under illumination and in batch reactor-like cell using UV-LEDS (375 nm) to initiate the photo-oxidation reaction. The relative intensity of desorbed to adsorbed cyclohexanone during reaction over an individual catalyst was found to be in agreement with the structure-activity relationship and indicated that the smaller TiO_x nanodomains are less active because formation of cyclohexanone is desorption limited. The structure-activity relationship for photo-oxidation of cyclohexane over the TiO_x nanodomains will be beneficial for future rational design of improved photo-oxidation catalysts.

1. Introduction

Titanium dioxide, TiO_2 , is well known as an effective photocatalyst for a variety of useful reactions. The majority of photocatalytic applications utilizing TiO_2 are environmentally beneficial processes that degrade organic compounds in air or water and photo-oxidize industrial solvents such as trichloroethane or other toxic chlorinated materials.¹⁻⁵ Many studies of TiO_2 -based photocatalysts have focused on modification of the material by the addition of dopants with the end goal being to increase photo-activity by tailoring of surface catalytic active sites, increasing surface area, increasing the trapping of photo-generated electrons and/or holes, or shifting the absorption of light to the visible region of the spectrum.⁵⁻¹⁰

Recently, the photo-oxidation of cyclohexane over TiO_2 has been subjected to a multitude of studies because the initial report of this photo-reaction by Giannotti *et al.* indicated a high selectivity to the highly desirable ketone product cyclohexanone (100% cyclohexanone over TiO_2 (anatase)).¹¹ Cyclohexanone is then used to produce ϵ -caprolactam and adipic acid, which are monomers of nylon-6 and nylon-6,6, respectively. The recent studies have focused on a broad range of factors affecting the activity and/or selectivity of photo-oxidation reactions: reactor design,¹²⁻¹⁵ intensity and wavelength of illumination,^{12,16} solvent,¹⁷ oxidizing reactants (O_2 , H_2O).^{17,18} Reactor studies have reported that the for cyclohexane photo-oxidation, the photonic efficiency of an internally illuminated monolith reactor is 0.062, which is lower than that obtained with a top illumination slurry reactor (0.151).¹³ The internally illuminated reactor, however, provides more facile catalysts separation and ease of catalyst illumination, whereas the top illumination slurry reactor must maintain a slurry density of no greater than 1 g TiO_2 per liter to prevent shielding of the illumination light from parts of the available reactor volume.^{12,14,15} Studies on the wavelength of light used for illumination have shown that the deep UV (< 275 nm) must be removed from the irradiation source to prevent photolysis, which served to benefit the selectivity to cyclohexanone.¹² Selectivity to mono-oxygenated products has also been demonstrated to be improved by addition of dichloromethane to the reactant solvent that acts to limit the adsorption of intermediates or by introducing H_2O to the oxidation reactant O_2 that acts to improve desorption of cyclohexanone products.^{17,18}

The TiO₂ catalyst structure has also been subjected to studies of the effect of surface area,¹² pretreatment conditions (calcinations temperature and environment),¹² particle size and crystallinity,¹⁹ crystal phase,²⁰ and dopants (Ag and Au).²¹⁻²⁴ The effect of particle size, crystallinity, and crystal structure all have particular interest because they have initiated the examination of the relevant properties that lead to the definition of structure-activity relationships for TiO₂ in the photo-oxidation reaction. Studies by Carneiro *et al.* have recognized the importance of developing structure-activity relationships for cyclohexane photo-oxidation.¹⁹ Their work demonstrated a correlation between small particle size (high surface area) and high surface hydroxyl concentration with increased production of cyclohexanone, but desorption of cyclohexanone was improved on large particles. This study, however, was done on particles containing only crystalline TiO₂ (anatase) and it is of interest to determine if other structures of titania have an effect on cyclohexane photo-oxidation activity.

The structure and catalytic activity of TiO₂ can be significantly affected by supporting titania on inert, high surface area metal oxide.²⁵⁻²⁸ In particular, it has been shown that the structure of TiO_x supported on SiO₂ varies with the weight percent loading of titania and these structures can be controlled during catalyst synthesis.^{26,27} Furthermore, the electronic properties of metal oxides (band gap or edge energy and photoluminescence) can be controlled by changing the nanodomain structure because the local electron density is affected by the metal oxide domain size.²⁹⁻³² The effect of weight percent loading on the physical and electronic structure of TiO_x nanodomains was discussed in Chapter 2 (Ch. 2, Figure 1). Based on the structural dependence on

TiO₂ loading and the well-defined nature of those structures, it is of great interest to study TiO₂ supported on SiO₂ for its activity in the photo-oxidation of cyclohexane in an attempt to derive structure-activity relationships. The present investigation employs the well-defined TiO₂/SiO₂ catalysts described above in the photo-reactor experiments to explore their potential structure-photoactivity relationship.

Photocatalytic reactions require the generation of excitons (electrons and holes) during irradiation of the catalyst material. The previous UV-vis-NIR results indicated a dependence of edge energy and photoluminescence properties on nanodomain structure, and this was shown to be true in Chapter 2 (Ch. 2, Figure 4).^{26,28} Tang *et al.* concluded that the lifetime of photo-generated holes in TiO₂ is a strong determinant of the ability of TiO₂ to split water.³³ Since PL emission is indicative of recombination of e⁻/h⁺ pairs, the PL emission decay is related to the lifetime of photo-generated holes (i.e. the slower the decay, the longer the lifetime). Thus, the time-resolved photoluminescence data from Chapter 2 will also be applied to the activity data for cyclohexanone production to determine if the decay properties of excitons in the TiO_x nanodomains potentially yield an electronic structure-activity relationship for cyclohexane photo-oxidation.

It is desirable to understand how photocatalyst structure affects the distribution of reaction intermediates to give additional insights into the mechanism. Information of this kind can be obtained through *in situ* infrared or Raman spectroscopic studies during photocatalysis, but they are typically done for gas phase reactants and products. Though studies on the mechanism of cyclohexane photo-oxidation have been

reported,^{12,16,17,34} spectroscopic evidence of the reaction mechanism is scarce. Attenuated Total Reflectance (ATR)-Fourier Transform Infrared (FTIR) spectroscopy, however, has been shown to be a technique that can successfully probe the solid-liquid interface that exists in many photocatalytic reaction systems.³⁵⁻³⁸ The technique has already been shown to be useful in probing the TiO₂-cyclohexane, solid-liquid interface for photo-oxidation of cyclohexane by Almeida *et al.* over the course of several recent studies that led to the identification of key adsorbed intermediates and the determination of a possible reaction mechanism.³⁹⁻⁴² The mechanism by which the catalyst deactivates has also been studied by ATR-FTIR, showing the broad range of useful information that this technique can provide for understanding the surface reactions at solid-liquid interfaces in photo-oxidation.¹⁵ The current study attempts to build on the work of Almeida *et al.* by using the well-defined nanodomains of TiO₂/SiO₂ catalysts in similar ATR-FTIR studies to relate the distribution of reaction intermediates and products to the potential structure-activity relationships found in reactor studies for cyclohexane photo-oxidation over TiO_x nanodomains.

2. Experimental

2.1 Catalyst Synthesis

Model supported TiO₂/SiO₂ catalysts were synthesized from Ti-isopropoxide/isopropanol precursor solutions and a SiO₂ support by incipient-wetness impregnation of varying amounts of Ti precursor, followed by drying and calcination in air. (A more complete description for obtaining various Ti loadings can be found in

references 26 and 28.) The silica support for this study was Cab-O-Sil (Cabot, EH-5) and this material was treated with water in order to condense its volume for easier handling. The wet SiO₂ was dried at 120 °C and subsequently calcined at 500 °C overnight. The resulting BET surface area was 332 m²/g. Titanium isopropoxide was obtained from Alfa Aesar (99.999% purity) and preparation was performed inside a glove-box with continuous flowing N₂. The samples were subsequently dried at 120 °C in flowing N₂ for 1 h and calcined at 500 °C in flowing air for 4 h. The catalysts will be referred to as x% TiO₂/SiO₂, where x is the weight percent loading of TiO₂ in each sample. Pure TiO₂ (anatase) was obtained commercially from Sigma-Aldrich (99.8% purity) and contains particles with an average size of ~24 nm.

2.2 Cyclohexane Photo-Oxidation Reaction

To evaluate catalyst performance in the selective photo-oxidation of cyclohexane, reactions were carried out in a Top Illumination Reactor (TIR).^{12,18,23} The catalysts were dried for 2h at 120 °C to remove adsorbed water. In a typical experiment 100 mL of cyclohexane containing a concentration of ~1.0 g/L of catalyst (~0.10 g of catalyst) was used (slurry system). The slurry was illuminated from the top of the reactor through a Pyrex window that cuts off the highly energetic UV radiation.^{12,13} A high pressure mercury lamp of 50 W was used (HBO50W from ZEISS). The light intensity of the lamp used in the wavelength absorption range of TiO₂ (275–388 nm) is 55 mW/cm² entering the suspension, which corresponds to 2×10^{-7} Einstein·cm⁻²·s⁻¹. This value was obtained by using the following equation:

$$I'' = \frac{E\lambda}{chN_A} \quad (1)$$

where I'' is the photon flux ($\text{Einst}\cdot\text{m}^{-2}\cdot\text{s}^{-1}$), E the radiant flux (W/m^2), k the wavelength (m), c the speed of light (3×10^8 m/s), h Planck's constant (6.63×10^{-34} J·s), and N_A Avogadro's number (6.02×10^{23} mol⁻¹).¹⁹

Air, dried over Molsieve 3 Å (Acros Organics) and pre-saturated with cyclohexane, was bubbled through the catalyst slurry at a rate of 30 mL/min. During the reaction, liquid was withdrawn and analyzed by gas chromatography (GC) over a 6 hour period. Organic compounds were quantitatively analyzed twice using a gas chromatograph with a flame ionization detector (Chrompack, CPwax52CB). Due to the relatively low activity of the supported TiO₂/SiO₂ samples, only cyclohexanone production was obtained. Hexadecane (1 mL) was used as an internal standard.

2.3 Thin Film Preparation

Thin films of the TiO₂ nanodomain containing supported TiO₂/SiO₂ samples and the pure TiO₂ (anatase) were prepared on the ZnSe crystal by first suspending the sample in 10 mL of DI-water. The suspensions were made so that the concentration of sample was 3.8 g/L. The suspension was treated at 30 min in a 35 kHz Elmasonic ultrasonic bath. Then 2 mL of the suspension were spread on the ZnSe crystal and dried under vacuum in the presence of a desiccant overnight.

2.4 *In Situ* ATR-FTIR During Photo-Oxidation of Cyclohexane

The ATR-FTIR cell used was a Harrick Horizon multiple internal reflections accessory coupled with a flow through cell. The flow through cell consisted of two plates; the top plate contained a quartz window for illumination of the sample and the bottom plate contained a ZnSe crystal as an internal reflection element (IRE). The

IRE had dimensions of $50 \times 10 \times 2 \text{ mm}^3$ and the 45° angle of entry of the IR beam yielded 11 internal reflections for the given geometry. The FTIR spectra were collected using a Bruker VERTEX 70 FTIR spectrometer equipped with a liquid-N₂ cooled MCT detector. Illumination of the sample during photo-oxidation was achieved using an array of 7 UV LEDs (375 nm, 42 mW). The photon flux at the sample surface was calculated to be $9 \times 10^{-9} \text{ Einstein}\cdot\text{cm}^{-2}\cdot\text{s}^{-1}$. More detailed information on the ATR cell can be found in a previous publication.³⁹

The cyclohexane (Sigma-Aldrich, 99.0%) was pre-saturated with O₂ by flowing air through the liquid at 310 mL/min for 1h. The ATR cell was operated in a batch mode and 2 mL of the saturated cyclohexane was introduced directly into the cell and onto the sample thin film. The O₂ saturated cyclohexane was allowed to adsorb onto the sample for 30 mins under ambient, dark conditions. Illumination of the sample was carried out for 100 mins during which time an ATR-FTIR spectrum (1 spectrum/min) was collected using 32 scans/spectrum and a resolution of 4 cm^{-1} . The background spectrum used in the time profile series of spectra was taken after the 30 min cyclohexane adsorption and collected with 64 scans/spectrum.

3. Results

3.1 Cyclohexanone Production and Activity: Top Illumination Reactor

The physical (domain structure and size) and electronic (E_g) structures of the well-defined nanodomains in the supported TiO₂/SiO₂ catalysts are summarized in Table 1. The various catalysts were screened for the production of cyclohexanone using the

Top Illumination Reactor (TIR) system in order to examine the influence of the molecular and electronic structure upon the photo-oxidation of cyclohexane. The cyclohexanone production (mmol) over 360 min for the supported TiO₂/SiO₂ catalysts is shown in Figure 1. The supported 60% TiO₂/SiO₂ catalyst, containing an average of ~11 nm TiO₂ (anatase) nanoparticles (NPs), produced the greatest amount of cyclohexanone during and the production was >2 times that of the supported 30% TiO₂/SiO₂ catalyst, which contains much smaller TiO₂ (anatase) NPs with a nanodomain size of ~4 nm. A small amount of cyclohexanone production was detected for the surface polymeric TiO₅ species present in the supported 12% TiO₂/SiO₂ catalyst, but it is ~10 times less than that of the supported 60% catalyst. The supported 1% TiO₂/SiO₂ catalyst showed no detectable cyclohexanone formation over the entire duration of the photo-reaction experiment.

Cyclohexanone production data during photo-oxidation of cyclohexane over pure TiO₂ (anatase) with a particle size of ~20 nm was previously obtained in the literature by Carneiro *et al.* using the same top-illuminated reactor system and experimental parameters.¹⁹ It was found that after 300 min of photo-reaction, ~0.10 mmol of cyclohexanone was formed. This datum point will be used in all subsequent calculations of activity at 300 min of photo-reaction time in an attempt to determine potential structure-activity relationships for this photo-reaction.

Employing the cyclohexanone production data from the literature for TiO₂ (anatase) at 300 min of reaction time allows plotting of the cyclohexanone production data at 300 min for the full range of supported TiO₂/SiO₂ catalysts as a function of weight

percent loading of TiO₂ and average domain size. These plots are shown in Figures 2a and 2b, respectively. When pure TiO₂ is included in the analysis, the trend is that cyclohexanone production increases with TiO₂ loading, in agreement with Figure 1. As indicated in Table 1, average domain size of the supported TiO₂/SiO₂ catalysts is directly related to the wt% loading of TiO₂. Therefore, Figure 2b shows the same relationship exists for cyclohexanone production as a function of average domain size since domain size also increases with titania loading on silica.

Although the same mass of catalyst was always used to create the slurry in the TIR, the mass of Ti in the samples differs greatly because of the varying titania content. To account for this difference, the activity of the supported TiO₂/SiO₂ catalysts for cyclohexanone production can be normalized by the mass of Ti used. A plot of activity (mmol/g Ti/h) as a function of average domain size is shown in Figure 3. There is almost no difference in activity for the ~4 nm and ~11 nm TiO₂ NPs in the supported 30 and 60% TiO₂/SiO₂ catalysts, respectively. The pure TiO₂ (anatase), with an average of ~20 nm NPs, exhibits just over twice the activity of the smaller supported TiO₂ nanodomains. This correlation in Figure 3, however, yields a false high activity of the ~4 and ~11 nm TiO₂ NPs in the supported 30 and 60% TiO₂/SiO₂ catalysts. The increased activity of the smaller domains relative to the production (see Figure 2b) can be attributed to a decrease in activity of the pure TiO₂ (anatase) that occurs with the normalization by mass of Ti, which incorrectly counts bulk TiO₂ sites as catalytically active.

A more accurate representation of photoactivity for cyclohexane photo-oxidation can be determined by estimating the dispersion (ratio of exposed Ti sites to total Ti sites) and using the dispersion to calculate the number of exposed Ti sites. The method for estimating dispersion and calculating the number of exposed Ti sites was previously discussed in the supporting information of Chapter 2. The dispersion and number of exposed sites for the mass of each catalyst used in the current study was determined and are summarized in Table 2. (A plot of the data can be found in the supporting information for this chapter, Figure S1) The results of the calculation show that the SiO₂-supported small TiO₂ (anatase) NPs and the surface polymeric TiO₅ species have a greater number of exposed Ti sites than the pure TiO₂ (anatase) powder because of the larger domain size of the latter. This difference in exposed sites is manifested in the specific activity which is defined as the activity normalized by the number of exposed Ti sites (mmol/exposed Ti site/h). A plot of specific photoactivity as a function of average domain size can be found in Figure 4. The trend in Figure 4 closely mimics that of the overall production of cyclohexanone in Figure 1. There is a smooth increase in specific photoactivity for the supported TiO₂/SiO₂ samples for cyclohexanone production that appears to be related the average nanodomain size present on the SiO₂ support. The unsupported, pure TiO₂ (anatase), possessing ~20 nm NPs, exhibits nearly four times the specific activity over the supported ~11 nm TiO₂ (anatase) NPs of the supported 60% TiO₂/SiO₂ catalyst.

3.2 *In Situ* ATR-FTIR of Supported TiO₂/SiO₂ Catalysts during Photo-Oxidation of Cyclohexane

The ATR-FTIR spectra were collected over 100 mins of reaction time under photocatalytic conditions for photo-oxidation of cyclohexane. The ATR cell that was used allowed for simultaneous collection of ATR-FTIR spectra through the ZnSe crystal in the bottom plate and illumination with 375 nm UV light through the quartz window in the top plate. The thin film of the catalyst sample is in direct contact with the ZnSe IRE and the sample volume above the film could be filled with the reactant cyclohexane. The reactant O₂ was provided by the pre-saturating cyclohexane liquid with molecular oxygen. The background for all FTIR spectra was collected after 30 min of cyclohexane adsorption under dark conditions. The ATR-FTIR spectra of the supported TiO₂/SiO₂ samples after 100 minutes of illumination under the reaction conditions are shown in Figure 5. Multiple intermediate and/or product FTIR peaks are formed during cyclohexane photo-oxidation as depicted in Figure 5. The intensity of the FTIR peaks qualitatively follows the trends found for cyclohexanone production with the highest intensity occurring for the pure TiO₂ (anatase). There is a significant drop in intensity from the supported 60% to the 40% TiO₂/SiO₂ catalyst, though trace peaks can still be seen in the spectra for the supported 40% and 30% TiO₂/SiO₂ catalysts. The ATR-IR spectrum for the pure SiO₂ support after 100 min of illumination during photo-oxidation of cyclohexane is also presented in Figure 5. This spectrum is useful as a reference as it shows the presence of negative consumption peaks despite its lack of intermediate or product peak formation. The negative consumption peak is also visible for the supported 1% and 12% TiO₂ catalysts, but it is not an indication of reaction because it is also present in the spectrum for the inert

support. The absence of observable intermediate and product FTIR peaks for the supported 1 and 12% TiO₂ catalysts agrees with the low cyclohexanone production results in Figure 1.

In addition to the positive FTIR peaks of reaction products dissolved in the bulk liquid cyclohexane phase and adsorbed intermediates, the ATR-FTIR spectra show the development of several negative consumption peaks that can be seen more clearly for the pure TiO₂ (anatase) catalyst and the supported 60% TiO₂/SiO₂ catalyst in Figures 6 and 7, respectively. The characteristic peaks at 1449, 1257, and 903 cm⁻¹ correspond to the scissoring, twisting, and rocking vibration of the CH₂ groups of cyclohexane.⁴³ These peaks are all present in Figure 6 and develop negatively over the 100 min reaction time indicating that cyclohexane is being consumed from the bulk as a reactant. The negative cyclohexane peak at 1449 cm⁻¹ indicating consumption of cyclohexane is visible for all catalysts in Figure 5, however the spectrum of the pure SiO₂ after 100 minutes of illumination under the same reaction conditions also showed a negative peak for cyclohexane. This is evidence of possible desorption and/or evaporation of the cyclohexane reactant. Therefore, the negative intensity of this peak is not necessarily an indication that reaction is taking place. The other peaks are evidence that reaction is taking place, but it must be stressed that quantitative comparisons of peak intensity should not be made without considering that the low activity of the lower loading supported TiO₂/SiO₂ catalysts may make peaks more difficult to detect at all.

To determine if the relative peak intensities observed are due to a particle size effect and not some contribution of Si sites, a physical mixture of 60% TiO₂ and 40% SiO₂ (by weight) was made and the *in situ* ATR-FTIR spectra were obtained using the same reaction conditions used for the other supported TiO₂/SiO₂ catalysts. If the support is active, it is expected that the physical mixture will have the same peak distribution and relative intensities as the supported 60% TiO₂/SiO₂ catalyst. Figure 8 shows the opposite to be true and that the peak distribution and relative intensities of the physical mixture match those found in the pure TiO₂ (anatase) sample. This observation is evidence that the hydroxyl groups in the SiO₂ support are inactive for cyclohexane photo-oxidation.

The complete time-resolved FTIR spectra (0-100 min of illumination) for cyclohexane photo-oxidation over the pure TiO₂ (anatase) sample appear in Figure 6 with each spectrum representing a 10 min interval. The photo-oxidation reaction is initiated by the illumination of the system with UV light and a broad range of peaks develop over time between 1800 and 800 cm⁻¹. The structures of the adsorbed species as proposed by Almeida *et al.* are displayed in Figure 6.³⁹ Cyclohexanone can be observed in two different forms in the spectrum: dissolved in the cyclohexane liquid phase and adsorbed on the photocatalyst. The liquid phase cyclohexanone molecules represent those reaction products that have desorbed into the liquid phase and are attributable to desorbed products. The dissolved cyclohexanone is readily identified by its FTIR peaks at 1712 and 1313 cm⁻¹ that correspond to the stretching vibration $\nu(\text{C}=\text{O})$ of the carbonyl group³⁹ and the bending mode of CH₂, $\delta(\text{CH}_2)$,

respectively.^{44,45} When cyclohexanone is adsorbed on the TiO₂ surface, its $\nu(\text{C}=\text{O})$ stretching vibration becomes less energetic and is red shifted to 1683 cm⁻¹ as seen in Figure 6.⁴⁴ The location of this FTIR peak for cyclohexanone was confirmed in the literature by studies of a solution of cyclohexanone in the presence and absence of a TiO₂ surface and can be seen in Figure 6.³⁹

There are also several other peaks in the FTIR spectra in Figure 6 and they correspond to several other adsorbed species. The strong FTIR peak at 1562 cm⁻¹ has been assigned to the carbonyl stretching $\nu(\text{C}=\text{O})$ vibration of adsorbed carbonates.^{46,47} The peak at 1409 cm⁻¹ and the broad region from 1072 - 1048 cm⁻¹ can be assigned to adsorbed carbonates.^{47,48} Finally, a weak peak at 880 cm⁻¹ is observed and has been assigned to surface peroxides.^{49,50} It is possible that this peak is linked to the formation of a hydroperoxide intermediate, but due to its relative weak intensity, irregularity, and proximity to the cut-off wavelength of the ZnSe IRE it will not be further considered in the present study.

The supported 60% TiO₂/SiO₂ catalyst also showed significant formation of products and intermediates during cyclohexane photo-oxidation. The time-resolved FTIR spectra of the peaks formed during 100 mins of illumination is shown in Figure 7 with each spectrum representing a 10 min interval. The corresponding peak assignments of the spectra of pure TiO₂ (anatase) (Figure 6) for liquid phase and adsorbed cyclohexanone, adsorbed carboxylates, and adsorbed carbonates are all found in the spectra for the supported 60% TiO₂/SiO₂ catalyst containing ~11 nm NPs. The three characteristic CH₂ vibrations of cyclohexane can also be seen as negative

peaks, again indicating consumption of the cyclohexane reactant from the liquid phase. Upon closer inspection of the relative intensities of the cyclohexanone peaks and the carbonate peaks, it is observed that the $\nu(\text{C}=\text{O})$ of adsorbed cyclohexanone at 1683 cm^{-1} is stronger than the $\nu(\text{C}=\text{O})$ stretch of the liquid phase cyclohexanone peak at 1712 cm^{-1} and the adsorbed carboxylate peak at 1562 cm^{-1} . In contrast, for pure TiO_2 (anatase) the $\nu(\text{C}=\text{O})$ intensity for the adsorbed cyclohexanone FTIR peak is weaker than the $\nu(\text{C}=\text{O})$ intensity of liquid phase cyclohexanone and the adsorbed carboxylate peak at 1562 cm^{-1} (see Figure 6).

4. Discussion

4.1 Cyclohexane Photo-Oxidation Structure-Activity Relationships as a Function of TiO_x Nanodomain Size

In heterogeneous catalysis, it is desirable to couple the quantitative structural properties with catalytic activity data to form a structure-activity relationship. This kind of relationship is important as it allows one to make critical decisions when rationally designing a catalyst to maximize activity and studies of this nature have greatly increased in the past decade.⁵¹ The same is true of photocatalytic reactions and it was indeed shown above in Figure 4 that the specific photoactivity for cyclohexane oxidation to cyclohexanone increases with TiO_2 domain size. The coupling of quantitative structural information with catalytic activity data to form structure-activity relationships has been previously applied to the photo-oxidation of cyclohexane on TiO_2 -containing catalysts.^{12,19,20} In particular, it was shown that on a

basis per mass of TiO_2 catalyst, the photoactivity to cyclohexanone decreases with increasing particle size. When the surface hydroxyl concentration is used to normalize the activity to account for the surface nature of the photocatalytic reaction, however, larger TiO_2 particles were found to be the most active. The latter finding is in agreement with the current structure-photoactivity relationship that normalizes activity by the number of exposed Ti sites available for surface photocatalytic reaction (see Figure 4). Despite being supported, the 30% and 60% $\text{TiO}_2/\text{SiO}_2$ catalysts contain TiO_2 (anatase) particles with an average size of ~ 4 and ~ 11 nm, respectively, and allows for the comparison of their activity to that of ~ 20 nm pure TiO_2 (anatase). Furthermore, the current structure-activity relationship reveals that the trend of decreased photoactivity continues as the domain size is decreased and surface polymeric TiO_5 polymers and surface isolated TiO_4 nanodomains are formed on supported 12% and 1% $\text{TiO}_2/\text{SiO}_2$ catalysts. Therefore, the current structure-activity relationship comprises a complete set of possible TiO_x nanodomain structures.

The structure-photoactivity relationship in the current study leaves the question open as to why the larger bulk structure in the supported $\text{TiO}_2/\text{SiO}_2$ catalysts contributes to the higher specific activity for photo-oxidation of cyclohexane. The improved activity of large particles found by Carneiro *et al.* was concluded to be related to improved desorption characteristics of large particles that have a higher availability of positively charged holes that promote product desorption.¹⁹ This conclusion, while plausible, requires additional experimental support. Photoluminescence (PL) spectroscopy, as discussed in Chapter 2, while a bulk technique, can yield information on the fate of the

resulting excitons, such as positively charged holes, which must migrate to the surface of the catalyst to be involved in surface photocatalytic reactions.^{7,52}

The PL decay properties of the supported TiO₂/SiO₂ catalysts were determined in Chapter 2 using time resolved PL spectroscopy. The PL decay of the nanodomains in the various catalysts was observed to contain a fast and a slow component (biexponential decay) and the relative contribution of the fast and slow component was determined. Because PL spectroscopy is a bulk technique, the overall lifetime excitons generated by nanodomains in supported TiO₂/SiO₂ catalysts is not an indicator of high photoactivity. This conclusion is supported in Chapter 2 and is true for cyclohexane photo-oxidation as well (see Figure S2). The relative contribution of the components of decay, however, allows for the semi-quantitative determination of the number of Ti sites that, upon photon absorption, generate excitons that decay with fast or slow kinetics. Excitons decaying with slow kinetics can be related to the surface photo-reaction, because they have a greater opportunity to migrate to the surface and participate in the photocatalytic process. As was invoked in Chapter 2, multiplying the total number of Ti sites by the relative contribution of the fast and slow component yields the number of Ti sites that generate excitons that decay with fast and slow kinetics, respectively. Larger TiO₂ (anatase) NPs, with their higher average size and larger cross sectional area, will absorb more photons at Ti sites at the surface *and* bulk of the catalyst particle.⁵³ (See Chapter 2, Section 4.3 for a complete discussion.)

Specific activity is plotted as a function of the number of Ti sites that generate excitons with slow recombination kinetics for the supported TiO₂/SiO₂ catalysts and is shown in Figure 9a. There exists a strong correlation between high specific activity and Ti sites generating a large number of excitons with slow recombination kinetics. Although it cannot be directly shown that all Ti sites produce excitons and that all generated electrons participate in the photo-oxidation, it is concluded that slow recombination kinetics are preferred. This conclusion is further supported by the finding that specific activity shows no correlation with the number of Ti sites generating excitons with fast recombination kinetics (Figure 9b). The large number of Ti sites in the bulk of large TiO₂ (anatase) particles, therefore, act as a reservoir for slow recombining excitons that are more likely to play a role in surface reactions, and Figure 9a reveals an electronic structure-photoactivity relationship for cyclohexane photo-oxidation over TiO_x nanodomains.

It has been proposed by Anpo *et al.* that a single site tetrahedral TiO₄ titanium oxide species incorporated in a zeolite framework has a relatively high activity in the reduction of CO₂ with H₂O and the decomposition of NO into N₂ and O₂.⁷ This finding disagrees with the current results for cyclohexane photo-oxidation, however, it has been shown by Yang *et al.* that carbon residue in the reactor during CO₂ photo-reduction with H₂O can lead to false positive results for the activity of this reaction.⁵⁴ Therefore, it is unclear whether the isolated TiO₄ site is truly active for CO₂ photo-reduction. It seems unlikely that the single site can provide a sufficient amount of

excitons to yield high activity during photo-reactions as has been shown to be necessary for cyclohexane photo-oxidation (see Figure 9a).

4.2 *In Situ* ATR-FTIR Evidence for the Dependence of Specific Activity on TiO_x Nanodomain Structure

It is qualitatively observed from Figure 5, that *in situ* ATR-FTIR supports the conclusion that a larger bulk structure in TiO_x nanodomains increases the specific activity for cyclohexanone production during cyclohexane photo-oxidation. The appearance of strong peaks in the pure TiO₂ (anatase) and supported 60% TiO₂/SiO₂ catalysts relative to the samples with less than 40% TiO₂ loading agrees with the overall production of cyclohexanone in the TIR experiments (Figure 1). The experimental design operated the ATR cell in a batch mode, which closely mimics the conditions found in the TIR. The positive peaks that were detected give not only information on adsorbed species, but also yield information on the formation of products in the liquid reactant phase. The lack of strong positive peaks in the supported 1% and 12% TiO₂/SiO₂ catalysts in Figure 5 supports the conclusion that small domains lacking a bulk structure (i.e. surface isolated TiO₄ and surface polymeric TiO₅) are less active than catalysts containing TiO₂ (anatase) particles. The effect of TiO₂ (anatase) particle size can then be inferred by examining the difference in the supported 30-60% TiO₂/SiO₂ catalysts. Figure 5 shows that significant product FTIR peaks are not present until a particle size of ~11 nm in the supported 60% TiO₂/SiO₂ catalyst is obtained. When the particles size is increase to ~20 nm in the pure TiO₂ (anatase) sample, the relative intensity of the FTIR peak for bulk liquid

phase cyclohexanone is further increased indicating that more product cyclohexanone is being formed (see Figures 6 and 7). Furthermore, a comparison of the adsorbed cyclohexanone peak intensity reveals that the pure TiO₂ (anatase) catalyst has improved desorption characteristics in agreement with previous studies and with the conclusions inferred from the PL spectroscopy results.

4.3 Effect of TiO_x Nanodomain Size on Cyclohexane Photo-Oxidation Reaction Pathways

It is possible to make comparisons of the relative intensity of product and adsorbed intermediate FTIR peaks that evolve during the reaction on a single catalyst to further understand how nanodomain size affects the cyclohexane photo-oxidation pathways, namely desorption and formation of unwanted further oxidation products. Figures 6 and 7 show the time profile for the formation of product cyclohexanone in the liquid phase (1712 cm⁻¹) and adsorbed cyclohexanone (1683 cm⁻¹) for the pure TiO₂ (anatase) and supported 60% TiO₂/SiO₂ catalysts, respectively, during 100 mins of illumination under reaction conditions. It is qualitatively observed that the pure TiO₂ (anatase) catalyst has a high intensity of product cyclohexanone than adsorbed cyclohexanone and that the opposite is true for the supported 60% TiO₂/SiO₂ catalyst. These differences give insight into the aforementioned reaction pathways.

Another way to examine this data is by tracking the FTIR peak intensity of the species over time as seen in Figure 10. Because the peak at 1712 cm⁻¹ is indicative of the formation of product cyclohexanone and it is known from the TIR studies that pure TiO₂ (anatase) is more active, it can be inferred that the high intensity of the product

cyclohexanone peak relative to the adsorbed peak is an indication of higher activity. Conversely, the supported 60% TiO₂/SiO₂ catalyst is less active in the TIR reactor and the high 1658 cm⁻¹ peak for this catalyst indicates that cyclohexanone is adsorbed on the surface rather than desorbing as a product. This finding on the supported 60% TiO₂/SiO₂ catalyst is an indication that the reaction is desorption limited on catalysts with a smaller particle size and smaller bulk structure. Because the pure TiO₂ (anatase) does not exhibit this accumulation of adsorbed cyclohexanone species, it is concluded that desorption is not as limiting for nanodomains with a larger bulk structure.

The distribution of the adsorbed carboxylates (1562 cm⁻¹) and adsorbed carbonates (1409 cm⁻¹) vary in relative intensity for the pure TiO₂ (anatase) and supported 60% TiO₂/SiO₂ catalysts. Carboxylates and carbonates are unwanted, further oxidation products of cyclohexane. Figure 10 shows that carboxylate and carbonate formation is relatively more significant for the pure TiO₂ (anatase) than for the supported 60% TiO₂/SiO₂ catalyst. Though a discussion of the mechanism of the reaction is outside the scope of the current study, it is important to point out that the increasing peak intensity is an indication of an accumulation of adsorbed species on the catalyst surface and a possible source of catalyst deactivation.³⁹ Recalling that the ATR cell is run in a batch reactor mode, it is quite possible that cyclohexanone readsorbs to form the carboxylates and carbonates. This appears to be the case in the pure TiO₂ catalyst which shows a higher relative intensity for the relevant peaks. Furthermore, given the higher activity, it was expected that the product cyclohexanone peak should have been

much stronger compared to the adsorbed cyclohexanone peak. If readsorption of product cyclohexanone is taking place, it would account for the seemingly low intensity of that respective peak. In the case of the supported 60% TiO₂/SiO₂ catalyst, the intensity of the carboxylate and carbonate peaks is relatively low compared to the cyclohexanone peaks. If product formation is desorption limited for the smaller TiO₂ (anatase) particle, then the cyclohexanone will remain on the surface and not readsorb as frequently to form carboxylates and carbonates. Thus they will not have a chance to accumulate on the catalyst surface. Carneiro *et al.* have studied the effect of TiO₂ (anatase) hydroxyl concentration and particle size for cyclohexane photo-oxidation and found that a high concentration of surface hydroxyls on small particle sizes TiO₂ (anatase) due to their higher surface area was beneficial to cyclohexanone activity, but large particles were more efficient at desorbing cyclohexanone.¹⁹

4.4 Relationships between Electronic Structure of TiO_x Nanodomains and Specific Photoactivity

The band gap of a material is a bulk property that has relevance to the photocatalytic process since it is related to the minimum energy required to generate excitons and make them available to photocatalytic processes.^{52,55} It is known from previous studies on the supported TiO₂/SiO₂ catalysts that the UV-vis-NIR edge energy E_g values, which are related to the optical band gap, decrease with increased TiO₂ loading that parallels increasing titania nanodomain size. A plot of specific photoactivity of cyclohexanone on the different model TiO₂ nanodomains as a function of E_g is depicted in Figure 11. A correlation between E_g and specific activity is not found

because the catalysts with >40% loading of TiO₂ exhibit the same E_g value as pure TiO₂ (anatase). The supported titania NPs with an average dimension of ~7 nm have the same electronic properties or E_g value as pure TiO₂ (anatase) due to their well developed crystalline TiO₂ (anatase) structure. Thus, it can be concluded that while E_g is an appropriate tool for the determination of the wavelength of light necessary to generate excitons in a given material, the bulk nature of the technique does not provide information on the critical surface photocatalytic reactions when nanodomain dispersion is less than 1 and, consequently, the UV-vis edge energy value cannot relate to the specific photoactivity of the model supported TiO₂ nanodomains. This finding corresponds to those found in Chapter 2 for the effect of E_g on photocatalytic water splitting (Ch. 2, Figure 11).

4.5 Role of the SiO₂ Support in Physical and Electronic Structure-Photoactivity Relationships

A physical mixture of 60% TiO₂ (anatase) and 40% SiO₂ support yielded the same ATR-FTIR spectrum as pure TiO₂ (anatase) during cyclohexane photo-oxidation (see Figure 8), but this only demonstrates that the SiO₂ support is inactive for the oxidation products. It is not conclusive as to whether the support plays some role in electronic structure that could result in the lower activity of the supported TiO₂ (anatase) nanoparticles found in the supported 60% TiO₂/SiO₂ catalyst. Participation of the SiO₂ support in trapping of excitons at inactive silanol sites provides an explanation for the desorption limitation of the supported 60% TiO₂/SiO₂ catalyst. PL spectroscopy studies in Chapter 2 indicate that SiO₂ has non-trivial PL decay

properties (Ch. 2, Table 2). The presence of Ti-O-Si bonds can facilitate the migration of electrons to trap states of the SiO₂ support that are inactive sites as indicated by the ATR-FTIR studies on pure SiO₂ and on the physical mixture of TiO₂ and SiO₂. The number of electrons that are likely to participate in surface reactions in the small TiO₂ nanoparticles of the supported 60% TiO₂/SiO₂ catalyst is already lower than in the pure TiO₂ (anatase) sample due to the smaller bulk structure (see Figure 9). If excitons are being trapped at inactive sites associated with the SiO₂ support, the number of excitons available to do the photo-reaction is further decreased. Desorption of cyclohexanone is predicted to require excitons in the form of positively charged holes and any additional causes for deficiency would be detrimental to cyclohexanone product formation.

5. Conclusions

The photo-oxidation of cyclohexane over well-defined TiO_x nanodomains was studied using a top illumination reactor and *in situ* ATR-FTIR spectroscopy to investigate the dependence of activity on nanodomain structure. The trend in cyclohexanone production of the nanodomains proceeded as follows: pure TiO₂ (anatase) (20 nm) > TiO₂ (anatase) nanoparticles (4-11 nm) > surface polymeric TiO₅ (~1 nm) > surface isolated TiO₄ (~0.4 nm). The specific photoactivity was calculated by normalization of the activity by the number of exposed Ti sites and revealed that despite the relatively low number of exposed Ti sites, pure TiO₂ (anatase) containing ~20 nm nanoparticles was the best catalyst for photo-oxidation of cyclohexane. It is

concluded that the contribution of the bulk to the nanodomain structure must be large to yield high specific activity of the photo-reaction. Combining the specific activity data with previous photoluminescence decay data showed that the bulk structure of the catalyst acts as a reservoir for producing a large number of long lived excitons that are more likely to participate in the surface photo-oxidation reaction. The discovery of the necessity of a large bulk structure led to a *structure-activity* relationship for the photo-oxidation of cyclohexane. The *in situ* ATR-FTIR data confirmed the general trend that the larger TiO₂ (anatase) particles are most active and this was evidenced by the formation of adsorbed reaction intermediates and product species detected in the reactant liquid phase. The accumulation of adsorbed cyclohexanone on the surface of less active catalysts containing smaller bulk structures indicates that the reaction is desorption limited on those nanodomains. Finally, it was shown that the SiO₂ support played no direct role in the formation of intermediates or products, but it can contribute to an increased deficiency in positively charged holes required for desorption of product cyclohexanone. The structure-photoactivity relationship between large bulk structure of TiO_x nanodomains and high photoactivity has been demonstrated for two different photocatalytic reactions and it should be taken into consideration for future rational design of improved photocatalysts for all photo-reactions using TiO₂-containing materials.

Acknowledgements:

This research was financially supported by Department of Energy-Basic Energy Sciences grant DE-FG02-93ER14350. Professor Guido Mul and Dr. Chieh-Chao Yang of the University of Twente, Enschede, The Netherlands are thanked for their collaboration in the collection of the ATR-FTIR data. The TIR data was collected at the Technical University of Delft, Delft, The Netherlands with the financial support of the NSF IREE, award No. 0609018.

References

- (1) Mills, A.; Davies, R. H.; Worsley, D. "Water purification by semiconductor photocatalysis," *Chem. Soc. Rev.* **1993**, 22, 417-425.
- (2) Linsebigler, A. L.; Lu, G.; Yates, J. T. Jr., "Photocatalysis on TiO₂ Surfaces: Principles, Mechanism, and Selected Results," *Chem. Rev.* **1995**, 95, 735-758.
- (3) Herrmann, J. M. "Heterogeneous photocatalysis: fundamentals and applications to the removal of various types of aqueous pollutants," *Catal. Today* **1999**, 53, 115-129.
- (4) Alfano, O. M.; Bahnemann, D.; Cassano, A. E.; Dillert, R.; Goslich, R. "Photocatalysis in water environments using artificial and solar light," *Catal. Today* **2000**, 58, 199-230.
- (5) Nishijima, K.; Ohtani, B.; Yan, X.; Kamai, T.; Chiyoya, T.; Tsubota, T.; Murakami, N.; Ohno, T. "Incident light dependence for photocatalytic degradation of acetaldehyde and acetic acid on S-doped and N-doped TiO₂ photocatalysts," *Chem. Phys.* **2007**, 339, 64-72.
- (6) Abe, R.; Kazuhiro, S.; Domen, K.; Arakawa, H. "A new type of water splitting system composed of two different TiO₂ photocatalysts (anatase, rutile) and a IO₃⁻/I⁻ shuttle redox mediator," *Chem. Phys. Lett.* **2001**, 344, 339-344.
- (7) Anpo, M.; Takeuchi, M. "The design and development of highly reactive titanium oxide photocatalysts operating under visible light irradiation," *J. Catal.* **2003**, 216, 505-516.

- (8) Kudo, A.; Kato, H.; Tsuji, I. "Strategies for the Development of Visible-light-driven Photocatalysts for Water Splitting," *Chem. Lett.* **2004**, 33, 1534-1539.
- (9) Usseglio, S.; Damin, A.; Scarano, D.; Bordiga, S.; Zecchina, A.; Lamberti, C. "(I₂)_n Encapsulation inside TiO₂: A Way to Tune Photoactivity in the Visible Region," *J. Am. Chem. Soc.* **2007**, 129, 2822-2828.
- (10) Irie, H.; Miura, S.; Kamiya, K.; Hashimoto, K. "Efficient visible light-sensitive photocatalysts: Grafting Cu(II) ions onto TiO₂ and WO₃ photocatalysts," *Chem. Phys. Lett.* **2008**, 457, 202-205.
- (11) Giannotti, C.; Le Greneur, S.; Watts, O. "Photooxidation of alkanes by metal oxide semiconductors," *Tetrahedron Lett.* **1983**, 24, 5071-5072.
- (12) Du, P.; Moulijn, J. A.; Mul, G. "Selective photo(catalytic)-oxidation of cyclohexane: Effect of wavelength and TiO₂ structure on product yields," *J. Catal.* **2006**, 238, 342-352.
- (13) Du, Peng; Carneiro, J. T.; Moulijn, J. A.; Mul, G. "A novel photocatalytic monolith reactor for multiphase heterogeneous photocatalysis," *Appl. Catal.* **2008**, 334, 119-128.
- (14) Carneiro, J. T.; Berger, R.; Moulijn, J. A.; Mul, G. "An internally illuminated monolith reactor: Pros and cons relative to a slurry reactor," *Catal. Today* **2009**, 147S, S324-S329.
- (15) Carneiro, J. T.; Moulijn, J. A.; Mul, G. "Photocatalytic oxidation of cyclohexane by titanium dioxide: Catalyst deactivation and regeneration," *J. Catal.* **2010**, 273, 199-210.

- (16) Brusa, M. A.; Grela, M. A. "Photon Flux and Wavelength Effects on the Selectivity and Product Yields of the Photocatalytic Air Oxidation of Neat Cyclohexane on TiO₂ Particles," *J. Phys. Chem. B* **2005**, 109, 1914-1918.
- (17) Boarini, P.; Carassiti, V.; Maldotti, A.; Amadelli, R. "Photocatalytic Oxygenation of Cyclohexane on Titanium Dioxide Suspensions: Effect of the Solvent and of Oxygen," *Langmuir* **1998**, 14, 2080-2085.
- (18) Carneiro, J. T.; Yang, C. -C.; Moulijn, J. A.; Mul, G. "The effect of water on the performance of TiO₂ in photocatalytic selective alkane oxidation," *J. Catal.* **2011**, 277, 129-133.
- (19) Carneiro, J. T.; Almeida, A. R.; Moulijn, J. A.; Mul, G. "Cyclohexane selective photocatalytic oxidation by anatase TiO₂: influence of particle size and crystallinity," *Phys. Chem. Chem. Phys.* **2010**, 12, 2744-2750.
- (20) Carneiro, J. T.; Savenije, T. J.; Moulijn, J. A.; Mul, G. "How Phase Composition Influences Optoelectronic and Photocatalytic Properties of TiO₂," *J. Phys. Chem. C* **2011**, 115, 2211-2217.
- (21) Vinu, R.; Madras, G. "Photocatalytic activity of Ag-substituted and impregnated nano-TiO₂," *Appl. Catal. A*, **2009**, 366, 130-140.
- (22) Carneiro, J. T.; Savenije, T. J.; Mul, G. "Experimental evidence for electron localization on Au upon photo-activation of Au/anatase catalysts," *Phys. Chem. Chem. Phys.* **2009**, 11, 2708-2714.

- (23) Carneiro, J. T.; Yang, C. -C.; Moma, J. A.; Moulijn, J. A.; Mul, G. "How Gold Deposition Affects Anatase Performance in the Photocatalytic Oxidation of Cyclohexane," *Catal. Lett.* **2009**, 129, 12-19.
- (24) Carneiro, J. T.; Savenije, T. J.; Moulijn, J. A.; Mul, G. "The effect of Au on TiO₂ catalyzed selective photocatalytic oxidation of cyclohexane," *J. Photochem. Photobiol. A* **2011**, 217, 326-332.
- (25) Deo, G; Andrzej, M.; Wachs, I. E.; Huybrechts, D. R. C.; Jacobs, P. A. "Characterization of titania silicalites," *Zeolites*, **1993**, 13, 365-373.
- (26) Gao, X.; Bare, S.R.; Fierro, J. L. G.; Banares, M. A.; and Wachs, I. E. "Preparation and in-Situ Spectroscopic Characterization of Molecularly Dispersed Titanium Oxide on Silica," *J. Phys. Chem. B* **1998**, 102, 5653-5666.
- (27) Lee, E. L.; Wachs, I. E. "Molecular Design and In Situ Spectroscopic Investigation of Multilayered Supported M1Ox/M2Ox/SiO₂ Catalysts," *J. Phys. Chem. C*, **2008**, 112, 20418-20428.
- (28) Ross-Medgaarden, E. I.; Wachs, I. E.; Knowles, W. V.; Burrows, A.; Kiely, C. J.; Wong, M. S. "Tuning the Electronic and Molecular Structures of Catalytic Active Sites with Titania Nanoligands," *J. Am. Chem. Soc.* **2009**, 131, 680-687.
- (29) Weber, R. S. "Effect of Local Structure on the UV-Visible Absorption Edges of Molybdenum Oxide Clusters and Supported Molybdenum Oxides," *J. Catal.* **1995**, 151, 470-474.

- (30) Gao, X.; Wachs, I. E. "Investigation of Surface Structures of Supported Vanadium Oxide Catalysts by UV-vis-NIR Diffuse Reflectance Spectroscopy," *J. Phys. Chem. B* **2000**, 104, 1261-1268.
- (31) Ross-Medgaarden, E. I.; Wachs, I. E. "Structural Determination of Bulk and Surface Tungsten Oxides with UV-vis Diffuse Reflectance Spectroscopy," *J. Phys. Chem. C* **2007**, 111, 15089-15099.
- (32) Tian, H.; Roberts, C. A.; Wachs, I. E. "Molecular Structural Determination of Molybdena in Different Environments: Aqueous Solutions, Bulk Mixed Oxides, and Supported MoO₃ Catalysts," *J. Phys. Chem. C* **2010**, 114, 14110-14120.
- (33) Tang, J.; Durrant, J. R.; Klug, D. R. "Mechanism of Photocatalytic Water Splitting in TiO₂. Reaction of Water with Photoholes, Importance of Charge Carrier Dynamics, and Evidence for Four-Hole Chemistry," *J. Am. Chem. Soc.* **2008**, 130, 13885-13891.
- (34) Almquist, C. B.; Biswas, P. "The photo-oxidation of cyclohexane on titanium dioxide: an investigation of competitive adsorption and its effects on product formation and selectivity," *Appl. Catal., A* **2001**, 214, 259-271.
- (35) Bürgi, T.; Baiker, A. "In Situ Infrared Spectroscopy of Catalytic Solid-Liquid Interfaces Using Phase-Sensitive Detection: Enantioselective Hydrogenation of a Pyrone over Pd/TiO₂," *J. Phys. Chem. B* **2002**, 106, 10649-10658.
- (36) Ortiz-Hernandez, I.; Williams, C. T. "In Situ Investigation of Solid-Liquid Interfaces by Attenuated Total Reflection Infrared Spectroscopy," *Langmuir* **2003**, 19, 2956-2962.

(37) Andanson, J. –M.; Baiker, A. “Exploring catalytic solid/liquid interfaces by *in situ* attenuated total reflection infrared spectroscopy.” *Chem. Soc. Rev.* **2010**, 39, 4571-4584.

(38) Mojet, B. L.; Ebbeson, S. D.; Lefferts, L. “Light at the interface: the potential of attenuated total reflection infrared spectroscopy for understanding heterogeneous catalysis in water.” *Chem. Soc. Rev.* **2010**, 39, 3643-4655.

(39) Almeida, A. R.; Moulijn, J. A.; Mul, G. “In Situ ATR-FTIR Study on the Selective Photo-oxidation of Cyclohexane over Anatase TiO₂,” *J. Phys. Chem. C* **2008**, 112, 1552-1561.

(40) Almeida, A. R.; Carneiro, J. T.; Moulijn, J. A.; Mul, G. “Improved performance of TiO₂ in the selective photocatalytic oxidation of cyclohexane by increasing the rate of desorption through surface silylation,” *J. Catal.* **2010**, 273, 116-124.

(41) Almeida, A. R.; Berger, R.; Moulijn, J. A.; Mul, G. “Photo-catalytic oxidation of cyclohexane over TiO₂: A novel interpretation of temperature dependent performance,” *Phys. Chem. Chem. Phys.* **2011**, 13, 1345-1355.

(42) Almeida, A. R.; Moulijn, J. A.; Mul, G. “Photocatalytic oxidation of cyclohexane over TiO₂: evidence for a Mars-van Krevelen mechanism,” *J. Phys. Chem. C* **2011**, 115, 1330-1338.

(43) Shimanouchi, T. *Tables of Molecular Vibrational Frequencies Consolidated Volume I*; National Bureau of Standards: Washington, D.C., **1972**; Vol. I.

- (44) Davydov, A. *Molecular Spectroscopy of Oxide Catalyst Surfaces*, Jon Wiley & Sons, Sussex, England, **2003**.
- (45) Bellamy, L. J. *The Infrared Spectra of Complex Molecules: Advances in Infrared Group Frequencies*, 3rd ed.; Chapman and Hall Ltd.: London, 1975; Vol. 2.
- (46) Araujo, P. Z.; Mendive, C. B.; Rodenas, L. A. G.; Morando, P. J.; Regazzoni, A. E.; Blesa, M. A.; Bahnemann, D. "FT-IR-ATR as a tool to probe photocatalytic interface," *Colloids Surf., A* **2005**, 265, 73-80.
- (47) Yates, D. J. C. "Infrared studies of the surface hydroxyl groups on titanium dioxide, and of the chemisorption of carbon monoxide and carbon dioxide" *J. Phys. Chem.* **1961**, 65, 746-753.
- (48) Connor, P. A.; Dobson, K. D.; McQuillan, A. J. "Infrared Spectroscopy of the TiO₂/Aqueous Solution Interface," *Langmuir* **1999**, 15, 2402-2408.
- (49) Ekstrom, G. N.; McQuillan, A. J. "In Situ Infrared Spectroscopy of Glyoxylic Acid Adsorption and Photocatalysis on TiO₂ in Aqueous Solution," *J. Phys. Chem. B* **1999**, 103, 10562-10565.
- (50) Nakamura, R.; Nakato, Y. "Primary Intermediates of Oxygen Photoevolution Reaction on TiO₂ (Rutile) Particles, Revealed by in Situ FTIR Absorption and Photoluminescence Measurements," *J. Am. Chem. Soc.* **2004**, 126, 1290-1298.
- (51) Wachs, I. E.; Roberts, C. A. "Monitoring surface metal oxide catalytic active sites with Raman spectroscopy," *Chem. Soc. Rev.* **2010**, 39, 5002-5017.
- (52) Shi, J; Chen, J; Feng, Z.; Chen, T.; Lian, Y.; Wang, X.; Li, C. "Photoluminescence Characteristics of TiO₂ and Their Relationships to the

Photoassisted Reaction of Water/Methanol Mixtures,” *J. Phys. Chem. C* **2007**, 111, 693-699.

(53) Murphy, A. B. “Band-gap determination from diffuse reflectance measurements of semiconductor films, and application to photoelectrochemical water-splitting,” *Sol. Energy Mater. Sol. Cells* **2007**, 91, 1326-1337.

(54) Yang, C. -C.; Yu, Y. -H.; van der Linden, B.; Wu, J. C. S.; Mul, G. “Artificial Photosynthesis over Crystalline TiO₂-Based Catalysts: Fact of Fiction?” *J. Am. Chem. Soc.* **2010**, 132, 8396-8406.

(55) Singha, A.; Dhar, P.; Roy, A. “A nondestructive tool for nanomaterials: Raman and photoluminescence spectroscopy,” *Am. J. Phys.* **2005**, 73, 224-233.

Table 1: Summary of the structure and average size as determined by XANES and TEM, respectively, of the supported TiO₂ nanodomains in the supported TiO₂/SiO₂ catalysts and for pure TiO₂ (anatase). Data is reproduced from reference 28 except where indicated.

x% TiO₂/SiO₂	Structure	Average Domain Size (nm)	E_g (eV)
1	Isolated Surface TiO₄ Species	0.4*	4.3
12	Polymeric Surface TiO₅ Species	1**	3.4
30	TiO₂ (anatase) – 2D Rafts	4	3.3
40	TiO₂ (anatase) – 2D Rafts	7	3.2
60	TiO₂ (anatase) – 3D Nanoclusters	11	3.2
100	TiO₂ (anatase) – Nanoparticles	20†	3.2

*Estimated for Isolated TiO₄ Unit **Estimated for Surface TiO₅ Polymer

†From reference 19

Table 2: Dispersion and number of exposed sites for the supported TiO₂/SiO₂ catalysts.

x% TiO ₂ /SiO ₂	Dispersion	Exposed Sites (x 10 ¹⁹)
1	1.00*	1.52
12	0.90	16.43
30	0.23	10.21
60	0.08	7.43
100	0.045	5.70

*Assumed to be fully dispersed since the sample contains only surface isolated TiO₄ sites.

Figure 1: Production of cyclohexanone over 6h in the TIR for supported 1, 12, 30, and 60% TiO₂/SiO₂ catalysts. The supported 12 and 30% TiO₂/SiO₂ catalysts have had their production normalized to reflect the same mass of TiO₂ as the supported 60% TiO₂/SiO₂ catalyst. No detectable product formation was observed for the supported 1% TiO₂/SiO₂ catalyst.

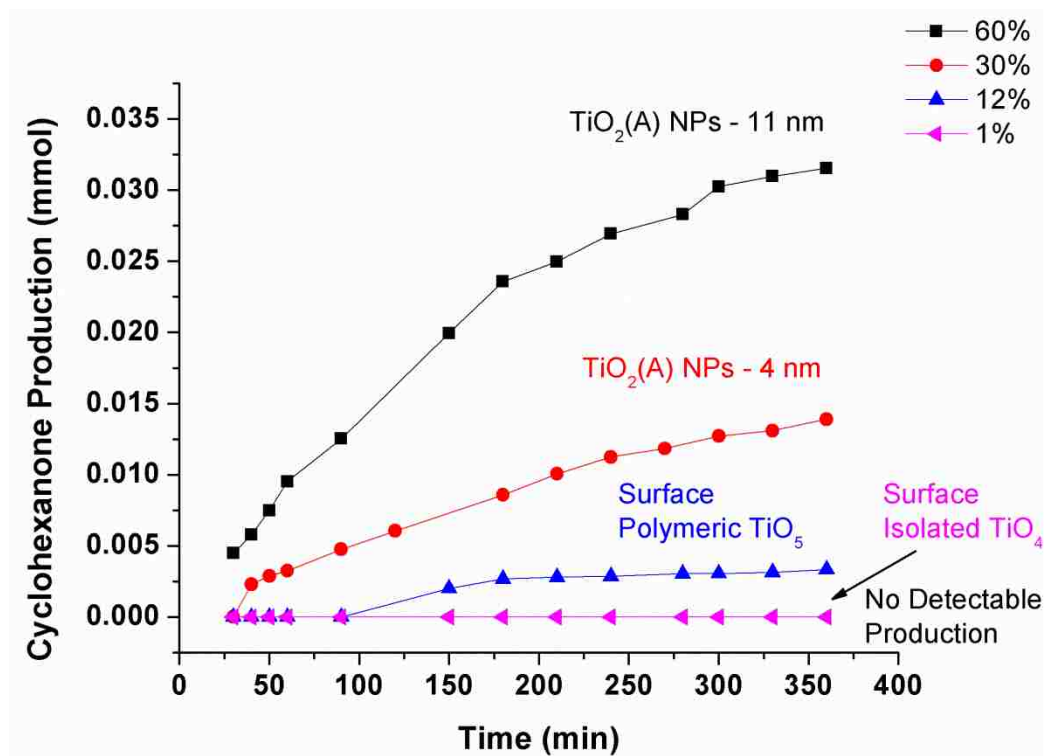


Figure 2: Cyclohexanone production at 5h reaction time as a function of (a) weight percent loading of TiO_2 and (b) average nanodomain size in the supported $\text{TiO}_2/\text{SiO}_2$ catalysts. Domain structure is indicated for reference.

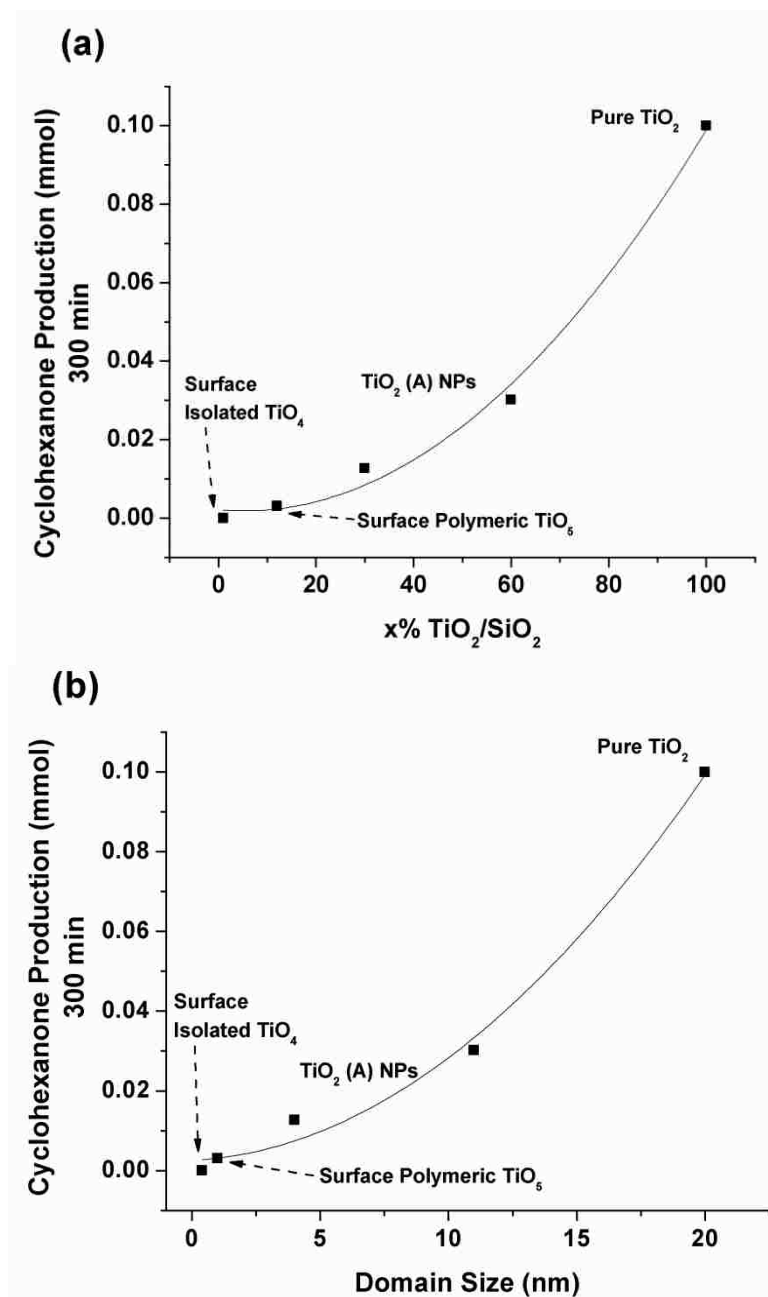


Figure 3: Cyclohexane photo-oxidation activity (mmol cyclohexanone/g Ti/h) for cyclohexanone production on TiO₂ nanodomains as a function of the average domain size. The TiO₂ nanodomain structure is shown for reference.

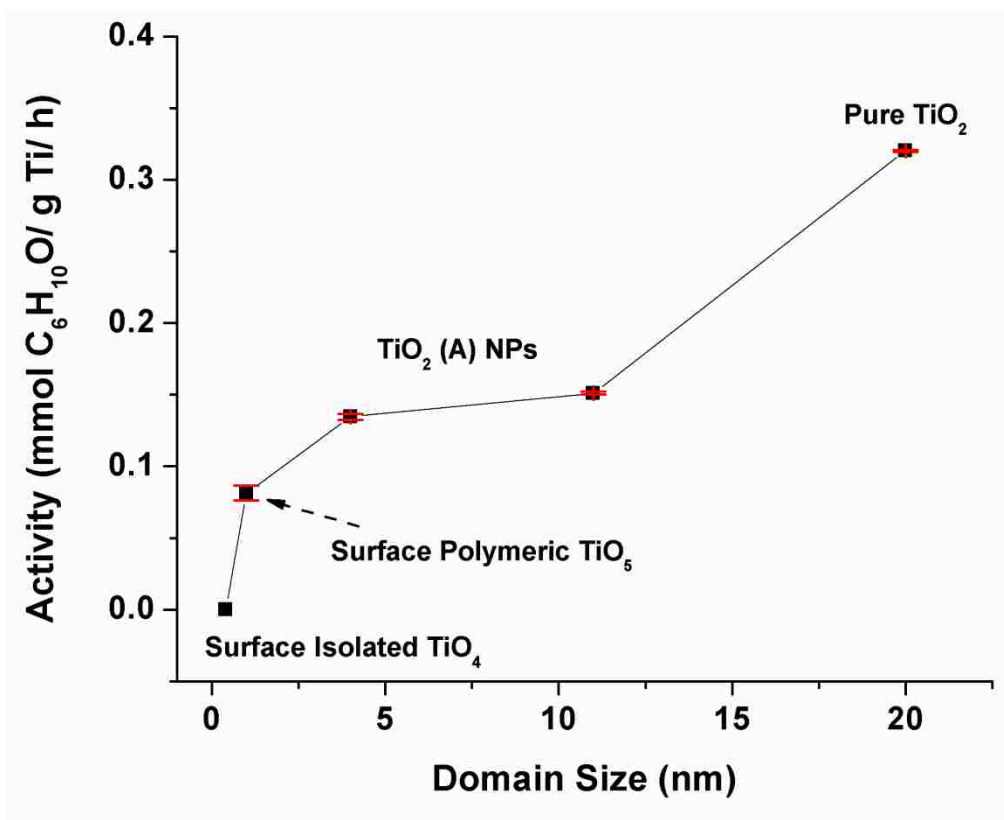


Figure 4: Specific activity (mmol cyclohexanone/exposed Ti site/h) of TiO₂ nanodomains for cyclohexanone production during photo-oxidation of cyclohexane as function of averages domain size. The TiO₂ nanodomain structure is shown for reference.

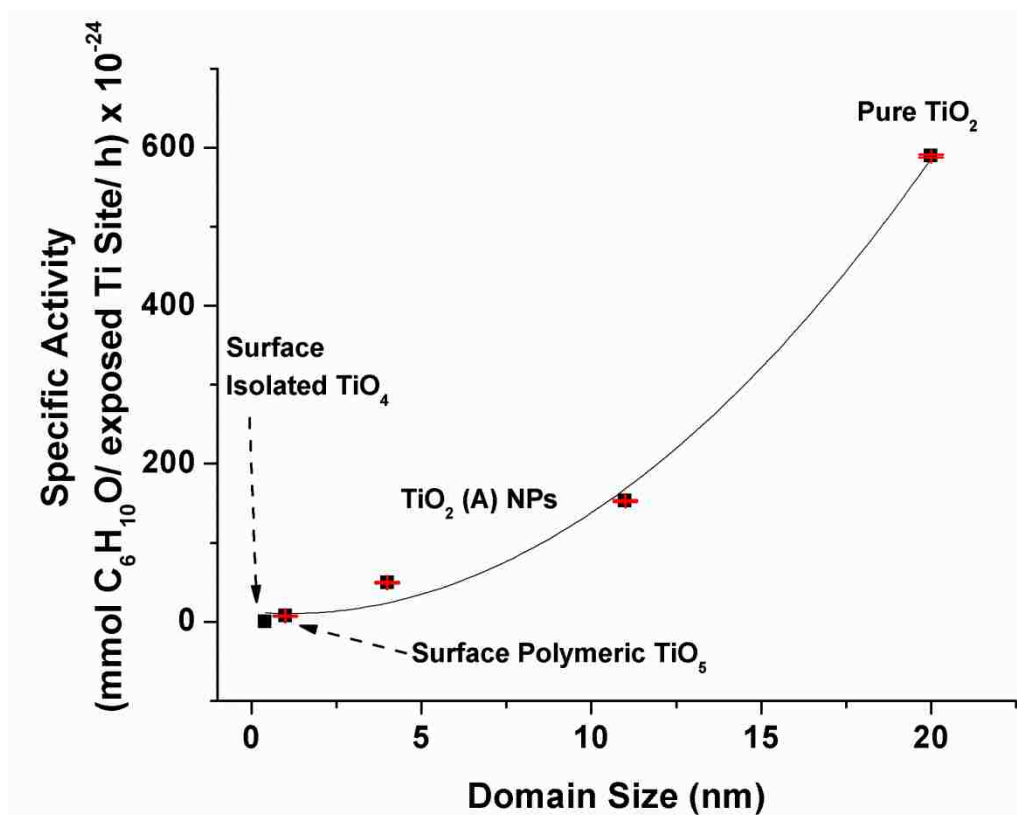


Figure 5: ATR-FTIR spectra of the supported $\text{TiO}_2/\text{SiO}_2$ catalysts after 100 minutes of illumination during photo-oxidation of cyclohexane. The spectrum for the pure SiO_2 support material is shown for reference.

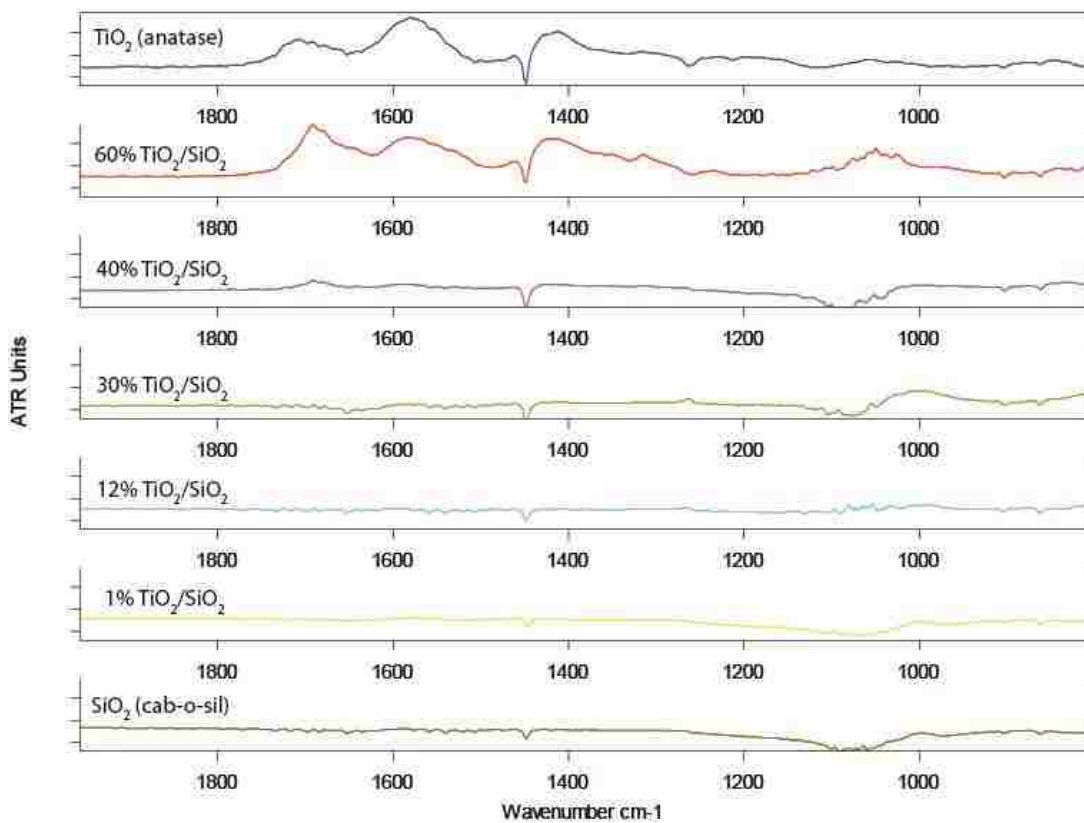


Figure 6: ATR-FTIR spectra composing the time profile (0-100 mins of illumination) for photo-oxidation of cyclohexane over pure TiO₂ (anatase). Negative peaks are due to reactant consumption. Each spectrum represents a 10 min interval.

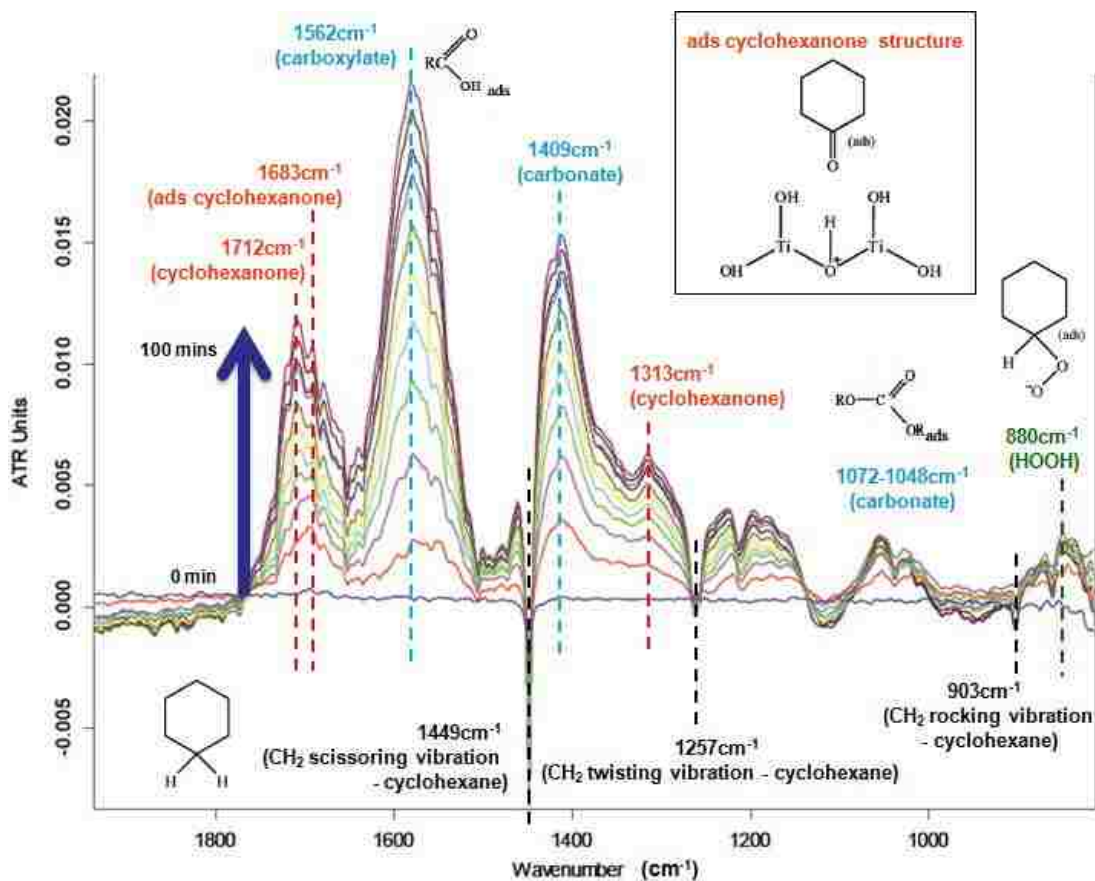


Figure 7: ATR-FTIR spectra composing the time profile (0-100 mins of illumination) for photo-oxidation of cyclohexane over the supported 60% TiO₂/SiO₂ catalyst containing ~11 nm spherical nanoparticles. Negative peaks are due to reactant consumption. Each spectrum represents a 10 min interval.

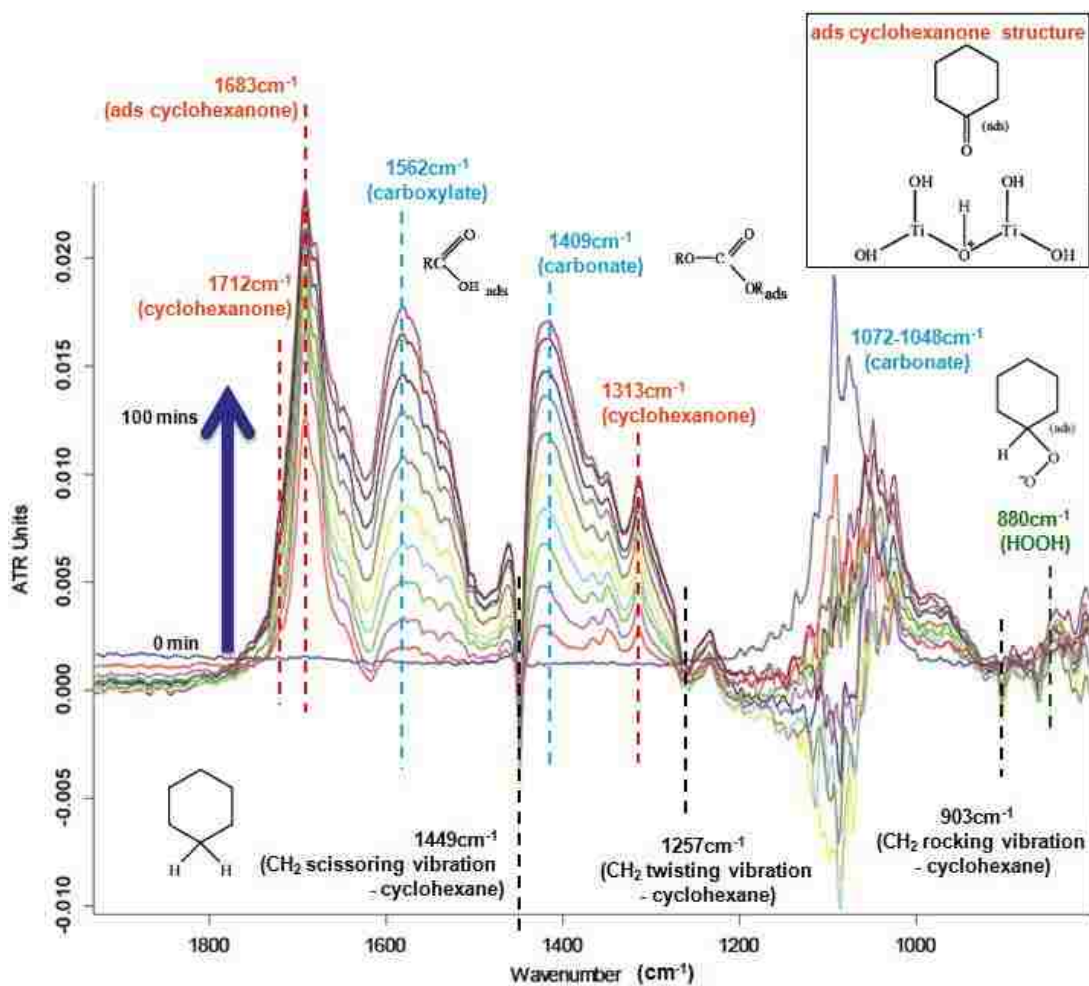


Figure 8: Comparison of the ATR-FTIR spectra composing the time profile (0-100 mins of illumination) for photo-oxidation of cyclohexane over pure TiO₂ (anatase) and a physical mixture of 60% TiO₂ (anatase) and 40% SiO₂ support by weight. The peaks highlighted in red correspond to cyclohexanone vibrations and the peaks highlighted in blue correspond to carbonate/carboxylate vibrations.

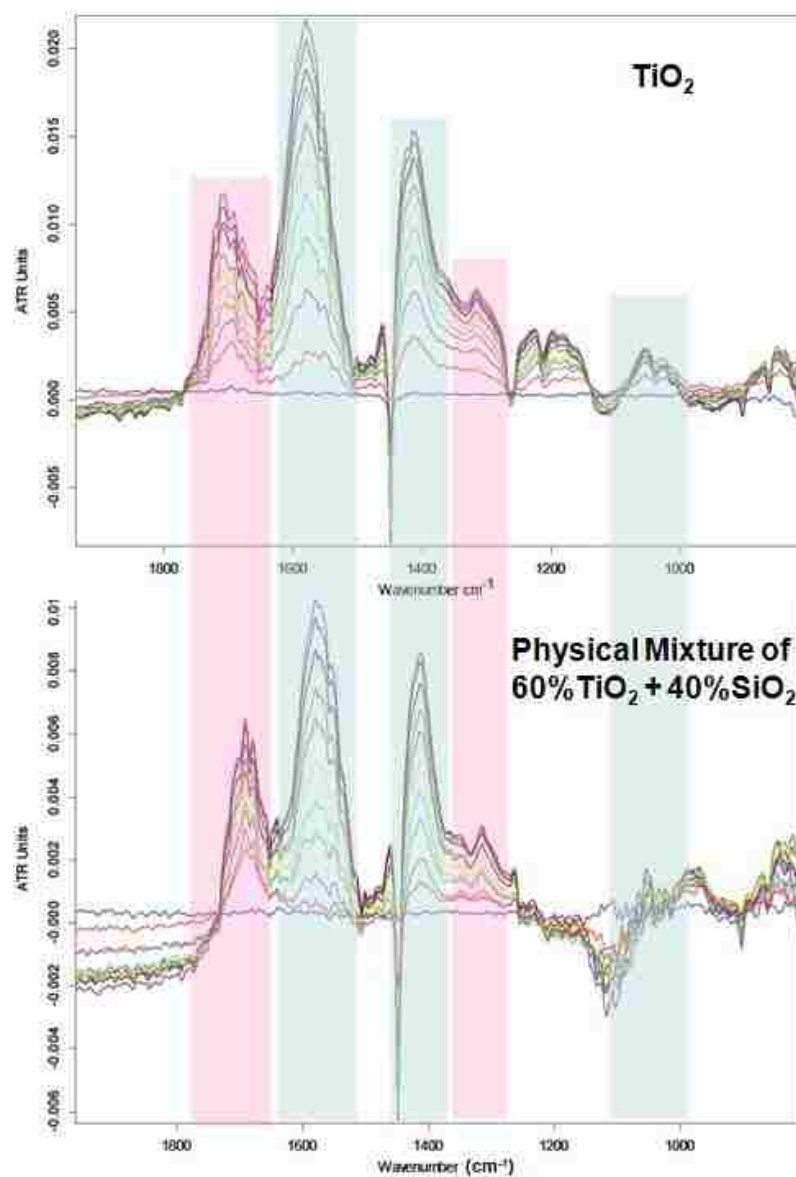


Figure 9: Specific activity (mmol cyclohexanone/exposed Ti site/h) of TiO₂ nanodomains for cyclohexanone production during photo-oxidation of cyclohexane as function of the relative contribution of the number of Ti sites producing electrons with (a) fast and (b) slow recombination dynamics.

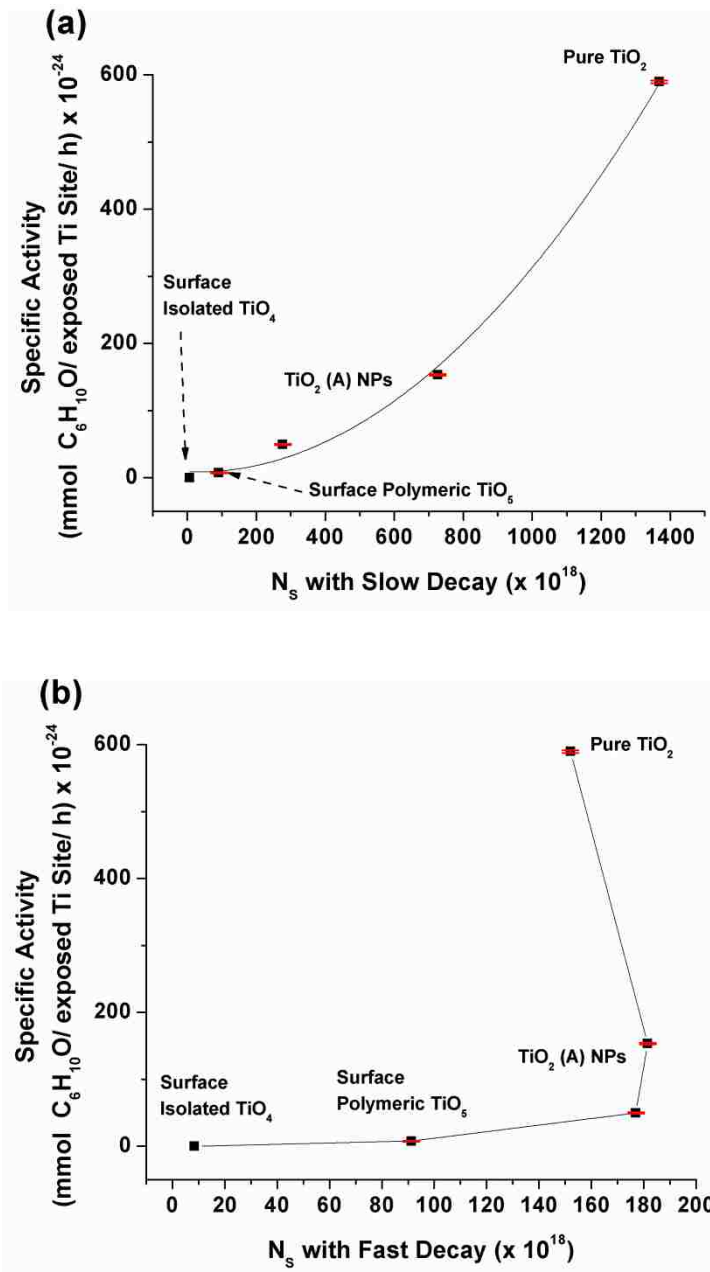


Figure 10: Evolution of the peak intensity for desorbed cyclohexanone (1710 cm^{-1}), adsorbed cyclohexanone (1680 cm^{-1}), carboxylates (1580 cm^{-1}), and carbonates (1414 cm^{-1}) over 100 mins of illumination time for pure (a) TiO_2 (anatase) and the (b) supported 60% $\text{TiO}_2/\text{SiO}_2$ catalyst.

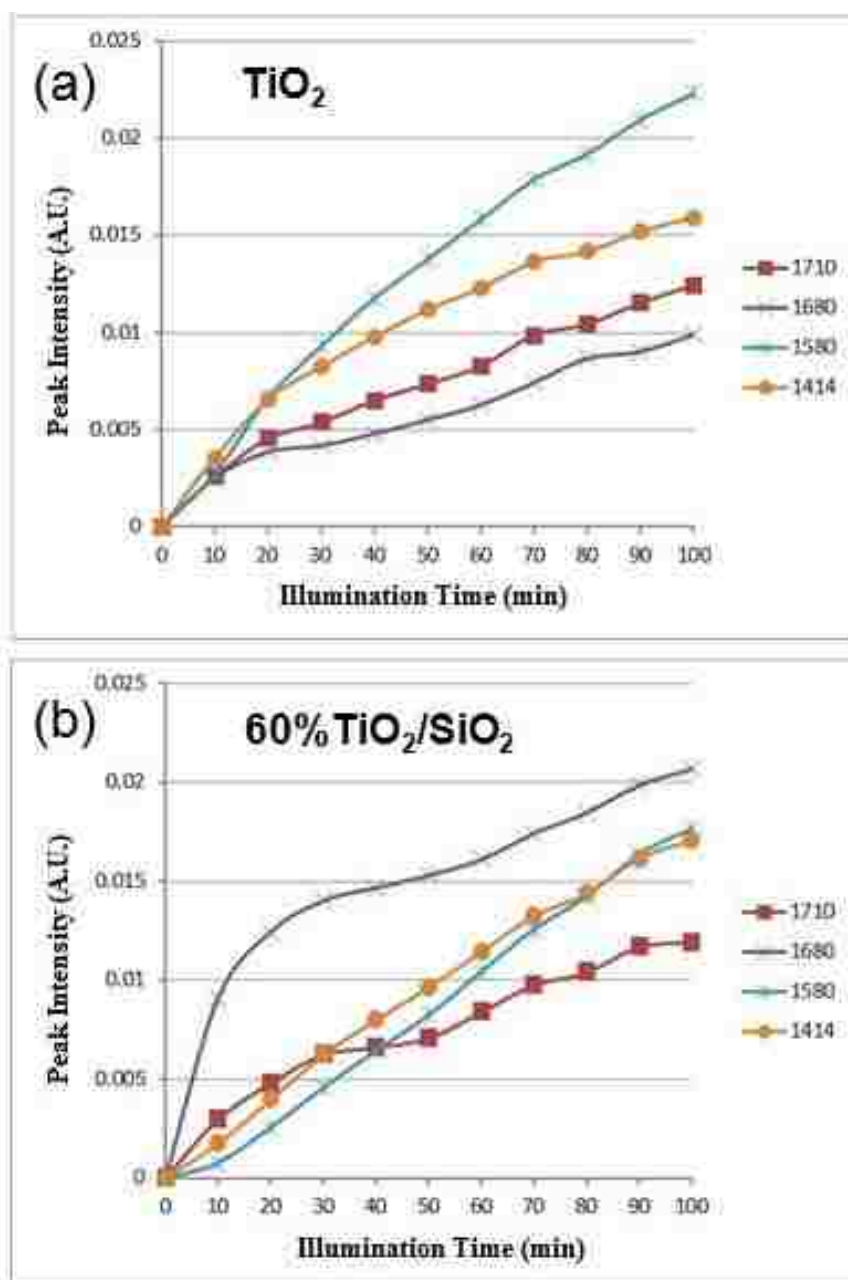
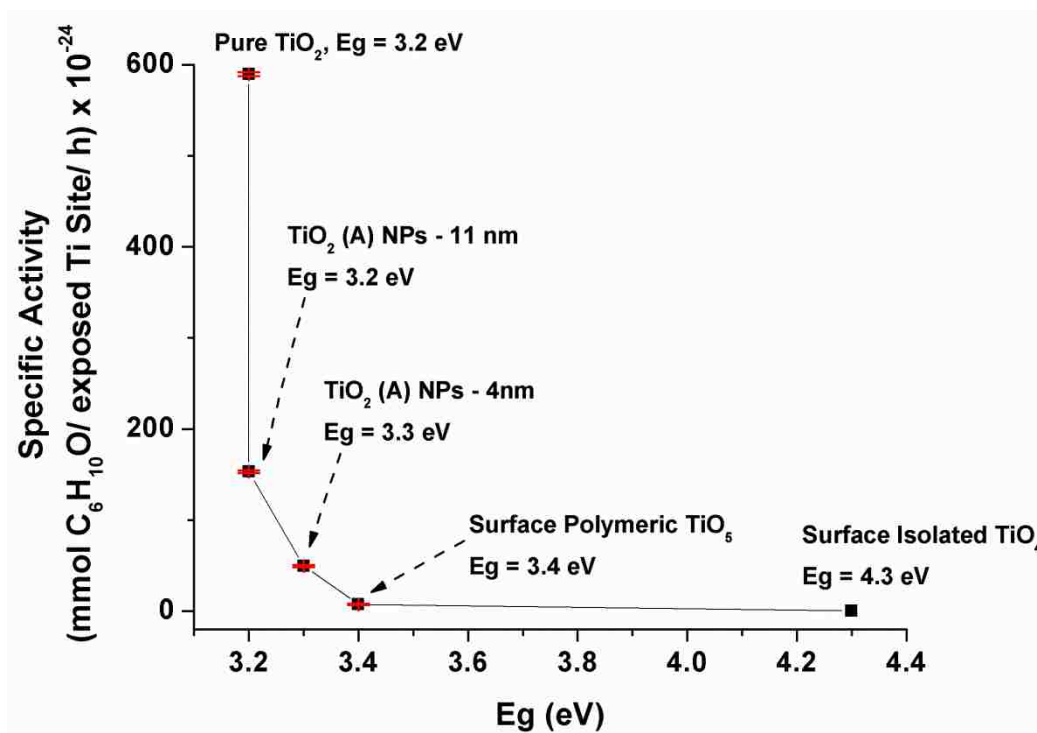


Figure 11: Specific activity (mmol cyclohexanone/exposed Ti site/h) of TiO₂ nanodomains for cyclohexanone production during photo-oxidation of cyclohexane as function of edge energy, Eg. The TiO₂ nanodomain structure and the exact Eg value are shown for reference.



Chapter 3

Supporting Information

The calculation of dispersion and the assumptions necessary to do so are discussed in Chapter 2 and the Supporting Information of Chapter 2 and the reader is referred to the relevant sections for more information. Figure S2 plots the dispersion and number of exposed Ti sites as a function of weight percent loading of TiO₂ for the supported TiO₂/SiO₂ catalysts. This is done for only the catalysts used in the study found in the current chapter. It is necessary to show this data a second time because the particle size of the pure TiO₂ (anatase) (20 nm average particle size) is different from that used in Chapter 2. Figure S2 shows that the number of exposed Ti sites for 20 nm particle size, pure TiO₂ (anatase) is still the lowest of all the TiO_x nanodomains found in the supported catalysts with a weight percent loading of 40 and above. The mass of TiO₂ in the supported 1% TiO₂/SiO₂ catalyst is significantly low so as to cause it to have the fewest number of exposed Ti sites.

Figure S2 shows the specific activity as a function of the decay time of photoluminescence (PL) as determined by the PL decay study on the supported TiO₂/SiO₂ catalysts in Chapter 2. In agreement with the findings of Chapter 2, Figure S2 shows that the longer decay time of the surface isolated TiO₄ nanodomain in the supported 1% TiO₂/SiO₂ catalyst is not an indication of high specific activity. This was thought to be a benefit to catalytic activity, however the property is irrelevant if an insufficient number of excitons are generated that decay with a long lifetime. The

low contribution of slow decay was shown to be the true for the smaller domain sizes and is believed to be related to the bulk of the nanodomain.

Figure S1: Dispersion (black) and the number of exposed Ti sites (blue) as a function of the average domain size in the supported $\text{TiO}_2/\text{SiO}_2$ catalysts. TiO_2 domain structure is indicated for reference.

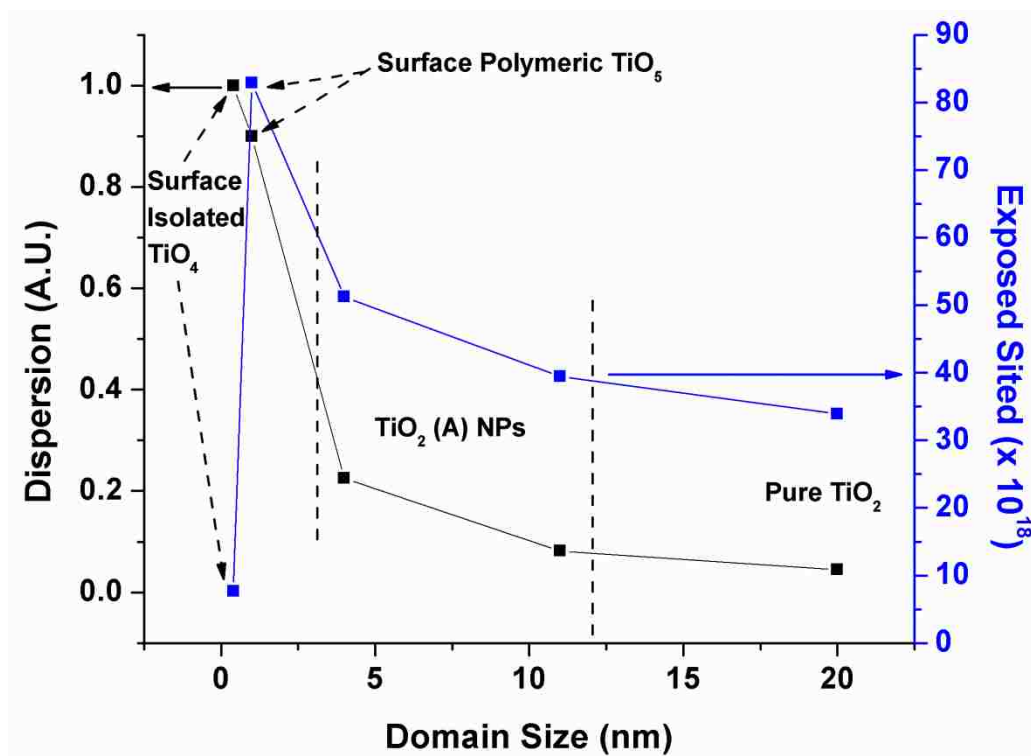
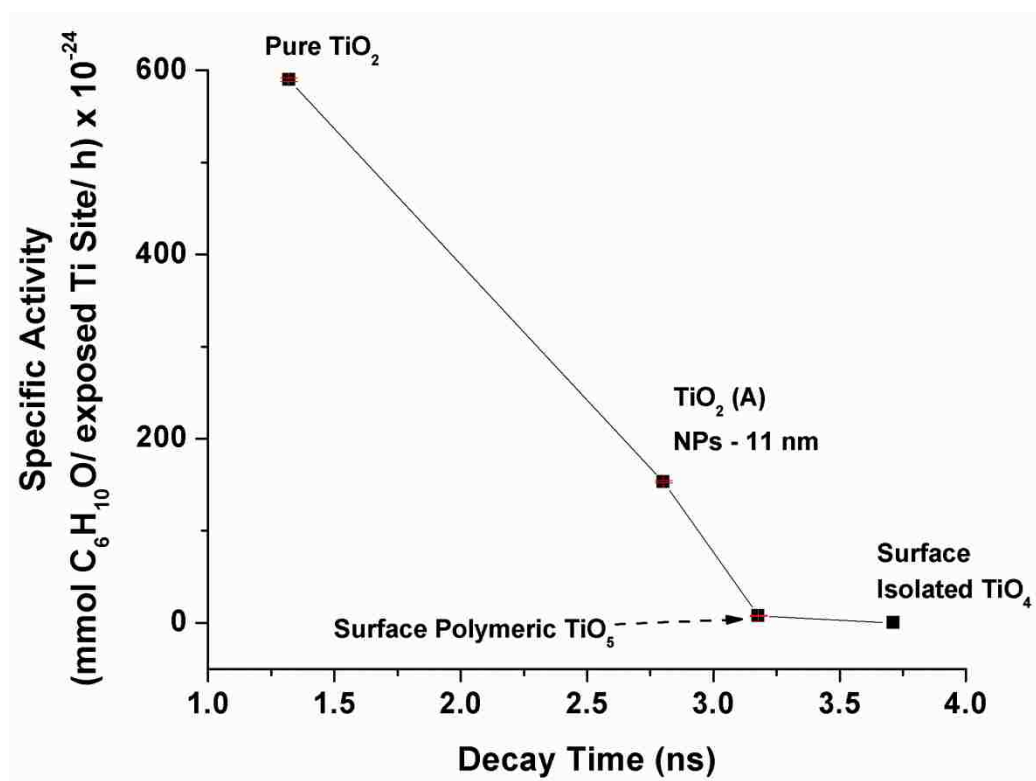


Figure S2: Specific activity (mmol/exposed Ti site/h) of TiO₂ nanodomains for cyclohexanone production during photo-oxidation of cyclohexane as function of the slow decay time, t₂, as determined the exponential decay of photoluminescence of the supported TiO₂/SiO₂ catalysts.



CHAPTER 4

***In situ* ATR-FTIR and Raman Spectroscopic Studies of Surface Reaction Intermediates during Photocatalytic Splitting of H₂O over TiO₂**

Abstract

Attenuated total reflectance (ATR) Fourier transform infrared (FTIR) spectroscopy was utilized to probe the formation of intermediates on TiO₂ thin films during the photocatalytic water splitting reaction. TiO₂ thin film thickness was calculated theoretically for the ideal penetration depth of the ATR evanescent wave and found to be insufficient for the collection of spectra due to the high absorption of liquid H₂O and the difficulties associated with forming an ideal thin film. Useful spectroscopic measurements were still made by observing the increase of a broad spectral region from 1000 – 1200 cm⁻¹ under UV illumination. The region was shown to be related to intermediates formed during water splitting and not an artifact of illumination by performing the experiment in the absence of H₂O. ATR-FTIR and Raman spectroscopy were performed during adsorption of was performed to assign possible intermediates in the 1000 – 1200 cm⁻¹. Raman spectroscopy was shown to be ineffective for intermediate detection during water splitting. The detection of superoxides by electron paramagnetic resonance spectroscopy during oxygen

adsorption, coupled with theoretical and experimental results, indicate that the 1000 – 1200 cm^{-1} region is related to a variety of species including superoxides, OH, and OOH vibrations. The absence of evidence for Ti-OOH vibrations is in agreement with the experimental conditions used and the kinetic relevance of such a species.

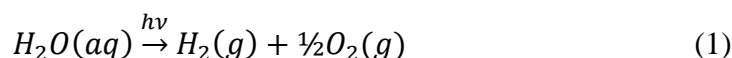
1. Introduction

Photocatalytic splitting of H_2O to H_2 and O_2 has been identified as a possible route to produce alternative, sustainable non-carbon fuel and improvements of the efficiency of such a process have motivated the study of this heterogeneous photocatalytic reaction. Electrolysis of H_2O into H_2 and O_2 on TiO_2 electrodes was discovered in 1972 and TiO_2 has become the most studied photocatalyst.¹ Titania-based materials, however, are semiconductor oxides with relatively wide bandgap energies (3.0 eV for rutile and 3.2 eV for anatase) and have been found to be relatively inefficient photocatalysts for H_2 production during water splitting when compared to a large variety of other photocatalysts for this reaction.² Furthermore, TiO_2 does not efficiently utilize the solar spectrum because excitation wavelengths of less than 400 nm are required to activate the photocatalyst.

In the last decade, modification of TiO_2 photocatalysts by doping³ and development of advanced semiconductor mixed metal oxide photocatalysts² have been developed in an attempt to improve the efficiency of water splitting. The improvements in efficiency of TiO_2 catalysts are accomplished via broadening light absorption into the visible range of the spectrum, preventing recombination of electron (e^-) and hole (h^+)

pairs, and increasing intrinsic catalysts properties such as phase, surface area, particle size, hydroxyl concentration.⁴⁻⁸ The advanced, non-TiO₂-based oxide catalysts have been shown to improve the activity for H₂ production by order of magnitude over TiO₂ (~100 μmol/g catalyst/h).² Kato *et al.* have developed a lanthanum-doped NaTaO₃ material impregnated with a NiO cocatalyst that has reported an H₂ activity of 19,800 μmol/g catalyst/h.⁹ Maeda *et al.* have developed a visible light active (Ga_{1-x}Zn_x)(N_{1-x}O_x) solid solution surface loaded with Rh and Cr yielding an H₂ activity of 3835 μmol/g catalyst/h.¹⁰ These novel water splitting catalysts, however, still fall below the desired solar efficiency. In addition, fundamental surface characterization studies still have not been reported and spectroscopic evidence of the mechanism is scarce. Therefore, despite the relatively low efficiency and activity of the reaction on TiO₂, spectroscopic investigation of TiO₂ during photocatalytic water splitting reaction conditions will greatly add to the fundamental understanding of mechanistic aspects such as surface adsorbed intermediates, catalytic active site, and rate-determining-step.

Photocatalytic decomposition of H₂O to H₂ and O₂, occurs via the half reaction:



The mechanism of water splitting is proposed to proceed in three main steps, qualitatively described as: 1) absorption of photons to form electron and hole pairs, 2) electron and hole separation and migration to surface catalytic active sites, and 3) the overall surface chemical reactions described by Equation 1.¹¹ The reaction steps of water splitting were schematically shown in Chapter 1 (Ch. 1, Figure 3). It is proposed that water is oxidized to form O₂ at surface catalytic active sites associated

with positively charge holes and that H^+ is reduced to H_2 at surface catalytic active sites associated with electrons. Regarding spectroscopic detection of the intermediates of the water splitting mechanism, two difficulties can be identified. First, the initiation of photocatalytic reactions is believed to proceed through the formation activated oxygen species, such as superoxide radicals (O_2^-), that must be formed through O_2 reduction by e^- and that the oxidizing h^+ excitons can generate surface hydroxyl radicals ($\bullet OH$).^{12,13} The formation of such strongly oxidizing radicals is believed to be the main driving force behind photocatalytic reactions on TiO_2 surfaces¹² and is in agreement with recent density functional theory (DFT) studies.¹⁴ The characteristic lifetimes of such species is believed to be quite short (< 100 ns), especially if they are not involved in the rate-determining-step of the reaction mechanism, which makes spectroscopic detection difficult.^{13,14} Second, the proposed intermediate structures such as surface hydroxyls, superoxides, and peroxides often yield spectral vibrations that are closely related to the characteristic FTIR bands of the reactant H_2O .^{14,15-17} Because H_2O has extremely high absorption of IR light, it can often mask such closely related, relevant reaction intermediates.¹⁸

The second difficulty can be addressed through the use of attenuated total reflectance (ATR) Fourier transform infrared (FTIR) spectroscopy. ATR-FTIR has been shown to be a technique that can successfully probe the solid-liquid interface that exists in many photocatalytic reaction systems.¹⁸⁻²² Almeida *et al.* used ATR-FTIR to study cyclohexane photo-oxidation and identified key adsorbed intermediates that allowed the proposal of a possible reaction mechanism.²³⁻²⁶ ATR-FTIR spectroscopy

also was employed during photo-oxidation of water over TiO₂ (rutile) to determine the primary reaction intermediates. It was found that surface peroxo species (Ti-OOH), stretching $\nu(\text{O-O})$ vibration at 838 cm⁻¹, accumulate on the titania surface with increasing reaction time.¹⁶ The appearance of this peak appears to be related to the presence of 10 mM Fe³⁺ used as an electron trapping agent in the H₂O reactant solution, which also shifts the pH to 2.4. It is still unclear, however, if Ti-OOH plays a vital role in the water splitting mechanism over TiO₂ in the absence of toxic chemicals that act as electron and/or hole traps.

The identification of surface Ti-OOH groups under relevant water splitting photo-reaction conditions is further complicated by the predicted transient nature of such an intermediate. Density functional theory (DFT) calculations by Valdés *et al.* find that the formation of surface hydroxyl groups at the coordinatively unsaturated TiO₂ sites is the rate-determining-step of water splitting and predict that because Ti-OOH is not involved in this step its presence will be difficult to experimentally detect.¹⁴ The detection of such a transient reaction intermediate would require spectroscopic collection times with a temporal resolution of the same scale. Using ATR-FTIR combined with rapid-scan collection, Sivasankar *et al.* observed a hydroperoxide intermediate on an iridium oxide-based catalyst during visible-light driven water photo-oxidation.²⁷ After a 1s pulse of excitation light, the detected OOH band at ~830 cm⁻¹ was observed only during the first 610 ms. The timescale of the detection is kinetically relevant for this short-lived reaction intermediate, especially if it is not involved in the rate-determining-step as proposed by DFT. Therefore, it will be

beneficial to use ATR-FTIR under relevant water splitting photo-reaction conditions to probe for the existence of other reaction intermediates that are more closely associated with the DFT-predicted rate-determining-step. A separate DFT study by Mattioli *et al.* calculated the predicted vibrations for a broad range of possible relevant adsorbed oxygen-containing surface intermediates on TiO₂ (anatase) during photo-reaction and their study will be used as an aid for the current ATR-FTIR studies on photocatalytic water splitting over TiO₂.¹⁷

2. Experimental

2.1 Thin Film Preparation and SEM Imaging

Thin films of TiO₂ were deposited on the ZnSe IRE for ATR-FTIR and on glass slides for scanning electron microscopy imaging using a technique developed by Kumnorkaew *et al.* and modified for the deposition of TiO₂ particles.²⁸ TiO₂ powder (Degussa P-25) was first suspended in ethanol (200 proof) at a concentration of ~0.18 g/mL, the resulting suspension having a paste like consistency. The suspension was then mixed well with a vortex mixer for 2-3 min. Thorough dispersion of the suspension was achieved using a sonic dismembrator (model 550, Fisher Scientific, Pittsburgh, PA). The sonication was performed for 1h in a pulse mode of 1 sec on/1 sec off at 20 kHz and 50% power. The suspension was then stirred with a spatula prior to deposition. A template for deposition was created using 3M Scotch Magic Tape #810 with a thickness of 62.5 μm. The tape was placed on both sides of the ZnSe crystal or parallel to the length of the glass slides to create a channel-like

template for deposition. Approximately 300 μL of the suspension was placed at one end of the channel and spread across the ZnSe or glass substrate using a glass slide as a deposition blade. The deposited suspension was allowed to dry for 10 minutes before the tape was removed. The film was allowed to dry overnight and was further treated at 100 $^{\circ}\text{C}$ for 1h prior to use to drive off any remaining ethanol.

Scanning electron microscopy (SEM) was performed using a FEI/Philips XL-30 ESEM (Environmental Scanning Electron Microscope) featuring a conventional hairpin tungsten source and using a secondary electron (SE) detector. The beam voltage was 5.00 kV and a working distance of 23.5 μm was used, resulting in a magnification of 1469x. The thin films prepared on glass slides were fractured along the width, mounted in the environmental chamber of the SEM, and the sample was tilted to 90 degrees to examine the thickness of the prepared thin films.

2.2 ATR-FTIR Spectroscopy Theory, Calculations, and Determination of Thin Film Thickness

The positioning of the TiO_2 catalyst/water reactant interface at the penetration depth of the evanescent wave associated with the ATR-FTIR technique allows direct spectroscopic measurement at the interface while minimizing the unwanted contribution of the liquid H_2O reactant's contribution to the spectrum. The evanescent wave is a standing wave and forms perpendicular to the IRE surface with a penetration depth d_p into the sample that is dependent on the wavelength of light λ , the angle of incidence θ , and the refractive indices of the IRE and the sample:

$$d_p = \frac{\lambda}{2\pi \sqrt{(n_1^2 \sin^2 \theta - n_2^2)}} \quad (2)$$

where n_1 is the refractive index of the IRE and n_2 is the refractive index of the sample.²² The calculation of penetration depth is complicated by the fact that the index of refractive of the sample is affected by the relative porosity of the material and by the material filling the pores. Mojet *et al.* calculated that the penetration depth for a sample with pores filled with water increased 1.3 times over a one with pores filled with air.¹⁸ The effect of the porosity and material filling the pore space can be reflected in a calculation of the effective refractive index n_{eff} of the sample:

$$n_{eff} = \sqrt{(1 - \phi)n_c^2 + \phi n_p^2} \quad (3)$$

where ϕ is the relative porosity and n_c and n_p are the refractive indices of the catalyst and the material filling the pores, respectively. Using Equations 2 and 3, the penetration depth can be calculated for an ATR-FTIR system studying water splitting on a TiO₂ thin film, but the theoretical prediction does not always work in practice due to difficulties in creating an ideal TiO₂ thin film.²¹

For the TiO₂ thin film in contact with a ZnSe IRE in the current study, the penetration depth of the evanescent wave can be estimated theoretically using Equations 2 and 3 for TiO₂ thin film coatings of varying porosity. The refractive index, though a function of wavelength, was taken to be constant for the sample materials and IRE. To calculate the effective refractive index for the sample using Equation 2, the refractive index at 2000 cm⁻¹ for TiO₂ and H₂O was used (2.40 and 1.33, respectively).²⁹ A constant refractive index for the ZnSe IRE of 2.42 was used to

calculate the penetration depth of the evanescent wave as a function of the wavelength (expressed in wavenumbers).²² Figure 1 shows the results of the calculation for various porosities using the effective refractive index of the TiO₂ coating with its pores filled with water. As the wavenumber of the light approaches the cutoff of the ZnSe IRE (~700 cm⁻¹) the penetration depth increases significantly. For the spectral range of interest (4000 – 800 cm⁻¹) the penetration depth remains below ~3 μm, especially at higher porosities. Therefore, it is theoretically estimated that a thin film coating of ~3 μm should allow direct probing of the solid-liquid interface during ATR-FTIR of water splitting on TiO₂ thin films.

Ortiz-Hernandez *et al.* showed that the theoretical predictions do not apply in practice due to the difficulties involved in creating an ideal sample thin film.²¹ This was also found to be true for the water splitting sample system in the current study, as the high contribution of the water background made collection of spectra impossible for thin films of ~3 μm (not shown). Therefore, their estimate of 5d_p was employed to avoid the contribution of water that is outside of the film. Using the film deposition technique described below, thin films averaging 15-20 μm were deposited on the ZnSe crystal for the current study. The film thickness was characterized by SEM imaging and is shown in Figure 2. The thin films were observed to be smooth and uniform in thickness and packing, however cracking of the film was still possible.

2.3 *In Situ* ATR-FTIR Spectroscopy

The ATR-FTIR cell used was a Harrick Horizon multiple internal reflections accessory coupled with a temperature controlled flow through cell. The flow through

cell consisted of two plates; the top plate contained a quartz window for illumination of the sample and the bottom plate contained a ZnSe crystal IRE. The sample volume of the cell was 0.47 mL. The ZnSe IRE had dimensions of $50 \times 10 \times 2 \text{ mm}^3$ and a 45° angle of incidence of the IR beam, yielding 11 internal reflections. Figure 3a shows a photo of the top plate of the ATR flow through cell containing the quartz window for illumination, inlet/outlet flow ports, and the thermocouple and heater port for temperature control. The FTIR spectra were recorded using a Thermo Scientific Nicolet 8700 Research FT-IR Spectrometer equipped with a liquid cooled MCT detector. Illumination of the sample during photocatalytic water splitting was achieved using a 150 W Xe lamp (Newport Apex Arc Lamp Source, model 71228) and light was directed to the sample using a standard grade fused silica fiber optic bundle (0.125in diameter, Newport).

In situ ATR-FTIR spectra were collected for water splitting on the TiO_2 thin films after first treating the samples at 100°C to remove residual ethanol using the temperature control capabilities of the cell. The sample was heated and cooled at a rate of $10^\circ\text{C}/\text{min}$ to avoid thermal damage to the ZnSe IRE. The reactant DI water was introduced into the cell under dark (no UV illumination) conditions by using an attached syringe to fill the sample volume of the flow through cell. Spectra were collected under dark conditions for 5 mins prior to illumination. Collection under illumination was done for 30 mins, followed by a post reaction collection under dark conditions. Figure 3b shows photo of the entire *in situ* ATR-FTIR experimental setup for illumination during photocatalytic water splitting with the syringe for liquid

injection into the sample volume and the fiber optic cable for illumination by the 150 W Xe lamp.

2.4 Raman Spectroscopy

Raman spectroscopy studies were performed with a Horiba-Jobin Yvon LabRam-IR High Resolution instrument equipped with a 532 nm visible light laser source (Coherent Compass 315M-150, Nd:YAG double diode pumped laser) and a 325 nm UV light laser source (Kimmon, model IK5751I-G, He-Cd laser). The Raman spectrometer was equipped with a confocal microscope equipped with a 50X long working distance objective (Olympus BX-30-LWD) for the visible laser and a 15X objective (OFR LMU-15X-NUV) for the UV laser. The spectrometer was optimized for the best spectral resolution by employing a 900 grooves/mm grating (Horiba-Jobin Yvon 51093140HR) for the visible laser and a 2400 grooves/mm grating (Horiba-Jobin Yvon 53011140HR) for the UV laser. The Raman spectral resolution for both gratings was $\sim 2 \text{ cm}^{-1}$. The Rayleigh scattered light was rejected with holographic notch filters (Kaiser Super Notch) with a window cutoff of $\sim 100 \text{ cm}^{-1}$ and $\sim 300 \text{ cm}^{-1}$ for the visible and UV lasers, respectively. The scattered light from the sample, after Rayleigh scattering removal, was directed to a UV/visible sensitive LN₂-cooled CCD detector (Horiba-Jobin Yvon CCD-3000V). The LabSpec 5 software was used to calibrate each laser line and grating to minimize errors in linearity across the full Raman spectrum range and to collect the Raman spectra. The ambient Raman spectra were collected on the TiO₂ thin films on glass slides. *In situ* Raman spectra were collected by using a micro-pipette to place liquid on the catalyst surface (DI H₂O or

HOOH, 30% solution in water, EMD Chemicals). During the *in situ* Raman spectroscopy using the visible laser line the 150 W Xe lamp described above for the ATR-FTIR experiments was employed to initiate the photocatalytic reaction. For *in situ* Raman spectroscopy using the UV laser line, the 325 nm laser itself was employed to initiate the photocatalytic reaction.

2.5 *In Situ* Electron Paramagnetic Resonance Spectroscopy

Electron paramagnetic spectroscopy (EPR) was performing using Bruker ESP 300 spectrometer operating at 9 GHz. The EPR spectrometer was equipped with an *in situ* cell with temperature control and gas flow capabilities. *In situ* EPR spectra were collected during the formation of defects on TiO₂ under reducing conditions (5% H₂/He at 30 mL/min). The temperature was ramped at 5 K/min to 505 K during reduction. Oxygen was introduced to the cell (10% O₂/He) to adsorb at defect sites on the catalyst sample. EPR spectra were collected during all experimental phases at a rate of ~1 spectrum/min.

3. Results

3.1 HOOH Adsorption and Intermediate Detection

The ATR-FTIR spectra were initially collected during the formation adsorbed HOOH species on the TiO₂ thin film surface. Spectra were taken every ~1.2 min for 30 min with a mirror velocity of 0.6329 cm/s and 72 scans/spectrum. The background used was the TiO₂ thin film in contact with a water layer to remove the contribution of the water in the HOOH solution. The spectral range centered around the peroxy

vibrations ($950\text{-}750\text{ cm}^{-1}$) are shown in Figure 4. The band at 877 cm^{-1} is assigned to the peroxy stretching $\nu(\text{O-O})$ vibration of unbound, aqueous HOOH and this FTIR band appears immediately.^{16,17} As HOOH adsorbs over time, the relatively broad band centered at 834 cm^{-1} increases in intensity and stabilizes after ~ 15 min. Nakamura *et al.* have assigned this band to the $\nu(\text{O-O})$ of an adsorbed peroxy species bound to Ti (Ti-OOH).¹⁶ The assignment is supported by DFT studies of the photo-reduction of oxygen on TiO_2 (anatase).¹⁷

An additional peak was observed in the spectral region between 1175 and 975 cm^{-1} shown in Figure 5. The minor peak at 1121 cm^{-1} was not identified in the experimental studies previously found in the literature. This peak can be assigned to $\nu(\text{O-O})$ for adsorbed superoxide (O_2^-) species and is in agreement with DFT predictions¹⁷ and superoxide oxygen stretches found experimentally on other oxide surfaces.³⁰

Raman spectra were also collected during adsorption of HOOH solutions. Pure 30% HOOH/ H_2O solution (not shown) was found to produce a very strong peak at 878 cm^{-1} for the $\nu(\text{O-O})$ vibration of aqueous, unbound hydrogen peroxide. To determine if the intensity of this peak was masking the adsorbed Ti-OOH vibration, solutions of 1.0 and 0.1% HOOH/ H_2O were prepared and used in adsorption experiments. The resulting Raman spectra after 10 min of HOOH adsorption for both solution concentrations are shown in Figure 6. Note that although Raman spectra are typically displayed as a function of increasing Raman shift, Figure 6 is displayed as a function of decreasing Raman shift for ease of comparison to the convention used in IR

spectroscopy. Raman spectroscopy is sensitive to TiO₂ (anatase) crystal vibrations, and an overtone from the TiO₂ (anatase) in the sample can be seen at a Raman shift of 795 cm⁻¹.³¹ For the 1.0% HOOH solution in Figure 6a, the 878 cm⁻¹ peak for HOOH(aq) is present however there is still no trace of the adsorbed Ti-OOH vibration. Further decreasing the solution concentration to 0.1% HOOH yielded a Raman spectrum that showed no signs of adsorption (Figure 6b)

3.2 *In Situ* ATR-FTIR and Raman Spectroscopy of Water Splitting on TiO₂ Thin Films

3.2.1 ATR-FTIR Spectroscopy

In situ ATR-FTIR spectra were collected under real photocatalytic water splitting reaction conditions (in air, ambient temperature and pressure, and UV illumination) using a series collection method. The mirror velocity was increased to 3.7974 cm/s and the 50 scans/spectrum was used resulting in a sampling interval of 12.11 sec/spectrum. The spectrometer maintained a resolution of 4 cm⁻¹. The background was collected after H₂O was injected into the sample volume and under dark conditions. Illumination began after ~2 minutes of collection time, illumination continued for 23 minutes, and finally the system was returned to dark conditions for the final 5 minutes of collection yielding a total experiment time of 30 minutes.

Figure 7a shows the results of the experiment as a 2D contour map with dark blue indicating areas of low intensity and red indicating areas of high intensity. The figure is labeled to explain the areas of extremely high intensity. These areas are related to liquid phase water that is not interacting with the TiO₂ photocatalyst and are assigned

to O-H stretching vibration $\nu(\text{O-H})$ at $\sim 3000\text{-}3600\text{ cm}^{-1}$ and the O-H scissors-bending mode $\delta(\text{O-H})$ centered at 1635 cm^{-1} .¹⁸ The area of high intensity at 700 cm^{-1} and below is related to the wavenumber cutoff of the ZnSe IRE. When the UV illumination begins at 2 minutes an area of increased intensity in the range $1000\text{ - }1200\text{ cm}^{-1}$ is observed for the duration of the illumination time. When the UV lamp is turned off, the intensity of this region begins to decrease. Vibrations in this region could be related to stretching vibrations $\nu(\text{O-O})$ from superoxides^{17,30} or the bending mode $\delta(\text{O-H})$ of peroxides.^{15,17} Specific peaks could not be resolved due to the high level of noise introduced by the inconsistent water background, but an analysis of the peak area from $1000\text{ - }1200\text{ cm}^{-1}$ quantitatively confirmed the change intensity with illumination (Figure 7b).

To ensure that the spectral features that appear in the range of $1000\text{-}1200\text{ cm}^{-1}$ were related to photocatalytic water splitting, the experiment was repeated several times and also performed in the absence of water. Figure 8 shows the peak area as a function of time for a UV illumination with and without the presence of water. The illumination was performed such that the dark/illuminated/dark durations of time were 5/30/15 min. For the experiment in the absence of water, the water was removed by pretreating the sample at $100\text{ }^{\circ}\text{C}$ prior to illumination and the background used was that of the dried TiO_2 thin film at ambient temperature. The spectral features in the $1000\text{ - }1200\text{ cm}^{-1}$ range do not appear in the absence of water indicating.

3.2.2 Raman Spectroscopy

In situ Raman spectroscopy during water splitting on TiO₂ thin films was performed using two techniques. It was first attempted to simultaneously illuminate the sample with the 150 W Xe lamp and collect Raman spectra with the visible 532 nm laser line as an excitation source. Simultaneous visible Raman and illumination proved to be impossible because the CCD detector was immediately saturated by the large amount of scattered light from the water on the TiO₂ thin film.

To simultaneously illuminate the sample to initiate photocatalytic water splitting and collect Raman spectra the UV laser (325 nm) was employed to serve both functions. The UV Raman requires long collection times (~2 min), therefore the laser was allowed to illuminate the sample for at least 10 min before collection of a spectrum. Spectra were collected under several conditions and are displayed in Figure 9. The Raman spectrum of the TiO₂ thin film is shown for reference and the strong bands associated with TiO₂ (anatase) phase are labeled “A” in the figure. The addition of the reactant water made no detectable difference in the spectrum. The same is true for using a 10 mM Fe³⁺/H₂O solution as was invoked in the literature.¹⁶ Two unidentified bands appear in all the spectra in Figure 9. These bands at 851 and 971 cm⁻¹ may be artifacts, but they are in no way involved with the water splitting reaction as they were present in the spectrum for ambient TiO₂ and are unaffected by the use of isotopically labeled D₂O as the reactant.

4. Discussion

4.1 Identification of Relevant Intermediates

It was necessary to identify possible intermediate vibrations in ATR-FTIR and Raman spectroscopy in order to later make peak assignments for the photo-reaction and facilitate understanding of what can be expected to occur during water splitting. Adsorption of HOOH experiments were carried out under ambient conditions in accordance with the study by Nakamura *et al.* to ensure the current experimental setup could reproduce the previous work and identify relevant intermediates. The HOOH adsorption ATR-FTIR measurements were found to be in agreement with Nakamura *et al.* for the $\nu(\text{O-O})$ stretching vibrations of both aqueous, unbound HOOH and adsorbed Ti-OOH giving confidence in the current experimental setup. An additional weak peak, however, was detected at 1121 cm^{-1} (Figure 5) and was not previously identified. This peak can be assigned to the $\nu(\text{O-O})$ stretch of adsorbed superoxide. This assignment is supported by DFT and experimental results on other oxide surfaces and will be discussed below.

Further support for the formation of relatively stable adsorbed superoxide (O_2^-) species was obtained from EPR spectroscopy. The formation of surface oxygen defects can be induced in the TiO_2 surface by treating the sample at elevated temperature in a reducing environment (5% H_2/He , 30 mL/min). When oxygen defects are formed, the defect can trap electrons at the anionic vacancies forming so-called F centers or color centers.³² The F center is highly EPR active and can be seen for reduced TiO_2 as an intense symmetric signal in Figure 10. Furthermore, F center formation can be induced by irradiation³² and the signal was found to increase with UV illumination (not shown). The addition of 10% O_2/He into the EPR cell after

reduction caused rapid consumption of the F center signal and resulting in the formation of asymmetric O_2^- signal (Figure 10). The signal shows resonance at applied magnetic fields that correspond to the g-tensor predicted for O_2^- species.³² From this data, which was obtained at high temperature, it can be concluded that the superoxide formation on TiO_2 should proceed at the ambient conditions found in photocatalytic water splitting. Furthermore, the formation of F centers is linked to UV illumination, therefore the formation of O_2^- can be expected to participate in water splitting and is a possible detectable intermediate.

Raman spectroscopy, unfortunately, yielded no useful information on adsorbed peroxy Ti-OOH or superoxy species. The use of 1.0 and 0.1% HOOH/ H_2O solutions was to be certain the intensity of the aqueous, unbound HOOH peak at 877 cm^{-1} . Figure 6a shows that despite the low intensity of this band for adsorption in the 1% HOOH/ H_2O solution, no additional signals could be found and this may be due to the broad tailing of the TiO_2 (anatase) overtone centered at 795 cm^{-1} . It is known from the ATR-FTIR experiments that under the experimental conditions used for HOOH adsorption, Ti-OOH readily forms on the surface. The absence of a Ti-OOH vibration, therefore, does not provide evidence that it is not present and it may be that it is Raman inactive or masked by the TiO_2 (anatase) overtone.

4.2 Intermediates Detected During *In Situ* Spectroscopy of Water Splitting Over TiO_2 Thin Films

The difficulty of creating an ideal TiO_2 thin film yielding highly resolved ATR-FTIR features is reflected in the 2D contour map of Figure 7a. The contribution of the

absorption of IR by H₂O can be clearly observed and, although the highest intensities are centered around the $\nu(\text{O-H})$ and $\delta(\text{O-H})$ vibrations, the water is likely to contribute to an inconsistent background over the entire spectral range and will be a detriment to resolving reaction intermediate FTIR peaks. Regardless of the inability to resolve specific FTIR peaks, meaningful spectral information was obtained by tracking the peak area in regions that were affected by UV illumination (Figure 7b). The increased intensity of the broad region from 1000 – 1200 cm⁻¹ coincides exactly with the start of UV illumination and the decrease in intensity similarly responds to the absence of UV illumination. The increased intensity is evidence for the formation of photo-reaction intermediate species related to water splitting and a large number of possible dioxygen vibrations have been assigned in this region. DFT calculations have predicted that the $\nu(\text{O-O})$ for adsorbed O₂⁻ occurs at 1194 cm⁻¹ on TiO₂ (anatase) (1 0 1).¹⁷ Adsorbed hydroperoxo species (Ti-OOH⁻) were predicted to have $\delta(\text{O-H})$ at 1151 cm⁻¹ and two-fold coordinated OH groups exhibit $\delta(\text{O-H})$ around 1075 cm⁻¹. Furthermore, the assignment of the previously unseen band at 1121 cm⁻¹ during HOOH adsorption (Figure 5) to adsorbed superoxide species agrees with the DFT results and experimental results for adsorbed O₂⁻ on CeO₂. The multitude of species yielding vibrations in this range supports the observation of increased peak area from 1100-1200 cm⁻¹ during illumination to initiate water splitting on TiO₂. The variety of species also contributes to the inability to resolve a single intense peak in this region.

The absence of an observable FTIR peak at 838 cm⁻¹ for the $\nu(\text{O-O})$ of Ti-OOH in Figure 7a may be due to the inconsistent background and the relative proximity of this

region to the ZnSe cutoff, but it is also likely due to the effect of pH on the formation of this species. The use of 10 mM Fe³⁺ solution was predicted to act an electron scavenger to suppress the formation of surface intermediates caused by electrons and to increase the number of intermediates formed by holes.¹⁶ The Fe³⁺ solution, however, also introduced an acidic environment of pH = 2.4. It was argued by Mattioli *et al.* that the experimental assignment of this band to a neutral OOH bound to Ti was not supported due to variations in the pH during the experiments.¹⁷ The presence of hydroperoxo groups is still possible, but DFT predicts their $\nu(\text{O-O})$ vibration to be closer to 971 cm⁻¹ and their $\delta(\text{O-H})$ vibrations to be in the 1000-1200 cm⁻¹ range of interest to the current study.

These conclusions based on pH considerations suggest that the absence the Ti-OOH FTIR peak in Figure 7a may not be only related to the inconsistent background. Furthermore, the importance of the experimental conditions, such as pH, is highlighted in regards to the identification of intermediates under relevant experimental conditions. It is not desirable to introduce Fe³⁺ to the reactant H₂O for photocatalytic water splitting if the process is to be clean especially when this accomplished using FeCl₃. Also, when a mechanism is proposed for water splitting over TiO₂, the species involved in the rate-determining-step are usually the most readily detectable by spectroscopic methods. If the detection of intermediates is affected by pH, mechanisms proposed are only applicable at that pH. DFT calculations by Valdés *et al.* suggest that Ti-OOH species do not play a role in the rate-determining-step and should be difficult to detect spectroscopically. Their calculations predict that the

formation of hydroxyl groups at the coordinatively unsaturated TiO₂ sites is the rate-determining-step. When this is coupled with the predicted vibrations for OH species and the observed increase in the 1000-1200 cm⁻¹ in the current ATR-FTIR studies, a more complicated picture of the relevant intermediates formed during water splitting on TiO₂ begins to form.

Regarding Raman spectroscopy of TiO₂ thin films under water splitting conditions utilizing the UV laser as both an excitation for Raman and to initiate the photo-reaction, it is apparent from Figure 9 that little could be concluded. The 325 nm laser contributes photons of high enough energy to initiate photo-excitation, however it may be that the power is not significant to produce detectable Raman bands. The odd bands that appear at 851 and 971 cm⁻¹ are concluded to be insignificant as they were present under dry conditions and were unaffected by isotopically labeled D₂O. 10 mM Fe³⁺/H₂O solution was used to see if the lower pH would yield an intermediate formation, but no change was observed. Because the simultaneous illumination with a high powered UV lamp and collection of Raman spectra was not possible, it is concluded that unless transient experiments are utilized, Raman spectroscopy is likely not an ideal experimental technique for monitoring intermediate formation on TiO₂ during photocatalytic water splitting.

4.3 ATR-FTIR in the Absence of H₂O.

It is necessary to confirm that the increase in the spectral region predicted to contain relevant photocatalytic intermediates (1000 – 1200 cm⁻¹) is not due to an artifact caused by shifts in the baseline related UV illumination. This was achieved by

performing the illumination in the absence of the reactant H₂O on a TiO₂ thin film that was first dehydrated for 1h at 100 °C. The spectral features in the 1000 – 1200 cm⁻¹ range do not appear in the absence of water indicating they are indeed related to photo-reaction over the TiO₂ catalysts. Furthermore, no significant increase in the baseline of the spectra was observed over the duration of the experiment under both illuminated and dark conditions. The species detected from 1000 – 1200 cm⁻¹ can also be concluded to be related to water splitting, rather than gaseous O₂ adsorption since they do not appear under UV illumination in the absence of H₂O. Finally, it can be seen in Figure 8 that the initial increase in intensity corresponding with the start of illumination is qualitatively observed to have different kinetics than the decrease in intensity when the UV illumination is ceased. This suggests that they are related to different mechanistic steps, i.e. adsorption and desorption. The decrease in the initial maximum intensity during illumination is also of interest as it is observed in both Figures 7b and 8. It is difficult to speculate what the cause of the fluctuations in intensity is because such a broad range of vibrations are being tracked and the changes cannot be linked to a specific resolved peak.

4.4 TiO₂ Thin Film Thickness

The ability to probe the solid/liquid interface using the ATR-IR technique depends on the penetration depth of the evanescent wave from the IRE/sample interface and the thickness of the sample coating on the IRE.^{18,21,22} If the sample coating is too thin, the liquid's contribution will be significant and it can mask the detection of intermediates. If the coating is too thick, the evanescent wave will interact only with the sample and

the solid/liquid interface will not be probed. Figure 1 shows the wavenumber dependence of the penetration depth of TiO₂ thin films on the ZnSe IRE. The increase in penetration depth at wavenumbers approaching the cutoff of ZnSe is in agreement with previous calculations in the literature giving confidence in the current calculations.¹⁸ The calculations show the penetration depth decreasing as porosity increases, but the trend is not significant. Only curves for porosities at and above $\phi = 0.5$ are shown because it was found that minimum porosity of the thin film is required any penetration to occur. This finding is not an issue because it has been shown that thin films of TiO₂ (P-25) prepared in a similar fashion have a porosity of $\phi \approx 0.8$.³³ It was concluded that a film thickness of $\sim 3 \mu\text{m}$ would be sufficient to approximate the penetration depth at relevant wavenumbers, i.e. 1200 cm^{-1} and below. It was found that this thickness was not sufficient to minimize the water contribution to the ATR-FTIR spectrum and this finding is in agreement with Ortiz-Hernandez *et al.* who showed explained that the difficulty lied in creating an ideal sample thin film.²¹ Therefore, their estimate of $5d_p$ was employed to avoid the contribution of water that is outside of the film. Despite the uniformity of the thickness and packing seen in the SEM image of the film shown in Figure 2 cracking of the film was observed and likely contributed to the inconsistent water background observed in the subsequent ATR-FTIR spectra in this study. Despite this finding, meaningful ATR-FTIR spectral features were still obtained, but film thickness is an area which requires further study into the optimization for water splitting. Better control and knowledge of the film thickness and porosity is required. These findings also suggest that the

calculation of film thickness cannot ignore the dependence of refractive index on wavelength for all the materials of the system, i.e. ZnSe, H₂O, and TiO₂.

5. Conclusions

ATR-FTIR and Raman spectroscopy were employed to identify the intermediates formed during photocatalytic water splitting. Adsorption of HOOH confirmed that Ti-OOH species could be detected using ATR-FTIR, but Raman spectroscopy provided no information on adsorbed peroxo species. Additionally, a previously undetected weak peak assigned to adsorbed O₂⁻ was detected as a possible intermediate during water splitting. ATR-FTIR of TiO₂ thin films under water splitting conditions is deterred by the contribution of high absorption by liquid H₂O and highly resolved peaks could not be detected. The region from 1000-1200 cm⁻¹, which is predicted to be related to various oxygen vibrations by DFT and experimental oxygen adsorption on other metal oxides, shows a significant increase in intensity during UV illumination under water splitting photo-reaction conditions. This region does not respond to UV illumination in the absence of reactant H₂O. It is concluded that the broad spectral region is related to surface superoxo $\nu(\text{O-O})$ vibrations and several OOH or OH $\delta(\text{O-H})$ vibrations. It cannot be determined if the OOH vibrations are related to Ti-OOH due to the absence of the associated $\nu(\text{O-O})$ vibrations and time resolved ATR-FTIR and DFT do not support Ti-OOH detection under relevant photo-reaction conditions. EPR spectroscopy and DFT calculations, however, support the presence of superoxides and OH species, respectively.

Acknowledgements:

This research was financially supported by Department of Energy-Basic Energy Sciences grant DE-FG02-93ER14350. Professor Guido Mul and Ana Rita Almeida of the Technical University of Delft, Delft, The Netherlands were instrumental in the design of the ATR-FTIR experiments. William Mushock of the Department of Materials Science and Engineering at Lehigh University is thanked for helping obtain the SEM images. Hervé Vezin at the École Nationale Supérieure de Chimie de Lille is thanked for aiding in the collection and interpretation of the EPR spectra. Jeff Christenson and his colleagues at Harrick Scientific are thanked for designing the flow through ATR cell.

References

- (1) Fujishima, A.; Honda, K. "Electrochemical photolysis of water at a semiconductor electrode," *Nature* **1972**, 238, 37-38.
- (2) Osterloh, F. E.; "Inorganic Materials as Catalysts for Photochemical Splitting of Water," *Chem. Mater.* **2008**, 20, 35-54.
- (3) Litter, M. I. "Heterogeneous photocatalysis, Transition metal ions in photocatalytic systems," *Appl. Catal. B* **1999**, 23, 89-114.
- (4) Anpo, M.; Takeuchi, M. "The design and development of highly reactive titanium oxide photocatalysts operating under visible light irradiation," *J. Catal.* **2003**, 216, 505-516.
- (5) Nishijima, K.; Ohtani, B.; Yan, X.; Kamai, T.; Chiyoya, T.; Tsubota, T.; Murakami, N.; Ohno, T. "Incident light dependence for photocatalytic degradation of acetaldehyde and acetic acid on S-doped and N-doped TiO₂ photocatalysts," *Chem. Phys.* **2007**, 339, 64-72.
- (6) Usseglio, S.; Damin, A.; Scarano, D.; Bordiga, S.; Zecchina, A.; Lamberti, C. "(I₂)_n Encapsulation inside TiO₂: A Way to Tune Photoactivity in the Visible Region," *J. Am. Chem. Soc.* **2007**, 129, 2822-2828.
- (7) Shi, J.; Chen, J.; Feng, Z.; Chen, T.; Lian, Y.; Wang, X.; Li, C. "Photoluminescence Characteristics of TiO₂ and Their Relationship to the Photoassisted Reaction of Water/Methanol Mixture," *J. Phys. Chem. C* **2007**, 111, 693-699.

- (8) Ingram, D. B.; Linic, S. "Water Splitting on Composite Plasmonic-Metal/Semiconductor Photoelectrodes: Evidence for the Selective Plasmon-Induced Formation of Charge Carriers near the Semiconductor Surface," *J. Am. Chem. Soc.* **2011**, 133, 5202-5205.
- (9) Kato, H.; Asakura, K.; Kudo, A. "Highly Efficient Water Splitting into H₂ and O₂ over Lanthanum-Doped NaTaO₃ Photocatalysts with High Crystallinity and Surface Nanostructure," *J. Am. Chem. Soc.* **2003**, 125, 3082-3089.
- (10) Maeda, K.; Teramura, K.; Saito, N.; Inoue, Y.; Domen, K. "Improvement of photocatalytic activity of (Ga_{1-x}Zn_x)(N_{1-x}O_x) solid solution for overall water splitting by co-loading Cr and another transition metal," *J. Catal.* **2006**, 243, 303-308.
- (11) Kudo, A.; Miseki, Y.; "Heterogeneous Materials for Water Splitting," *Chem. Soc. Rev.* **2009**, 38, 253-278.
- (12) Fox, M. A.; Dulay, M. T. "Heterogeneous Photocatalysis," *Chem. Rev.* **1993**, 93, 341-357.
- (13) Mills, A.; Le Hunte, S. "An overview of semiconductor photocatalysis," *J. Photochem. Photobiol. A* **1997**, 108, 1-35.
- (14) Valdés, A.; Qu, Z.-W.; Kroes, G.-J.; Rossmeisl, J.; Nørskov, J. K. "Oxidation and Photo-Oxidation of Water on TiO₂ Surface," *J. Phys. Chem. C* **2008**, 112, 9872-9879.
- (15) Nakamura, R.; Imanishi, A.; Murakoshi, K.; Nakaoto, Y. "In Situ FTIR Studies of Primary Intermediates of Photocatalytic Reactions on Nanocrystalline TiO₂ Films in Contact with Aqueous Solutions," *J. Am. Chem. Soc.* **2003**, 125, 7443-7450.

- (16) Nakamura, R.; Nakato, Y. "Primary Intermediates of Oxygen Photoevolution Reaction on TiO₂ (Rutile) Particles, Revealed by in Situ FTIR Absorption and Photoluminescence Measurements," *J. Am. Chem. Soc.* **2004**, 126, 1290-1298.
- (17) Mattioli, G.; Filippone, F.; Bonapasta, A. A. "Reactions Intermediates in the Photoreduction of Oxygen Molecules at the (1 0 1) TiO₂ (anatase) Surface," *J. Am. Chem. Soc.* **2006**, 128, 13772-13780.
- (18) Mojet, B. L.; Ebbeson, S. D.; Lefferts, L. "Light at the interface: the potential of attenuated total reflection infrared spectroscopy for understanding heterogeneous catalysis in water." *Chem. Soc. Rev.* **2010**, 39, 3643-4655.
- (19) Hind, A. R.; Bhargava, S. K.; McKinnon, A. "At the solid/liquid interface: FTIR/ATR – the tool of choice," *Adv. Coll. Int. Sci.* **2001**, 93, 91-114.
- (20) Bürgi, T.; Baiker, A. "In Situ Infrared Spectroscopy of Catalytic Solid-Liquid Interfaces Using Phase-Sensitive Detection: Enantioselective Hydrogenation of a Pyrone over Pd/TiO₂," *J. Phys. Chem. B* **2002**, 106, 10649-10658.
- (21) Ortiz-Hernandez, I.; Williams, C. T. "In Situ Investigation of Solid-Liquid Interfaces by Attenuated Total Reflection Infrared Spectroscopy," *Langmuir* **2003**, 19, 2956-2962.
- (22) Andanson, J. -M.; Baiker, A. "Exploring catalytic solid/liquid interfaces by *in situ* attenuated total reflection infrared spectroscopy." *Chem. Soc. Rev.* **2010**, 39, 4571-4584.

(23) Almeida, A. R.; Moulijn, J. A.; Mul, G. "In Situ ATR-FTIR Study on the Selective Photo-oxidation of Cyclohexane over Anatase TiO₂," *J. Phys. Chem. C* **2008**, 112, 1552-1561.

(24) Almeida, A. R.; Carneiro, J. T.; Moulijn, J. A.; Mul, G. "Improved performance of TiO₂ in the selective photocatalytic oxidation of cyclohexane by increasing the rate of desorption through surface silylation," *J. Catal.* **2010**, 273, 116-124.

(25) Almeida, A. R.; Berger, R.; Moulijn, J. A.; Mul, G. "Photo-catalytic oxidation of cyclohexane over TiO₂: A novel interpretation of temperature dependent performance," *Phys. Chem. Chem. Phys.* **2011**, 13, 1345-1355.

(26) Almeida, A. R.; Moulijn, J. A.; Mul, G. "Photocatalytic oxidation of cyclohexane over TiO₂: evidence for a Mars-van Krevelen mechanism," *J. Phys. Chem. C* **2011**, 115, 1330-1338.

(27) Sivasankar, N.; Weare, W. W.; Frei, H. "Direct Observation of a Hydroperoxide Surface Intermediate upon Visible Light-Driven Water Oxidation at an Ir Oxide Nanocluster Catalysts by Rapid-Scan FT-IR Spectroscopy.

(28) Kumnorkaew, P.; Ee, Y. -K.; Tansu, N.; Gilchrist, J. F. "Investigation of the Deposition of Microsphere Monolayers for Fabrication of Microlens Arrays," *Langmuir* **2008**, 12150-12157.

(29) *CRC Handbook of Chemistry and Physics*, ed. W. M. Haynes, CRC Press/Taylor and Francis, Boca Raton, FL, 92nd Edition, **2011**.

- (30) Davydov, A. *Molecular Spectroscopy of Oxide Catalyst Surfaces*, Jon Wiley & Sons, Sussex, England, **2003**.
- (31) Deo, G.; Wachs, I. E. "Effect of Additives on the Structure and Reactivity of the Surface Oxide Phase in V₂O₅/TiO₂ Catalysts," *J. Catal.* **1994**, 146, 335-345.
- (32) Anpo, M.; Che, M.; Fubini, B.; Garrone, E.; Giamello, E.; Paganini, M. C. "Generation of superoxide ions at oxide surfaces," *Top. Catal.* **1999**, 8, 189-198.
- (33) O'Regan, B.; Lenzmann, F.; Muis, R.; Wienke, J. "A Solid-State Dye-Sensitized Solar Cell Fabricated with Pressure-Treated P25-TiO₂ and CuSCN: Analysis of Pore Filling and IV Characteristics," *Chem. Mater.* **2002**, 14, 5023-5029.

Figure 1: Theoretical estimation of the penetration depth of the evanescent wave as a function of the wavelength (expressed in wavenumbers) of IR light for a TiO₂ thin film with various porosities on a ZnSe IRE. The pores are assumed to be filled with water.

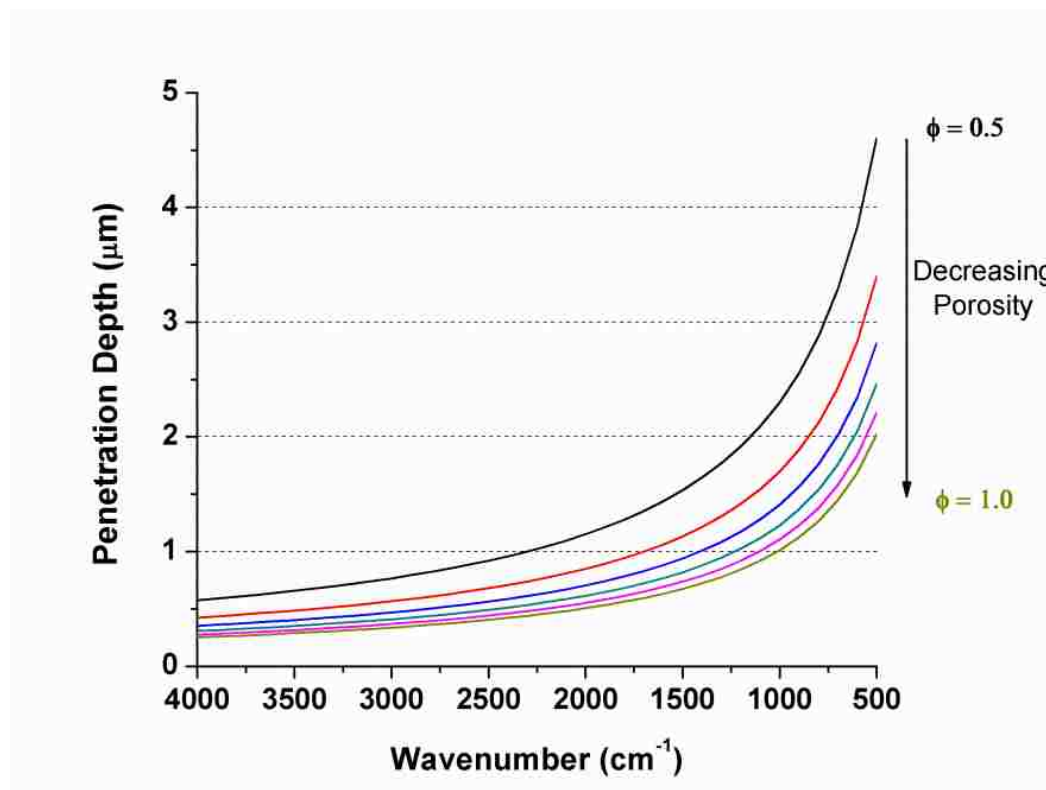


Figure 2: SEM image of the TiO₂ thin film thickness as prepared on a glass slide.

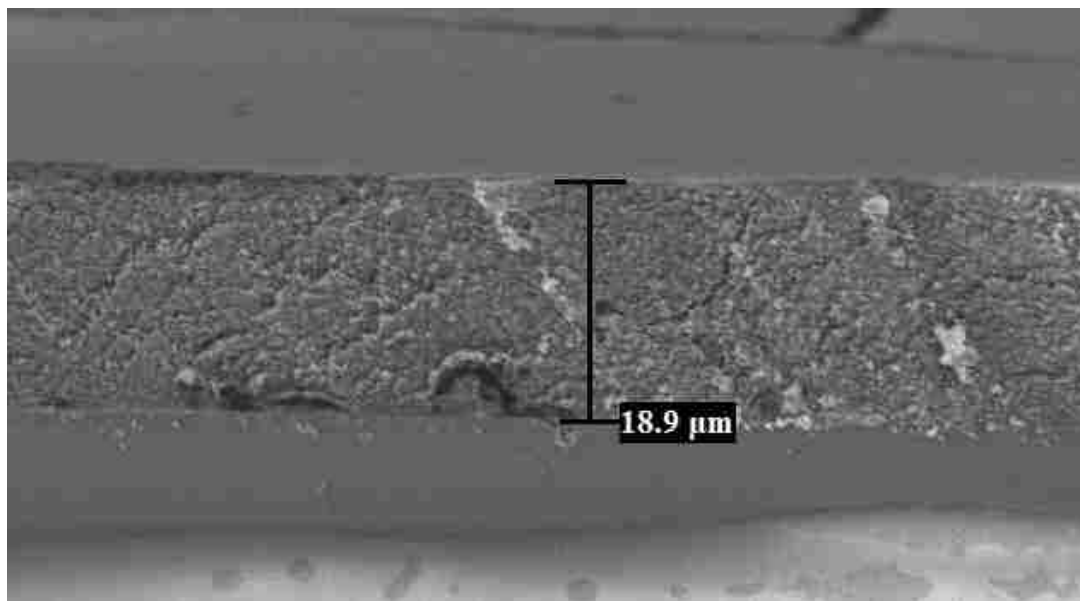
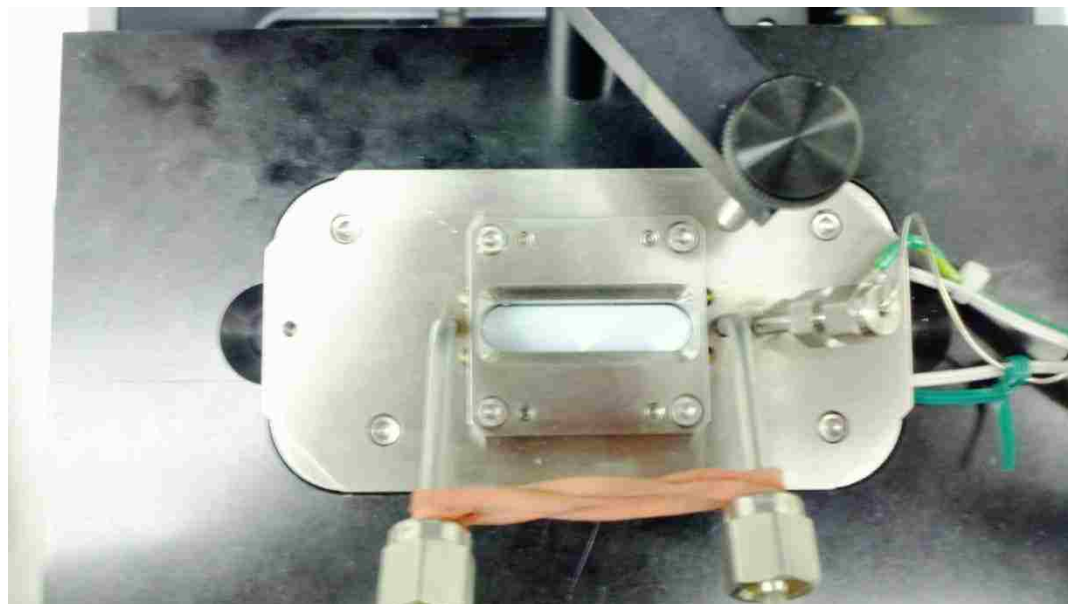


Figure 3: (a) Top view of the top plate of the ATR flow through cell. (b) *In situ* ATR experimental setup for illumination during photocatalytic water splitting.

(a)



(b)

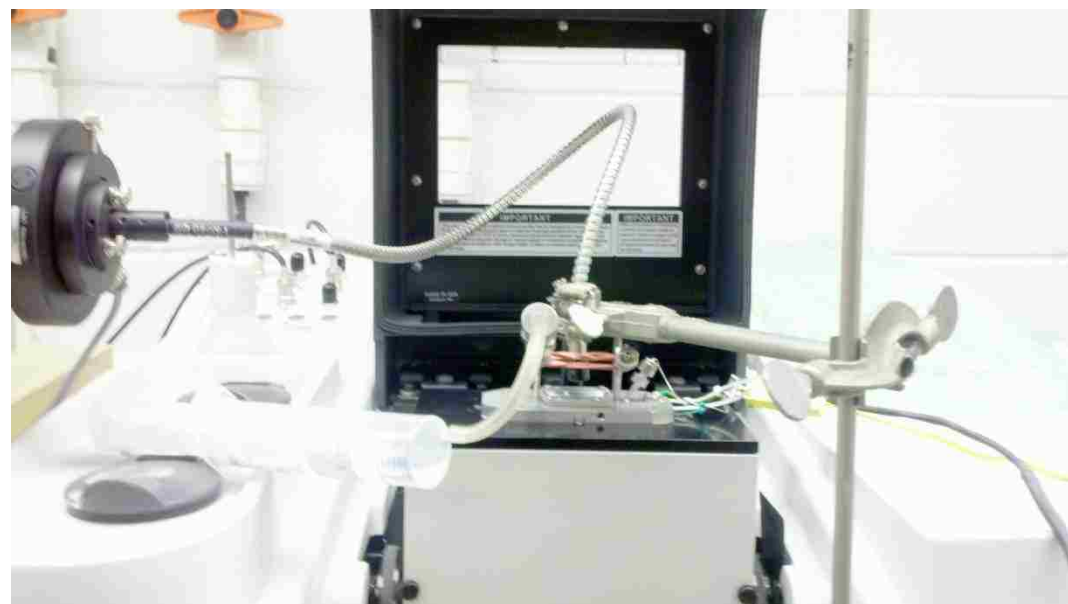


Figure 4: Time profile of ATR-FTIR spectra centered around the peroxide spectral region during HOOH adsorption on a TiO₂ thin film under ambient conditions using a 30% HOOH/H₂O solution. The background used was TiO₂ in H₂O.

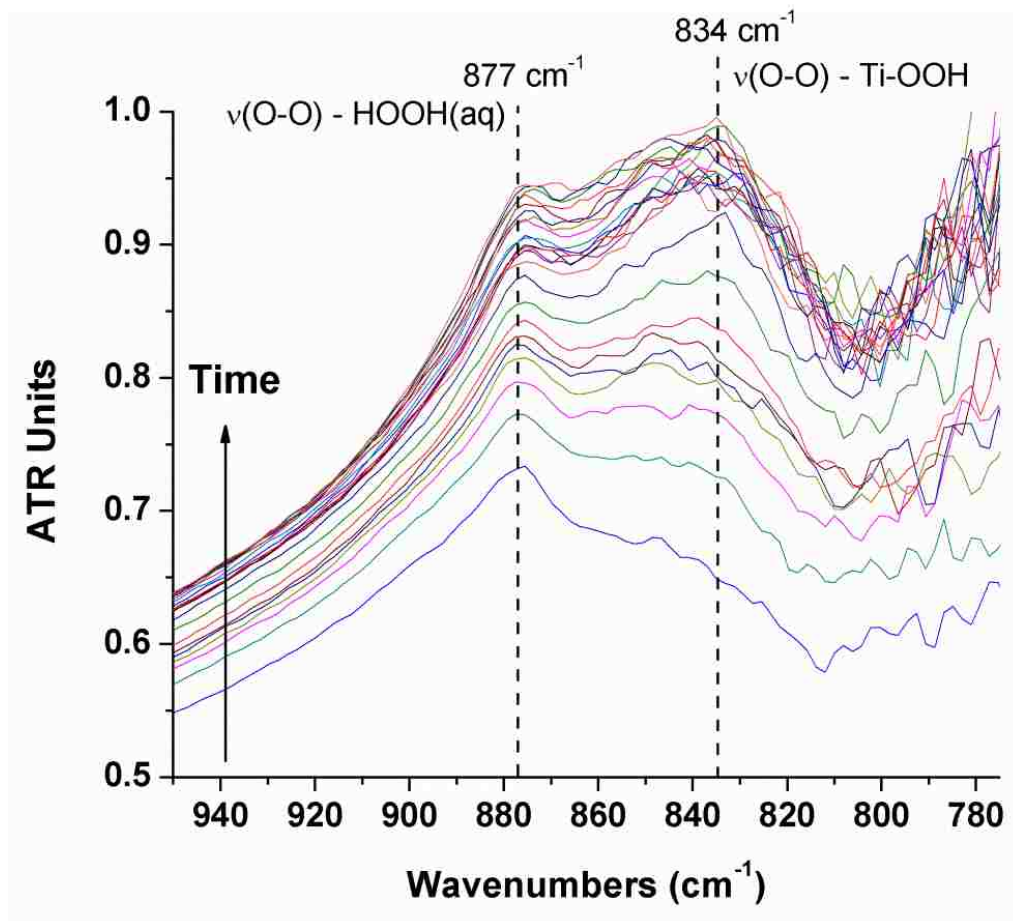


Figure 5: Time profile of ATR-FTIR spectra centered around the superoxide spectral region during HOOH adsorption on a TiO₂ thin film under ambient conditions using a 30% HOOH/H₂O solution. The background used was TiO₂ in H₂O.

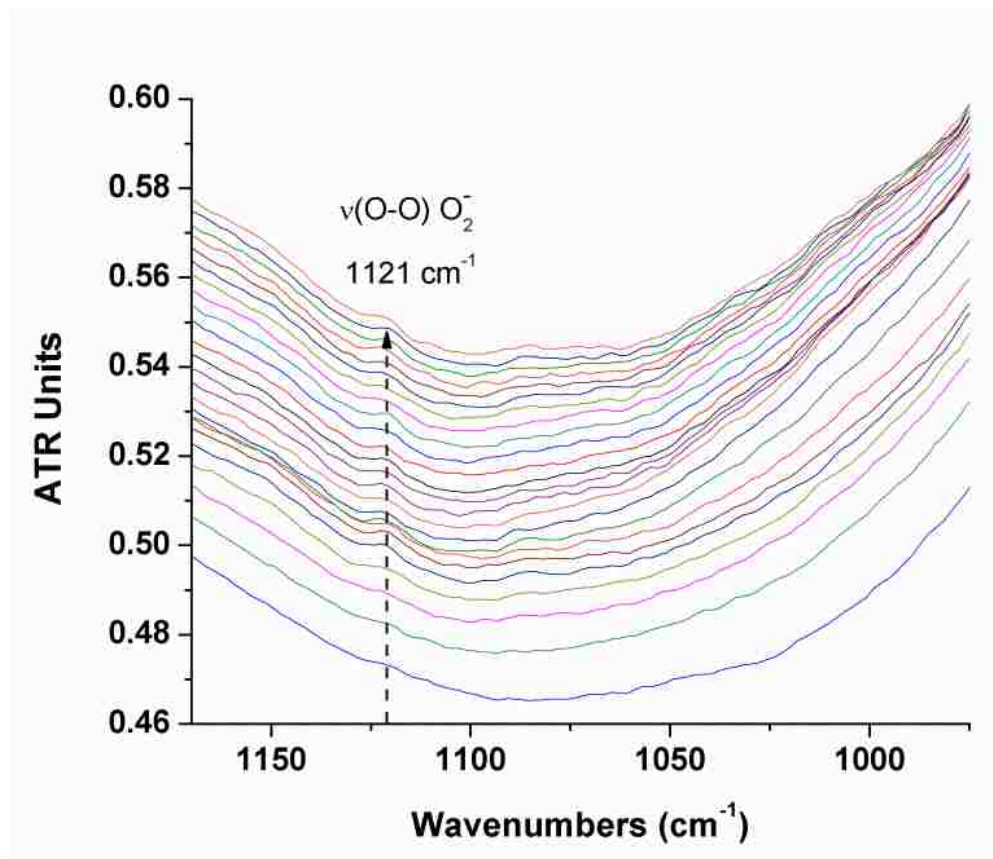


Figure 6: Visible (532 nm) Raman spectra during HOOH adsorption on a TiO₂ thin film under ambient conditions using (a) 1.0% and (b) 0.1% HOOH/H₂O solution. Note that the convention of plotting as function of decreasing wavenumber is adopted for ease of comparison to the ATR-FTIR spectra.

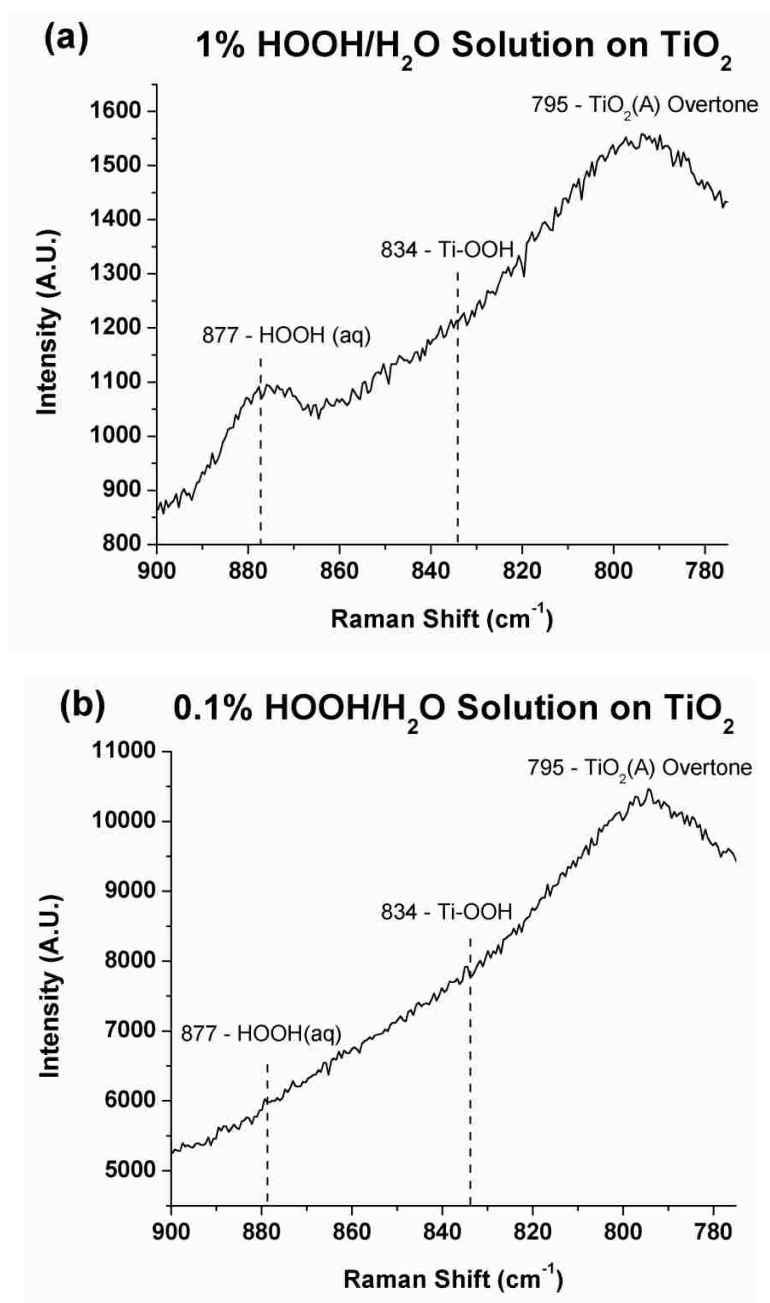


Figure 7: (a) Time profile 2D contour map of *in situ* ATR-FTIR spectra during photocatalytic water splitting on a TiO₂ thin film and under dark and illuminated conditions. (b) Peak area (1000-1200 cm⁻¹) as a function of time for the same experiment. The background used was TiO₂ in H₂O under dark conditions.

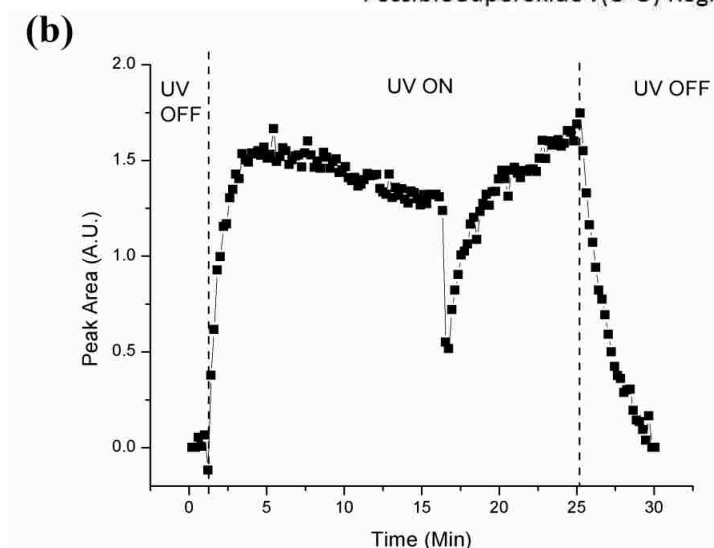
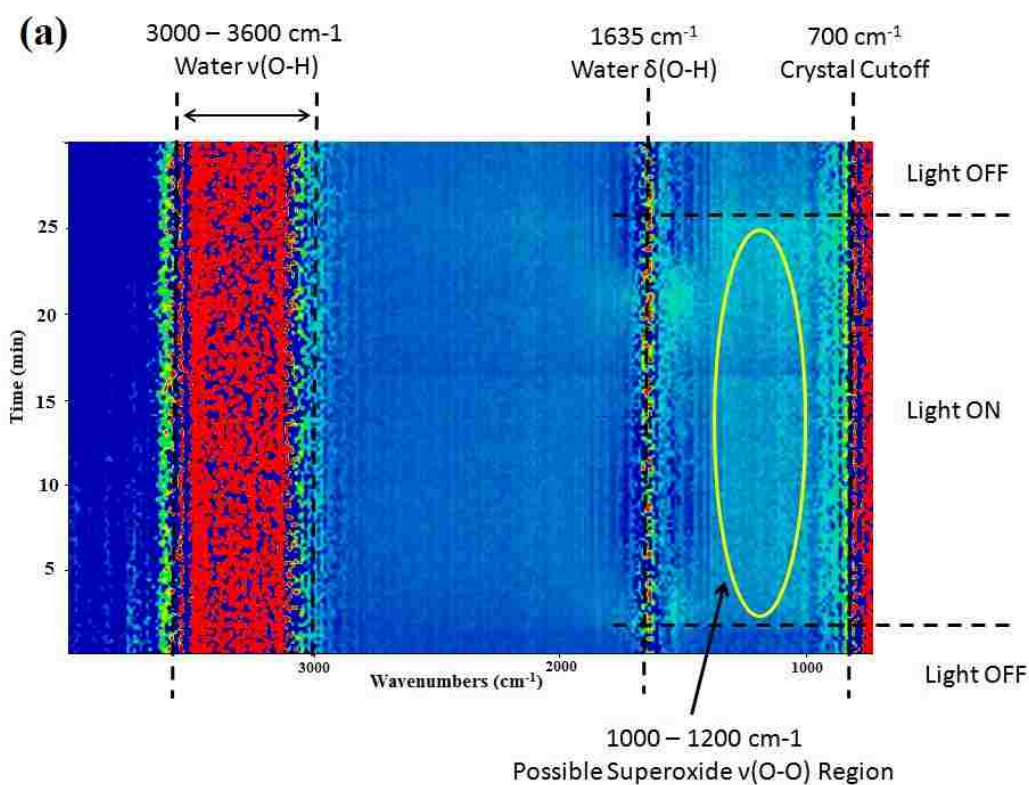


Figure 8: Peak area ($1000\text{-}1200\text{ cm}^{-1}$) as a function of time for *in situ* ATR-FTIR during photocatalytic water splitting on a TiO_2 thin film and under dark and illuminated conditions (Red). The black curve is the same experiment in the absence of H_2O reactant.

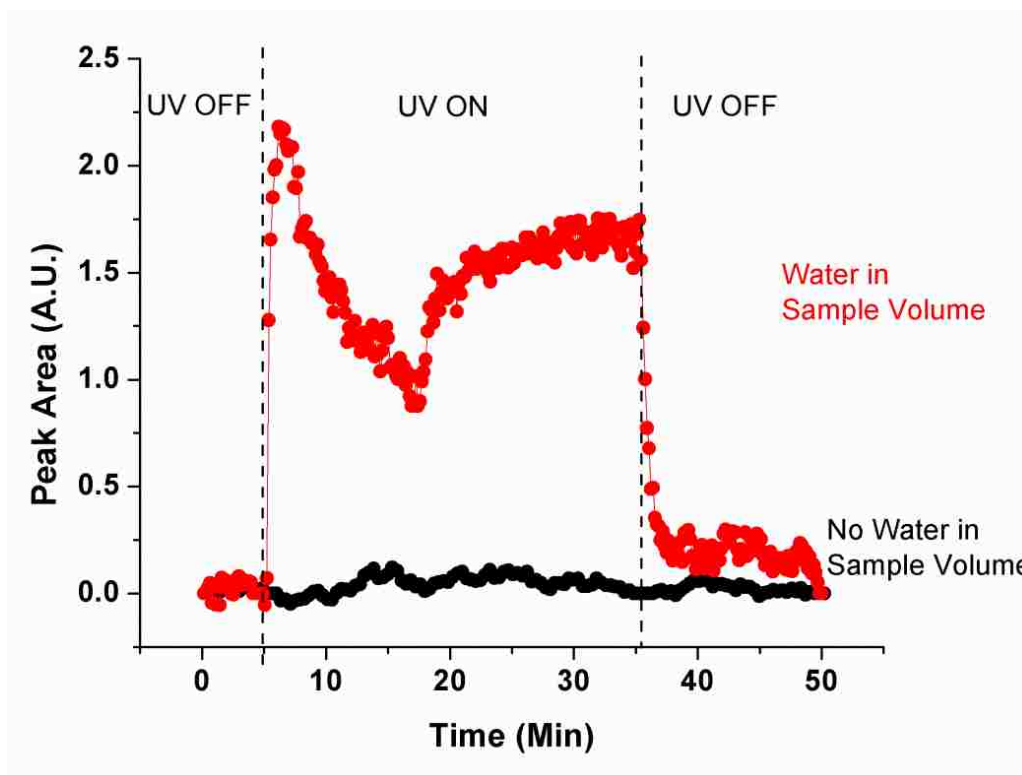


Figure 9: UV Raman spectra after 10 min of excitation using the UV laser line (325 nm) in absence of H₂O and in the presence of various reactants (H₂O, 10 mM Fe³⁺/H₂O, and D₂O)

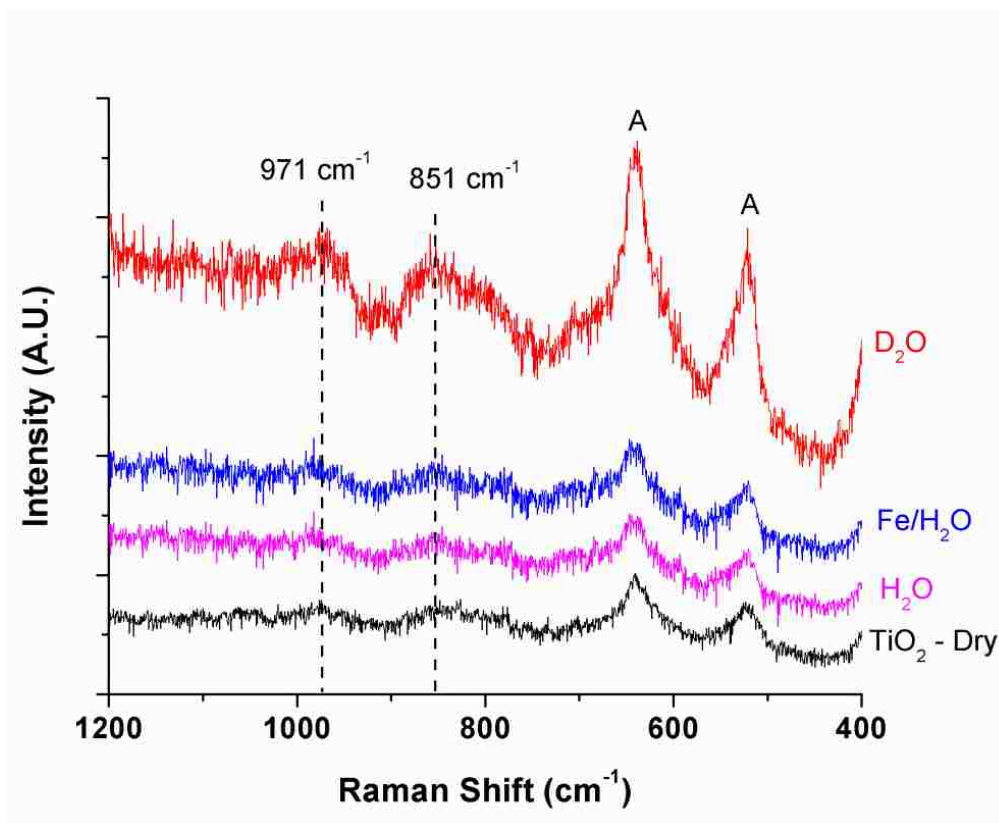
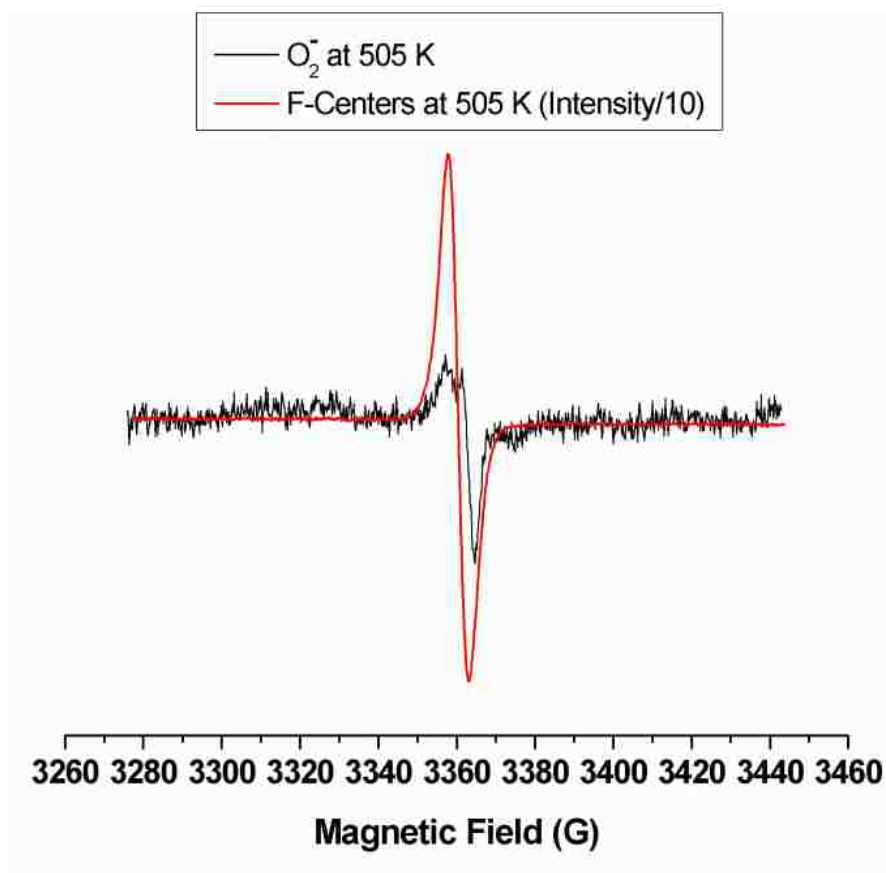


Figure 10: *In situ* EPR spectra of TiO₂ under reducing conditions (red) followed by the introduction of 10% O₂/He flow (black) at elevated temperature.



CHAPTER 5

Structure/Composition-Photoactivity Relationships for Titanate Nanotubes

Abstract

The following reports the successful synthesis of hydrogen titanate nanotubes (H-Ti-NT) and TiO₂ (anatase) nanotubes, their thermal solid-state transformational chemistry, clarifies some of the confusion surrounding their literature Raman vibrational assignments, and examines the effect of nanotube composition and structure on photoactivity. Hydrothermally prepared titanate nanotube powders with negligible (<0.1 wt% Na, H-Ti-NT) and high (~7.0 wt% Na, Na/H-Ti-NT) Na content, that underwent freeze-drying and thermal treatments, were prepared and characterized with ambient and *in situ* Raman spectroscopy. The H-Ti-NT phase gives rise to Raman bands at ~195, 285, 458, ~700, 830 and 926 cm⁻¹. The Raman bands above 650 cm⁻¹ were found to be sensitive to the presence of moisture, which indicates that they are related to surface vibrational modes. The titanate nanotube Raman band at ~926 cm⁻¹ was shown not be related to a Na-O-Ti vibration, which was previously assigned in the literature, since its intensity does not vary with Na content, which varied by a factor of >70. The anatase H-Ti-NT phase was found to be thermally stabilized up to 700 °C by Na that had been entrapped during synthesis. The Na-free

H-Ti-NT phase, however, transformed to TiO₂ (anatase) nanotubes upon heating above 200 °C and the anatase phase was stable up to 700 °C, however microscope imaging reveals that the collapse of nanotube structures to nanorods and nanowires begins around 500 °C. The Ti-NTs were examined for their photoactivity for decomposition of 4-chlorophenol and the splitting of H₂O to H₂ and O₂. The optimum photoactivity was found when the initial Ti-NT titanate phase was transformed to TiO₂ (anatase) corresponding to thermal treatments at 400-500 °C. The presence of Na in the Ti-NTs was detrimental and significantly decreased the photoactivity.

1. Introduction

Hydrothermally prepared titanate nanotube (Ti-NT) powders have excellent potential as heterogeneous catalysts,¹⁻⁵ hydrogen storage materials,^{6,7} and secondary batteries⁸⁻¹⁰ because of their nanoscale tubular shape (outer diameter ~1 nm) and large internal open structure (internal diameter ~0.6–0.8 nm). These characteristics are responsible for the high surface area and large pore volume of titanate nanotubes. It has been reported that these titanate nanotubes are easily converted into nanospherical or rod-like particles at temperatures above 500 °C in air.¹¹ If the nanotubular shaped titanate is thermally converted to high surface area titania without changing its morphology, it potentially can have applications as a photo or thermal catalyst and as a catalytic support material. Nanotubular titania has especially strong merit as a humidity sensor or catalytic support material. The large surface area of such a nanotubular titanate can support and disperse relatively large amounts of active

catalytic components such as Pt, MoO₃, WO₃, V₂O₅, etc. Furthermore, the large external and internal surfaces with planar sites of the nanotubular titanate would facilitate uniform reaction over its surface.^{2,4,12,13}

The ideal oxide support material for a stable gas sensor or heterogeneous catalyst should not show any changes in physical properties such as shape, crystalline structure, and surface area during thermal treatments and under realistic operating environments. The nanotubular titanate phase changes during thermal treatments, however, have not previously been clearly established or tracked. This lack of uniform conclusions is a consequence of differing reports about the TiO₂ or titanate phase in the as-prepared or dried powders and about the remaining content of Na in the powder, which differed among the limited literature reports.^{1,3,14-16} In order to address these synthesis variables upon the resulting nanotubular titanate structures, the present study employs Raman spectroscopy to investigate the crystalline phases of Ti-NT powders prepared by hydrothermal and freeze-drying methods with negligible and high Na contents. The freeze-drying method was employed to exclude any thermal effects on the crystallinity that may be caused by the rapid removal of H₂O or H⁺ from the powder and to also study the effect of water on the crystallinity of the Ti-NT powder. The elemental Na content in the as-prepared powders was controlled by varying the number of water-washing treatments and employing an additional ion-exchange technique.

Raman spectroscopy is an ideal characterization method for oxide powders since it can provide both bulk and surface molecular structural information under various

environmental conditions.¹⁷ Furthermore, Raman spectroscopy can also readily discriminate between the different crystalline morphologies of TiO₂ (anatase, rutile, brookite, B and Ti-NT)¹⁸⁻²² and tungsten oxide phases (bulk WO₃ and surface WO_x species)²³⁻²⁵ that are many times added as promoters to TiO₂ catalysts.

Since the pioneering discovery of the effect of photosensitization of TiO₂ electrodes on the electrolysis of H₂O into H₂ and O₂ by Fujishima and Honda in 1972, photocatalysis by TiO₂ semiconductors has received much attention.²⁶ In the following decades photocatalytic reactions utilizing TiO₂ have been studied, especially for the oxidation of organic compounds and dyes.²⁷⁻³¹ An application such as photo-oxidation of industrial solvents and other toxic chlorinated material, such as trichloroethane²⁸ and 4-chlorophenol,³² have obvious environmental benefits. TiO₂ based catalysts have also been modified or tailored to increase photoactivity, trap photo-generated holes, or shift the activity to the visible region of the spectrum.^{31,33-37} These same photocatalytic reactions have also been studied for Ti-NT containing catalysts of various kinds and with various modifications.³⁸⁻⁴⁶ Ti-NT, TiO₂ nanotubes, and other nano-structured Ti-containing materials have attracted interest because they have the intrinsic properties of high crystallinity, high surface area, and high concentration of surface hydroxyl groups; all of which are beneficial to photocatalytic activity. The water splitting reaction over TiO₂ catalysts has been greatly studied recently due to the possibility of producing a clean, renewable source of energy in the form of H₂ and Ti-NT structures have been explored as possible photocatalysts.⁴⁶⁻⁴⁸

Furthermore, Ti-NT can be structured into arrays which have been shown to be useful in improving charge separation during photochemical water splitting.^{46,49-51}

The hydrothermal preparation method for Ti-NT nanotubes often results in a catalyst that has a lower activity than the standard TiO₂ (P-25) catalyst due to Na impurities in the “as-prepared” catalyst.^{46,52} Improvement to the activity can be made through further transformation of the catalyst by removal of Na impurities and by transformation of the catalyst with thermal treatments into a more active, crystalline TiO₂ form such as anatase. These methods for improving photocatalytic activity will be examined by detailed characterization and the resulting catalysts will be tested for their activity in both decomposition of a chlorinated material (4-chlorophenol) and the water splitting reaction.

2. Experimental

2.1 Ti-NT Preparation and Imaging

Commercial P-25 powder (Degussa) was used as the source of TiO₂ for preparation of the Ti-NT powder. A precursor solution of P-25 and 10 M NaOH in a 304 stainless steel autoclave was subjected to heat treatment at 130 °C for 24 hrs. The autoclave was lined with a Ni plate to protect it from corrosion by the strongly basic NaOH solution. After hydrothermal synthesis, the precipitated titanates were washed with distilled water (pH = 7.0) several times. At this point, a small amount of sample was collected and termed as Na/H-Ti-NT. The Na content of this sample was found to be 7.02 atom %. The remaining sample was treated with 0.1 N HCl solution (pH = 1.0)

and constantly stirred for 24 hrs at room temperature. It was further washed with distilled water at pH = 7.0 to reduce the Na content. The obtained sample was termed as H-Ti-NT and found to contain less than 0.1 atom % of Na. The elemental Na contents were measured with EDS (Energy Dispersive Spectroscopy) attached to a scanning electron microscopy (SEM S-4700, Hitachi Co.). During the 24 hrs stirring procedure, fresh aqueous HCl solution was introduced every 4 hr to ensure rapid ion exchange of the Na ions in the titanate with H ions. The as-prepared Ti-NT powders were obtained after complete washing by freeze-drying at -57 °C for 24 hrs in a liquid nitrogen solution. In addition, thermo-gravimetric analysis (TGA) experiments (STA-1500, Sinco Co.) were conducted to measure the H₂O content of the dried Ti-NT samples. Transmission electron microscopy (TEM, JEOL-2010) was employed to image the titanate particle structures present in the sample.

2.2 Raman Spectroscopy

The Raman studies were performed with a Horiba-Jobin Yvon LabRam-IR High Resolution instrument equipped with a visible light laser source (YAG double-diode pumped laser, Coherent 315 m, 20 mW). The Raman spectrometer was equipped with a confocal microscope (Olympus BX-30), notch filter (532 nm), 50X objective and a single stage monochromator with 900 grooves/mm grating. The Raman spectral resolution was better than 2 cm⁻¹. The laser power was kept below 0.5 mW at the sample so as to minimize any laser-induced alterations of the sample. The scattered light from the sample was passed through the monochromator grating and collected with a visible sensitive LN₂-cooled CCD detector (Horiba-Jobin Yvon CCD-3000V).

The LabSpec 5 software was used to operate the experimental set up and collect the Raman spectra. The ambient Raman spectra were collected by putting the samples on a glass slide under ambient conditions. The *in situ* Raman spectra were collected in an environmental reaction cell (Linkam T 1500). During the *in situ* Raman analysis, a heating rate with 60 °C /min was maintained and 10% O₂/Ar was flown through the cell at 30 sccm. The Raman spectra were collected after maintaining 10 minutes at the desired temperature during the temperature ramping experiments.

2.3 Photocatalytic Activity

To evaluate photocatalytic properties of the calcined powders, 0.1 g of a sample was mixed together with 0.1 mM aqueous 4-chlorophenol (4-CP) solution. Then UV-A light source (PowerArc UV-100, UV Process Co.) with ~400 nm of wavelength and 100 W of power was irradiated on the mixed solution for 3 hours to initiate the photocatalytic reaction. After the reaction, the remaining organic carbon in the mixed solution was measured using a total organic carbon (TOC) analyzer (TOC-VCPH, Shimadzu Co.) to determine the extent of photocatalytic decomposition of 4-CP.³²

The H₂O splitting photocatalytic activity of the various Ti-NT catalysts was determined with UV (wavelengths > 290 nm) irradiation using a 450 W Hg lamp. A reaction cell made of Pyrex was employed and filled with 250 mL condensed liquid-phase water. The reactor was connected to a glass, closed-gas circulation system. About 200 mg of the photocatalyst was suspended in the reaction cell and stirred with a magnetic stir bar. The air in the remaining volume of the reactor was evacuated to

facilitate product detection. The reactor was maintained at room temperature and gas chromatography was used to analyze H₂ production for 5 hours.

3. Results

3.1 Raman Spectroscopy of As-Prepared and Dried Ti-NT

The Raman spectra of the as-prepared, freeze dried H-Ti-NT and Na/H-Ti-NT ambient powders with long nanotubular shapes, which have also been reported by other researchers,^{5,11} are presented in Figure 1. The Raman spectrum of the Na/H-Ti-NT powder has the bands characteristic of the titanate phase (197, 288, 458, 710, 830 and 926 cm⁻¹).¹⁹⁻²² The crystalline structure of Na/H-Ti-NT, however, is still uncertain due to the coexistence of mixed orthorhombic and monoclinic crystalline phases. The Raman spectrum of the low Na-containing H-Ti-NT powder exhibits somewhat broader Raman bands of the titanate phase that are slightly blue shifted (193, 283, 458, 683, 830 and 926 cm⁻¹) and contains additional bands at 144 and 402 cm⁻¹ from a trace amount of TiO₂ (anatase).⁵³ The titanate Raman spectrum was compared with reference Raman spectra (Figure S1) of different TiO₂ phases (anatase, rutile, brookite, and B), and anatase was the only additional phase found to be present in the titanate samples. The Raman spectrum of the ambient H-Ti-NT powder has a somewhat broader band in the 600-720 cm⁻¹ range (circled area in the Figure 1) than the Raman spectrum of the ambient Na/H-Ti-NT powder. The broadening of the Raman bands is related to the moisture content of the H-Ti-NT powder.⁵⁴

To further examine the effect of water content on the broadening of the Raman bands around 700 cm^{-1} , comparisons of multiple freeze-drying cycles and drying methods were made as shown in Figure 2. The numbers contained in Figure 2a indicate the number of freeze-drying cycles to decrease the amount of H_2O in the powder. For example, #5 means the freeze-drying cycle was carried out 5 times and for 24 hrs each time without raising the temperature. Referencing to the total moisture weight loss after calcination at $1000\text{ }^\circ\text{C}$ by thermo-gravimetric analysis, the total H_2O content of the H-Ti-NT powder decreased from 44 to 12 wt% with these multiple freeze-drying cycles. The H_2O content dropped from 44 wt% to 10 and 8.6 wt% for convection drying and vacuum drying at $105\text{ }^\circ\text{C}$, respectively. With decreasing H_2O content in the powder, the broad Raman band around 700 cm^{-1} becomes narrower with freeze-drying (Figure 2a) and further sharpens with the more efficient drying at $105\text{ }^\circ\text{C}$ (Figure 2b).

3.2 *In Situ* Raman Spectroscopy during Thermal Treatment of Ti-NT

In situ Raman measurements were conducted between $100\text{-}550\text{ }^\circ\text{C}$ in an oxidizing atmosphere to monitor the thermal behavior of the H-Ti-NT and Na/H-Ti-NT powders and the corresponding spectra are presented in Figures 3a and 3b, respectively. Up to $350\text{ }^\circ\text{C}$ for H-Ti-NT (Figure 3a), the initially broad band at $600\text{-}720\text{ cm}^{-1}$ sharpens and splits into two bands corresponding to the titanate phase at 710 cm^{-1} and to the anatase phase at 641 cm^{-1} . At $550\text{ }^\circ\text{C}$ the H-Ti-NT has completely transformed into the anatase phase as indicated by the band at 632 cm^{-1} and the complete absence of the 710 cm^{-1} band. In contrast, the Raman bands of the Na/H-Ti-NT powder contain

almost the same intensity up to 200 °C, though they are slightly decreased at higher temperatures due to thermal broadening and also become blue shifted due temperature effects (Figure 3b). However, the Na/H-Ti-NT phase does not transform to TiO₂ (anatase) at or below 550 °C and a new minor band appears at ~117 cm⁻¹ that is reminiscent of Na₂Ti₃O₇.⁵⁵

The morphology of the titanate particles during thermal treatments was imaged with transmission electron microscopy (TEM, JEOL-1010). The TEM image of the anatase Ti-NT powder obtained after calcination at 400 °C for 30 minutes is shown in Figure 4. The image shows that the powder still largely consists of a long nanotube shape that is unaffected by calcination at 400 °C, though some nanorods or nanowires may also be present. The image was also used to estimate the inner and outer diameters of the nanotubes at ~1 and ~0.75 nm, respectively, with an estimated error of 10-20%.

The Raman spectra of the ambient H-Ti-NT and Na/H-Ti-NT titanate powders after calcination at 700 °C for 3 hrs in air are presented in Figure 5. These Raman spectra show sharp bands at 138, 191, 393, 513, 638 and 796 cm⁻¹ corresponding to the TiO₂ (anatase) phase crystals of micron-sized particles and only traces of the TiO₂ (rutile) phase, weak bands at 450 and 614 cm⁻¹. The anatase and rutile phases are marked A and R, respectively, in Figure 5. The complete absence of TiO₂ (rutile) during calcination of H-Ti-NT below 700 °C for 3 hrs indicates that the TiO₂ (anatase) nanostructures are thermally stable as anatase below 700 °C. The nanostructures at this temperature, however, likely consist of a mixture of nanotubes, -rods, -wires, and completely collapsed particles (see Figure S5).

The Raman spectrum of the Na/H-Ti-NT powder after calcination at 700 °C contains bands that are characteristic of multiple titanate phases. Qamar *et al.* previously reported that the titanate nanotube particles with almost the same Na content as that of Na/H-Ti-NT in the present study changed into nano-spherical or -rod shaped particles at high temperatures above 500 °C in air with corresponding Raman bands of TiO₂ (anatase), Na₂Ti₃O₇, Na₂Ti₆O₁₃, etc.¹¹ Comparison of the current Raman spectrum of Na/H-Ti-NT calcined to 700 °C with those reported by Horvth *et al.*,⁵⁵ Papp *et al.*⁵⁶ and Mao *et al.*⁵⁷ suggests that the Raman bands of the calcined Na/H-Ti-NT powder in Figure 5 corresponds to Na₂Ti₃O₇ and Na₂Ti₆O₁₃, but the bands are slightly shifted. Thus, calcination of Na/H-Ti-NT at 700 °C results in a mixture of H-Ti-NT, Na₂Ti₃O₇, Na₂Ti₆O₁₃ and a small amount of TiO₂ (anatase) and calcination of H-Ti-NT with negligible Na at the same temperature yields the TiO₂ (anatase) phase with a trace of TiO₂ (rutile).

Raman spectroscopy was used to probe for the presence of surface Na in titanate nanotubes by examining the effect of Na on the vibrations of dehydrated supported WO₃/titanates. The surface W=O vibration is extremely sensitive to the presence of surface alkali, thus, the Raman spectrum of the dehydrated Ti-NTs can indicate if surface Na is present.^{58,59} The mono-oxo surface O=WO₄ species vibrate at ~1010-1020 cm⁻¹ and the presence of surface alkali can shift the W=O band to ~900-950 cm⁻¹ under dehydrated conditions by complexing with the surface tungstate species.^{58,59} The *in situ* Raman spectra of the supported ~12% WO₃/titanate powders were taken at 700 °C, as shown in Figure S4, and neither samples possesses a strong Raman band at

$\sim 805\text{ cm}^{-1}$ characteristic of crystalline WO_3 NPs.²⁰ The supported $\text{WO}_3/\text{Na}/\text{H-Ti-NT}$ sample exhibits $\text{W}=\text{O}$ Raman bands at 905 and 922 cm^{-1} reflecting the presence of surface Na complexing with the surface WO_x species. The supported $\text{WO}_3/\text{H-Ti-NT}$ sample, however, contains the $\text{W}=\text{O}$ vibration at 1009 cm^{-1} consistent with the almost complete absence of surface Na in this nanotubular titanate powder.^{58,60,61} Furthermore, a sample with $\sim 0.10\text{-}0.15$ atom % Na resulted in a shift of the $\text{W}=\text{O}$ Raman band to $\sim 950\text{ cm}^{-1}$ (not shown for brevity) Thus, the H-Ti-NT titanate powder prepared in this investigation is almost completely free of surface Na.

3.3 Photocatalytic Activity of Ti-NT Samples

The photocatalytic decomposition of 4-chlorophenol (4-CP) over H-Ti-NT samples with various thermal treatments is shown in Figure 6.³² For reference, the reaction was run with no catalyst and negligible decomposition was detected. The as-prepared H-Ti-NT sample showed the lowest percentage of decomposition of 4-CP. TiO_2 powder (P-25) exhibited a moderate amount of decomposition at $\sim 20\%$. Thermal treatment of the H-Ti-NT sample in air was performed to transform the H-Ti-NT to the anatase crystalline phase of the samples while maintaining the high surface area intrinsic to the Ti-NT structure. Treatment at $400\text{ }^\circ\text{C}$ for 2h yielded the best results, with $\sim 55\%$ decomposition of 4-CP. While $500\text{ }^\circ\text{C}$ obtained a sample that was a slight improvement over P-25, the higher calcination temperature decreased the H-Ti-NT photoactivity. An initial thermal treatment at $400\text{ }^\circ\text{C}$ followed by a thermal treatment at $500\text{ }^\circ\text{C}$ resulted in slightly better ($\sim 27\%$ decomposition) relative to the straight 500

°C thermal treatment, but the photoactivity was still significantly lower than the 400 °C treatment.

The Ti-NTs were also examined for the production of H₂ during the photocatalytic splitting of H₂O and the activity results are summarized in Table 1. The as-prepared low Na-content H-Ti-NT (0.12% Na) produced 11.0 μmol of H₂ over the 5h reaction time. If the sodium content remains high as in the Na/H-Ti-NT sample (7.02% Na), the effect is detrimental to the water splitting activity and production drops to 5.3 μmol of H₂ over the same period. Thermal treatment at 500 °C in air is used to obtain nanotubes with an increased content of TiO₂ (anatase) and the result is a much improved water splitting catalyst with H₂ production of 28.7 μmol. However, the low Na-content and increased TiO₂ (anatase) content are not sufficient to create a water splitting catalyst superior to the bulk TiO₂ (P-25) powder that produces 69.0 μmol of H₂ over the same 5h period and may be related to the collapse of some of the nanotube structures to nanorods or nanowires.

4. Discussion

4.1 Raman Spectroscopy of As-Prepared and Dried Ti-NT

In the present study, the nanotubular H-Ti-NT powder was successfully synthesized with only a trace of TiO₂ (anatase) and negligible Na content (see Figure 1). The relative Raman cross-sections of the Ti-NT and TiO₂ (anatase) phases were semi-quantitatively determined from a series of physical mixtures of the two crystalline phases (see supplemental Figures S2 and S3), and a rough estimate of the amount of

the TiO₂ (anatase) suggests that ~1.0 wt% TiO₂ (anatase) is present in the H-Ti-NT powder. Kasuga *et al.* reported the preparation of TiO₂ (anatase) nanotube powder from continuous washing and ion-exchange using an aqueous HNO₃ solution. The SEM and TEM images of the final powder prepared by Kasuga *et al.* contained short or disrupted nanotube shapes and the corresponding Raman spectrum was dominated by vibrations from the TiO₂ (anatase) phase with only weak titanate bands at ~280 and 700 cm⁻¹.^{62,63} From analysis of the Raman spectra of the physical mixtures of Ti-NT and TiO₂ (anatase) in Figures S2 and S3, it is estimated that powders in the Kasuga *et al.* study contained ~40 wt% TiO₂ (anatase). It was also observed in the present study that after extensive washing and ion-exchange treatments that the original Ti-NT micron long nanotubes changed into very short tubes with strong TiO₂ (anatase) Raman bands. Thus, with extensive washing a significant portion of the titanate phase transforms into the TiO₂ (anatase) phase with concomitant destruction of the nanotubular shape and almost complete removal of Na.

Several of the H-Ti-NT Raman bands were found to be sensitive to moisture suggesting that they may be related to surface vibrational modes since only the vibrations of surface states respond to moisture content.^{54,64} The Raman band for the H-Ti-NT titanate at ~700 cm⁻¹ sharpens and shifts from ~683 to ~710 cm⁻¹ upon dehydration suggesting that this band is a surface vibrational mode. Similarly, the weaker bands at ~830 and ~926 cm⁻¹ may also be related to surface vibrational modes. The other major Raman bands below 600 cm⁻¹, however, are not sensitive to the moisture content implying that they are associated with bulk vibrational modes.^{54,64}

4.2 Effect of Na Content on Raman Spectra of Ti-NT

The as-prepared H-Ti-NT samples were estimated to contain ~1% TiO₂ (anatase), while the Na/H-Ti-NT does not contain even a trace of anatase Raman bands (see Figure 1). The absence of TiO₂ (anatase) in the NA/Ti-NT nanotubes is consistent with the observation that the relative intensity of the small TiO₂ (anatase) Raman band increased as the Na content was decreased during the intermediate ion-exchange stages in the preparation of H-Ti-NT (not shown). The current observation is in agreement with similar observations previously reported by Kasuga *et al.*^{62,63}

The Raman spectra of ambient Na/H-Ti-NT and H-Ti-NT titanates exhibit a small band at 926 cm⁻¹ (see Figures 1 and 2) that was previously assigned to bridging Na-O-Ti bonds formed by surface Na on the titanate particles.^{19,55,65-67} Note that this broad Raman band sharpens upon dehydration (see Figures 2a and 2b). The comparable intensity of this Raman band for the Na/H-Ti-NT and H-Ti-NT titanates, with the former containing >70 times more Na than the latter, strongly suggests that this band the 926 cm⁻¹ band is not related to the bridging Na-O-Ti vibrations and that the ~926 cm⁻¹ titanate Raman band may be related to an overtone of the 453-458 cm⁻¹ band.

With regards to TiO₂ (anatase) formation, Figure 3a shows that at 550 °C, the H-Ti-NT phase completely transforms to the anatase phase (632 cm⁻¹). TiO₂ (anatase) begins to form by 350 °C which is indicated by the splitting of the broad band into two peaks at 641 and 710 cm⁻¹. In contrast, the titanate Raman bands of the Na/H-Ti-NT powder exhibit nearly the same intensity up to 200 °C. A slight decrease and blue shift in the titanate bands at higher temperatures can be observed due to thermal

broadening and due temperature effects, respectively. However, the Na/H-Ti-NT phase does not transform to TiO₂ (anatase) below 550 °C and a new minor band appears at ~117 cm⁻¹ that is reminiscent of Na₂Ti₃O₇.⁵⁵ These comparative thermal studies clearly demonstrate that Na stabilizes the H-Ti-NT titanate phase at elevated temperatures and that in the absence of Na the H-Ti-NT phase transforms to TiO₂ (anatase).

It is possible that nanorods and nanowires exist in the thermally treated samples without significant Na content. Temperature, phase transitions, and moisture can cause the collapse of nanotubes into these other structures. Figure S5 shows STEM high angle annular dark field (HAADF) images of H-Ti-NT (low Na) that has been impregnated with WO_x species and calcined at 550 °C. Analysis of the images shows that while the nanotubular structure is still preserved in some cases (Figure S5a), the collapse of nanotubes to nanowires can also be observed (Figure S5b).

4.3 Structure-Activity Relationships for Photocatalytic Reactions Over Ti-NT

Combining the structural characterization information (Raman spectroscopy and TEM) with photoactivity data allows for establishing fundamental structure-activity relationships for the photocatalytic reactions examined over the Ti-NT nanotubes. For the photocatalytic decomposition of 4-CP, the relative activities of the catalysts were found to be H-Ti-NT (400 °C) >> H-Ti-NT (400+500 °C) > H-Ti-NT (500 °C) >> H-Ti-NT (as-prepared). The strong influence of calcination temperature upon the photocatalytic performance is directly a consequence of the Ti-NT structural changes. The poor performance of the as-prepared H-Ti-NT is related to the greater degree of

disorder present for the titanate phase relative to the more crystalline TiO₂ (anatase) phase that is readily detectable in by its sharp Raman bands. The high photoactivity of the thermally treated H-Ti-NT nanotubes are ascribed to the more ordered TiO₂ (anatase) phase crystalline NT formed during thermal treatments since increased crystallinity of a material provides fewer defects to act as sites for the recombination of electron (e⁻) and holes (h⁺) generated during excitation and, thus, these e⁻/h⁺ pairs are made more readily available to photocatalytic reactions.^{35,46} This explains the increased activity for decomposition of 4-CP for the catalyst treated at 400 °C over the as-prepared H-Ti-NT, which had the lowest activity. Further thermal treatments at 500 °C and above, even if they are performed incrementally (400 + 500 °C), start to cause the collapse of the H-Ti-NT nanotube structure as shown by the STEM-HAADF in Figure S5 and the current observation is supported by the literature.¹¹ The smaller surface area of these structures, despite the TiO₂ (anatase) crystallinity, is the reason why they exhibit a reduced photoactivity for 4-CP decomposition that closely matches that of P-25.

Similar trends can be seen for H₂ production during photocatalytic water splitting over the H-Ti-NT catalysts. The thermal treatment at 500 °C enhanced the photoactivity for H₂ production relative to the as prepared H-Ti-NT titanate phase. Although a 400 °C thermally activated H-Ti-NT was not examined for water splitting, it should have generated twice as much H₂ as the H-Ti-NT (500 °C) photocatalyst because of the partial decomposition of the TiO₂ nanotubes with the higher thermal treatment. Sodium ions are a known poison to photocatalytic activity as they have

been attributed to the increase in recombination centers for electron and hole pairs, preventing the participation of such excitons in the photocatalytic process.^{22,52,68} The presence of significant Na in the as prepared Na-Ti-NT reduced the photoactivity for H₂ production, reflecting this poisoning effect. Furthermore, the inability of the Na-Ti-NT titanate nanotubes to be thermally activated by conversion to the crystalline TiO₂ (anatase) nanotubes suggests that alkali-containing Ti-NTs cannot be thermally activated as the H-Ti-NT nanotubes.

The relative photoactivity of the H-Ti-NT nanotubes differed somewhat relative to that of TiO₂ (P-25) depending on the specific photocatalytic reaction. While the H-Ti-NT(500 °C) was slightly more active than the TiO₂ (anatase) for photodecomposition of 4-CP it was less active than TiO₂ (P-25) for splitting of water. These slight photoactivity differences may reflect the different requirements of dissimilar photoreactions or possibly reflect the sensitivity of the H-Ti-NT to minor synthesis conditions.

A DFT study by Valdés *et al.* showed that the calculated that the active site for water oxidation is a coordinatively unsaturated site on the TiO₂ surface and the breaking of the Ti-O-Ti bond, though a possible route, is energetically unfavorable.⁶⁹ The TEM in Figure 4 revealed that the H-Ti-NT structures have a wall thickness of ~1-2 nm and surfaces of this thickness contain a greater percentage of Ti-O-Ti bonds rather than bulk TiO₂ surfaces. Therefore, the lower number of surface coordinatively unsaturated surface sites may be another reason for the lower water splitting activity of thermally treated H-Ti-NT compared to TiO₂ (P-25) powder.

5. Conclusions

Hydrothermally prepared titanate nanotube powders with negligible and high Na content were prepared and characterized with Raman spectroscopy as a function of synthesis procedures and thermal treatments. The structural characterization was then used to explain photocatalytic activity in the samples. The as-prepared nanotube powders primarily consist of the H-Ti-NT phase (Raman bands at ~ 195 , 285 , 458 , ~ 700 , 830 and 926 cm^{-1}). Moisture was found to broaden the Raman bands at ~ 700 , 830 and 926 cm^{-1} suggesting that they are related to surface vibrational modes. The titanate Raman band at 926 cm^{-1} , which was previously assigned in the literature as originating from Na-O-Ti vibrations, is present in both titanate samples, where the Na content varies by a factor of > 70 , revealing that this band is not related to a Na-O-Ti vibration. The Na-containing titanate powder is thermally stabilized by Na and decomposes at $700\text{ }^\circ\text{C}$ to multiple titania phases (H-Ti-NT, $\text{Na}_2\text{Ti}_3\text{O}_7$, $\text{Na}_2\text{Ti}_6\text{O}_{13}$ and a small amount of TiO_2 (anatase)). The H-Ti-NT phase with negligible Na, however, readily transforms to TiO_2 (anatase) nanotubes upon calcination between $200\text{-}700\text{ }^\circ\text{C}$. Thus, the above reports on the successful synthesis of Na/H-Ti-NT and H-Ti-NT nanotubes and clarifies some of their Raman assignments and their thermal solid-state chemistry.

Photocatalytic decomposition of 4-chlorophenol and photocatalytic water splitting on the as-prepared H-Ti-NT samples showed that thermal treatment to increase the TiO_2 (anatase) content was beneficial in both reactions. At $500\text{ }^\circ\text{C}$, the nanotubes begin to collapse to nanorods or nanowires, and this proved detrimental to the Ti-NT

activity for water splitting as there was no improvement over bulk TiO₂ activity. The activity of the decomposition of 4-CP, however, was not deterred by the collapse of the nanotube structure, reflecting the possible different requirements of high activity for dissimilar photoreactions. The poisoning effect of residual Na impurities was observed for water splitting as the Na/H-Ti-NT catalyst exhibited a decreased production of H₂ product. Furthermore, the inability of Na/H-Ti-NT to form TiO₂ (anatase) nanotubes was concluded to be a negative structural aspect when attempting to transform as-prepared nanotubes into photocatalytically more active forms of crystalline TiO₂, namely TiO₂ (anatase).

Acknowledgements:

Professor Sun-Jae Kim of Sejong University, Seoul, Korea is thanked for providing the catalysts for this study, the TEM image, and the dye decomposition data. This research was financially supported by the DeNO_x catalysis development program of the Electric Power Industry Research & Development Project as well as by the Seoul Research & Business Development Project (NT070123). Lehigh researchers gratefully acknowledge the support by the Department of Energy-Basic Energy Sciences grant DE-FG02-93ERG14350. Wu Zhou and Christopher Kiely of the Department of Materials Science and Engineering of Lehigh University are thanked for the STEM-HAADF images of the supported WO₃/Ti-NT photocatalyst.

References

- (1) Kasuga, T. "Formation of titanium oxide nanotubes using chemical treatments and their characteristic properties," *Thin Solid Films* **2005**, 496, 141-145.
- (2) Cortes-Jacome, M. A.; Angeles-Chaves, C.; Morales, M.; Lopez-Salinas, E.; Toledo-Antonio, J. A. "Evolution of titania nanotubes-supported WO_x species by in situ thermo-Raman spectroscopy, X-ray diffraction and high resolution transmission electron microscopy," *J. Solid State Chem.* **2007**, 180, 2682-2689.
- (3) Cortes-Jacome, M. A.; Ferrat-Torres, G.; Ortiz, L. F. F.; Angeles-Chavez, C.; Lopez-Salinas, E.; Escobar, J.; Mosqueira, M. L.; Toledo-Antonio, J. A. "In situ thermo-Raman study of titanium oxide nanotubes," *Catal. Today* **2007**, 126, 248-255.
- (4) Yu, K. -P.; Yu, W. -Y.; Kuo, M. -C.; Liou, Y. -C.; Chien, S. -H. "Pt/titania-nanotube: A potential catalyst for CO₂ adsorption and hydrogenation," *Appl. Catal, B* **2008**, 84, 112-118.
- (5) Qamar, M.; Yoon, C. R.; Oh, H. J.; Lee, N. H.; Park, K.; Kim, D. H.; Lee, K. S.; Lee, W. J.; Kim, S. J. "Preparation and photocatalytic activity of nanotubes obtained from titanium dioxide," *Catal. Today* **2008**, 131, 3-14.
- (6) Lim, S. H.; Luo, J.; Zhong, Z.; Ji, W.; Lin, J. "Room-Temperature Hydrogen Uptake by TiO₂ Nanotubes," *Inorg Chem* **2005**, 44, 4124-4126.
- (7) Jung, Y. H.; Kim, D. H.; Kim, S. J.; Lee, K. S. "Synthesis and Characterization of Titanate Nanotube for Hydrogen Storage Using Hydrothermal Method with Various Alkaline Treatment," *J. Nanosci. Nanotechnol.* **2008**, 8, 5094-5097.

- (8) Zhang, H.; Gao, X. P.; Li, G. R.; Yan, T. Y.; Zhu, H. Y. "Electrochemical lithium storage of sodium titanate nanotubes and nanorods," *Electrochim. Acta* **2008**, 53, 7061–7068.
- (9) Kim, D. H.; Lee, K. S.; Yoon, J. H.; Jang, J. S.; Choi, D.-K.; Sun, Y.-K.; Kim, S.-J.; Lee, K. S. "Synthesis and electrochemical properties of Ni doped titanate nanotubes for lithium ion storage," *Appl. Surf. Sci.* **2008**, 254, 7718-7722.
- (10) Zhao, Z. W.; Guo, Z. P.; Wexler, D.; Ma, Z. F.; Liu, H. K. "Titania nanotube supported tin anodes for lithium intercalation," *Electrochem. Commun.* **2007**, 9, 697-702.
- (11) Qamar, M.; Yoon, C. R.; Oh, H. J.; Kim, D. H.; Jho, J. H.; Lee, K. S.; Lee, W. J.; Lee, H. G.; Kim, S. J. "Effect of post treatments on the structure and thermal stability of titanate nanotubes," *Nanotechnology* **2006**, 17, 5922-5929.
- (12) Liu, J.; Fu, Y.; Sun, Q.; Shen, J. "TiO₂ nanotubes supported V₂O₅ for the selective oxidation of methanol to dimethoxymethane," *Micro. Meso. Mater.* **2008**, 116, 614-621.
- (13) Escobar, J.; Toledo-Antonio, J. A.; Cortes-Jacome, M. A.; Mosqueira, M. L.; Perez, V.; Ferrat, G.; Lopez-Salinas, E.; Torres-Garcia, E. "Highly active sulfided CoMo catalyst on nano-structured TiO₂," *Catal. Today* **2005**, 106, 222-226.
- (14) Bavykin, D. V.; Cressey, B. A.; Light, M. E.; Walsh, F. C. "An aqueous, alkaline route to titanate nanotubes under atmospheric pressure conditions," *Nanotechnology* **2008**, 19, 275604/1-275604/5

- (15) Peng, H. R.; Lia, G. C.; Zhang, Z. K. "Synthesis of bundle-like structure of titania nanotubes," *Mater. Lett.* **2005**, 59, 1142-1145.
- (16) Nian, J.-N.; Teng, H. "Hydrothermal Synthesis of Single-Crystalline Anatase TiO₂ Nanorods with Nanotubes as the Precursor," *J. Phys. Chem. B* **2006**, 110, 4193-4198.
- (17) Banares, M. A.; Wachs, I. E. "Molecular Structures of Supported Metal Oxide Catalysts Under Different Environments," *J. Raman Spectrosc.* **2002**, 33, 359-380.
- (18) Deo, G.; Wachs, I. E. "Predicting molecular structures of surface metal oxide species on oxide supports under ambient conditions," *J. Phys. Chem.* **1991**, 95, 5889-5895.
- (19) Wachs, I. E.; Kim, T.; Ross, E. I. "Catalysis science of the solid acidity of model supported tungsten oxide catalysts," *Catal. Today*, **2006**, 116, 162-168.
- (20) Kim, T.; Burrows, A.; Kiely, C. J.; Wachs, I. E. "Molecular/electronic structure–surface acidity relationships of model-supported tungsten oxide catalysts." *J. Catal.* **2007**, 246, 370-381.
- (21) Ross-Medgaarden, E. I.; Knowles, W. V.; Kim, T.; Wong, M. S.; Zhou, W.; Kiely, J.; Wachs, I. E. "New insights into the nature of the acidic catalytic active sites present in ZrO₂-supported tungsten oxide catalysts," *J. Catal.* **2008**, 256, 108-125.
- (22) Bavykin, D. V.; Friedrich, J. M.; Walsh, F. C. "Protonated Titanates and TiO₂Nanostructured Materials: Synthesis, Properties, and Applications," *Adv. Mater.* **2006**, 18, 2807-2824.

- (23) Qian, L.; Du, Z. L.; Yang, S. Y.; Jin, Z. S. "Raman study of titania nanotube by soft chemical process," *J. Mol Struct.* **2005**, 749, 103-107.
- (24) Yao, B. D.; Chan, Y. F.; Zhang, X. Y.; Zhang, W. F.; Yang, Z. Y.; Wang, N. "Formation mechanism of TiO₂ nanotubes," *Appl. Phys. Lett.* **2003**, 82, 281-283.
- (25) (X) Hodos, M.; Horvath, E.; Haspel, H.; Kukovecz, A.; Konya, Z.; Kiricsi, I. "Photosensitization of ion-exchangeable titanate nanotubes by CdS nanoparticles," *Chem. Phys. Lett.* **2004**, 399, 512-515.
- (26) Fujishima, A.; Honda, K. "Electrochemical photolysis of water at a semiconductor electrode," *Nature* 1972, 238, 37-38.
- (27) Mills, A.; Davies, R. H.; Worsley, D. "Water purification by semiconductor photocatalysis," *Chem. Soc. Rev.* **1993**, 22, 417-425.
- (28) Linsebigler, A. L.; Lu, G.; Yates, J. T. Jr., "Photocatalysis on TiO₂ Surfaces: Principles, Mechanism, and Selected Results," *Chem. Rev.* **1995**, 95, 735-758.
- (29) Herrmann, J. M. "Heterogeneous photocatalysis: fundamentals and applications to the removal of various types of aqueous pollutants," *Catal. Today* **1999**, 53, 115-129.
- (30) Alfano, O. M.; Bahnemann, D.; Cassano, A. E.; Dillert, R.; Goslich, R. "Photocatalysis in water environments using artificial and solar light," *Catal. Today* **2000**, 58, 199-230.
- (31) Nishijima, K.; Ohtani, B.; Yan, X.; Kamai, T.; Chiyoya, T.; Tsubota, T.; Murakami, N.; Ohno, T. "Incident light dependence for photocatalytic degradation of

acetaldehyde and acetic acid on S-doped and N-doped TiO₂ photocatalysts,” *Chem. Phys.* **2007**, 339, 64-72.

(32) Lee, N. -H.; Oh, H. -J.; Jung, S. -C.; Lee, W. -J.; Kim, D. -H.; Kim, S. -J. “Photocatalytic Properties of Nanotubular-Shaped TiO₂ Powder with Anatase Phase Obtained through Various Thermal Treatments,” *Int. J. Photoenergy* 2011, 327821, 7 pp.

(33) Abe, R.; Kazuhiro, S.; Domen, K.; Arakawa, H. “A new type of water splitting system composed of two different TiO₂ photocatalysts (anatase, rutile) and a IO₃⁻/I⁻ shuttle redox mediator,” *Chem. Phys. Lett.* **2001**, 344, 339-344.

(34) Anpo, M.; Takeuchi, M. “The design and development of highly reactive titanium oxide photocatalysts operating under visible light irradiation,” *J. Catal.* **2003**, 216, 505-516.

(35) Kudo, A.; Kato, H.; Tsuji, I. “Strategies for the Development of Visible-light-driven Photocatalysts for Water Splitting,” *Chem. Lett.* **2004**, 33, 1534-1539.

(36) Usseglio, S.; Damin, A.; Scarano, D.; Bordiga, S.; Zecchina, A.; Lamberti, C. “(I₂)_n Encapsulation inside TiO₂: A Way to Tune Photoactivity in the Visible Region,” *J. Am. Chem. Soc.* **2007**, 129, 2822-2828.

(37) Irie, H.; Miura, S.; Kamiya, K.; Hashimoto, K. “Efficient visible light-sensitive photocatalysts: Grafting Cu(II) ions onto TiO₂ and WO₃ photocatalysts,” *Chem. Phys. Lett.* **2008**, 457, 202-205.

- (38) Zhang, M.; Jin, Z.; Zhang, J.; Guo, X.; Yang, J.; Li, W.; Wang, X.; Zhang, Z. "Effect of annealing temperature on morphology, structure and photocatalytic behavior of nanotubed $H_2Ti_2O_4(OH)$," *J. Molec. Catal. A* **2004**, 217, 203-210.
- (39) Lin, C. -H.; Lee, C. -H.; Chao, J. -H.; Kuo, C. -Y.; Cheng, Y. -C.; Huang, W. -N.; Chang, H. -W.; Huang, Y. -M.; Shih, M. -K. "Photocatalytic Generation of H_2 Gas from Neat Ethanol over Pt/TiO₂ Nanotube Catalysts," *Catal. Lett.* **2004**, 98, 61-66.
- (40) Yu, J.; Yu, H.; Cheng, B.; Trapalis, C. "Effects of calcination temperature on the microstructures and photocatalytic activity of titanate nanotubes," *J. Molec. Catal. A* **2006**, 249, 135-142.
- (41) Yu, H.; Yu, J.; Cheng, B. "Preparation, characterization and photocatalytic activity of novel TiO₂ nanoparticle-coated titanate nanorods," *J. Molec. Catal. A* **2006**, 253, 99-106.
- (42) Yu, Y.; Xu, D. "Single-crystalline TiO₂ nanorods: Highly active and easily recycled photocatalysts," *Appl. Catal. B* **2007**, 73, 166.
- (43) Xiao, M.-W.; Wang, L. -S.; Wu, Y.-Dan; Huang, X. -J.; Dang, Z. "Preparation and characterization of CdS nanoparticles decorated into titanate nanotubes and their photocatalytic properties," *Nanotechnology* **2008**, 015706/1-015706/7.
- (44) Zhou, H.; Park, T. -J; Wong, S. S. "Synthesis, characterization, and photocatalytic properties of pyrochlore Bi₂Ti₂O₇ nanotubes," *J. Mater. Res.* **2006**, 21, 2941-2947.

- (45) Song, H.; Jiang, H.; Liu, T.; Liu, X.; Meng, G. "Preparation and photocatalytic activity of alkali titanate nano materials $A_2Ti_nO_{2n+1}$ ($A = Li, Na$ and K)," *Mater. Res. Bull.* **2007**, 42, 334.
- (46) Bavykin, D. V.; Walsh, F. C. *Titanate and Titania Nanotubes: Synthesis, Properties and Applications*, RSC Publishing, Cambridge, UK, **2010**.
- (47) Kitano, M.; Mitsui, R.; Eddy, D. R.; El-Bahy, Z. M. A.; Matsuoka, M.; Ueshima, M.; Anpo, M. "Synthesis of Nanowire TiO_2 Thin Films by Hydrothermal Treatment and their Photoelectrochemical Properties," *Catal. Lett.* **2007**, 119, 217-221.
- (48) Tsai, C. -C.; Teng, H. "Chromium-doped titanium dioxide thin-film photoanodes in visible-light-induced water cleavage," *Appl. Surf. Sci.* **2008**, 254, 4912-4918.
- (49) Shankar, K.; Mor, G. K.; Prakasam, H. E.; Yoriya, S.; Paulose, M.; Varghese, Oommen K.; Grimes, C. A. "Highly-ordered TiO_2 nanotube arrays up to 220 μm in length: use in water photoelectrolysis and dye-sensitized solar cells," *Nanotechnology* **2007**, 18, 065707/1-065707/11.
- (50) Macak, J. M.; Zlamal, M.; Krysa, J.; Schmuki, P. "Self-organized TiO_2 nanotube layers as highly efficient photocatalysts," *Small*, **2007**, 3, 300-304.
- (51) Liu, Y.; Li, J.; Zhou, B.; Chen, H.; Wang, Z.; Cai, W. "A TiO_2 -nanotube-array-based photocatalytic fuel cell using refractory organic compounds as substrates for electricity generation," *Chem. Comm.* **2011**, DOI: 10.1039/c1cc13388h.

(52) Suetake, J.; Nosaka, A. Y.; Hodouchi, K.; Matsubara, H.; Nosaka, Y. "Characteristics of Titanate Nanotube and the States of the Confined Sodium Ions," *J. Phys. Chem. C* **2008**, 112, 18474.

(53) Deo, G.; Turek, A. M.; Wachs, I. E.; Machej, T.; Haber, J.; Das, N.; Eckert, H. "Physical and chemical characterization of surface vanadium oxide supported on titania: influence of the titania phase (anatase, rutile, brookite and B)," *Appl. Catal. A* **1992**, 91, 27-42.

(54) Chan, S. S.; Wachs, I. E.; Murrell, L. L.; Wang, L.; Hall, W. K. "In Situ Laser Raman Spectroscopy of Supported Metal Oxides," *J. Phys. Chem.* **1984**, 88, 5831-5835.

(55) Horvath, E.; Kukovecz, A.; Konya, Z.; Kiricsi, I. "Hydrothermal Conversion of Self-Assembled Titanate Nanotubes into Nanowires in a Revolving Autoclave," *Chem. Mater.* **2007**, 19, 927-931.

(56) Papp, S.; Korosi, L.; Meynen, V.; Cool, P.; Vansant, E. F.; Dekany, I. "The influence of temperature on the structural behaviour of sodium tri- and hexa-titanates and their protonated forms," *J. Solid State Chem* **2005**, 178, 1614-1619.

(57) Mao, Y.; Wong, S. S. "Size- and Shape-Dependent Transformation of Nanosized Titanate into Analogous Anatase Titania Nanostructures," *J. Am. Chem. Soc.* **2006**, 128, 8217-8226.

(58) Ostromecki, M. M.; Burcham, L. J.; Wachs, I. E.; Ramani, N.; Ekerdt, J. G. "The influence of metal oxide additives on the molecular structures of surface

tungsten oxide species on alumina: I. Ambient conditions,” *J. Molec. Catal.* **1998**, 132, 43-57.

(59) Ostromecki, M. M.; Burcham, L. J.; Wachs, I. E. “The influence of metal oxide additives on the molecular structures of surface tungsten oxide species on alumina: II. In situ conditions,” *J. Molec. Catal. A* **1998**, 132, 59-71.

(60) Wang, X.; Wachs, I. E. “Designing the activity/selectivity of surface acidic, basic and redox active sites in the supported $K_2O-V_2O_5/Al_2O_3$ catalytic system,” *Catal. Today* **2004**, 96, 211-222.

(61) Lewandowska, A. E.; Calatayud, M. n.; Lozano-Diz, E.; Minot, C.; Banares, M. A. “Combining theoretical description with experimental in situ studies on the effect of alkali additives on the structure and reactivity of vanadium oxide supported catalysts,” *Catal. Today* **2008**, 139, 209-213.

(62) Kasuga, T.; Hiramatsu, M.; Akihiko Hoson; Sekino, T.; Niihara, K. “Titania Nanotubes Prepared by Chemical Processing,” *Adv. Mater.* **1999**, 11, 1307-1311.

(63) Kasuga, T.; Hiramatsu, M.; Hoson, A.; Sekino, T.; Niihara, K. “Formation of Titanium Oxide Nanotube,” *Langmuir* **1998**, 14, 3160-3163.

(64) Jehng, J. M.; Deo, G.; Weckhuysen, B. M.; Wachs, I. E. “Effect of water vapor on the molecular structures of supported vanadium oxide catalysts at elevated temperatures,” *J. Molec. Catal.* **1996**, 110, 41-54.

(65) Bavykin, D. V.; Friedrich, J. M.; Lapkin, A. A.; Walsh, F. C. “Stability of Aqueous Suspensions of Titanate Nanotubes,” *Chem. Mater.* **2006**, 18, 1124-1129.

(66) Kolen'ko, Y. V.; Kovnir, K. A.; Gavrilov, A. I.; Garshev, A. V.; Frantti, J.; Lebdev, O. I.; Churagulov, B. R.; Tendeloo, O. G. V.; Yoshimura, M. "Hydrothermal Synthesis and Characterization of Nanorods of Various Titanates and Titanium Dioxide," *J. Phys. Chem. B* **2006**, 110, 4030-4038.

(67) Riss, A.; Berger, T.; Grothe, H.; bernardi, J.; Diwald, O.; Knozinger, E. "Chemical control of photoexcited states in titanate nanostructures," *Nano Lett.* **2007**, 7, 433-438.

(68) Tada, H.; Tanaka, M. "Dependence of TiO₂ Photocatalytic Activity upon Its Film Thickness," *Langmuir* **1997**, 13, 360-364.

(69) Valdés, A.; Qu, Z- W.; Kroes, G- J.; Rossmeisl, J.; Nørskov, J. K. "Oxidation and Photo-Oxidation of Water on TiO₂ Surface," *J. Phys. Chem. C* **2008**, 112, 9872-9879.

Table 1: H₂ production over 5h during photocatalytic water splitting for Ti-NT catalysts with various pretreatment conditions. A TiO₂ (P-25) catalyst is also shown for comparison.

Catalyst	Pretreatment	H₂ Produced (μmol/5h)
H-Ti-NT (0.12% Na)	As-Prepared	11.0
Na/H-Ti-NT	As-Prepared	5.3
H-Ti-NT	Calcined 500 °C in Air	31.9
TiO ₂ (P-25)	None	69.0

Figure 1 Raman spectra of the as-prepared titanate powders with negligible Na content (H-Ti-NT) and with 7.02 at% Na content (Na/H-Ti-NT) under ambient conditions.

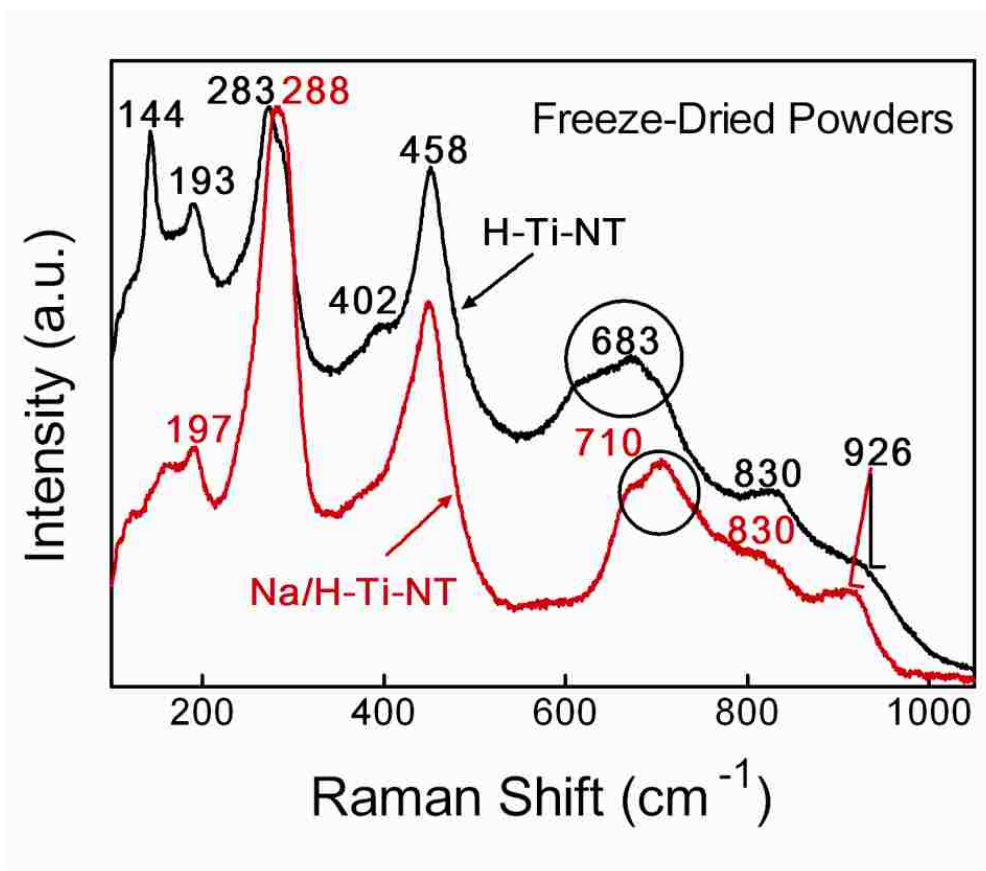


Figure 2 Raman spectra of the titanate powders with negligible Na content (H-Ti-NT) freeze-dried multiple times (a) and of the powders with various drying methods (b) under ambient conditions.

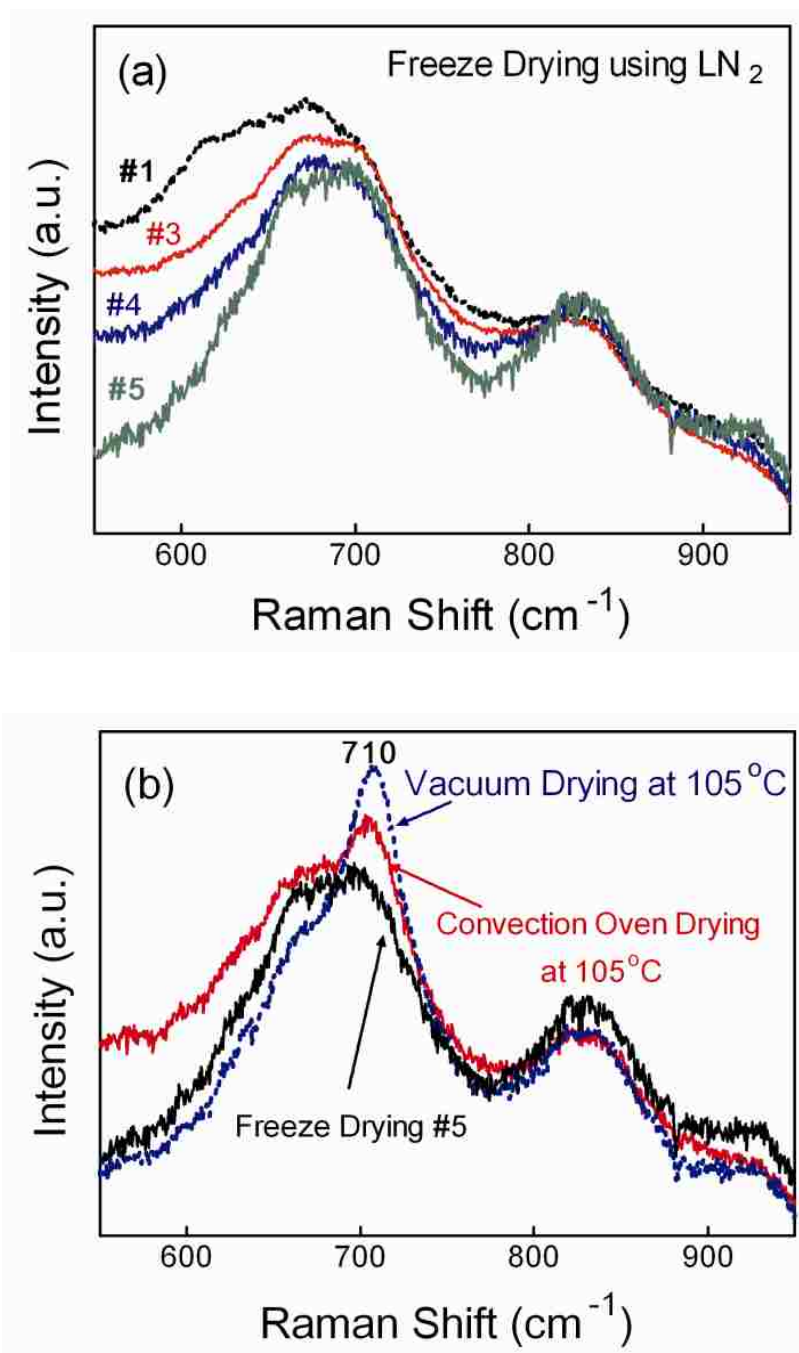


Figure 3 *In situ* Raman spectra of the titanate powders (a) with negligible Na content (H-Ti-NT) and (b) with 7.02 atom % Na content (Na/H-Ti-NT) taken at temperatures of 100 °C to 550 °C with a flowing 10% O₂/Ar (30 sccm).

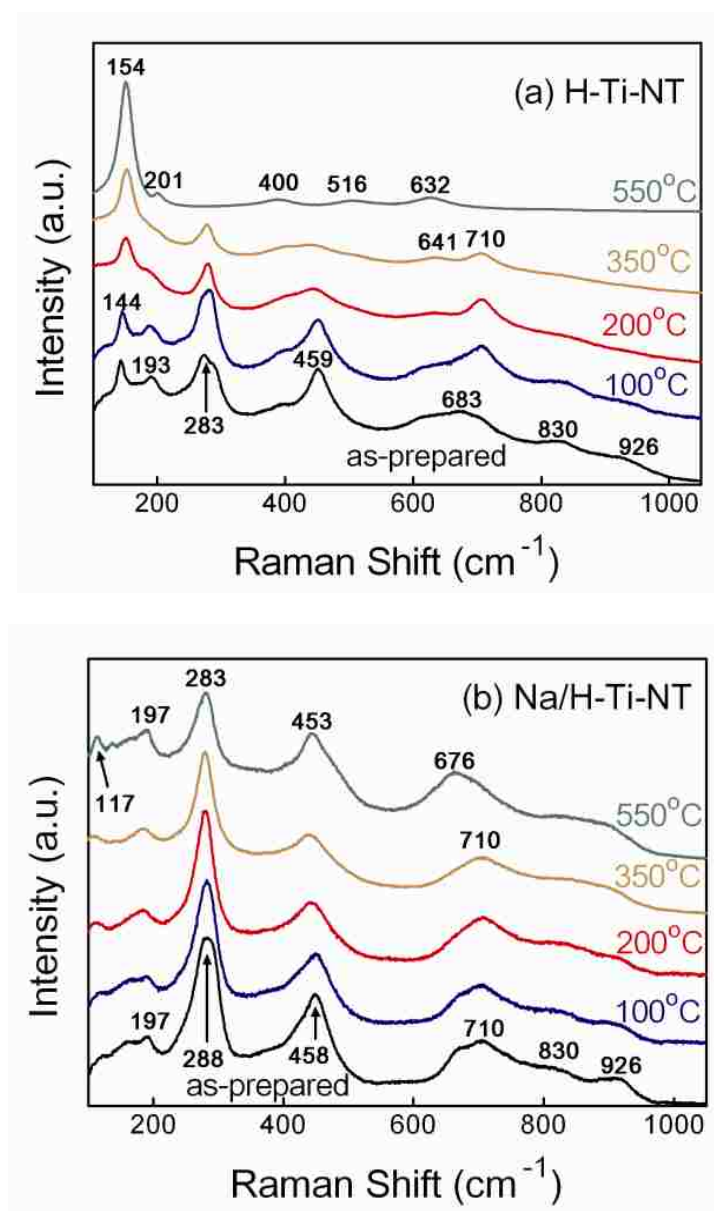


Figure 4 TEM image for the H-Ti-NT powder after heat treatment at 400 °C for 30 minutes in air.

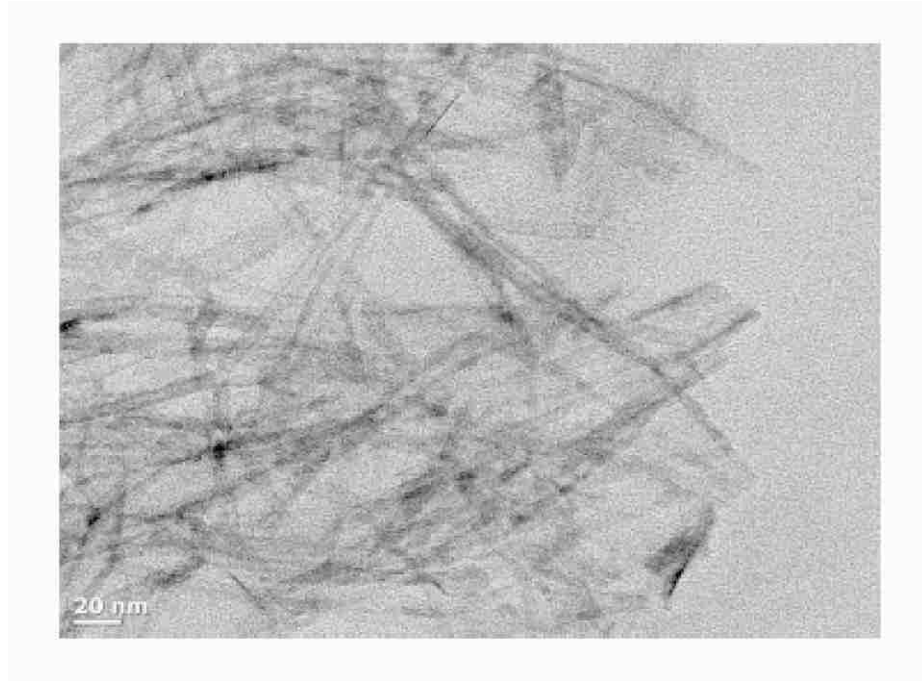


Figure 5 Raman spectra of the titanate powders with negligible Na content (H-Ti-NT) and with 7.02 at% Na content (Na/H-Ti-NT) under ambient conditions after calcining at 700 °C for 3 hrs in air. (A: anatase phase, R: rutile phase)

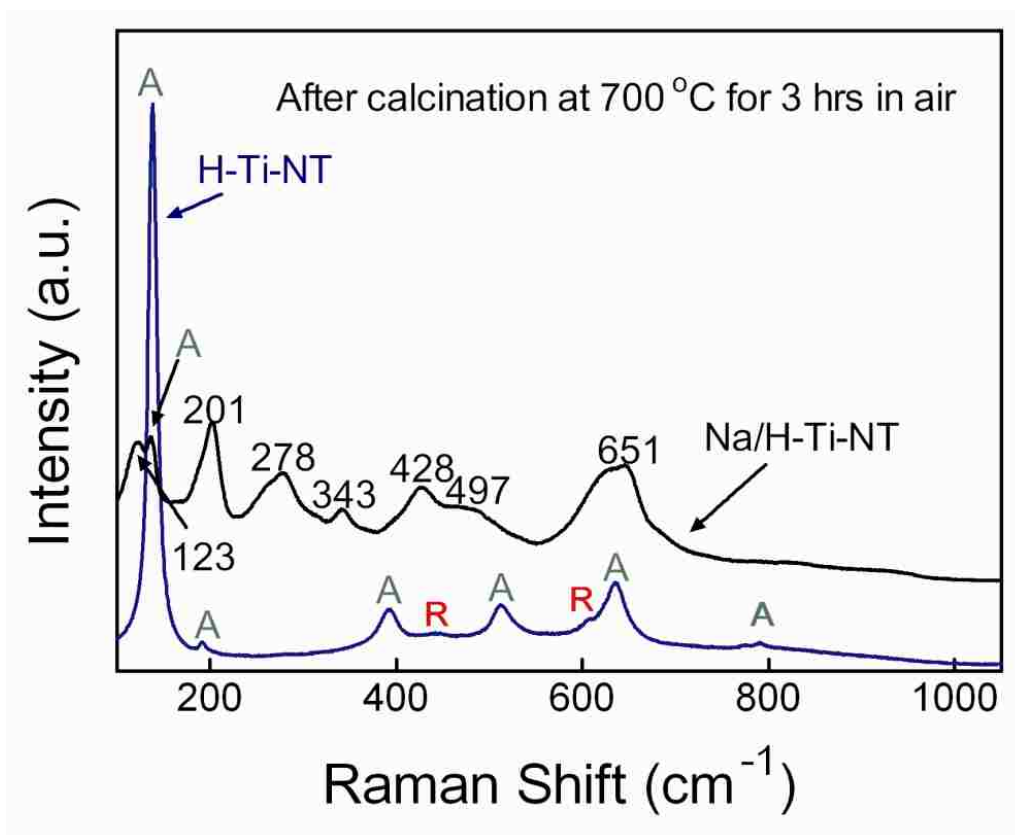
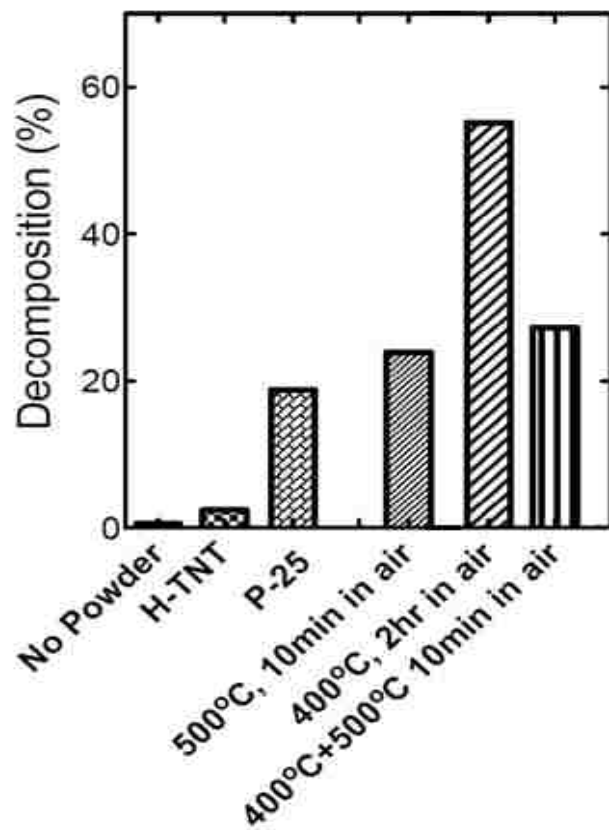


Figure 6: Photocatalytic decomposition of 4-chlorophenol over Ti-NT catalysts after various pretreatment procedures. A pure TiO₂ (P-25) sample was also run for comparison.³²



Chapter 5

Supporting Information

The initial analysis of the as-prepared H-Ti-NT was accomplished by comparison to reference Raman spectra of the various TiO₂ phases: anatase, rutile, brookite, and TiO₂ (B). Figure S1 shows these spectra normalized to the same scale alongside the as-prepared H-Ti-NT spectrum. As indicated in the manuscript, the main spectral features present in the H-Ti-NT are those identified in the literature as indicative of titanate species. The dashed lines in Figure S1 label the major features of the H-Ti-NT spectrum and indicate that there is a trace amount of anatase present corresponding to the presence of the vibration at 144 cm⁻¹. This band is further analyzed semi-quantitatively below. There also appears to be a slight rutile contribution to the spectrum, however, analysis of the relative intensity of the rutile spectral features indicates that a band at ~614 cm⁻¹ should also be present in the case of rutile. The broad band at ~600–720 cm⁻¹ could be misconstrued as this rutile contribution, but the later drying treatments shown in Figure 2 of the manuscript show that this peaks sharpens with the removal of water and is indeed a titanate vibration. Finally, it is clear that the brookite and TiO₂ (B) phases are absent since their most intense Raman peaks at ~156 cm⁻¹ and ~122 cm⁻¹, respectively, do not contribute to the H-Ti-NT spectrum.

In order to semi-quantitatively estimate the amount of TiO₂ (anatase) present in the titanate nanotubes, physical mixtures of TiO₂ (anatase) and Na/H-Ti-NT nanotube

powders were prepared. The pure TiO₂ (anatase) powder was obtained by thermally transforming H-Ti-NT, with negligible Na, by calcination in air at 700 °C for 3 hrs to form the TiO₂ (anatase) nanotubes. The resulting TiO₂ (anatase) nanotube powder only contained a trace of TiO₂ (rutile) as shown in Figure 4. The physical mixtures were combined with ethanol dried in a convection oven at 105 °C for 2 hrs. Raman spectra of the ambient physical mixtures are shown in Figure S2 and S3. As can be seen in Figure S2, the TiO₂ (anatase) phase has a much stronger Raman cross-section than the TiO₂ (titanate) phase. Furthermore, only the TiO₂ (anatase) Raman bands are present at 50 wt% TiO₂ (anatase) and higher contents. Below 50 wt% TiO₂ (anatase), it is possible to estimate the amount of TiO₂ (anatase) present in the H-Ti-NT titanate by comparing the Raman bands of the titanate (288 cm⁻¹) and anatase (138 cm⁻¹). Comparison of the Raman spectrum of the 1.6 wt% TiO₂ (anatase) + 98.4% Na/H-Ti-NT physical mixture with the Raman spectrum of the as prepared H-Ti-NT titanate nanotube suggests that the TiO₂ (anatase) content in the H-Ti-NT titanate powder is slightly less than 1.0 wt%.

The *in situ* Raman spectra of the supported WO₃/titanate catalyst powders with 7.0 atom% Na content (Na/H-Ti-NT) and with negligible Na content (H-Ti-NT) taken after maintaining for 10 minutes at 700 °C with flowing 10% O₂/Ar (30 sccm) are presented in Figure S4. The H-Ti-NT and Na/H-Ti-NT nanotube powders were used as support materials to prepare the supported 12 wt% WO₃/Ti-NT samples by incipient wetness impregnation of aqueous ammonium meta-tungstate (Pfaltz and Bauer). The amount of tungsten oxide was estimated based on monolayer surface

coverage of the surface WO_x species on the Ti-NT supports by assuming that the Ti-NT materials did not undergo significant loss in surface area upon calcination. The supported $\text{WO}_3/\text{Ti-NT}$ catalyst samples were then dried at 105 °C for 24 hrs. Their *in situ* Raman spectra were collected under flowing 30 sccm of 10% O_2/Ar and a heating rate of 60 °C/min and holding the temperature at 700 °C for 10 minutes. The resulting Raman spectra of the supported $\text{WO}_3/\text{Ti-NT}$ samples are shown in the 750-1050 cm^{-1} range. The supported $\text{WO}_3/\text{H-Ti-NT}$ catalyst exhibits one Raman band at 1009 cm^{-1} and the supported $\text{WO}_3/\text{Na/H-Ti-NT}$ catalyst possess two broad bands at ~905 and 922 cm^{-1} .

Figure S1. Reference Raman spectra for different TiO₂ phases compared to the Raman Spectrum of as-prepared H-Ti-NT powder. Dashed lines indicate major Raman bands present for the H-Ti-NT spectrum.

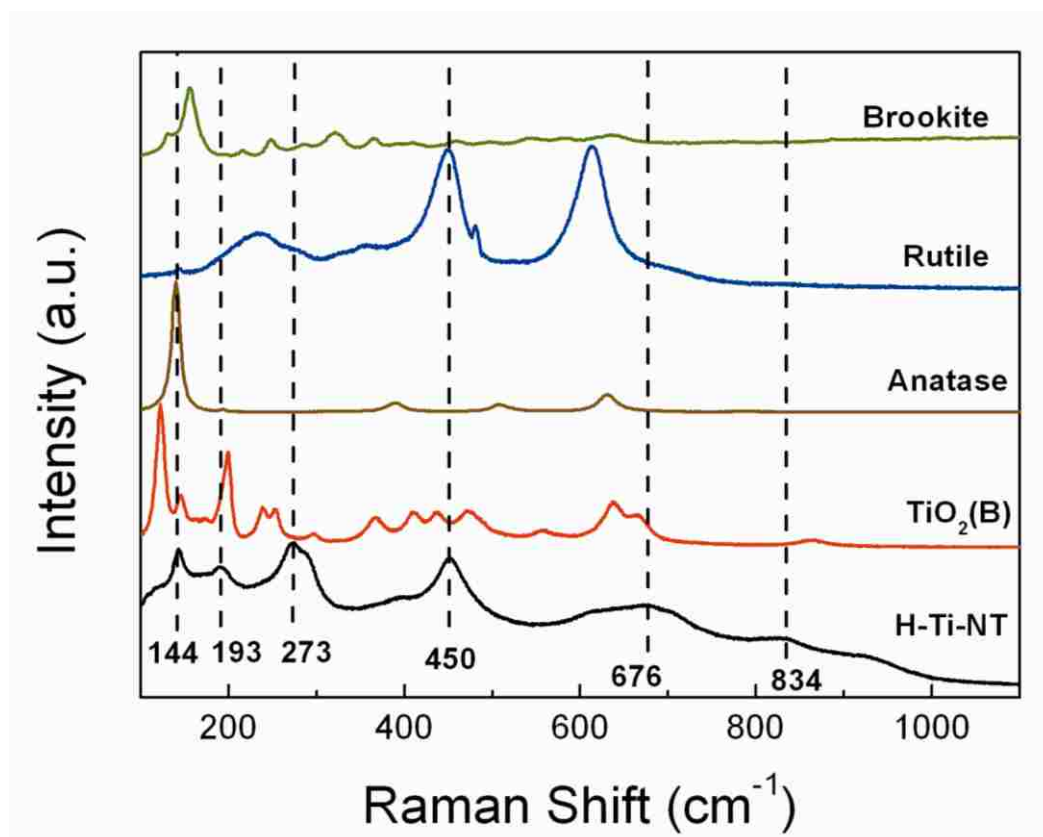


Figure S2. Ambient Raman spectra of physically mixed H-Ti-NT powders and TiO₂ powders as a function of different weight ratios.

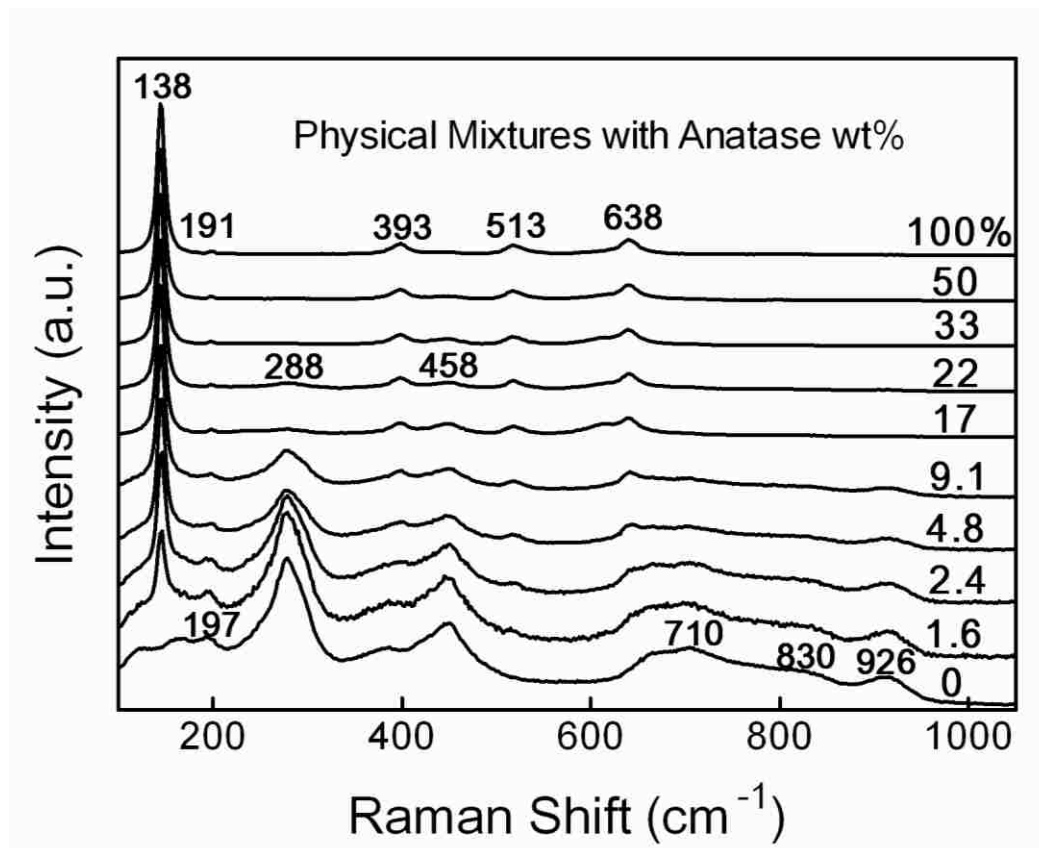


Figure S3. Phase intensities (%) of anatase TiO₂ phase at 138 cm⁻¹ and H-Ti-NT phase at 288 cm⁻¹ estimated from the ambient Raman spectra presented in Figure S1.

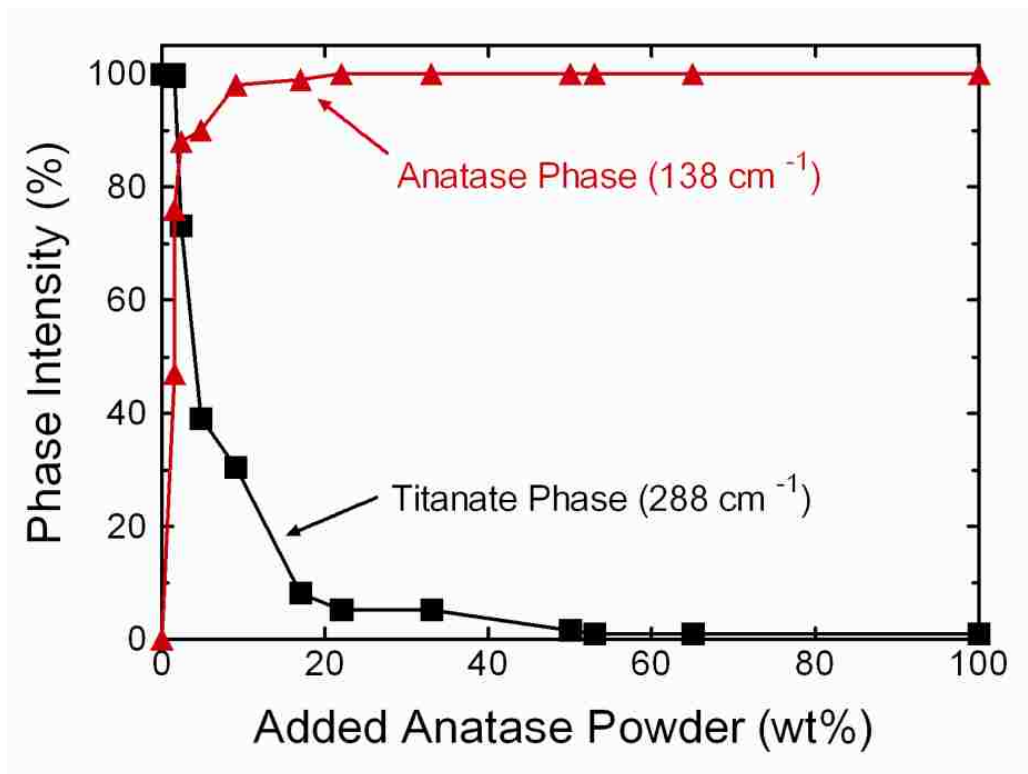


Figure S4. In-situ Raman spectra for ammonium metatungstate supported on Na/H-Ti-NT and H-Ti-NT powders obtained during calcination at 700 °C in presence of 10% O₂/Ar.

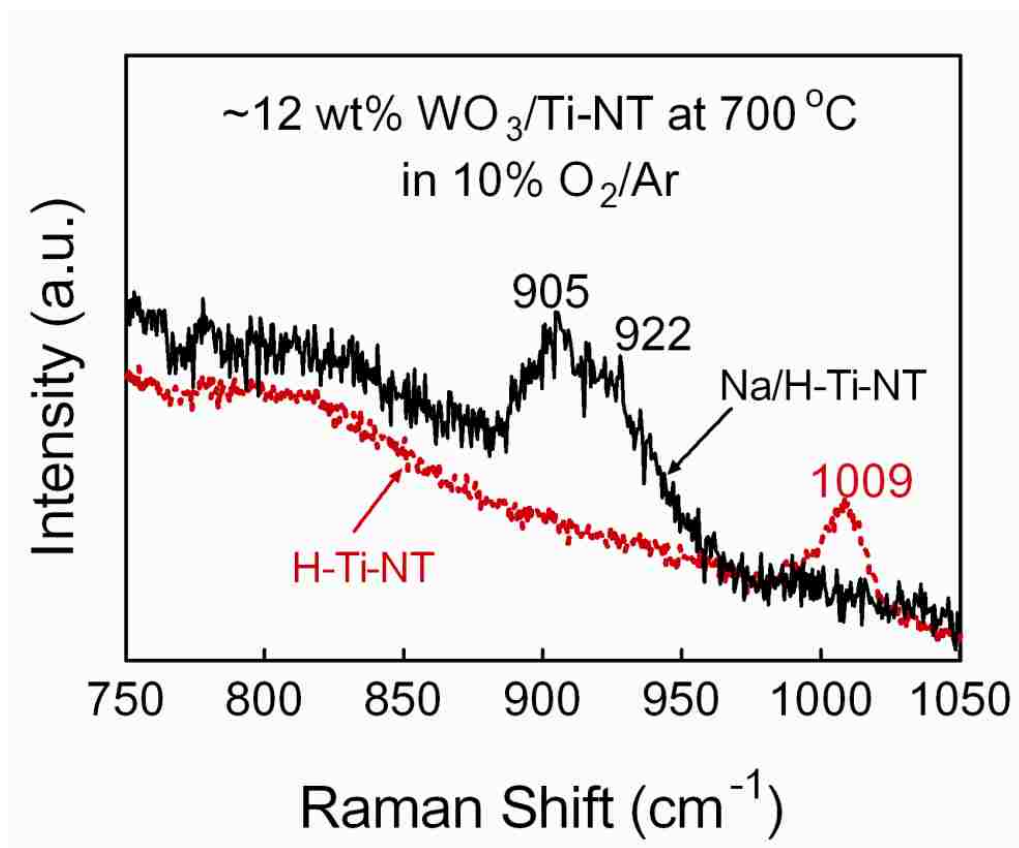
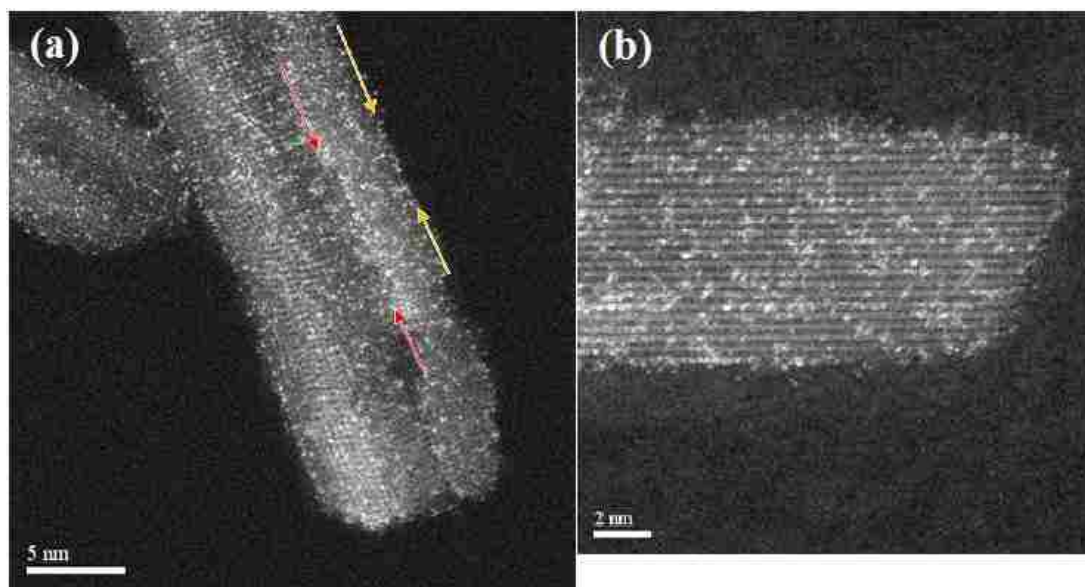


Figure S5: STEM-HAADF images of 11.2% WO_x impregnated on H-Ti-NT (0.12% Na) and calcined at 550 °C showing both nanotube structure (a) and nanowire structures (b). For the nanotube structure in (a) the yellow lines indicate the outer wall and the red lines indicate the inner wall.



CHAPTER 6

Conclusions and Future Outlook

1. Conclusions

The inefficient use of light or solar energy by heterogeneous photocatalysts during potentially useful reactions such as production of H₂ fuel by photocatalytic water splitting has prompted researchers to examine the relationships between the fundamental structural (physical and electronic) properties of photocatalytic semiconductor materials and their photoactivity. The ability to create well-defined TiO_x nanodomains with known physical and electronic structures by supporting varying amounts of titania on a silica support has inspired the current study to use model photocatalysts of this kind as a basis for determining structure-photoactivity relationships. The photoactivity for water splitting and cyclohexane photo-oxidation was determined using reactor studies to monitor the production of H₂ and cyclohexanone, respectively. Spectroscopic investigations were carried out using photoluminescence (PL), attenuated total reflectance (ATR) Fourier transform infrared FTIR, and Raman spectroscopies. Although it is related to the bulk semiconductor property of edge energy, PL spectroscopy is indirectly related to the surface reaction because it yields information on the generation and recombination of excitons utilized by the surface reaction. In several cases ATR-FTIR and Raman spectroscopy gave further insight into the role of adsorbed intermediates in the resulting structure-

photoactivity relationship. The main conclusions of each chapter containing the research performed for this dissertation are summarized below.

Chapter 2

An investigation into the existence of a structure-photoactivity relationship for photocatalytic water splitting on well-defined TiO₂ nanodomains was performed. The trend in H₂ specific activity (μmol H₂/exposed Ti site/h) for the nanodomains proceeded as: pure TiO₂ (anatase) (24 nm) > TiO₂ (anatase) nanoparticles (NPs) (4-11 nm) > polymeric TiO₅ (~1 nm) > isolated TiO₄ (~0.4 nm). Thus, this trend defined a *structure-photoactivity relationship* for water splitting on TiO_x nanodomains related to increased domain size and crystalline quality. High temporal resolution, transient PL spectroscopy measurements revealed that the contribution of slow recombination kinetics was also a function of increasing TiO_x nanodomain size. The generation of excitons with slow recombination kinetics reflects the ability of larger bulk structure of TiO₂ (anatase) NPs to act as a reservoir for these excitons, providing a greater opportunity for exciton migration to surface active sites prior to recombination. The SiO₂ support appears to play a role in trapping excitons at inactive sites and provides an explanation for the low specific photoactivity of supported TiO₂ (anatase) NPs (11 nm) compared to unsupported TiO₂ NPs (24 nm). The SiO₂ support as well as the relative high concentration of inactive Ti-O-Ti sites on isolated TiO₄ and polymeric TiO₅ domains explains their low specific photoactivity.

Chapter 3

The *structure-photoactivity relationship* found for cyclohexane photo-oxidation on supported TiO_x nanodomains also showed increasing specific photoactivity for cyclohexanone production with larger nanodomain structure. The transient PL spectroscopy measurements from Chapter 2 were also applied to the specific activity data and the large bulk structure of TiO_2 (anatase) NPs similarly contribute excitons with slow recombination dynamics with a greater opportunity to participate in surface catalytic reactions. ATR-FTIR spectroscopy detected the formation of adsorbed and bulk liquid phase product cyclohexanone and confirmed the trend of the structure-photoactivity relationship. The obtained spectra also showed that the unsupported TiO_2 (anatase) NPs exhibit better desorption characteristics than supported TiO_2 (anatase) NPs. The decreased desorption characteristics of the smaller supported TiO_x nanodomains can be explained by a decrease in crystalline quality or the trapping of excitons at inactive SiO_2 support sites.

Chapter 4

ATR-FTIR and Raman spectroscopy were employed to identify the intermediates formed during photocatalytic water splitting. HOOH adsorption on TiO_2 thin films was employed to identify the vibrations of relevant adsorbed species. Peroxo (Ti-OOH) and superoxo (Ti-OO) were detected using ATR-FTIR, but Raman spectroscopy was inactive for adsorbed species and only detected unbound, aqueous HOOH. ATR-FTIR at the water/ TiO_2 thin film interface is deterred by the extremely high absorption of IR wavelengths by H_2O . It was not possible to resolve peaks in the peroxo or superoxo spectral regions, however the peak area from $1000\text{-}1200\text{ cm}^{-1}$ was

found to increase in relation to UV illumination. This region does not respond to illumination in the absence of H₂O. It was concluded that the broad spectral region is related to surface superoxo $\nu(\text{O-O})$ vibrations and several OH and OOH $\delta(\text{O-H})$ vibrations. EPR spectroscopy showed that superoxides readily form at defects sites that are generated by UV illumination and DFT studies have shown that the Ti-OOH species is not a part of the rate-determining-step, so it should be extremely difficult to detect with spectroscopic methods. It is not possible to conclude with certainty that the peaks observed in the current study indicate that superoxides are the reactive intermediate associated with the rate-determining-step, but the increase in the spectral range associated with superoxide, OH, and OOH vibrations is supported by EPR and DFT.

Chapter 5

Hydrothermally prepared titanate nanotubes with negligible and high Na content were prepared and characterized with Raman spectroscopy as a function of thermal treatments that were employed to induce phase transformation and form TiO₂ (anatase) nanotubes. It was shown that Na is a detriment to increasing photocatalytic activity because it acts as a poison and stabilizes the titanate structure, preventing the transformation to the higher crystalline quality phase with higher photoactivity. Removal of the Na impurities was accomplished and TiO₂ (anatase) nanotubes were formed at < 400 °C. The increased surface area of TiO₂ (anatase) nanotubes over NPs was beneficial in to the photo-decomposition of 4-chlorophenol. The nanotube structure, however, was not as stable and TiO₂ nanowire formation was observed.

This affected the photoactivity of H₂ production during water splitting, and the larger bulk structure of TiO₂ (anatase) NPs remained the more active photocatalyst.

General Conclusions

It has now been shown in for two separate photo-reaction, water splitting (Chapter 2) and cyclohexane photo-oxidation (Chapter 3), that the increasing bulk structure of TiO₂ (anatase) NPs and is responsible for structure-photoactivity relationships in each reaction. Both photo-reactions also support the conclusion that the bulk acts as a reservoir of excitons with slow recombination dynamics that are more likely to participate in the surface reactions. The ATR-FTIR results of the cyclohexane photo-oxidation study indicate that the supported TiO₂ (anatase) NPs have decreased desorption characteristics compared to unsupported TiO₂ (anatase) NPs. When PL spectroscopy measurements are considered with respect to the necessity of holes for desorption to take place, the lack of excitons with slow recombination kinetics would be the cause of the decrease in desorption. If the water splitting reaction is also desorption limited, this explanation would also apply for that reaction. The SiO₂ support is inactive for both reactions, yet it exhibits clear PL intensity, so it is inferred that it contains trap states that are inactive and a detriment to photoactivity in both reactions. The structure-activity relationship for photocatalysis on TiO_x domains was also found to be useful in explaining the photoactivity of titanate and TiO₂ (anatase) nanotubes, suggesting that the relationship is general for photocatalysis. Therefore, this structure-photoactivity relationship should be seriously considered when

attempting future rational design of new and novel photocatalysts for improved photoactivity.

2. Future Outlook

The most difficult area of research in this dissertation was the attempted identification of relevant adsorbed intermediates during photocatalytic water splitting. The extreme absorption of IR wavelengths by H₂O, the reactant liquid for this reaction, makes *in situ* ATR-FTIR spectroscopy a true challenge. The typical ATR-FTIR spectrum of H₂O on a ZnSe internal reflection element (IRE) in Figure 1 makes the problematic nature of IR absorption by H₂O readily apparent. Although the deposition of thin films of a thickness equal to the penetration depth works well in situations where the relevant intermediates do not overlap with the characteristic vibrations of H₂O,¹ in practice the catalyst coating must be thicker than theoretically predicated.² In the case of water splitting on TiO₂, however, even the application of thicker films failed to provide highly resolved spectroscopic evidence for relevant adsorbed species. The work of Nakamura *et al.* is a well documented instance of the identification of the possible peroxo intermediate Ti-OOH, but the use of Fe³⁺ solution (from FeCl₃) during their study calls in to question the relevance of the intermediate under the desirable conditions of water splitting, i.e. pure, clean H₂O.³ Furthermore, the density functional theory (DFT) study by Valdés *et al.* concludes that peroxo species should be difficult to observe experimentally since its conversation does not represent the rate-determining-step.⁴ Their predication of the rate-determining-step is

the dissociation of water into surface adsorbed OH and H⁺ and an electron (e⁻), therefore making all subsequent intermediates difficult to observe spectroscopically. Given an adsorbed OH is so closely related to the characteristic bands of H₂O, the difficulty of identifying an intermediate of this nature becomes further increased.

There are several possible routes for improving the experimental design of ATR-FTIR measurement of water splitting intermediates under real photocatalytic reaction conditions. The first requires greater control of the TiO₂ film thickness and porosity. The contribution of unbound, liquid H₂O to the resulting ATR-FTIR spectrum must be kept to an absolute minimum. Continual increase of the thickness of film will work to an extent, but if the thickness becomes too great, the evanescent wave will no longer penetrate to the H₂O/catalyst interface and no meaningful data will be collected. Therefore, it is also necessary to accurately calculate the effective refractive index of the thin film, which requires exact knowledge of the porosity and prevention of defect formation such as cracking during deposition. Second, the effect of wavelength of the IR light should also be considered. The peroxy $\nu(\text{O-O})$ stretching vibration spectral region around 800-900 cm⁻¹ begins to experience a rapid increase in penetration depth. It is suggested that the thin film be tailored to maximize its benefits around this region or any region of interest to improve measurement of the specific vibrations. Finally, careful design of experiments utilizing isotopically labeled water (D₂O or H₂¹⁸O) or ¹⁸O exchange of surface hydroxyls on the TiO₂ surface prior to reaction could be a means to shift relevant intermediate vibrations away from H₂O absorption regions.

Another means of elucidating information on intermediates formed during water splitting could be achieved by increasing the temporal resolution of ATR-FTIR spectrum collection. Because intermediates like Ti-OOH are theorized to be short-lived, evidence of their existence may come from transient experiments where a pulse of excitation light is used to initiate reaction followed by ATR-FTIR detection at a rapid speed, similar to the photoluminescence decay study in Chapter 2. The ability of FTIR spectrometers to accomplish high temporal resolution collection has been significantly improved using techniques called rapid-scan and step-scan, which can collect spectra on the order of milliseconds and nanoseconds, respectively.⁵ The nanosecond time-scale of the step-scan technique is particularly attractive given the characteristic times of electron-involving steps of the photocatalytic process. The technique, however, requires the reaction to be performed multiple times to generate a full spectrum, thus necessitating a highly reproducible experiment which is likely difficult for the water splitting given the above issues for the ATR-FTIR thin film technique. Nonetheless, the technique has been utilized successfully for other reaction systems⁶ and coupled with ATR-FTIR.⁷ Sivasankar *et al.* recently showed that rapid-scan and ATR-FTIR could be combined to detect an OOH intermediate during water photo-oxidation on a iridium nanocluster catalyst on the time scale of 610 ms.⁸ These techniques, therefore, should be further investigated for use during water splitting.

The relatively low activity of TiO₂ for photocatalytic splitting of H₂O should also be considered. Presumably a more active catalyst will yield a greater concentration of surface adsorbed intermediates, leading to a more facile spectroscopic measurement.

There exist a great number of oxide semiconductor materials with a higher activity of H₂ production during water splitting and a few of these materials are compiled in Table 1.⁹ If the thin film ATR-FTIR spectroscopy technique were applied to the most active water splitting catalysts, it is possible that chances of identifying the relevant reactive intermediates would increase.

It is also suggested that these novel, more efficient catalysts be subjected to the rigors of determining structure photo-activity relationships and this requires more characterization studies on these novel water splitting materials. The structure-photoactivity relationship found for TiO_x nanodomains for water splitting and cyclohexane photo-oxidation suggests that the bulk structure found in large domains contributes significantly to improving activity. Thus, it is no surprise that the best oxide materials discovered to date are low surface area, bulk oxides. It would be of interest to understand how the multiple oxide components of such complex bulk, mixed-metal oxide catalysts contribute to the individual steps of the photocatalytic process. From the conclusions of this dissertation, it is hypothesized that certain materials will play a role in acting as a reservoir for excitons with slow recombination dynamics, while materials found at the surface or surface modifications must increase the concentration of active hydroxyls or exhibit improved desorption characteristics.

The determination of structure-activity relationships by coupling quantitative structural properties with activity data is a fundamental goal in traditional heterogeneous catalysis.¹⁰ The research in this dissertation extended that ideology to heterogeneous photocatalysis, yet much remains to be understood. Despite the

emergence of structure-photoactivity relationships in the literature,^{11,12} the efficiency of heterogeneous photocatalytic reactions remains well below what is considered commercially viable. Additionally, if photocatalytic reactions are to be driven by renewable solar energy, their efficiency is further reduced due to the inability of large bandgap semiconductors to absorb a large portion of the solar spectrum. For this reason, materials exhibiting relatively high photoactivity for H₂ production during water splitting with improved visible light absorption, such as the GaN:ZnO solid solution reported by Maeda *et al.*,¹³ must be subjected to the ideologies and methodologies of traditional heterogeneous catalysis to further improve the photoactivity and quantum efficiency to industrially viable levels.

Heterogeneous photocatalysis may not be the only answer to the energy problems facing the globe. It is, however, a technology that shows promise for decreasing our dependence on carbon-based fuels. The scientific community is not at a point where the best or only solution to the energy issue can be clearly defined, so research must continue to be done to explore all possible technologies and methods of solving energy problems for the growing world population. It may well be that the answer is a combination of technologies. The research in this dissertation is intended to be a step, however small, in the right directions. On a personal note, I for one believe in the ingenuity of the human race. I am reminded of a statement I first heard from Dr. Mark J. McCready, my professor for undergraduate reaction engineering at The University of Notre Dame: “The stone age did not end because we ran out of stone.”

References

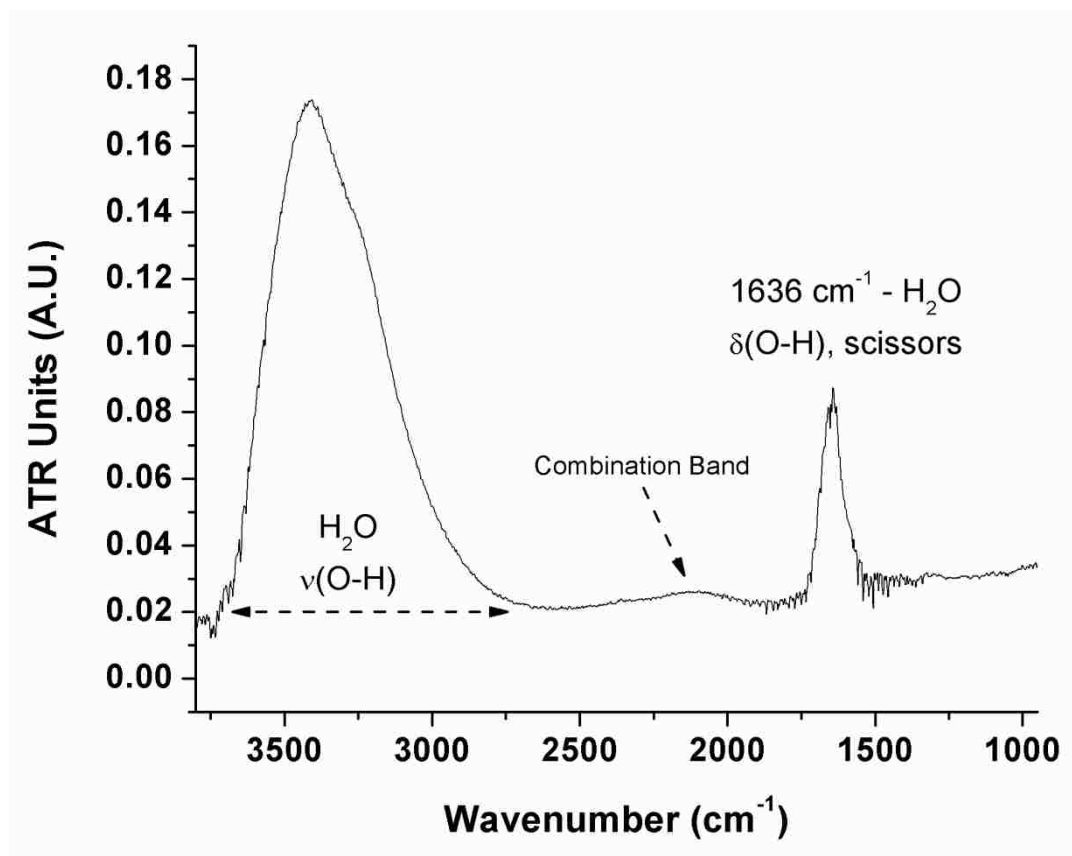
- (1) Mojet, B. L.; Ebbeson, S. D.; Lefferts, L. "Light at the interface: the potential of attenuated total reflection infrared spectroscopy for understanding heterogeneous catalysis in water." *Chem. Soc. Rev.* **2010**, 39, 3643-4655.
- (2) Ortiz-Hernandez, I.; Williams, C. T. "In Situ Investigation of Solid-Liquid Interfaces by Attenuated Total Reflection Infrared Spectroscopy," *Langmuir* **2003**, 19, 2956-2962.
- (3) Nakamura, R.; Nakato, Y. "Primary Intermediates of Oxygen Photoevolution Reaction on TiO₂ (Rutile) Particles, Revealed by in Situ FTIR Absorption and Photoluminescence Measurements," *J. Am. Chem. Soc.* **2004**, 126, 1290-1298.
- (4) Valdés, A.; Qu, Z.-W.; Kroes, G.-J.; Rossmeisl, J.; Nørskov, J. K. "Oxidation and Photo-Oxidation of Water on TiO₂ Surface," *J. Phys. Chem. C* **2008**, 112, 9872-9879.
- (5) Yeom, Y.-H.; Frei, H. "Time-Resolved Step-Scan and Rapid-Scan Fourier-Transform Infrared Spectroscopy," from *In-situ Spectroscopy of Catalysts*, ed. Bert M. Weckhuysen, American Scientific Publishers, **2004**.
- (6) Andersen, L. K.; Frei, H. "Dynamics of CO in Mesoporous Silica Monitored by Time Resolved Step-Scan and Rapid-Scan FT-IR spectroscopy," *J. Phys. Chem. B* **2006**, 110, 22601-22607.
- (7) Mul, G.; Wasylenko, W.; Hamdy, M. S.; Frei, H. "Cyclohexene photo-oxidation over vanadia catalyst analyzed by time resolved ATR-FT-IR spectroscopy," *Phys. Chem. Chem. Phys.* **2008**, 10, 3131-3137.

- (8) Sivasankar, N.; Weare, W. W.; Frei, H. "Direct Observation of a Hydroperoxide Surface Intermediate upon Visible Light-Driven Water Oxidation at an Ir Oxide Nanocluster Catalysts by Rapid-Scan FT-IR Spectroscopy.
- (9) Osterloh, F. E.; "Inorganic Materials as Catalysts for Photochemical Splitting of Water," *Chem. Mater.* **2008**, 20, 35-54, and references therein.
- (10) Wachs, I. E.; Roberts, C. A. "Monitoring surface metal oxide catalytic active sites with Raman spectroscopy," *Chem. Soc. Rev.* **2010**, 39, 5002-5017.
- (11) Carneiro, J. T.; Almeida, A. R.; Moulijn, J. A.; Mul, G. "Cyclohexane selective photocatalytic oxidation by anatase TiO₂: influence of particle size and crystallinity," *Phys. Chem. Chem. Phys.* **2010**, 12, 2744-2750.
- (12) Carneiro, J. T.; Savenije, T. J.; Moulijn, J. A.; Mul, G. "Toward a Physically Sound Structure-Activity Relationship of TiO₂-Based Photocatalysts," *J. Phys. Chem. C* **2010**, 114, 327.
- (13) Maeda, K.; Takate, T.; Hara, M.; Saito, N.; Inoue, Y.; Kobayashi, H.; Domen, K. "GaN:ZnO Solid Solution as a Photocatalyst for Visible-Light-Driven Overall Water Splitting," *J. Am. Chem. Soc.* **2005**, 127, 8286-8287.

Table 1: Activity for H₂ production during photocatalytic water splitting over various novel metal oxides studied in the literature. The activity for TiO₂ is shown for comparison.

Catalyst	Activity (μmol/hr/g cat)	Reference
TiO ₂	69	Current Study
SrTiO ₃	100	K. Domen, <i>Chem. Phys. Lett.</i> , 2001 , 92, 433
Ta ₂ O ₅	1154	H. Kato, <i>Chem. Phys. Lett.</i> 1998 , 295, 487
K ₂ La ₂ Ti ₃ O ₁₀	444	T. Takata, <i>Chem. Mater.</i> 1997 , 9, 1063
Sr ₂ Nb ₂ O ₇	402	H.G. Kim, <i>Chem. Commun.</i> 1999 , (12), 1077
NaTaO ₃ :La	19800	H. Kato, <i>J. Am. Chem. Soc.</i> 2003 , 125, 3082
Sr ₂ SnO ₄	16	J. Sato, <i>J. Phys. Chem. B.</i> 2001 , 105, 6061

Figure 1: Typical ATR-FTIR spectrum for H₂O on a ZnSe IRE.



CURRICULUM VITAE

Charles Alexander Roberts

Address: 25 Maple Rd., Franklin, NJ 07416

Phone: (973) 271-7822

Email: car205@lehigh.edu

Place of Birth: Newton, NJ, USA

Date of Birth: January 5, 1983

Parents: Charles A. and Diane P. Roberts

EDUCATION

Lehigh University, Bethlehem, PA January 2012

- Ph.D. Chemical Engineering, Cum. GPA: 3.71/4.0

University of Notre Dame, Notre Dame, IN May 2005

- B.S. Chemical Engineering, Cum. GPA: 3.4/4.0

RESEARCH EXPERIENCE

Lehigh University, Research Assistant, Chemical Engineering Department
2006-present

- Utilized *in situ* infrared (attenuated total reflectance), Raman, and UV-vis spectroscopy and reactor-based studies to determine structure-activity relationships for photocatalytic water splitting on TiO₂.
- Designed experiments with environmental control for time-resolved emission decay photoluminescence spectroscopy at Oak Ridge National Lab to quantify the recombination of excitons under UV illumination.
- Collaborated with a visiting scientist from South Korea to perform Raman characterization of the thermal treatment of titanate nanotubes for improved photocatalytic performance.
- Investigated the activity of formic acid decomposition over bulk transition and precious metal catalysts to demonstrate that bulk heat of formation of the respective metal oxide does not correlate with the surface reaction activity.
- Characterized the physical and electronic structure of catalytic materials such as supported MoO₃ and titanate nanotubes using *in situ* Raman and UV-vis spectroscopy.

Technical University of Delft, Delft, The Netherlands 2008

- Performed cyclohexane photo-oxidation reactor experiments and acquired the knowledge of ATR-IR equipment and methodologies for probing solid/liquid interfaces.

ENSC Lille, Lille, France 2007

- Acquired experience in *in situ* UV-Raman and electron paramagnetic resonance spectroscopy for oxygen adsorption on metal oxides.

University of Notre Dame, Research Assistant, Nanoscale Bioengineering Lab,
Department of Chemical and Biomolecular Engineering 2003 and 2004

- Measured and monitored the growth of photosynthetic bacteria (*R. viridis*) in varying media and toxins.
- Developed a standardized technique for extraction of bacteriochlorophyll from *R. viridis* using sonication and centrifugation techniques.

TEACHING EXPERIENCE

Teaching Assistant, Chemical Eng. Department, Lehigh University

- Elements of Bioengineering , 2005
- Fluid Dynamics, 2008
- Physical Chemistry Laboratory, 2009

PROFESSIONAL DEVELOPMENT

Lehigh University Unique Surface Analysis Symposium, Bethlehem, PA, 2011

Lehigh University Nano-Energy Workshop, Bethlehem, PA, 2010

NSF Engineering Education Awardees Conference, Reston, VA, 2009

Gordon Research Conference in Catalysis, Colby-Sawyer College, New London, NH, 2008

SpectroCat 2007, Ecole Nationale Supérieure D'Ingenieurs de Caen, Caen, 2007

2006 XAFS Studies of Nanocatalysis and Chemical Transformations, NSLS, Brookhaven National Laboratory, 2006

Interfacial Sciences Meetings, Lehigh University, Bethlehem, 2006

PROFESSIONAL AFFILIATIONS

- American Chemical Society
- American Institute of Chemical Engineers
- North American Catalysis Society
- Catalysis Society of Metropolitan New York
- Catalysis Club of Philadelphia

AWARDS

- **Graduate Student Senate Champion** – Lehigh University student appreciation award, 2011
- **NSF International Research in Engineering and Education**, Award No. 0609018, 2007-2008
- **Kokes Award** - 20th North American Catalysis Society Meeting, Houston
- **Gotshall Fellowship** - Lehigh University

ACTIVITIES

President, Lehigh Chemical Engineering Graduate Association, 2007-2008 and 2008-2009

Vice President, Lehigh Chemical Engineering Graduate Association, 2006-2007
Unit Representative for Chemical Engineering Department, Lehigh Graduate Student Senate, 2005-2010

NCAA ATHLETICS

University of Notre Dame Track and Field

- Three-year Monogram winner, 2003-2005
- Team Captain 2005
- Big East Champion – Hammer Throw 2005
- Two-time All-Big East selection, 2004-2005

PUBLICATIONS

1. “Top Illumination Reactor and *In Situ* ATR-FTIR Investigation of Structure-Activity Relationships for Photo-Oxidation of Cyclohexane over Well-Defined TiO_x Nanodomains,” Charles A. Roberts, Chieh-Chao Yang, Guido Mul, Israel E. Wachs. (*in preparation*)
2. “Determination of a Structure-Photocatalytic Relationship for Water Splitting on Well-Defined TiO₂ Nanodomains,” Charles A. Roberts, Alexander A. Puztzky, Somphonh Peter Phivilay, Israel E. Wachs, *J. Phys. Chem. C* (*to be submitted*).
3. “Monitoring Surface Metal Oxide Catalytic Active Sites with Raman Spectroscopy,” Israel E. Wachs, Charles A. Roberts, *Chem. Soc. Rev.* **2010**, 39(12), 5002-5017.
4. “Molecular Structural Determination of Molybdena in Different Environments: Aqueous Solutions, Bulk Mixed Oxides, and Supported MoO₃ Catalysts,” Hanjing Tian, Charles A. Roberts, Israel E. Wachs, *J. Phys. Chem. C* **2010**, 114 (33), 14110-14120
5. “Characterization of Hydrothermally Prepared Titanate Nanotube Powders by Ambient and *In Situ* Raman Spectroscopy,” Kim, Sun-Jae; Yun, Yeong-Ung; Oh, Hyo-Jin; Hong, Sung Ho; Roberts, Charles A.; Routray, Kamalakanta; Wachs, Israel E., *J. Phys. Chem. Lett.* 2010, 1, 130-135.

INVITED SPEAKER

1. “*In Situ* Time-Resolved Spectroscopic Studies of Metal Oxide Photocatalysts for Water Splitting,” C. Roberts, A. Puztzky, S. Phivilay, and I. Wachs, Applications of Raman Microscopy to Nanoscience Workshop, Argonne National Lab (October 22, 2010)
2. “Structure-Photocatalytic Relationships of Well-Defined TiO₂ Nanodomains,” C. Roberts, A. Puztzky, S. Phivilay, & I. Wachs, April 2009 - Catalysis Club of Philadelphia April Meeting.

ORAL PRESENTATIONS

1. "Photocatalytic Properties of Nanostructured TiO₂ Containing Materials for Splitting of H₂O," Charles A. Roberts, Alexander A. Puzovskiy, Somphonh Peter Phivilay, Sun-Jae Kim, Israel E. Wachs, ACS National Meeting, Anaheim, CA (March 30, 2011).
2. "Fundamental Surface Structure-Photoactivity Relationships of Advanced Photocatalysts," Somphonh Peter Phivilay, Charles A. Roberts, Xiaofang Yang, Guangzhi Frank Liu, Bruce Koel, Israel Wachs, ACS National Meeting, Anaheim, CA (March 30, 2011).
3. "In Situ Time Resolved Spectroscopic Studies of Metal Oxide Photocatalysts for Water Splitting" C.A. Roberts, A.A. Puzovskiy, S.P. Phivilay, and I.E. Wachs, 21st International Symposium on Chemical Reaction Engineering, Philadelphia, PA (June 16, 2010).
4. "In Situ Time Resolved Spectroscopic Studies of Metal Oxide Photocatalysts for Water Splitting" C.A. Roberts, A.A. Puzovskiy, S.P. Phivilay, and I.E. Wachs, ACS National Meeting, San Francisco, CA (March 21, 2010).
5. "Structure-Photocatalytic Relationships of Well-Defined TiO₂ Nanodomains" C.A. Roberts, A.A. Puzovskiy, S.P. Phivilay, and I.E. Wachs, 2008 AIChE Annual Meeting, Philadelphia, PA (November 20, 2008).
6. NS NIRT outreach meeting, Rice University, Houston, TX, June 2007

POSTER PRESENTATIONS

1. "*In Situ* ATR-FTIR Study of Photocatalytic Reactions Over TiO₂ and Supported TiO_x Nanodomains," C. Roberts, C.-C. Yang, S. P. Phivilay, G. Mul, and I. E. Wachs, November 17th, 2011, The Catalysis Club of Philadelphia Student Poster Competition.
2. "Synthesis and Thermal Stability of Hydrothermally Prepared Titanate Nanotube Powders," Sun-Jae Kim, Yeong-Ung Yun, Hyo-Jin Oh, Charles A. Roberts, Kamalakanta Routray, Israel E. Wachs, March 2011 - Catalysis Society of Metropolitan New York Spring Symposium.
3. "Structure-Photocatalytic Relationships of Well-Defined TiO₂ Nanodomains," C. Roberts, A. Puzovskiy, S. Phivilay, & I. Wachs, September 2010 - Lehigh University Nano-Energy Workshop 2010.
4. "*In Situ* Time Resolved Spectroscopic Studies of Metal Oxide Photocatalysts for Water Splitting" C.A. Roberts, A.A. Puzovskiy, S.P. Phivilay, and I.E. Wachs, March 2010 - Catalysis Society of Metropolitan New York Spring Symposium.
5. "*In Situ* Time Resolved Spectroscopic Studies of Metal Oxide Photocatalysts for Water Splitting" C.A. Roberts, A.A. Puzovskiy, S.P. Phivilay, and I.E. Wachs, March 2010 - Catalysis Club of Philadelphia Annual Poster Contest.
6. "Structure-Photocatalytic Relationships of Well-Defined TiO₂ Nanodomains," C. Roberts, A. Puzovskiy, S. Phivilay, & I. Wachs, November 2009 – Oak Ridge National Laboratory, Center for Nanophase Materials Sciences - DOE review.

7. "Structure-Photocatalytic Relationships of Well-Defined TiO₂ Nanodomains," C. Roberts, A. Puretzky, S. Phivilay, & I. Wachs, March 2009 - Catalysis Society of Metropolitan New York Spring Symposium.
8. "Structure-Photocatalytic Relationships of Well-Defined TiO₂ Nanodomains," C. Roberts, A. Puretzky, S. Phivilay, & I. Wachs, March 2009 - Catalysis Club of Philadelphia Annual Poster Contest.
9. "Photocatalytic Structure-Activity Relationship of Well-Defined TiO₂ Nanodomains," C. Roberts, E. Berrier, H. Vezin, E. Payen, & I. Wachs, June 2008 - Gordon Research Conference on Catalysis.
10. "Photocatalytic Structure-Activity Relationship of Well-Defined TiO₂ Nanodomains," C. Roberts, E. Berrier, H. Vezin, E. Payen, & I. Wachs, March 2008 - Catalysis Society of Metropolitan New York Spring Symposium.
11. "Photocatalytic Structure-Activity Relationship of Well-Defined TiO₂ Nanodomains," C. Roberts, E. Berrier, H. Vezin, E. Payen, & I. Wachs, March 2008 - Catalysis Club of Philadelphia Annual Poster Contest.
12. "Investigating the Volcano Curve Correlation for Formic Acid Decomposition on Bulk Metal Catalysts," C. Roberts & I. Wachs, June 2007 - 20th North American Catalysis Society.
13. "Investigating the Volcano Curve Correlation for Formic Acid Decomposition on Bulk Metal Catalysts," C. Roberts & I. Wachs, March 2007 - Catalysis Society of Metropolitan New York Spring Symposium.
14. "Investigating the Volcano Curve Correlation for Formic Acid Decomposition on Bulk Metal Catalysts," C. Roberts & I. Wachs, March 2007 - Catalysis Club of Philadelphia Annual Poster Contest.